GEOLOGICAL SURVEY OF CANADA
OPEN FILE 7550

TILL GEOCHEMICAL SIGNATURES OF THE KIGGAVIK URANIUM DEPOSIT, NUNAVUT

S.V.J. Robinson, R.C. Paulen, C.W. Jefferson, M.B. McClenaghan, D. Layton-Matthews, D. Quirt, and P. Wollenberg

2014

Natural Resources Canada | Ressources naturelles Canada

Canada

GEOLOGICAL SURVEY OF CANADA
OPEN FILE 7550

Till geochemical signatures of the Kiggavik uranium deposit, Nunavut

S.V.J. Robinson[1], R.C. Paulen[2], C.W. Jefferson[2], M.B. McClenaghan[2], D. Layton-Matthews[1], D. Quirt[3], and P. Wollenberg[4]

[1]Department Geological Sciences, Queen's University, Kingston, Ontario
[2]Geological Survey of Canada, Ottawa, Ontario
[3]AREVA Resources Canada Inc., Saskatoon, Saskatchewan
[4]Formerly AREVA Resources Canada Inc., Saskatoon, Saskatchewan

2014

doi:10.4095/293857

This publication is available for free download through GEOSCAN (http://geoscan.nrcan.gc.ca/)

Recommended citation
Robinson, S.V.J., Paulen, R.C., Jefferson, C.W., McClenaghan, M.B., Layton-Matthews, D., Quirt, D., and Wollenberg, P., 2014. Till geochemical signatures of the Kiggavik uranium deposit, Nunavut; Geological Survey of Canada, Open File 7550. doi:10.4095/293857

Publications in this series have not been edited; they are released as submitted by the author.

Contribution to the Geological Survey of Canada's Geo-Mapping for Energy and Minerals (GEM) Program 2008-2013

TABLE OF CONTENTS

Figures

Tables

TILL GEOCHEMICAL SIGNATURES OF THE KIGGAVIK URANIUM DEPOSIT, NUNAVUT, CANADA

S.V.J. Robinson[1], R.C. Paulen[2], C.W. Jefferson[2], M.B. McClenaghan[2], D. Layton-Matthews[1], D. Quirt[3], and P. Wollenberg[4]

[1]Department Geological Sciences, Queen's University, Kingston, Ontario K7L 3N6
[2]Geological Survey of Canada, 601 Booth Street, Ottawa, Ontario K1A 0E8 (e-mail: rogerpaulen@nrcan-rncan.gc.ca)
[3]AREVA Resources Canada Inc., 817 45th Street West, Saskatoon, Saskatchewan S7L 5S2
[4]Formerly AREVA Resources Canada Inc., 817 45th Street West, Saskatoon, Saskatchewan S7L 5S2

ABSTRACT

In 2010, a drift prospecting study was initiated over the Kiggavik uranium deposit under the Geomapping for Energy and Minerals (GEM) Program. The objective of this study was to document the till geochemical signatures of the Kiggavik uranium deposit and to apply these geochemical characteristics for future exploration for buried, drift-covered uranium deposits. The study area is within the zone affected by the migration of the Keewatin Ice Divide of the Laurentide Ice Sheet. Mineralized bedrock and surface till samples (n=71) were collected directly overlying, up-ice, and at various distances (50 m, 100 m, 200 m, 500 m, 1 km, 2 km, 3 km, 5 km, and 10 km) in a fan-shaped pattern down-ice from the deposit with respect to the dominant north-northwest, northwest, and west ice-flow directions.

Samples containing the highest metal contents were located directly to the west of the deposit in locally derived, basement-dominated grey till, which markedly contrasts with the regional red till dominated by material eroded from the Baker Lake and Wharton Groups of the Dubawnt Supergroup. Till geochemistry exhibits a polymetallic dispersal signature down-ice of the Kiggavik Main Zone outcrop. Uranium, Bi, Mo, Au, Ag, Co, Cs, Pb, and W range from elevated to anomalously high concentrations up to 1 km down-ice of the Main Zone and thus can be utilized as pathfinder elements. These pathfinder elements are also present down-ice from other U deposits within the Kiggavik camp, demonstrating their broad applicability to U exploration in basement rocks near the Thelon Basin. Analysis of the <0.063 mm and <0.002 mm fraction of the till matrix shows that elemental abundances are significantly greater in the finer fraction, indicating a strong geochemical partitioning based on grain size.

Laboratory gamma-ray spectrometry, Pb isotopic analysis, and X-ray diffraction were conducted on the till samples. Results show that eU and Pb isotope ratios ($^{206}Pb/^{204}Pb$, $^{207}Pb/^{204}Pb$, $^{207}Pb/^{206}Pb$) in the till matrix share a strong correlation with U content in till and can be used as a geochemical tool for U exploration. The clay mineralogy of samples with elevated to anomalously high U is enriched in illite and kaolinite relative to quartz. Pebble lithological and Pb isotope ratio analyses have trends that can be applied to deciphering till matrix provenance.

INTRODUCTION

The Athabasca Basin of Saskatchewan and Alberta is the template for analysis of the Thelon Basin of Nunavut and Northwest Territories (Miller and LeCheminant, 1985). Current production of U in Saskatchewan is from super high-grade unconformity-associated deposits (Jefferson et al., 2007) at McArthur River and Rabbit Lake with production from Cigar Lake imminent (Saskatchewan Mining Association web site; http://www.saskmining.ca/commodity-info/Commodities/29/uranium.html, accessed 2013-11-11). As reported by Jefferson et al. (2007), the Athabasca Basin contains past plus current resources of 587,063 tonnes of U at a grade of 1.97%, whereas the Thelon Basin contained 48,939 tonnes of U at a grade of 0.41%. The Athabasca U in-ground reserves and inferred resources were worth about $14.6 and $4.7 billion, respectively, at the end of 2005 (Lydon, 2007) although those value estimates did not consider the costs of development, mining, and reclamation.

Twelve additional Paleo- to Mesoproterozoic sedimentary basins in Canada either contain or are considered to have potential to host U deposits of various styles (Jefferson et al., 2007). All of these basins were overridden by continental glaciers during the Quaternary (Dyke and Prest, 1987) and their geochemical signatures were subsequently entrained in glacial sediment, particularly till. Mineral exploration in Canada and Fennoscandia has successfully utilized till geochemistry for Au (e.g. Averill, 1988; McClenaghan, 2001), base metals (e.g. Kaszycki et al., 1996; Parkhill and Doiron, 2003), and rare earth elements (e.g. McConnell and Batterson, 1987). Most of the published case studies that document the geochemical dispersal signatures from U deposits (e.g. Earle, 2001; Campbell, 2009) are from the Athabasca Basin, and very little has been published about other basins that can be applied to drift prospecting in northern Canada. The northeastern part of the Thelon Basin, located in the Kivalliq Region of Nunavut (Figs. 1, 2), is an ideal

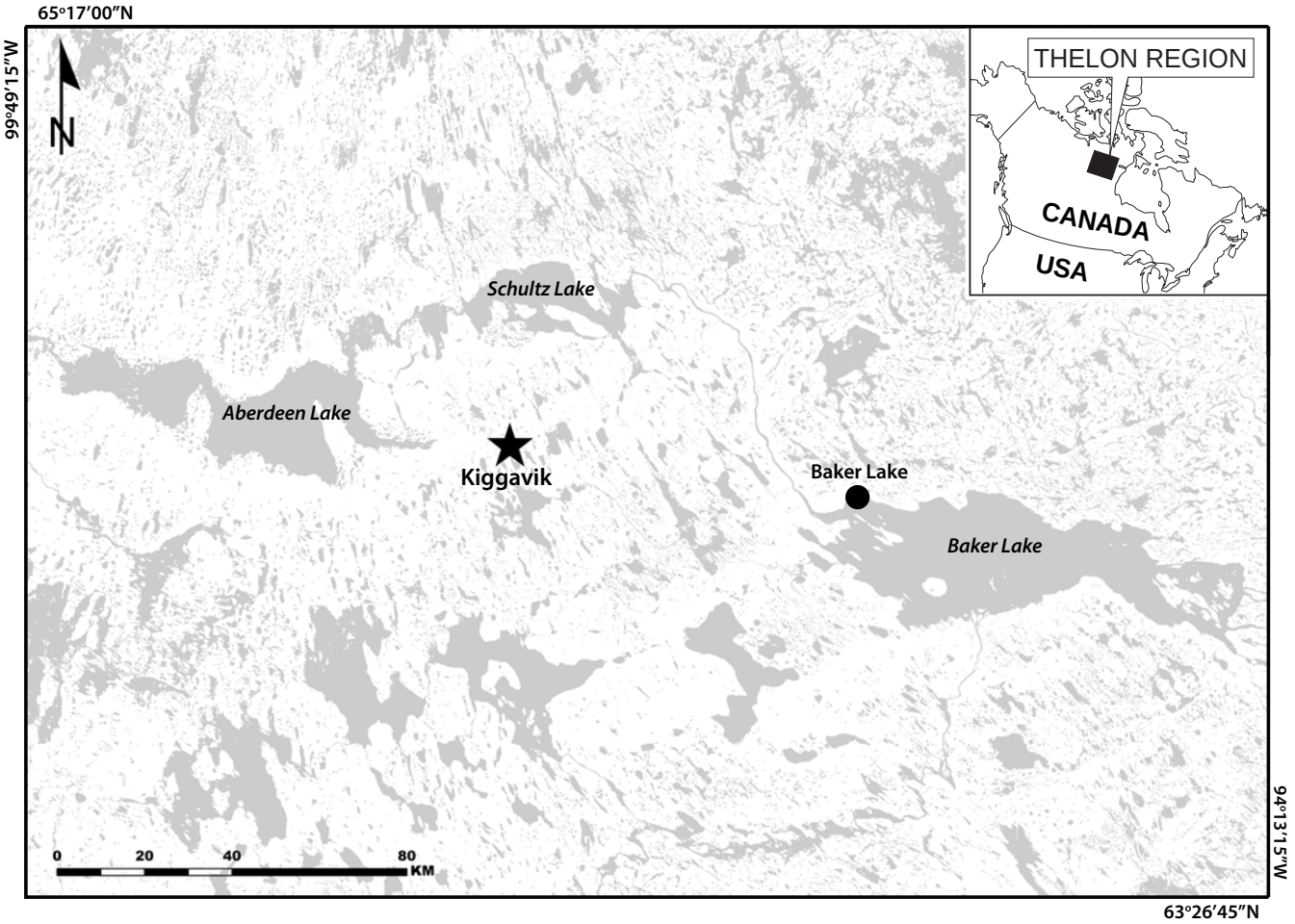

Figure 1. Location map of the Kiggavik study area in central Kivalliq, Nunavut.

location for such studies as an integral part of the GEM Uranium Project (Jefferson et al. 2011a,b,c; 2013a,b).

To better understand the till geochemical signatures of unconformity-associated U deposits in northern Canada, and to test the concept that drift prospecting methods for other deposit types can be adapted to U deposits, the Geological Survey of Canada (GSC) through its GEM Program (2008–2013) in collaboration with the Queen's Facility for Isotope Research at Queen's University and AREVA Resources Canada Incorporated (AREVA), collected and analyzed a suite of bedrock and till samples from the Kiggavik U deposit, Nunavut. For this specific geochemistry study, the GSC collected a total of 71 till samples to document the geochemical dispersion of the Kiggavik deposit.

The Kiggavik U deposit was chosen for this study because (a) the Kiggavik camp is known to have multiple U deposits and prospects (Fig. 3); (b) the Kiggavik Main Zone (KMZ) deposit outcrops and thus was directly eroded by glaciers; and (c) the surficial geology surrounding the KMZ is favourable, consisting of scattered outcrops and till veneer. The ultimate objectives of this study were to document till geochemical signatures associated with the KMZ, establish background concentrations for U and the associated pathfinder elements, and document the elemental partitioning in both the <0.063 mm fraction and the <0.002 mm fraction with modern analytical procedures. The Meadowbank iron formation Au deposit is hosted in the same supracrustal belt, therefore some potential exists in the Kiggavik part of this belt for undiscovered lode Au, concomitant with its pathfinder elements.

Project location and physiography

The Kiggavik U deposits are located in the central Kivalliq Region of Nunavut, in the Schultz Lake topographic map sheet (NTS 66A/05; Fig. 1). The KMZ outcrop is situated approximately 80 km west of the community of Baker Lake at 64º26' north and 97º38' west (UTM easting 565133, northing 7146899; Datum NAD83, zone 14). The study area lies on the northern edge of the Kazan Upland, at the intersection of the Thelon Plain, Back Lowland, and Wager Plateau physiographic divisions of the Kazan Region of the Canadian Shield (Bostock, 1970). The region is under-

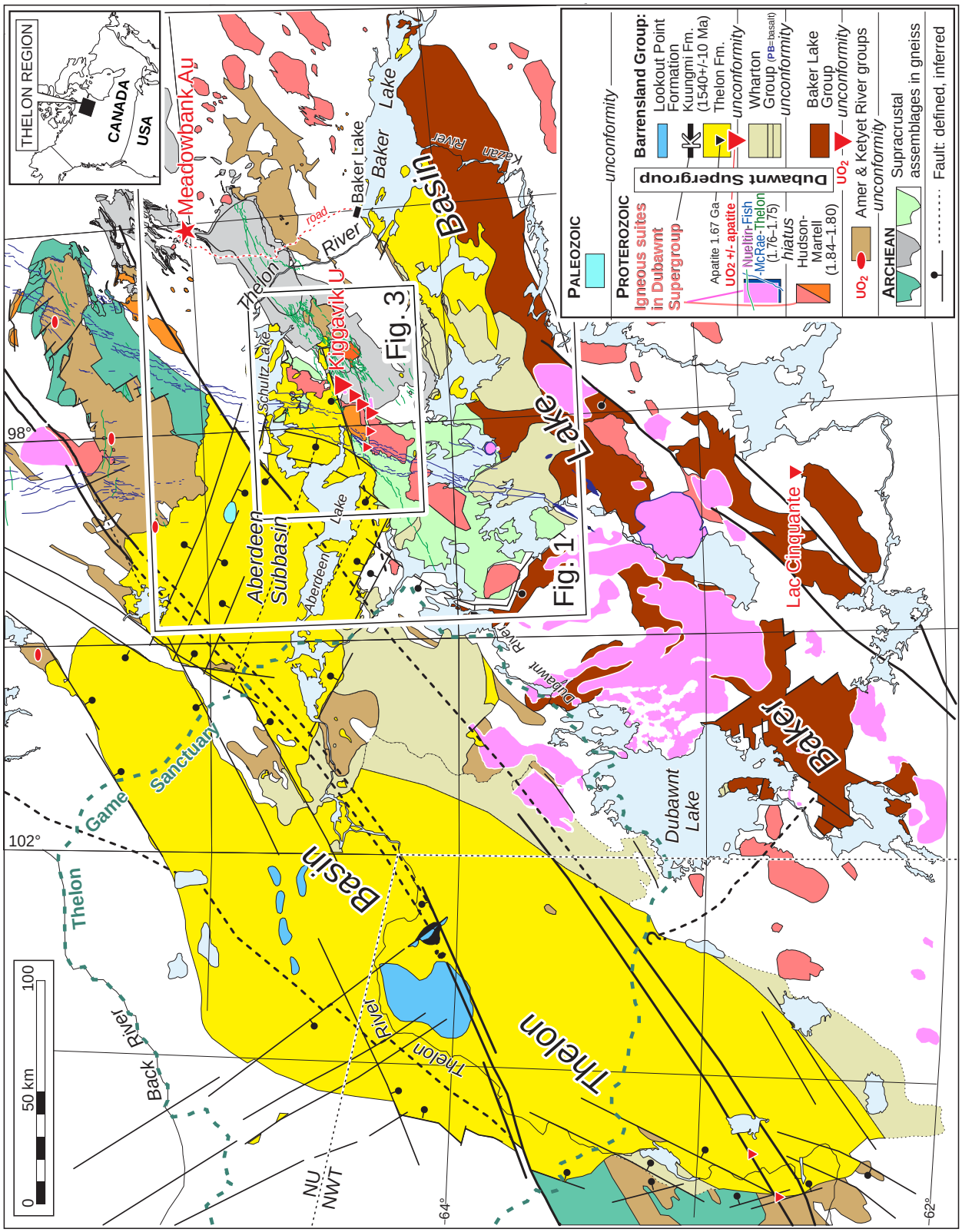

Figure 2. Regional geological map of the Baker Lake and Thelon basins, the Dubawnt Supergroup, and older supracrustal belts (after Jefferson et al., 2011c, 2013a). U showings and occurrences are annotated by red triangles; the Kiggavik deposit is indicated by the largest. Baker Lake community is denoted by a black rectangle. Outlines show the locations of Figures 1 and 3.

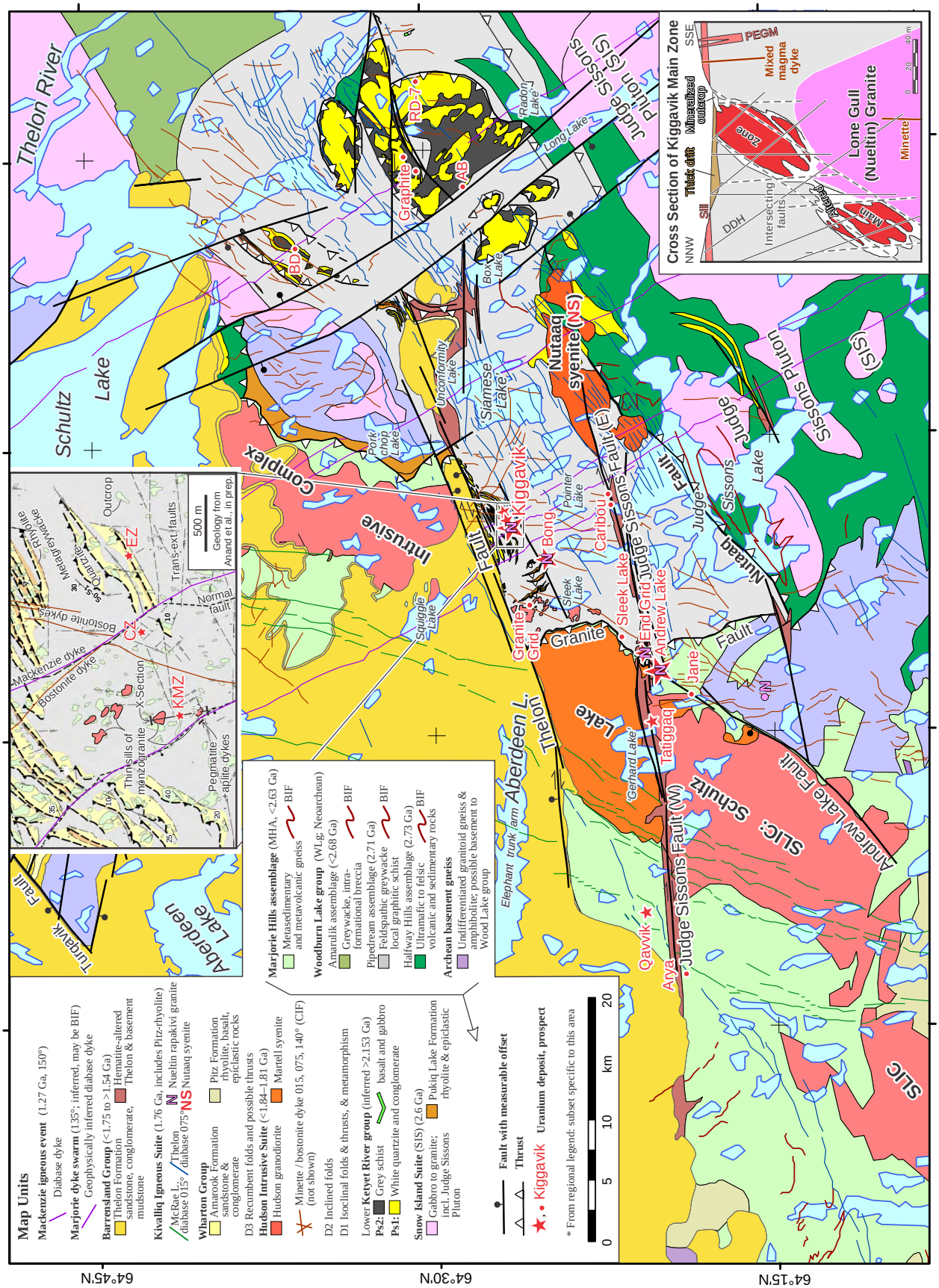

Figure 3. Bedrock geology of the Kiggavik camp, in the western Schultz Lake and eastern Aberdeen Lake map areas (NTS 66A, B, respectively). Details of the Kiggavik deposit are shown in the inset map at the top and the cross section at the bottom-right (modified from Jefferson et al., 2013b).

lain by continuous permafrost with the depth of the active layer varying from 15–200 cm, depending on the sediment type and drainage conditions (McMartin et al., 2006). The vegetation is characteristic of open tundra (dwarf trees, shrubs, sedges, and grasses). In the study area around Kiggavik, the relief is low and glacially streamlined, bogs are thinly developed, and the abundant shallow-water bodies range from 25 m ponds to 5 km lakes. These freeze solid in winter, with the exception of the deeper lakes that are greater than 1–2 km in diameter.

Bedrock geology

The late Paleoproterozoic Thelon Basin comprises a 500 by 200 km western portion and a 100 x 110 km northeastern portion, termed the Aberdeen Subbasin (Fig. 2). The Kiggavik U deposits are basement-hosted, occurring just outside the Aberdeen Subbasin, on its southeast corner, and separated from the Subbasin by the Thelon Fault (Fig. 3). The basement rocks are dominantly metasedimentary, with subordinate metavolcanic and intrusive rocks. The Neoarchean and early Paleoproterozoic metasedimentary and minor metavolcanic rocks are highly deformed but weakly metamorphosed, interfolded, and thrust-repeated (Jefferson et al., 2011c, 2013b).

The Neoarchean-Paleoproterozoic structural package was intruded by late- to post-orogenic granite sills of the Hudson Suite and numerous ultrapotassic mafic to felsic dykes, all in the order of 1.83 Ga (Peterson et al., 2002). The first major sequence of the Dubawnt Supergroup is the Baker Lake Group, deposited from 1.84 to 1.81 Ga in the Baker Lake and related basins to the south and east of Kiggavik (Fig. 2; Rainbird et al., 2003). The Baker Lake Group comprises intercalated conglomerate and sandstone intercalated with ultrapotassic bimodal volcanic rocks whose intrusive equivalents in the Kiggavik camp include the Martell syenite (mingled with the Hudson granite) and abundant minette (lamprophyre) plus bostonite (microsyenite) dykes that transect the camp. The latter were altered as part of the mineralization process but are essentially barren of ore phases (Figs. 2, 3).

The region was peneplaned, deeply weathered, and unconformably overlain by sandstone and conglomerate of the Amarook Formation, which is the lower part of the Wharton Group and middle sequence of the Dubawnt Supergroup. Shortly thereafter, undeformed bimodal products of the 1.75 Ga Kivalliq Igneous Suite (KIS; Peterson et al., in prep.) included volcanic and epiclastic rocks of the Pitz Formation (upper part of the Wharton Group) and multiple intrusive phases: the Nueltin granite, anorthositic gabbro, and two sets of diabase dykes — the McRae and Thelon swarms. These were all unconformably overlain in the study area by the three major sequences of the Dubawnt Supergroup: conglomerate, red mudstone, and pale pink sandstone of the Thelon Formation, basal units of the Wharton Group, and basal units of the Barrensland Group (Fig. 3).

Detailed mapping of the Kiggavik camp by Pehrsson et al. (2010), Jefferson et al. (2011c), and McEwan et al. (2011) elucidated the Kiggavik host rocks as follows. Most of the ore is in Neoarchean quartzofeldspathic metagreywacke with minor iron formation and metapelite. These are unconformably overlain in succession by 2.6 Ga quartz-feldspar porphyritic rhyolite (also an ore host and locally known as "quartz-eye quartzite") and early Paleoproterozoic quartzite that is barren of U. The basal subunit of the quartzite is highly micaceous (locally known as sericite schist). The three-part sequence of greywacke-rhyolite-quartzite forms multiple structural intercalations in an east-west panel flanking the south side of the Thelon Fault and in a north-south panel west of the Bong deposit. Most workers infer that sandstone and conglomerate of the Thelon Formation once covered the Kiggavik deposits but was removed by erosion such that the closest outcrops of the Thelon Formation are on the north side of the Thelon Fault, 2 km to the north of the KMZ (Fuchs and Hilger, 1989). The Ayra occurrence, one of the new discoveries by Cameco Corp. (R. Hunter, oral presentation, Nunavut Mining Symposium, April 5, 2011) is overlain by an outlier of the Thelon Formation, supporting the unconformity-association for the basement-hosted uraninite. Another host rock for U is the border phases of the porphyritic Lone Gull granite intrusion, hypabyssal Nueltin granite that is part of the KIS (ca. 1750 Ma zircon U/Pb: Scott et al., 2010, in prep; Peterson et al., 2010).

The above described ductile deformation and igneous history was overprinted by hydrothermal alteration that was most strongly developed along steeply dipping, intersecting brittle fault zones. Two of the most prominent and regional faults are the east-northeast-trending Thelon Fault, some 2 km north of Kiggavik, and the Judge Sissons fault, about 8.5 km to the south (Fig. 3). These are only part of an array of such faults, one or more of which trend directly through the Kiggavik deposits. The deposits are localized by intersections of these faults with northeast- and northwest-trending faults. The existence of these fault systems has been recognized by exploration geologists from soon after discovery (Fuchs and Hilger, 1989) to the present day (R. Hunter, oral presentation, Nunavut Mining Symposium, April 5, 2011).

Three ore zones have been defined in the immediate Kiggavik area. The Main and Center zones (KMZ and CZ) are approximately 600 m apart and both are on a 065°-trending fault zone. The East zone (EZ) is 500 m

Table 1. List of the Kiggavik U deposit ore and associated minerals (Fuchs et al., 1985; Weyer et al., 1987; Pacquet, 1993; Reyx, 1994; Robinson et al., in prep).

Mineral	Chemical Formula
Uraninite	UO_2
Coffinite	$(U^{4+},Th)(SiO_4)_{1-x}(OH)4x$
Uranophane	$Ca(UO_2)2[HSiO_4]_2$ - $5H_2O$
Gold	Au
Molybdenite	MoS_2
Pb-rich Apatite	$Ca_5(Pb)(PO_4)3(F,CL,OH)$
Rutile / Anatase	TiO_2
Pyrite / Marcasite	FeS
Hematite	Fe_2O_3
Limonite	$FeO(OH)$ - nH_2O
Galena	PbS
Chalcopyrite	$CuFeS_2$
Bismuthinite	Bi_2S_3
Electrum	(Au,Ag)
Brannerite (U-rich)	$(U^{4+},REE,Th,Ca)(Ti,Fe^{3+},Nb)_2(O,OH)_6$
Covellite	CuS
Digenite	Cu_9S_5
Bi-Ag Tellurides - sulphates	Bi,Ag,SO_4^{2-}

east of the CZ (Campbell and Clark, 2009). The KMZ is the largest, being described as having two major subparallel en echelon lenses within the same fault zone. These lenses are elongated, plunging to the east-northeast at ~25º to a depth of 150–190 m, and hosted by both metagreywacke and the border phase of the Lone Gull granite (Fuchs and Hilger, 1989; Weyer et al., 1987). Most of the KMZ subcrops beneath <10 m of glacial till but a small part of it is exposed on the surface and has been trenched and was sampled during this study. The CZ also comprises two defined lenses; these are hosted by metagreywacke and metarhyolite sandwiching a barren orthoquartzite body that dips shallowly to the north (Fuchs and Hilger, 1989). The EZ, located approximately 150 m along strike, is similar to that of the CZ in that the disseminated uraninite is shallow to within 100 m of the surface (Fuchs et al., 1985; Fuchs and Hilger, 1989).

The ore zones are enclosed by intense alteration haloes characterized by desilicification and conversion of feldspar and mica to clay minerals, dominantly illite and sericite (Fuchs and Hilger, 1989; Pacquet, 1993). The main ore minerals are uraninite and coffinite; minor uranophane is present in weathered ore at surface (Fuchs et al., 1985). The ore minerals are finely (<100 μm) disseminated, predominantly along foliation planes and/or in veinlets parallel to the foliation, but also fill fractures (Weyer et al., 1987; Fuchs and Hilger, 1989; Reyx, 1994) and forms vermiform microroll-front textures. The ore contains subordinate pyrite, marcasite, galena, and hematite/limonite with common calcite stringers. Multiple additional minerals and metals, which are present only in trace amounts, are listed in Table 1. Of interest as potential geochemical tracers are fine-grained gold (<50 μm), molybdenite and Bi-Ag telluride group minerals (Reyx, 1994). The KMZ and CZ zones contain inferred resources of 12,383 and 3992 tonnes of U metal grading 0.48%, 0.50% U, respectively (Berthet and Osorio 2011a, b). The EZ contains a bulk historical resource of about 495 tonnes of U metal, grading 0.05% (Jefferson et al., 2007). Additional resources have been identified in the Kiggavik Camp at the Andrew Lake and End Grid deposits, located about 15 km south-southwest of the KMZ, with inferred resources of 20,003 and 14,696 tonnes U grading 0.50% and 0.40%, respectively (recalculated from Berthet (2011) and Osorio (2011), respectively). The Bong deposit, located about 3.9 km southwest of the KMZ, has an historical bulk resource of about 1650 tonnes U grading 0.23% (Jefferson et al., 2007).

Exploration history of the Kiggavik uranium camp

Exploration for U in Proterozoic supracrustal successions within the Churchill structural province was initiated after reconnaissance bedrock mapping during the 1950s by Wright (1955) and subsequent stratigraphic work by Donaldson (1965). With the discovery of the high-grade Rabbit Lake U deposit in the Athabasca Basin, U exploration in and around the late Paleoproterozoic Thelon Basin began due to its geological similarities with the Athabasca camp of northern Saskatchewan (Miller and LeCheminant, 1985). Exploration in the vicinity of the Kiggavik deposit (initially named the Lone Gull Deposit) has been ongoing since the 1970s when Urangesellschaft Canada Limited (UGC) selected this area for its similarity to the eastern part of the Athabasca Basin (Fuchs et al., 1985). In 1974 much of the Thelon Formation and the adjacent basement rocks underwent a systematic exploration program that included lake sediment, water, and airborne radiometric surveys. This program led to the discovery of a strong geochemical anomaly hosted in radioactive frost boils overlying what is now termed the KMZ (Reilly, 1997). Drilling in the late 1970s discovered significant U in structurally controlled zones within metagreywacke ("dirty quartzites" of Griep (1978)).

Further exploration through gravimetric, EM-16 VLF, resistivity, overburden drilling, and geochemical soil sampling took place in the late 1970s leading to the discovery of two smaller deposits that subcrop (later named CZ and EZ), located approximately 600 m and 1200 m to the east-northeast of the KMZ (Griep et al., 1980). This early stage of exploration resulted in the drilling of over 25,000 m in 200 diamond drill holes that outlined two cigar-shaped bodies of the KMZ and

CZ zones, in addition to the discovery of more radiometric anomalies to the west and southwest of the KMZ at ~6 and 15 km respectively. In 1988, open pit mining was proposed for both the KMZ and CZ with minable reserves of 14,307 t U at 0.424% (Beak Consultants Limited, 1988).

Mineralogical, petrographic, and structural studies of the Kiggavik deposit were undertaken during the late 1980s and early 1990s (Fuchs et al., 1985; Weyer et al., 1987; Weyer, 1992). By 1985, regional programs were terminated and UGC began to concentrate on the KMZ. With the addition of venture partners Daewoo and PNC, airborne geophysics using the Dighem IV system soon discovered resistivity and ground gravity lows along the east-northeast trending Judge Sissons fault, which led to the discovery of two new buried deposits (Andrew Lake, Endgrid) located 15–17 km southwest of Kiggavik (Reilly, 1997).

In 1993, COGEMA Incorporated (COGEMA) became the operator of the project by acquiring 69% of Urangesellschaft. Detailed petrographic studies were completed on the host rocks, alteration, and mineralization mineralogy of the Kiggavik deposit (Pacquet, 1993; Reyx, 1994). No further exploration took place and little work was done on the Kiggavik deposit until late 1997 when J.H. Reedman and Associated Limited conducted a pre-feasibility study on behalf of COGEMA (Morrison, 2009).

From 1997 to 2006, partial rehabilitation and field inspection/assessment work was conducted, resulting in many of the original Kiggavik camp buildings being destroyed in addition to the radioactive core being relocated. Cleanup of the exploration camp continued until work began in mid-2006 to prepare for future feasibility studies on the Kiggavik, End Grid, and Andrew Lake deposits (Morrison, 2009). During the 2008 summer drilling program, COGEMA changed its name to AREVA Resources Canada and expanded exploration outside of the main deposits to determine prospective areas (Morrison, 2009). This program saw 19 diamond drillholes sunk, primarily for geotechnical and/or metallurgical purposes, at Kiggavik, Andrew Lake, and End Grid, in addition to 10 drillholes to evaluate prospects at Bong and Granite Grid (D. Quirt, pers. comm., 2012) (Fig. 3).

Surficial geology

The Kiggavik deposit is located within the area of the Keewatin Ice Divide of the Laurentide Ice Sheet (Aylsworth and Shilts, 1989; McMartin and Henderson, 2004). Located in the central part of the Keewatin Sector of the Laurentide Ice Sheet, this area was constantly ice-covered from the beginning of the Wisconsin (Dyke et al., 2002) through the Late Wisconsin Maximum (18–13 ^{14}C ka BP) with complete deglaciation only between 7.2 and 6.0 ^{14}C ka BP (Dyke, 2004).

Surficial features in the Keewatin region (e.g. eskers, ribbed moraines, streamlined landforms) form a distribution pattern that is roughly concentric about the Keewatin Ice Divide (Aylsworth and Shilts, 1989). Surficial geology near Kiggavik is dominated by low hummocky moraine and featureless plains that are, in part, a discontinuous veneer of till over bedrock. There is an absence of eskers and ribbed moraines around the Kiggavik deposit and in the Schultz Lake area (Aylsworth and Shilts, 1989).

The Schultz Lake map area is described as a well developed glacial landscape with numerous drumlins, striations, and chatter marks of older subglacial erosion on bedrock, which suggests wet-based, erosive conditions during the last glaciation (McMartin et al., 2006). The land surface surrounding the Kiggavik deposit is commonly streamlined in different directions (Aylsworth and Shilts, 1989). Thin till veneer (<2 m) occurs on bedrock highs and more resistant bedrock, whereas lower lying areas, and those occurring above metasedimentary and sedimentary rocks. are typically dominated by till blankets (2–25 m) and hummocky till (Fig. 4). Sections along the Thelon River (McMartin et al., 2006) and diamond drillholes sunk by Urangesellschaft in the 1980s (cf. Pacquet, 1993) indicate that till is the dominant surficial material.

During deglaciation, the retreating ice mass, centred approximately 60 km to the southeast of the Kiggavik deposit, prevented the natural drainage of the Thelon River. This inundated the region and deposited lake sediments in low-lying areas in the Thelon River Valley and Princess Mary Lake basin between 7 and 6 ^{14}C ka BP (Dyke, 2004; McMartin et al., 2006). Post-glacial marine and/or glaciolacustrine sediments occur solely in poorly drained, low-lying areas and glaciofluvial sediments are non-existent. Minor outwash sediments, consisting of a mixture of boulders, glaciofluvial and mixed sediments do occur immediately to the southeast and east of the Kiggavik deposit. Bedrock outcrops make up less than 10% of the land surface (Fig. 4) and are exposed solely in hills that are dominated by Proterozoic quartzite and Mesoarchean – Early Proterozoic granitoid rocks. These exposures, particularly the Proterozoic quartzite units to the north of the Kiggavik deposit, display faceted and striated surfaces indicative of multiple ice-flow trajectories.

Ice-flow indicators

Tyrrell (1897) was the first to measure striations in the Schultz Lake map area in 1893. Tyrrell (ibid.) documents several sets of striations that indicate opposite flows occurred between Schultz Lake and Baker Lake. Cunningham and Shilts (1977) mapped ice-flow direc-

a)

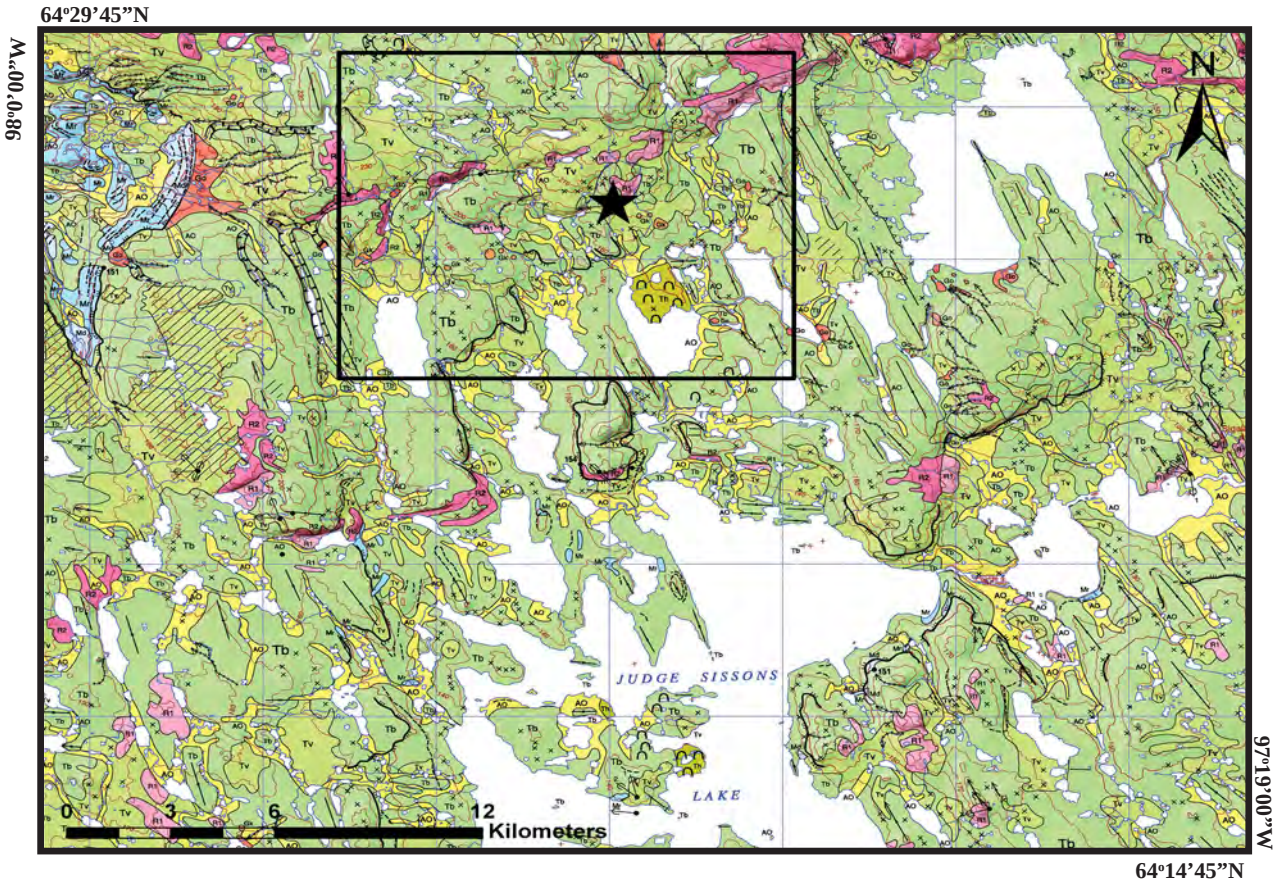
64°29'45"N
98°00'00"W
97°19'00"W
64°14'45"N
JUDGE SISSONS
LAKE
0 3 6 12
Kilometers
N

b)

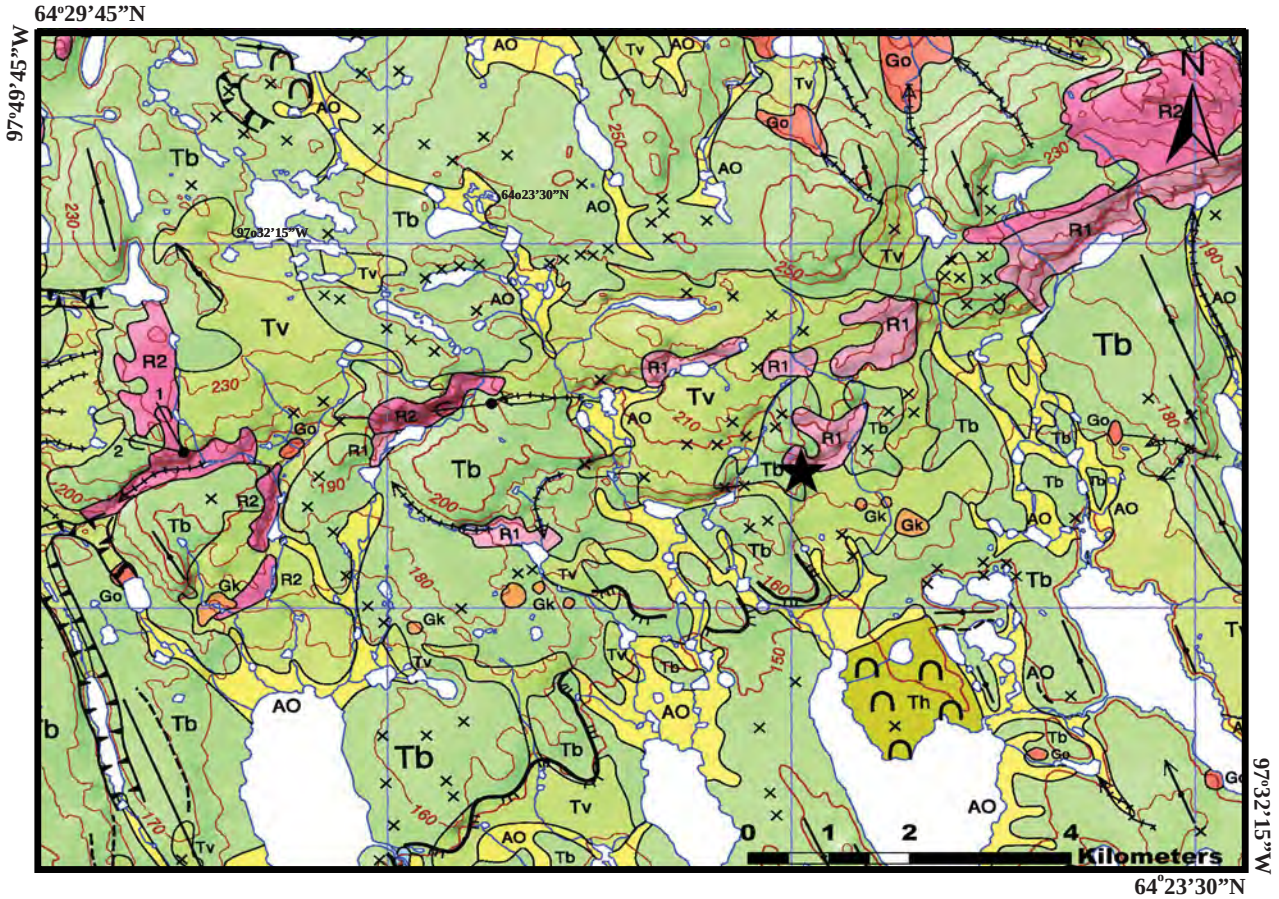
64°29'45"N
97°49'45"W
97°32'15"W
64°23'30"N
64o23'30"N
97o32'15"W
0 1 2 4
Kilometers
N

LEGEND

QUATERNARY GEOLOGY

POST-LAST GLACIATION

ALLUVIAL DEPOSITS: stream-deposited material within active drainage systems formed since the retreat of the post-glacial sea, proglacial lakes, or glacial ice; 1 m to several metres thick

A — **Alluvium:** sand, gravel, and cobbles; 1-10 m thick; deposited in channels and on floodplains, or as deltaic sediments where modern streams enter lakes.

AO — **Alluvium and marine or outwash sediments, undifferentiated:** sand or silt, minor gravel; 1-5 m thick; modern alluvium mixed with fine-grained sediments washed from till slopes by wave action or with glaciofluvial outwash sediments in stream valleys or abandoned channels above marine limit; occurs in topographic lows or on gently sloping surfaces; commonly covered by a thin organic mat; high water table and rare ice-wedge polygons.

MARINE DEPOSITS: materials deposited in the post-glacial Tyrell Sea from 6500 +500 BP to about 500 years ago; mainly derived from reworking of glacial deposits by wave and current action during marine regression; 1 m to several m.

Md — **Deltaic sediments:** sand, pebbly sand, gravel; 2–20 m thick; deposited by glacial or non-glacial draining into the sea.

Mr — **Littoral sediments:** generally well-sorted sand, gravel, cobbles, or boulders; 1–5 m thick; deposited as beaches, bars, spits, and shore ice-push ridges derived from the reworking of upland surficial deposits.

LAST GLACIATION

GLACIOFLUVIAL DEPOSIT: generally well sorted material deposited by meltwater streams behind, at, and in front of the ice margin; 2 m to several metres thick.

Gk — **Ice-contact sediments:** poorly stratified sand and gravel; 5–15 m thick; deposited in, over, or around ice or in subglacial ice tunnels; forming isolate kame terraces near marine limit.

Go — **Outwash sediments:** stratified sand and gravel; 2–15 m thick; deposited in a proglacial environment by subaerial meltwater streams in areas above local sea level as valley trains, terraces, and fans; surfaces locally terraced, hummock, and kettled; grading to deltaic sediments near marine limit.

GLACIAL DEPOSITS: poorly sorted sediments with distinctive forms deposited directly by glacial ice; 1 m to several metres thick; lithic composition generally reflects a local provenance and a net transport direction to the northwest, except in the southeast extremity of the map area where the youngest flow was to the southeast. Till located mainly southwest of the Thelon River has a reddish matrix and a significant Dubawnt Supergoup clast content; till composition northeast of the river generally reflects underlying bedrock types.

TM — **Till and marine sediments, undifferentiated:** till and glacial marine diamictons mixed with patches of marine offshore and sublittoral sediments; 1–5 m thick; forming till-cored landforms veneered by marine silt and silty sand, or marine deposits in depressions among till landforms; includes areas of till reworked from marine and current action; may occur anywhere below marine limit, but distribution is patchy from 60 m.a.s.l.

Tb — **Till blanket:** glacial diamicton; 2–25 m thick; deposited mainly in a subglacial environment; forming gently undulating till plains or streamlined landforms; includes areas of boulder lags as a result of wave-washing or meltwater erosion.

Tv — **Till veneer:** glacial diamicton; 1–2 m thick; discontinuous cover mimicking underlying bedrock topography; includes numerous small bedrock outcrops and boulder fields.

Tr — **Ribbed moraine:** generally bouldery till, in places sand and gravel; forming straight to sinuous ridges, less than 1 km long and 2–19 m high; ridges generally oriented at right angles to the direction of ice flow.

Th — **Hummocky till:** glacial diamicton, occurring as 5–20 m high rounded hummocks; surfaces lack a significant boulder cover.

PRE-QUATERNARY

BEDROCK: Archean to Paleoproterozoic supracrustal and intrusive igneous and metamorphic rocks; red volcanic rocks, and unmetamorphosed sediments; surface comprises more than 80% outcrop.

R1 — **Polydeformed and metamorphosed supracrustal and intrusive rocks:** Neoarchean metasedimentary and metavolcanics supracrustal rocks of the Woodburn Group, and late Archean granitoid complexes; Paleoproterozoic, clastic-dominated supracrustal rocks of the Ketyet River Group; minor Mesoarchean gneissic remnants of the basement of the Woodburn Group.

R2 — **Paleoproterozoic Dubawnt Supergroup rocks:** undeformed and unmetamorphosed red volcanic and sedimentary rocks; include distinctive quartz sandstone and conglomerate units of the Thelon Formation, and red volcanics rocks of the Pitz and Christopher Island formations.

Figure 4. a) Regional- and **b)** deposit-scale surficial geology of the Schultz Lake area and Kiggavik deposit (modified from Aylsworth and Shilts, 1989; McMartin et al., 2007).

tions based on striations and streamlined landforms in the region between Baker and Schultz lakes and postulated that the Keewatin Ice Divide migrated to the south and east during the latter stages of deglaciation. Shilts et al. (1979) re-evaluated the Keewatin sector of the Laurentide Ice Sheet, and returned to Tyrrell's (1898) original concept of an ice centre in central Keewatin. More recent work conducted by Aylsworth and Shilts (1989) and Aylsworth et al. (1990), based mainly airphoto interpretation of landforms, indicate that the area surrounding the Kiggavik deposit was dominated by a northwest glacial ice flow with minor evidence of ice that flowed to the west.

A regional till sampling and surficial mapping project of the Schultz Lake area undertaken by McMartin et al. (2006) observed that faceted and striated bedrock surfaces and palimpsest streamlined landforms record multiple ice flows. A total of six sets of ice-flow sequences were recorded by McMartin and Dredge (2005): southwest, south-southeast, southeast, north-northwest, northwest, and west (Fig. 5).

Previous surficial geochemistry studies

Although no detailed studies focusing on the surficial geochemistry of the Kiggavik deposit have been published, there are reports of regional surficial geochemistry surveys. The Kivalliq (Keewatin) sector of central Nunavut received much attention by the GSC in the 1970s (Shilts and Klassen, 1976; Klassen and Shilts, 1977a,b; Shilts and Cunningham, 1977; Dilabio, 1979). These studies carried out by the GSC focused on techniques to indicate U as well as base metal mineralization. Work conducted in the Kaminak Lake and Baker Lake areas (~300 km south-southeast and 80 km east of Kiggavik) by Klassen and Shilts (1977a) observed that U preferentially partitioned to the <0.002 mm (clay) fraction of till, with higher concentrations found in wet clay. It was discovered that 75% of till samples of Aphebian metasedimentary rocks near Kaminak Lake had low-background U contents, suggesting that U mineralization potential in such rocks is reciprocated by high U concentrations in till (Klassen and Shilts, 1977a). The Baker Lake study (Klassen and Shilts, 1977a) found that sites of known mineralization did not correspond to U content in till samples. Klassen and Shilts (1977a) concluded that dispersal tails and curves would be difficult to detect unless a small sampling grid was utilized. Elevated contents of U (>20 ppm U) reported to the northeast of Baker Lake (Klassen and Shilts, 1977b; Shilts and Cunningham, 1977) were determined to be associated with the underlying felsic volcanic rocks and not necessarily sites of mineralization. Such observations were also reported by McMartin et al. (2006), who illustrated that higher U contents are commonly associated with felsic granitoid

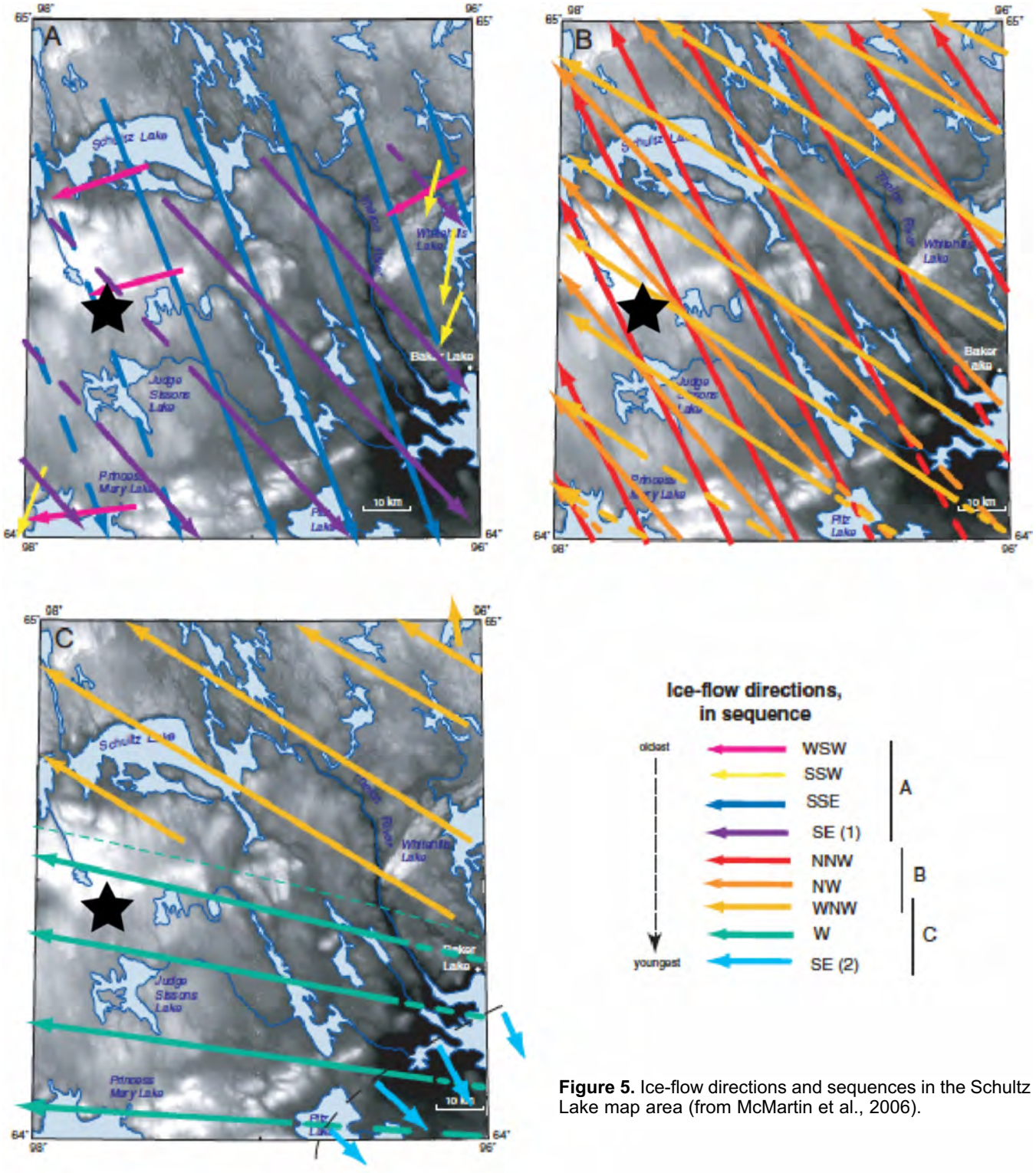

Figure 5. Ice-flow directions and sequences in the Schultz Lake map area (from McMartin et al., 2006).

rocks and Archean gneiss, and are not related to zones of mineralization.

A more focused study on drift prospecting around zones of U and base-metal mineralization south of Baker Lake found small dispersal trains of U originating from a site of pitchblende-bearing fracture fillings in gneiss (Dilabio, 1979). This dispersal train, defined by the <0.002 mm fraction, displayed U levels up to 280 ppm as well as high amounts of Mo and Pb (Dilabio, 1979). These findings had been missed by the earlier reconnaissance survey sampling (approximately 1.6 km spacing) of Klassen and Shilts (1977a).

In 2004, McMartin et al. (2006) carried out a regional till composition and provenance survey of the Shultz Lake map area (NTS Zone 66A), with Kiggavik in the mid-west section of the survey area. Sample

spacing was, on average, 10–15 km. Higher U contents in addition to equivalent U (eU) and equivalent Th (eTh) (concentrations determined indirectly from daughter products ^{214}Bi and ^{208}Tl and are assumed to be in equilibrium with their parents isotopes) occur in the northeast section of the map area (~75 km northeast of Kiggavik) and are associated with Archean gneiss, supracrustal rocks, and Proterozoic granitic bodies (McMartin et al., 2006). The most proximal sample to the Kiggavik deposit was collected 4 km to the west-northwest and displayed low to moderate metal contents with a U concentration of 2.6 ppm U (INAA: McMartin et al., 2006). Over the entire survey area, the U concentrations in till ranged from 0.25 to 6.9 ppm U, with an average of 2.54 ppm.

METHODS

Geologists from the GSC, AREVA, and Queen's University collected till and rock samples from hand-dug pits, outcrops, and diamond drill core at the Kiggavik deposit during the summer of 2010. Till samples were collected around the KMZ and drill core was sampled from holes previously drilled in both the KMZ and the CZ.

Ice-flow measurements

Assessment of glacial history within the study area included observation of the orientation of large-scale glacially streamlined landforms to small-scale erosional ice-flow indicators on bedrock such as glacial striae, grooves and outcrop sculpting. Landform mapping encompassed examination of large subglacial bedforms such as drumlins and flutings from aerial photographs. Evidence from the landforms was supplemented with other investigations, such as detailed striation mapping because the final flow phase indicated by glacial landforms may differ from dominant sediment transport paths (e.g. Stea et al., 2009).

Outcrop locations for striation measurements were selected based upon accessibility by foot or helicopter traverses and the potential for striae preservation (i.e. striations on fine-grained bedrock lithologies weather more slowly than coarse-grained granitic rocks). Striations were measured on relatively flat outcrop surfaces and care was taken not to bias data collection by preferentially measuring sites on stoss slopes of the last major ice flow. Relative ages of striated facets are determined (where possible) by evaluating their relative positions on an outcrop according to the criteria defined by Lundqvist (1990) and McMartin and Paulen (2009). A total of 24 outcrops were visited in a 320 km^2 region, proximal to the Kiggavik deposit, of which 21 sites had multiple striation azimuths with crosscutting relationships. Striation site locations and measurements are given in Appendix A1.

Field sampling

Based on the knowledge of ice-flow patterns throughout the area from previous work and observations made during this field program, a fan-shaped distribution of sample sites was designed, extending to the west and northwest of the Kiggavik deposit (Fig. 6) to test the most likely range of glacial transport directions down-ice from the Kiggavik deposit. Till samples were collected up-ice, overlying, and down-ice of the deposit by foot and helicopter traverses, from hand-dug holes (15–45 cm deep) in active and inactive frost boils. Frost boils were selected as a sample medium because the sampling area experiences continuous permafrost with an active layer in the summer. This causes freeze-thaw conditions where the diapiric nature of frost boils causes mixing of till and thus soil profiles on frost boils are poorly developed (Shilts, 1973, 1978; McMartin and McClenaghan, 2001; McMartin and Campbell, 2009).

A total of 71 till samples (3–5 kg) were collected in the Kiggavik area for till matrix geochemical analysis from seven fan-shaped transects 0.25, 0.5, 1, 2, 3, 5, and 10 km down-ice from the Kiggavik deposit to account for the dominant ice-flow directions (Fig. 6). Three sample sites were field duplicates collected to test for field variability; sample 10-PTA-113 is a field duplicate of 10-PTA-095, 10-PTA-119 is a duplicate of 10-PTA-118, and 10-PTA-133 is a duplicate of 10-PTA-128. During sampling, the surface of each frost boil was scraped clean of organic material, rocks, and other debris prior to collection. Till sample locations, field descriptions, and site photos are listed in Appendices A2 and A3.

Grain size, Munsell colour, and matrix carbon content

Grain-size distribution of the matrix of the till samples were determined in the GSC's Sedimentology Lab, Ottawa. The percentages of clay (<0.002 mm), silt (0.002–0.63 mm), and sand (0.063-2.0 mm) were determined by wet sieving in a stack of sieves for the >0.063 mm and using a Lecotrac LT-100 Particle Size Analyzer for the <0.063 mm. Total C, organic and inorganic C contents, and loss on ignition (LOI) were determined at the GSC using the LECO Cr 412 Carbon Determinator. Total %C and inorganic %C were determined for samples heated to 1350ºC and LOI was determined for samples heated to 500ºC for 1 hour. Munsell colour was determined on moist samples. Selected samples were analyzed using the CM 5015 Coulometer/Acid Evolution to determine percentages of calcite and dolomite; however, the samples contained less than the detection limit values for CO_2 and thus the data have not been reported. An unsieved 500 g split of each sample was air-dried and archived at the

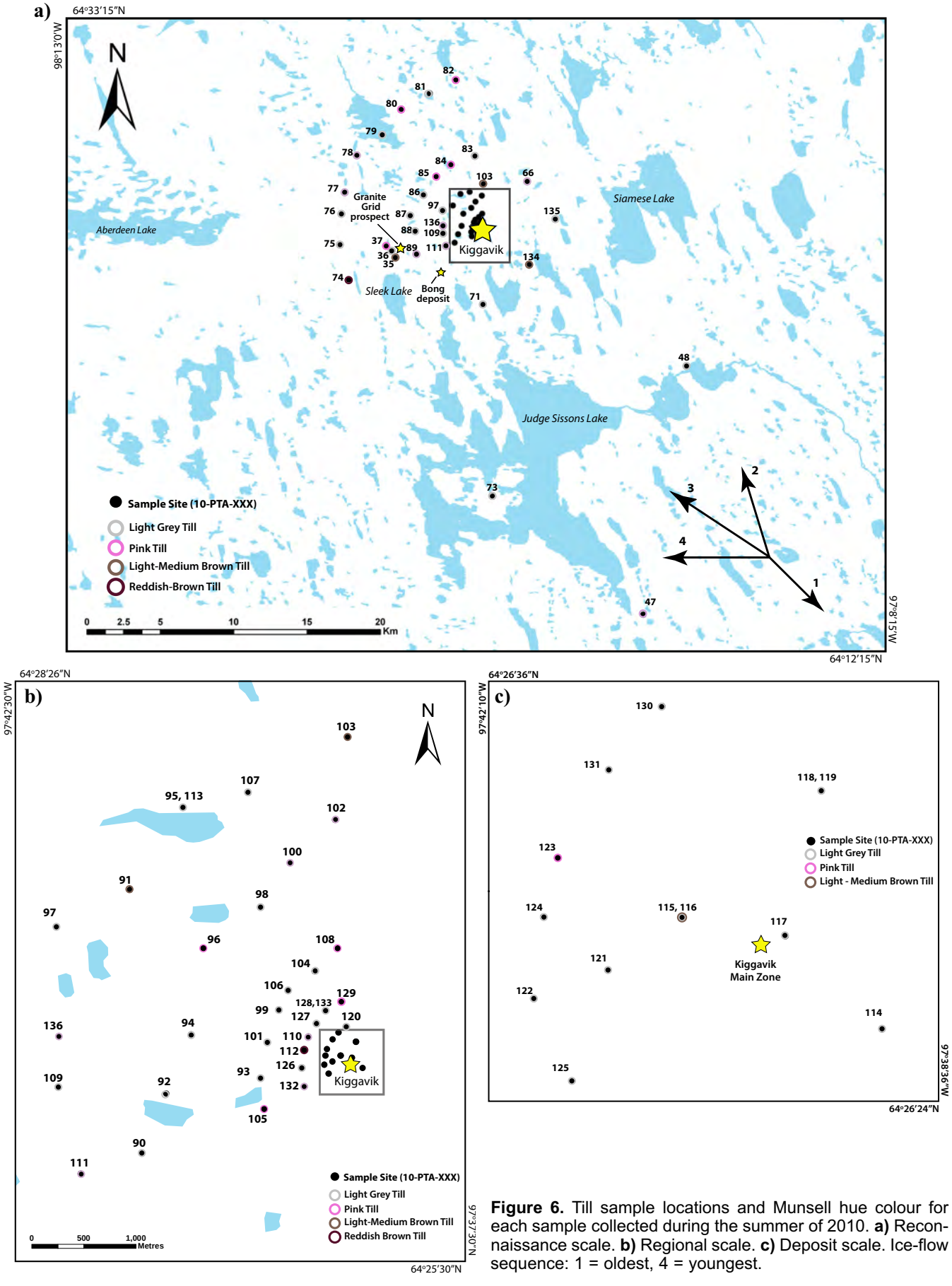

Figure 6. Till sample locations and Munsell hue colour for each sample collected during the summer of 2010. **a)** Reconnaissance scale. **b)** Regional scale. **c)** Deposit scale. Ice-flow sequence: 1 = oldest, 4 = youngest.

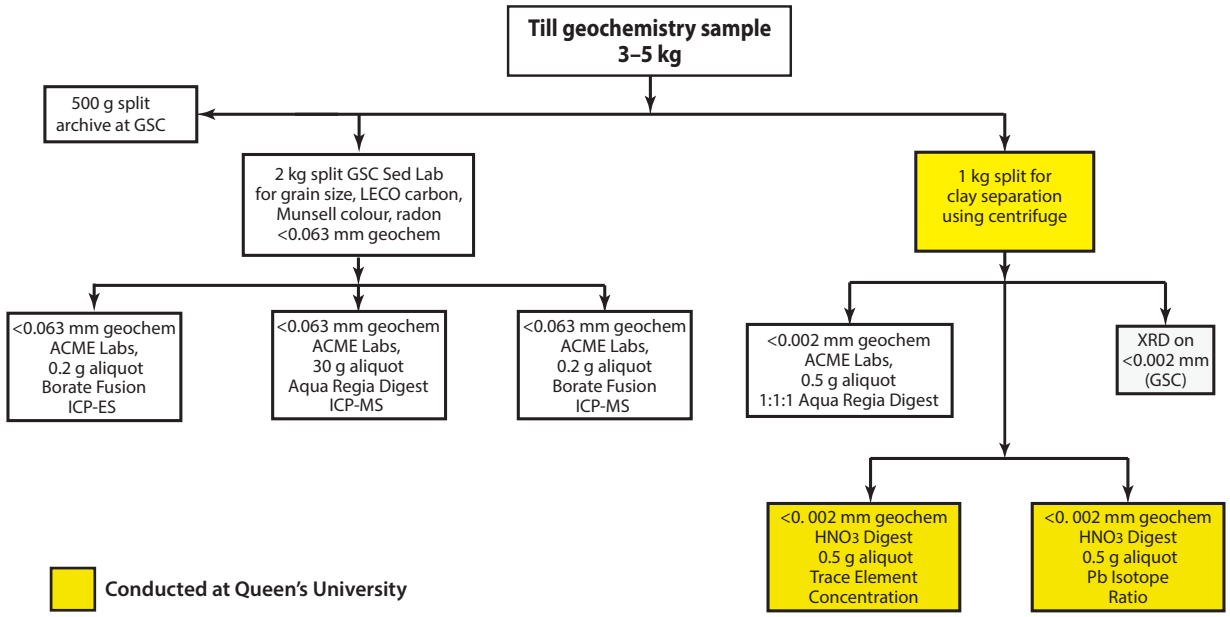

Figure 7. Flow chart of the various geochemical analyses undertaken for each sample (3–5 kg).

GSC, Ottawa. Analytical methods have been described in detail in the GSC Sedimentology Lab Manual (Girard et al., 2004). Sample data are listed in Appendix B.

Geochemical analysis

Till samples (3–5 kg) were split and air-dried to provide a 500 g archive at the GSC and a 2 kg split for grain size, LECO carbon, and Munsell colour determinations (Girard et al. 2004), gamma-ray spectrometry analysis (cf. Dredge et al., 2005; Ford et al., 2008), and the preparation of the <0.063 mm (silt and clay) fraction at the GSC Sedimentology Laboratory for contract geochemical analysis. An additional 1 kg was split for clay separation at Queen's University using centrifugal methods to recover the <0.002 mm (clay) fraction for contract geochemical analysis and in-house Pb ratio and trace element geochemistry (Fig. 7).

Silt and clay (<0.063 mm)

Samples were sent to Acme Analytical Laboratories (ACME) in Vancouver for geochemical analysis. Total abundances of major oxides and several minor elements were reported for a 0.2 g aliquot analyzed by inductively coupled-plasma emission spectrometry (ICP-ES) following a lithium metaborate / tetraborate fusion (borate) and dilute nitric digestion (nitric; Acme Group 4A method). Rare earth and refractory elements were determined by Inductively Couples Plasma-Mass Spectrometry (ICP-MS) following a borate and nitric digestion of a 0.2 g aliquot (ACME Group 4B method). All samples were also analyzed at ACME using ICP-MS after an ultratrace aqua regia digestion (aqua regia) (ACME Group 1F method) of 30 g of material for a full suite of 53 elements. All analytical results of the silt and clay fraction are listed in Appendix C.

Clay (<0.002 mm)

The separated clay-sized material was analyzed at ACME using ICP-MS following an aqua regia digestion (0.5 g aliquot) for a full suite of 53 elements (ACME Group 1F method) (Appendix D1).

Pb isotope analysis and HNO_3 weak acid digestion

Pb isotope analyses were conducted on 0.5 g clay separates (<0.002 mm fraction) of 65 till samples. Five grams of 2% HNO_3 was added to a polyurethane tube that contained the clay separate. Tubes were covered and placed in an ultrasonic bath for 2 hours, then centrifuged for 10 minutes at 3500 rpm. Following centrifuging, 1 ml (1 g) of the supernatant fluid was removed from each tube and placed in 60 ml Nalgene bottle using a calibrated pipette. The volume was then increased to 50 ml (50 g) with 2% HNO_3 spiked with 1 ppb 115In. As this time, the supernatant fluid removed and the weight of the removed fluid and the final weight of the diluted supernatant fluid were recorded. Lead isotopic ratios and trace element contents were measured using Finnigan MAT element high-resolution ICP-MS; measurements of the material and fluids are listed in Appendix D2.

Quality assurance/quality control

Analyses of laboratory duplicate samples and analytical standards (CANMET certified reference materials TILL-4 and UTS-1) were used to monitor the analytical accuracy and precision of geochemical results according to the procedures established by the GSC

Table 2. Analytical precision of laboratory duplicates for the <0.063 mm and <0.002 mm fractions. Precision is represented as relative standard deviation %. Good Reproducibility = <+5%; Moderate Reproducibility = +5% to +10%; Fair Reproducibility = +10% to +25%; Poor Reproducibility = >+25%.

	<0.063 mm Fraction			
	Good Reproducibility	**Moderate Reproducibility**	**Fair Reproducibility**	**Poor Reproducibility**
Aqua Regia (ICP-MS)	Al, As, Ba, Bi, Ce, Fe, Ga, K, La, Mg, Nb, P, Sc, Sr, Th, Ti, V, Y	Ag, Ca, Co, Cr, Cs, Hf, Li, Mn, Rb, U, W, Zn	Au, Be, Cd, Na, Ni, Sn	Ge, Hg, Re, Pd, Pt
Borate Fusion (ICP-MS)	Dy, Sr, Tb, Co, Rb, Pr, Yb, Sm, Cs, La, Nb, Lu, Ga, Ce, Ba, Y, Gd, Er, Tm, Eu, V, Nd, Hf, Zr, Th	Zr, Th, Be	Sb, Nb, In, Au, Te, Hg	Pt, Pd, Se, Re

	<0.002 mm Fraction			
	Good Reproducibility	**Moderate Reproducibility**	**Fair Reproducibility**	**Poor Reproducibility**
Aqua Regia (ICP-MS)	V, W, Ba, Fe, Rb, Mg, Ga, Sc, Cs, As, Bi, Na, Y, Mn, P, Zn, Ni, Sr, K, Al, Cr, La, Ce, Tl, Li, Ag, U, Co, Ti, Ca, Hf, Sn	Zr, Th, Be	Sb, Nb, In, Au, Te, Hg	Pt, Pd, Se, Re
Weak Acid Leach (ICP-MS)	Na, Ce, Sr, La, Cu, Zn, Fe, Mn, Y, Mg, Pr, Be, Ca, Nd, V, Co, Pb, Al, Th, K, Ba, Si, P, U, B	Li, Ti, Sm, Ga, Eu, Gd, Ho, Sc, Tb, Dy, Er, Tl, Cr, Rb, Bi	Ni, Tm, Yb, Zr, Lu, Ge, As, Hg, Mo, Sn, Se, Cs, Nb, Cd, W, S, Pd, Sb	Au, Pt

Sedimentology Laboratory (Girard et al., 2004). The analytical precision of laboratory duplicates was calculated using relative standard deviation and is presented as a percentage. Table 2 summarizes element analytical precision for both the <0.063 mm and <0.002 mm fraction, and more detailed reports are listed in Appendix C.

During laboratory analysis at Queen's University, 16 standards were inserted for quality control purposes. The relative standard deviation (RSD) for these control standards has very good reproducibility (+5%) for $^{207}Pb/^{206}Pb$, $^{208}Pb/^{206}Pb$, $^{206}Pb/^{204}Pb$, $^{207}Pb/^{204}Pb$, and $^{208}Pb/^{204}Pb$. Furthermore, quality assurance/quality control (QA/QC) for the <0.002mm fraction of 65 till samples after a HNO_3 digestion displays an average RSD value of +2.3% for $^{207}Pb/^{206}Pb$, +2.9% for $^{208}Pb/^{206}Pb$, +2.2% for $^{206}Pb/^{204}Pb$, +2.2% for $^{207}Pb/^{204}Pb$, and +2.6% for $^{208}Pb/^{204}Pb$ (Appendix E1).

Clay mineralogy (X-ray diffraction)

Semi-quantitative X-ray Diffraction (XRD) was completed at the GSC on 15 samples to observe fluctuations in clay mineralogy with distance from the deposit. Mineralogy of bulk materials was determined by XRD using the clay separates from the original till samples. Samples were suspended in water and later pipetted onto glass slides to be air-dried. X-ray patterns of the press-powder and air-dried samples were recorded on a Bruker D8 Advance Powder Diffractometer equipped with a graphite monochromator, Co Kα radiation set at 40 kV and 40 mA. The samples were exposed to X-rays following saturation with ethylene glycol and heat treatment (550ºC). Mineral identification was made using EVA software (Bruker AXS Inc.) with comparison to reference powder-diffraction mineral patterns from the International Centre for Diffraction Data and other available databases. Quantitative analysis was carried out using TOPAS software (Bruker AXS Inc.), which is a program that performs Rietveld refinement of XRD spectra. Detailed description of the methods and the data for standards are included in Appendix F.

Laboratory gamma-ray spectrometry analyses

A total of 71 samples were analyzed for K, eU, and eTh by laboratory gamma-ray spectrometry (LGRS) at the GSC. Following a sample split, larger pebbles (>1 cm) were picked by hand or removed with a 5.6 mm (#4) sieve. The till was then placed in a 230 g seamless tin that was lined with plastic wrap to avoid any possible metal contamination prior to LGRS analysis. Equivalent U and eTh contents measured by LGRS are based on measurements of the gamma-ray activity originating from daughter products of their respective decay series (^{214}Bi for U and ^{208}Tl for Th), which assumes the

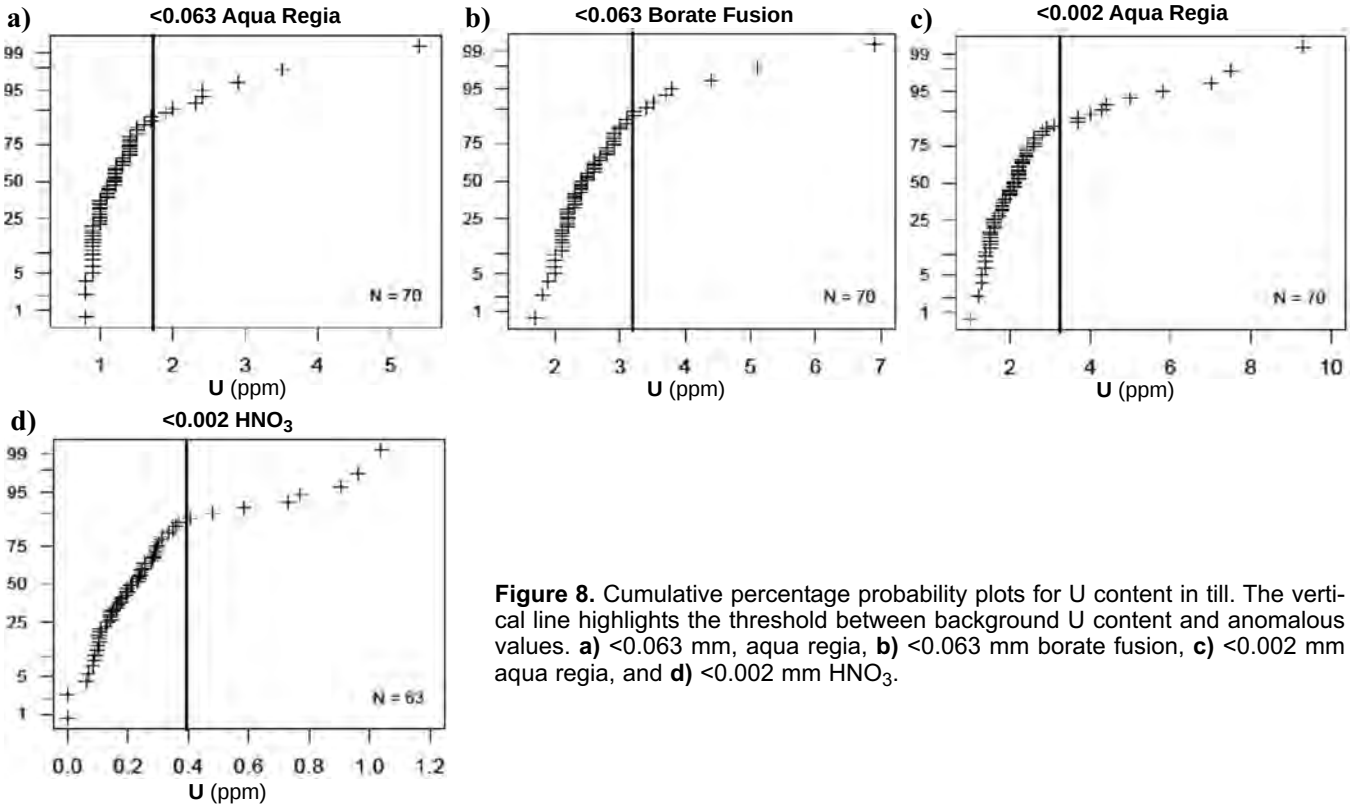

Figure 8. Cumulative percentage probability plots for U content in till. The vertical line highlights the threshold between background U content and anomalous values. **a)** <0.063 mm, aqua regia, **b)** <0.063 mm borate fusion, **c)** <0.002 mm aqua regia, and **d)** <0.002 mm HNO_3.

measured isotope and parent are in equilibrium. Potassium concentrations were determined directly from 40K (Friske et al., 2012). Quality control for LGRS was monitored using three control reference materials recognized by the International Atomic Energy Agency. Repeat analysis was performed on randomly selected samples at a rate of 1 per 10 samples (Friske et al., 2010).

Pebble lithology analysis

Pebbles (>5.6 mm) from 21 samples were visually examined using a hand lens and binocular microscope after a cone and quarter split. The total number of clasts identified in each sample varied from 300 to 588; the results are reported as a count % and weight % (Appendix H.1). Pebble lithology was divided into 10 categories: 1) granitoid gneiss, consisting of foliated to schistose Archean rocks with strong metamorphic fabric; 2) intrusive rocks, which includes felsic to intermediate granitoid and mafic compositions; 3) metasedimentary and metavolcanic rocks; 4) Thelon sandstone, consisting of Paleoproterozoic quartz arenite, siltstone, and other fluvial sandstone derived from the Thelon Basin; 5) Paleoproterozoic quartzite (Woodburn Group quartzite units); 6) quartz vein, consisting of pure quartz clasts that are not quartzite; 7) Pitz volcanic rocks, including undifferentiated Dubawnt Supergroup volcanic units; 8) Pitz volcanic rocks and clasts with quartz veining; 9) iron formation; and 10) other. Images of the classified pebbles and proportional dot maps for each lithological group are provided in Appendix H.

Statistics

All geochemical values reported as less than the lower detection limit were assigned values of one half of the lower detection limit for calculating statistics and the production of charts and graphs. Several statistical methods were used to establish elemental relationships with U as well as any elemental concentration variability throughout the sample set. Correlations coefficients (Pearson, r) and related significance values were calculated for the 71 till simples. Correlation coefficients were also calculated for 70 of the 71 the samples. Sample 10-PTA-117 was excluded because it was collected immediately above the deposit and was found to contain exceptionally high concentrations of ore elements that would skew the data set. A combination of Tukey box plots, median+2 median absolute deviations, empirical cumulative distribution function, and cumulative percentage probability plots (Fig. 8) were used to determine and compare the background, elevated, and anomalous contents of various elements. Statistical plots of elements of interest are shown in Appendix I.

Data plotting

Data for all samples have been plotted on maps at two scales: local (1:8,500) and regional (1:85,000). These maps were created using several types of data: 1) aqua

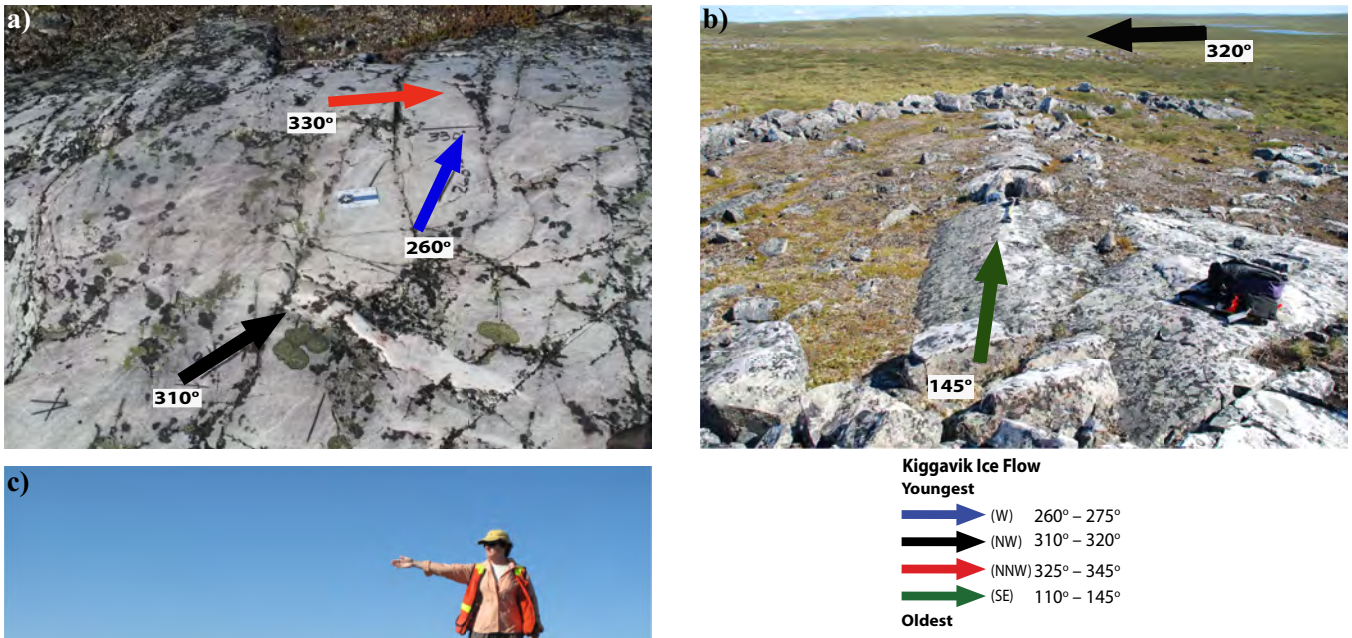

Figure 9. a) Glacially polished quartzite outcrop 2.5 km northeast of the Kiggavik deposit. This strongly striated surface displayed evidence of three directions of ice flow. **b)** Two sets of ice-flow indicators on a quartzite outcrop 2 km northeast of the Kiggavik deposit. This location preserved rare evidence for an older southeastward flow. **c)** Sculpted metavolcanic outcrop along the shore of Judge Sissons Lake, south of the Kiggavik deposit displaying two sets of ice-flow indicators. The older northwest flow indicators occur as glacial grooves and striae in the lee of the more recent west ice-flow features.

regia for the <0.063 mm fraction, 2) aqua regia for the <0.002 mm fraction, 3) weak acid leach for the <0.002 mm fraction, and 4) Pb/Pb ratios after weak acid leach for the <0.002 mm fraction. Elemental content maps were plotted using the 50th, 75th, 90th, 95th, and 98th percentiles for 70 of the 71 till samples (Appendices J and K). Samples that fell within the 90th percentile or higher were plotted in red to highlight that their values are above the upper threshold and thus are considered anomalous. As sample 10-PTA-117 was collected directly above the KMZ, its elemental contents plot as extreme outliers. For this reason, sample 10-PTA-117 was omitted to avoid skewing the data set.

RESULTS

Ice-flow history

Previously published ice-flow history interpretations of the area at and around the KMZ were re-examined (Aylsworth and Shilts, 1989; Stokes and Clark, 2003; McMartin and Henderson, 2004; McMartin et al., 2006). McMartin et al. (2006) reported four sequences of distinctly different flows, which can be summarized as follows (oldest to youngest):

1. Earliest preserved ice-flow indicators in the Schultz Lake area are subtle with poorly preserved striations trending 227–260º.
2. Well preserved striations oriented south-southeast at 159–178º. At this point the ice shifted southeasterly, as indicated by striations trending 122–152º. The preservation of southeasterly trending crag-and-tail landforms east and southeast of Schultz Lake, in addition to the lack of landforms associated with south-southeast flow, suggests that the southeast flow postdated the south-southeast flow.
3. A major flow reversal occurred in the entire Schultz Lake map area producing striations trending 336–348º. Crosscutting striations document that the north-northwest ice flow then shifted to the northwest (316–334º) and then to the west-northwest (284–315º).
4. The latest ice-flow produced striations trending 268–283º, and westerly trending short drumlinoid features. This westerly flow in the Schultz Lake area is attributed to the major late-glacial Dubawnt Lake ice stream (Stokes and Clark, 2003).

Four phases of ice-flow trajectories were recorded around the Kiggavik deposit as well as a few distal observations (Fig. 9). The oldest ice-flow was oriented east-southeast (~110º) and was only observed at a few quartzite outcrops. The second oldest ice-flow trajectory was north-northwest (~340º) and was probably short-lived. This was followed by the most prevalent

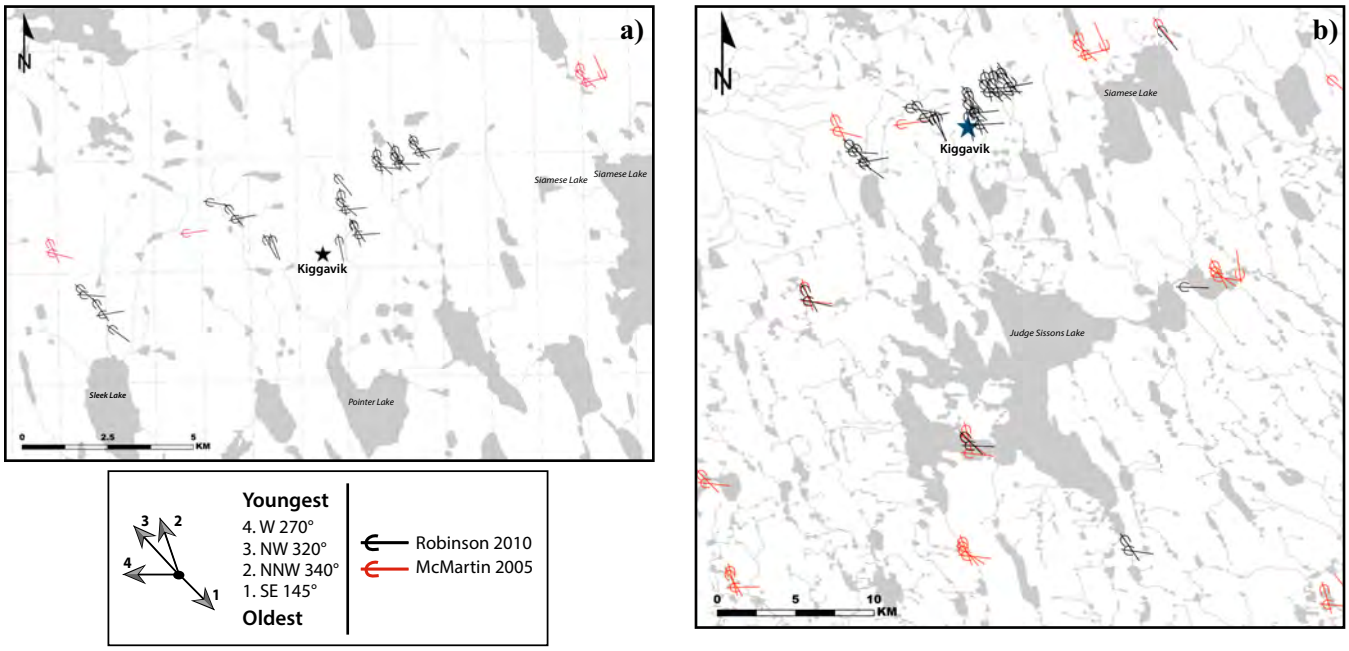

Figure 10. Ice-flow measurements collected in 2005 (McMartin et al., 2006) and 2010 (this study) at **(a)** deposit-scale (1:50,000) and **(b)** regional-scale (1:150,000).

ice-flow, which is represented by the majority of the large streamlined landforms oriented at ~320º and is believed to be related to the Last Glacial Maximum. A fourth, and youngest recorded ice-flow is commonly observed on outcrops and smaller streamlined landforms built on the larger landforms. In many places this is the dominant bedrock-sculpting ice-flow. This youngest flow is oriented west (~270º) (Fig. 10) and is most likely related to the Dubawnt Ice Stream event (Stoke and Clark, 2003), which was also noted by McMartin et al. (2006). Palimpsest landforms were observed around the east end of Schultz Lake, where west-northwest-trending drumlins are found superimposed on long northwest-trending till landforms.

In summary, ice-flow observations around the Kiggavik deposit were similar to the four sequences of ice-flow documented by McMartin et al. (2006). The preserved record of divergent flows, the paleoland surfaces observed in the Schultz Lake regional work, and the work conducted around Kiggavik are indicative of a transitory ice divide as described by Aylsworth and Shilts (1989), McMartin and Henderson (2004), McMartin et al. (2006).

Grain size, Munsell colour, and matrix carbon

The till at the Kiggavik deposit is composed of a silty sand matrix, containing on average 57% sand, 40% silt, and 2.5% clay (Fig. 11). The till matrix colour is variable: some samples are light grey (Munsell hue 10YR); several samples are reddish brown to pinkish grey (Munsell hue 5–7.5YR); and several are brown (Munsell hue 10YR) (Figs. 6, 12). Overall, the till matrix for all 71 samples has an average of 0.4% total

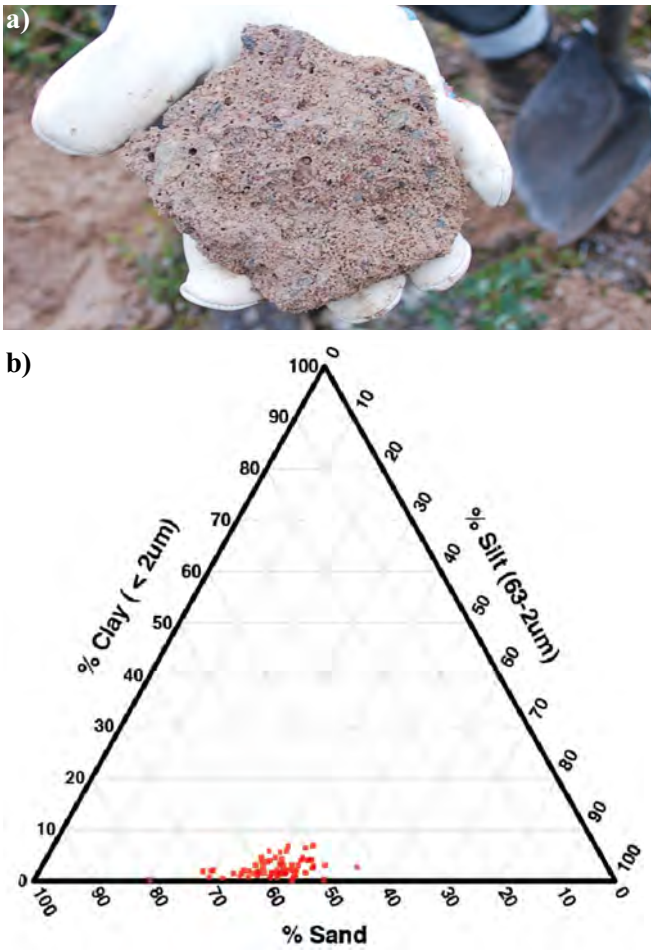

Figure 11. a) An example of till from a frost boil displaying the dominant silty sand texture that was observed in this study. **b)** Ternary diagram illustrating the average textural composition of till samples from the study area.

Figure 12. Munsell colour variability of the till matrix: **a)** light medium brown (7.5YR 6/3), **b)** light grey (10YR 7/2), **c)** light reddish brown (5YR 6/3), and **d)** pink-grey (7.5YR 7/2).

C with an error of + 0.1% and less than detection limit values (<0.1%) of inorganic C. Loss on ignition values are relatively low, varying from 0 to 3.2% (Appendix B).

Till matrix geochemistry (<0.063 mm fraction)

Geochemical data for the <0.063 mm fraction of 71 till samples are listed in Appendix C. Proportional dot maps have been created for selected elements determined by aqua regia/ICP-MS on 30 g aliquot: U, Au, Ag, Bi, Co, Cs, Cu, Mo, Ni, Pb, Ti, and W at a regional, deposit, and reconnaissance scale (Appendix J). Proportional dot maps have also been plotted for the <0.002 mm fraction for selected elements (U, Au, Ag, Bi, Co, Cs, Cu, Mo, Ni, Pb, Ti, W) determined by aqua regia/ICP-MS and weak acid leach (U) on 0.5 g aliquots (Appendix D). Correlation matrices for the elements determined by aqua regia/ICP-MS on both the <0.063 and <0.002 mm fractions are displayed in Tables 3 and 5, respectively. Strong positive correlations are those with R values >0.8, significant correlations include R values between 0.6 and 0.8, and moderate correlations include R values between 0.4 and 0.6. Samples stated to be anomalous are fall within the >90th percentile; elevated samples fall between the 75th and 90th percentile.

Sample 10-PTA-117

Sample 10-PTA-117 (Fig. 6c) was taken proximal (~5 m) to the KMZ and was not included in the statistical analysis or data plotting, as many of the elements, particularly those of interest, are an order of magnitude higher when analyzed by ICP-MS after an aqua regia digestion (Table 3). This sample is particularly enriched in U, Au, Te, and Pt (>10 times the mean concentration of 71 samples) and has moderately elevated (>2 times the mean concentration of 71 samples) in Mo, Ag, Bi, V, B, K, Hg, Se, Cs, Rb, Be, Li, and Pd (Table 4). This sample also had anomalously low Ba (<50% of the mean concentration of 71 samples). The U content in the <0.063 mm fraction after a borate fusion digestion shows similar results to that of the aqua regia digestion. Uranium exhibits a 20 times greater concentration in sample 10-PTA-117 than the average U concentration for the entire sample suite.

Uranium

Aqua regia ICP-MS (30 g aliquot)

Till samples (excluding sample 10-PTA-117) contain between 0.8 and 5.4 ppm U with a median value of 1.2 ppm U. Anomalous samples (≥90th percentile) range

Table 3. Correlation matrix for selected elements in the <0.063 mm fraction.

	Mo	Cu	Pb	Zn	Ag	Ni	Co	Mn	Fe	Al	U	Au	Th	Sr	Cd	Sb	Bi	V	Ca	P	La	C	Mg	Ba	Ti	B	Al	Na	K	W	Sc	S	Hg	Se	Te	Ga	Cs	Ge	Hf	Nb	Rb	Sn	Zr	Y	Li	Pd	Pd
Mo	1																																															
Cu	0.63	1																																														
Pb	0.22	0.23	1																																													
Zn	0.31	0.72	0.19	1																																												
Ag	0.43	0.75	0.32	0.85	1																																										
Ni	0.24	0.56	0.02	0.82	0.62	1																																									
Co	0.50	0.71	0.16	0.84	0.69	0.91	1																																									
Mn	0.22	0.50	0.24	0.76	0.61	0.80	0.85	1																																								
Fe	0.38	0.67	0.20	0.83	0.63	0.89	0.91	0.85	1																																							
Al	0.06	0.35	0.20	0.53	0.42	0.63	0.57	0.68	0.63	1																																						
U	0.65	0.59	0.24	0.35	0.43	0.27	0.45	0.19	0.39	-0.03	1																																					
Au	0.09	0.04	0.10	0.03	0.18	-0.07	0.04	0.10	0.04	0.01	0.10	1																																				
Th	-0.04	0.14	0.32	0.31	0.35	0.22	0.18	0.25	0.26	0.08	0.21	-0.05	1																																			
S	0.03	-0.03	0.69	0.01	0.06	-0.09	-0.05	0.11	0.11	0.02	0.14	0.00	0.59	1																																		
Cd	-0.03	0.19	0.22	0.32	0.39	0.10	0.20	0.35	0.16	0.16	-0.05	0.52	0.17	0.08	1																																	
Sb	-0.12	0.11	0.08	0.40	0.23	0.58	0.45	0.59	0.61	0.73	-0.03	0.10	0.33	0.21	0.17	1																																
Bi	0.92	0.68	0.28	0.42	0.60	0.27	0.53	0.29	0.42	0.12	0.59	0.21	0.01	0.04	0.17	-0.11	1																															
V	0.37	0.58	0.24	0.81	0.60	0.89	0.90	0.82	0.96	0.59	0.41	0.01	0.29	0.19	0.11	0.59	0.4	1																														
Ca	0.23	0.32	0.44	0.44	0.43	0.29	0.37	0.50	0.49	0.21	0.17	0.08	0.59	0.66	0.27	0.37	0.25	0.51	1																													
P	0.09	-0.03	0.45	-0.02	0.06	-0.22	-0.11	0.05	0.03	-0.12	0.01	0.13	0.40	0.73	0.22	0.07	0.11	0.07	0.77	1																												
La	0.16	0.16	0.68	0.19	0.25	0.04	0.12	0.20	0.28	0.04	0.39	0.12	0.67	0.89	0.12	0.25	0.17	0.34	0.69	0.71	1																											
C	0.16	0.46	0.01	0.75	0.51	0.98	0.84	0.75	0.87	0.65	0.20	-0.12	0.20	-0.06	0.02	0.64	0.19	0.88	0.24	-0.23	0.04	1																										
Mg	0.31	0.59	0.06	0.90	0.68	0.95	0.92	0.80	0.88	0.55	0.34	-0.07	0.26	-0.06	0.11	0.49	0.35	0.91	0.36	-0.17	0.09	0.91	1																									
Ba	-0.02	0.08	0.65	0.27	0.25	0.26	0.21	0.38	0.37	0.33	0.09	0.03	0.54	0.86	0.16	0.47	0.03	0.45	0.65	0.53	0.78	0.30	0.26	1																								
Ti	0.62	0.48	0.55	0.37	0.43	0.08	0.32	0.23	0.35	0.06	0.56	0.14	0.05	0.42	0.16	-0.07	0.62	0.39	0.51	0.51	0.56	0.04	0.20	0.32	1																							
B	-0.10	0.22	-0.02	0.52	0.36	0.63	0.48	0.57	0.56	0.42	0.06	-0.14	0.65	0.17	0.05	0.60	-0.09	0.56	0.38	-0.06	0.18	0.62	0.62	0.36	-0.25	1																						
Al	0.18	0.53	0.04	0.86	0.65	0.94	0.85	0.79	0.86	0.60	0.27	-0.10	0.36	-0.04	0.09	0.58	0.22	0.87	0.33	-0.22	0.08	0.91	0.95	0.28	0.05	0.78	1																					
Na	0.44	0.64	0.34	0.76	0.72	0.60	0.67	0.61	0.70	0.40	0.42	-0.05	0.46	0.29	0.25	0.31	0.50	0.70	0.61	0.25	0.42	0.53	0.67	0.41	0.54	0.49	0.67	1																				
K	0.13	0.50	0.12	0.79	0.68	0.75	0.67	0.70	0.72	0.52	0.20	-0.13	0.61	0.17	0.18	0.56	0.19	0.70	0.52	0.02	0.24	0.70	0.78	0.40	0.07	0.88	0.89	0.77	1																		
W	0.80	0.51	0.20	0.30	0.46	0.24	0.47	0.24	0.38	0.09	0.46	0.21	0.00	0.09	0.16	-0.04	0.87	0.40	0.28	0.20	0.20	0.17	0.30	0.07	0.61	-0.13	0.17	0.48	0.14	1																	
Sc	0.19	0.55	0.08	0.84	0.63	0.93	0.84	0.81	0.89	0.60	0.25	-0.09	0.37	0.05	0.10	0.60	0.22	0.91	0.48	-0.06	0.17	0.90	0.93	0.35	0.14	0.74	0.95	0.70	0.85	0.2	1																
Tl	0.43	0.65	0.30	0.87	0.81	0.71	0.77	0.68	0.79	0.52	0.50	0.09	0.43	0.19	0.26	0.44	0.52	0.78	0.47	0.04	0.35	0.65	0.80	0.39	0.43	0.57	0.81	0.85	0.82	0.44	0.76																
S	-0.06	-0.09	0.61	-0.11	-0.08	-0.12	-0.11	-0.03	-0.04	-0.06	0.07	-0.07	0.22	0.68	-0.04	-0.01	-0.06	0.03	0.27	0.40	0.58	-0.08	-0.15	0.60	0.25	-0.09	-0.16	0.02	-0.12	-0.09	-0.09	1															
Hg	-0.12	-0.13	0.01	-0.10	-0.13	-0.08	-0.07	0.03	-0.03	-0.03	-0.06	0.44	0.04	0.11	0.59	0.19	-0.04	-0.03	0.00	0.14	0.08	-0.09	-0.13	0.08	-0.06	0.01	-0.11	-0.10	-0.11	0.03	-0.12	-0.03	1														
Se	0.37	0.24	0.00	0.33	0.33	0.32	0.36	0.25	0.30	0.19	0.11	0.04	0.06	0.03	0.01	0.12	0.40	0.33	0.18	0.01	0.05	0.29	0.34	0.08	0.27	0.17	0.32	0.33	0.31	0.42	0.29	-0.08	-0.17	1												
Te	0.25	0.55	0.11	0.28	0.38	0.14	0.21	0.07	0.22	0.12	0.14	0.04	-0.01	-0.12	0.17	-0.01	0.36	0.12	-0.03	-0.11	0.01	0.11	0.13	-0.09	0.21	-0.14	0.07	0.13	0.04	0.30	0.07	-0.03	-0.13	0.21	1											
Ga	0.33	0.61	0.15	0.91	0.74	0.89	0.87	0.78	0.88	0.53	0.42	-0.03	0.40	0.08	0.13	0.52	0.38	0.90	0.42	-0.08	0.24	0.85	0.95	0.35	0.27	0.69	0.96	0.76	0.87	0.32	0.92	-0.10	-0.10	0.38	0.12	1										
Cs	0.34	0.61	0.25	0.86	0.75	0.81	0.81	0.75	0.84	0.57	0.45	0.00	0.47	0.19	0.15	0.56	0.39	0.85	0.47	-0.03	0.33	0.76	0.88	0.44	0.30	0.72	0.91	0.79	0.89	0.33	0.88	-0.07	-0.10	0.33	0.13	0.95	1									
Ge	0.31	0.16	0.44	-0.01	0.04	-0.06	0.09	0.00	0.08	-0.06	0.25	-0.04	0.15	0.51	0.04	-0.04	0.24	0.12	0.33	0.43	0.51	-0.07	-0.06	0.35	0.45	-0.16	-0.13	0.18	-0.09	0.21	-0.06	0.60	-0.01	0.13	0.08	-0.02	-0.02	1								
H	0.03	0.21	0.22	0.39	0.47	0.24	0.21	0.26	0.21	0.04	0.06	-0.11	0.78	0.34	0.19	0.15	0.08	0.23	0.56	0.36	0.40	0.17	0.28	0.32	0.07	0.57	0.38	0.53	0.65	0.05	0.41	0.09	-0.07	0.09	-0.05	0.40	0.43	0.07	1							
Nb	0.18	0.03	0.44	-0.18	-0.17	-0.23	-0.13	-0.20	-0.06	-0.10	0.37	0.09	-0.20	0.35	-0.18	-0.13	0.13	-0.02	-0.08	0.10	0.37	-0.17	-0.22	0.24	0.45	-0.43	-0.28	-0.16	-0.42	0.11	-0.26	0.39	0.03	-0.06	0.11	-0.18	-0.11	0.27	-0.44	1						
Rb	0.31	0.59	0.21	0.84	0.74	0.76	0.74	0.69	0.80	0.56	0.40	-0.06	0.51	0.19	0.11	0.53	0.37	0.79	0.45	-0.03	0.31	0.72	0.83	0.43	0.27	0.74	0.89	0.80	0.92	0.30	0.84	-0.09	-0.12	0.35	0.12	0.94	0.98	-0.04	0.48	-0.15	1					
Sn	0.17	0.20	0.37	0.37	0.31	0.30	0.37	0.47	0.56	0.29	0.33	0.21	0.51	0.64	0.14	0.53	0.17	0.59	0.70	0.56	0.75	0.31	0.37	0.65	0.48	0.39	0.37	0.51	0.44	0.27	0.45	0.19	0.15	0.18	-0.06	0.49	0.56	0.22	0.26	0.21	0.53	1				
Zr	0.08	0.30	0.34	0.50	0.55	0.36	0.34	0.43	0.37	0.21	0.10	-0.09	0.83	0.47	0.24	0.31	0.14	0.40	0.72	0.45	0.52	0.29	0.40	0.49	0.18	0.65	0.49	0.67	0.76	0.12	0.54	0.15	-0.08	0.17	-0.04	0.51	0.56	0.13	0.94	-0.39	0.60	0.42	1			
Y	0.21	0.43	0.46	0.61	0.60	0.44	0.50	0.57	0.63	0.32	0.37	0.15	0.63	0.57	0.25	0.46	0.26	0.65	0.83	0.61	0.77	0.41	0.50	0.63	0.54	0.43	0.48	0.72	0.59	0.27	0.61	0.25	-0.03	0.16	0.05	0.60	0.65	0.29	0.55	0.01	0.61	0.78	0.71	1		
Li	0.46	0.68	0.23	0.89	0.74	0.86	0.91	0.79	0.87	0.54	0.51	0.01	0.27	0.05	0.15	0.41	0.51	0.89	0.38	-0.10	0.22	0.80	0.93	0.31	0.38	0.57	0.90	0.77	0.77	0.43	0.86	-0.09	-0.07	0.37	0.11	0.95	0.92	0.01	0.28	-0.07	0.88	0.43	0.41	0.54	1	
Pd	-0.09	-0.03	-0.12	-0.01	-0.06	0.11	0.00	-0.04	0.00	0.05	-0.08	-0.02	-0.04	-0.07	-0.05	0.16	-0.12	-0.02	-0.02	-0.09	-0.15	0.12	0.03	0.01	-0.18	0.08	0.08	0.00	0.08	-0.12	0.08	-0.03	0.00	-0.09	-0.10	0.00	0.02	-0.08	0.03	-0.05	0.03	-0.06	0.02	-0.07	-0.04	1	
Pt	0.07	0.08	0.15	0.17	0.20	0.22	0.15	0.11	0.22	0.16	0.10	0.23	0.05	0.08	0.00	0.16	0.16	0.24	0.09	-0.04	0.10	0.25	0.19	0.17	0.15	0.12	0.23	0.14	0.17	0.08	0.21	0.08	-0.03	0.27	0.07	0.24	0.24	-0.05	0.01	0.19	0.25	0.19	0.06	0.13	0.21	0.19	1

Table 4. Element contents in the <0.002 mm fraction of sample 10-PTA-117 in comparison to the remainder of the samples.

<0.0063 mm Fraction by Aqua Regia ICP-MS									
Element	Sample Suite Average (n=71)	Sample 10-PTA-117	Difference	Ratio of Element Content in Sample 10-PTA-117 to Sample Suite Average	Element	Sample Suite Average (n=71)	Sample 10-PTA-117	Difference	Ratio of Element Content in Sample 10-PTA-117 to Sample Suite Average
Mo (ppm)	1.92	6.87	4.95	3.6:1	**Al** (%)	0.74	1.40	0.66	1.9:1
Cu (ppm)	17.74	31.31	13.57	1.8:1	**Na** (%)	0.00	0.01	0.00	1.8:1
Pb (ppm)	13.91	16.78	2.87	1.2:1	**K** (ppm)	0.11	0.39	0.28	3.6:1
Zn (ppm)	25.42	31.90	6.48	1.3:1	**W** (ppm)	1.04	2.60	1.56	2.5:1
Ag (ppb)	36.04	223.00	186.96	6.2:1	**Sc** (ppm)	2.18	3.30	1.12	1.5:1
Ni (ppm)	19.09	26.10	7.01	1.4:1	**Tl** (ppm)	0.07	0.37	0.30	5.4:1
Co (ppm)	6.83	9.80	2.97	1.4:1	**S** (ppm)	0.01	0.01	0.00	0.97:1
Mn (ppm)	215.30	212.00	3.30	0.98:1	**Hg** (ppm)	7.03	52.00	44.97	7.4:1
Fe (%)	1.88	2.21	0.33	1.2:1	**Se** (ppm)	0.17	0.50	0.33	2.9:1
As (ppm)	7.37	5.90	1.47	0.8:1	**Te** (ppm)	0.04	0.66	0.62	17.5:1
U (ppm)	2.16	59.40	57.24	27.5:1	**Ga** (ppm)	3.13	5.40	2.27	1.7:1
Au (ppb)	8.43	127.30	118.87	15.1:1	**Cs** (ppm)	1.00	2.26	1.26	2.3:1
Th (ppm)	9.37	10.30	0.93	1.1:1	**Ge** (ppm)	0.07	0.10	0.03	1.5:1
Sr (ppm)	87.08	72.60	14.48	0.83:1	**Hf** (ppm)	0.18	0.29	0.11	1.6:1
Cd (ppm)	0.05	0.04	0.01	0.88:1	**Nb** (ppm)	0.47	0.33	0.14	0.71:1
Sb (ppm)	0.19	0.14	0.05	0.75:1	**Rb** (ppm)	7.69	22.40	14.71	2.9:1
Bi (ppm)	0.63	4.16	3.53	6.6:1	**Sn** (ppm)	0.43	0.60	0.17	1.4:1
V (ppm)	26.07	80.00	53.93	3.1:1	**Zr** (ppm)	11.41	21.50	10.09	1.9:1
Ca (%)	0.31	0.35	0.04	1.1:1	**Y** (ppm)	8.02	14.33	6.31	1.8:1
P (%)	0.11	0.10	0.00	0.96:1	**Ce** (ppm)	72.21	68.90	3.31	0.9:1
La (ppm)	38.51	39.50	0.99	1.0:1	**In** (ppm)	0.01	0.01	0.00	0.7:1
Cr (ppm)	33.08	43.60	10.52	1.3:1	**Re** (ppm)	1.19	2.00	0.81	1.9:1
Mg (%)	0.41	0.62	0.21	1.5:1	**Be** (ppm)	0.54	1.30	0.76	2.4:1
Ba (ppm)	271.61	136.40	135.21	0.5:1	**Li** (ppm)	11.33	24.00	12.67	2.1:1
Ti (%)	0.04	0.05	0.01	1.2:1	**Pd** (ppb)	5.37	20.00	14.63	3.7:1
B (ppm)	6.06	42.00	35.94	6.9:1	**Pt** (ppb)	4.77	256.00	251.23	54.6:1

<0.063 mm Fraction by Borate Fusion ICP-MS				
Element	Sample Suite Average (n=71)	Sample 10-PTA-117	Difference	Ratio of Element Content in Sample 10-PTA-117 to Sample Suite Average
U (ppm)	3.65	73.60	69.95	20.2:1

Legend
>10
>2–10
<0.5

from 2 to 5.4 ppm U. The majority of anomalous samples occur <1 km from the KMZ, with the highest U content in samples 10-PTA-115 and 10-PTA-116 (field duplicates) collected ~75 m west of the KMZ (Appendix J1). Sample 10-PTA-034 (4 km southeast) is the only sample located >1 km from the KMZ that is to be considered have anomalously high U. Samples with elevated U contents (75–90th percentile) occur predominantly within 1 km of the Kiggavik deposit; however, they can also occur at distances of 3 and 10 km, respectively. (Appendix J2).

Though U does not exhibit any strong positive correlation with other elements, there is a significant correlation with Mo and a moderate correlation with several elements (Cu, Bi, Ti, Li, Tl, Co, Cs, W, Ag, Ga, V, Na, Rb and Fe: Table 3). Uranium displays negative correlations with elements Pd, In, Hg, Cd, Sb, and As.

Borate fusion ICP-MS (0.2 g aliquot)

Till samples contain between 1.7 and 6.9 ppm U with a median value of 2.4 ppm U. Anomalous samples (3.4–6.9 ppm U) occur <1 km west and northwest from the KMZ. Similar to aqua regia digestion results, samples 10-PTA-115 and 10-PTA-116 have the greatest U contents and samples containing elevated U (75–90th percentile) occur predominantly within a 1 km distance of the KMZ. Although U does not display any strong or significant correlations with other elements, moderate correlations with Be, W, and Eu were observed. Uranium exhibits negative correlations with Zr and Hf.

Sample 10-PTA-117 was collected almost directly above the deposit and is an extreme outlier (U contents are 60 ppm U (aqua regia) and 80 ppm U (borate)) and for this reason is excluded from statistical calculations. Seven samples are considered to be anomalous and

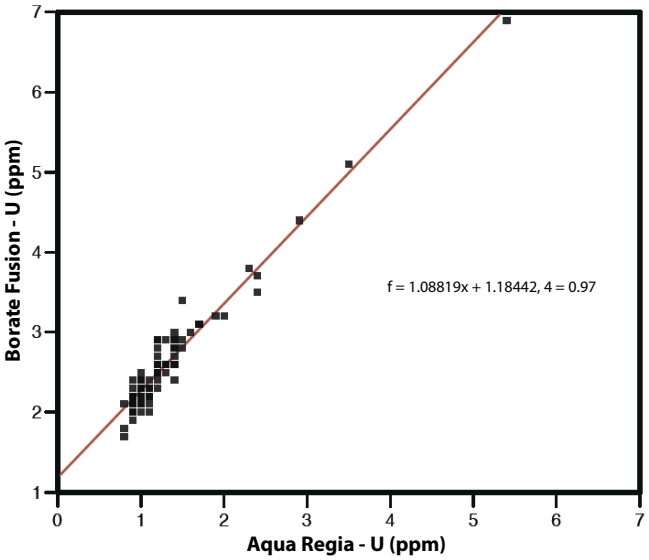

Figure 13. Comparison of the U content in the <0.063 mm fraction of the till matrix of each sample (n = 70) determined by aqua regia versus borate fusion digestion.

were all collected within 4 km of the KMZ; and six of the seven were collected less than 1 km from the deposit (Appendix H). The sample with the highest U concentration (sample 10-PTA-115) was collected ~75 m west of the KMZ (Appendix J1). Sample 10-PTA-116 (field duplicate taken from the same frost boil as sample 10-PTA-115) and sample 10-PTA-124 (collected 200 m west of the KMZ) also have anomalously high U contents (3.5 and 2.9 ppm U, respectively) and fall within the 95th percentile. Samples 10-PTA-106, -114, -128, and -134 have U contents in the 90th percentile (1.9–2.4 ppm U).

Uranium in the <0.063 mm fraction (aqua regia ICP-MS) does not exhibit a strong positive correlation with any element. It does, however, exhibit a significant correlation with Mo and a moderate correlation with a number of other elements (Cu, Bi, Ti, Li, Tl, Co, Cs, W, Ag, Ga, V, Na, Rb, and Fe (Table 3). When examining variability between different digestion methods, U contents determined by aqua regia ICP-MS (30 g) and borate fusion (0.2 g) present a very strong positive correlation (R=0.97: Fig 13). Although both digestion methods display a very good correlation, borate fusion results typically have higher U values. This can potentially be explained by the greater ability of borate fusion to fully digest minerals such as zircon and monazite, which frequently contain trace amounts of U.

Molybdenum

As determined by aqua regia (30 g aliquot) ICP-MS, the Mo contents in till samples (excluding sample 10-PTA-117) ranged between 0.3 and 14.8 ppm, with a median value of 0.8 ppm Mo. Anomalous samples contain between 3.9 and 14.8 ppm Mo, with the highest content (14.8 ppm Mo) recorded from sample 10-PTA-131, which was collected approximately 250 m to the northwest of the KMZ. All of the seven anomalous samples (>90th percentile, >3.9 ppm Mo) were collected within 2 km of the deposit and 6 of these samples from less than 500 m of the KMZ (Appendix J1). None of the samples collected up-ice of the deposit has anomalously high Mo contents. All of the samples collected more than 2 km from the KMZ had <2.2 ppm Mo, with the majority of these samples having less than 0.8 ppm Mo. Molybdenum has strong positive correlations with Bi and W, significant positive correlations with U, Cu, and Ti, and moderate positive correlations with Li, Ag, Na, Tl, Fe, Be, V, and Se.

Bismuth

Bismuth contents in the till samples ranged from 0.13 to 2.7 ppm Bi, with a median value of 0.36 ppm Bi, when determined by aqua regia (30 g aliquot). Anomalous values are those containing >1.3 ppm Bi. The sample with the highest contents of Bi was collected immediately to the west of the KMZ (sample 10-PTA-116) and all anomalous samples (>1.3 ppm Bi) are from within 2 km down-ice of the KMZ. Six of these seven anomalous samples are from within 500 m of the deposit (Appendix J1). Samples 10-PTA-035 and 10-PTA-036 were collected ~6 km west from the KMZ and have elevated (75–90th percentile) Bi contents whereas the common trend of samples from >2 km from the KMZ is typically below the 50th percentile. Bismuth exhibits strong positive correlations with Mo and W, significant positive correlations with Cu, Ti, and Ag, and moderate correlations with U (R=0.59), Co, and Li.

Gold

Gold contents in till samples at Kiggavik as determined by ICP-MS after an aqua regia (30 g) digestion in the silt plus clay fraction ranged from 0.3 to 26.9 ppb, with a median of 5.2 ppb Au. Anomalous samples contain >15.4 ppb Au. Sample 10-PTA-120, which was collected ~300 m north of the KMZ, had the highest Au concentration (Appendix J1). Samples 10-PTA-104, -083, -134, and -132 contain between 14 and 21 ppb Au (90th percentile) and have a random distribution in comparison to other elements of interest (i.e., U, Mo, Bi, and Cu). Sample 10-PTA-134 was collected ~4 km southeast of KMZ, sample 10-PTA-132 from 500 m southwest, and sample 10-PTA-104 from 1 km to the north-northwest. Samples that contain 21–25 ppb Au (95th percentile)() include 10-PTA-083 and 10-PTA-035, which were collected 3 km to the northwest and the 6.2 km to the west-southwest of the KMZ, respectively. Samples 10-PTA-036 and -037, from immediately down-ice of sample 10-PTA-035), has elevated contents Au of 13.1 and 10 ppb, respectively. Gold does not display any strong positive correlations

(R>0.8) with any element and only has moderate correlation with In (R=0.58), Cd (R=0.52), and Hg (R=0.44).

Silver

Silver content, determined by aqua regia (30 g) ICP-MS, ranged from 13 to 68 ppb, with a median value of 31 ppb Ag. Anomalous samples have >51 ppb Ag, the highest contents occurred in sample 10-PTA-128, collected ~500 m northwest of the KMZ (Fig. 6b). Samples 10-PTA-121 and 10-PTA-124 both contain 65 ppb Ag (95th percentile) and are from 150 and 200 m west of the deposit, respectively (Fig. 6c). Samples in the 90th percentile include 10-PTA-112, -129, -037 and -086. Samples 10-PTA-112 and -129 are from within 500 m of the KMZ whereas samples 10-PTA-086 and -037 are from 4.7 and 6.2 km from the deposit, respectively. The majority of distal samples (>2 km) are within the 50th percentile. Of particular interest are the elevated (75–90th percentile) Ag signatures in samples collected north and northeast of Sleek Lake, near the Granite Grid U prospect, where samples 10-PTA-036 and 10-PTA-089 have elevated Ag contents. Samples with anomalous Ag have similar trends to those that have anomalous U, Mo, Cu, Cs, and Co. Silver exhibits strong positive correlations (R>0.8) with Zn and Tl; significant correlations (R=0.6–0.8) with Cu, Cs, Li, Ga, Rb, Na, Co, K, Mg, Al, Fe, Sc, Ni, Mn, V, Y, and Bi; and moderate correlations (R=0.4–0.6) with Be, Zr, Cr, Hf, W, Ca, U, Mo, Ti, As, and Cd.

Copper

Copper contents in till samples determined by aqua regia (30 g) ICP-MS ranged from 4.5 to 101 ppm, with a median value of 14.6 ppm Cu. Anomalous samples have >27 ppm Cu and similar to Ag, sample 10-PTA-128 (~400 m northwest of the KMZ) has the highest Cu contents. Samples 10-PTA-115 and 10-PTA-116 (~75 m west-northwest of KMZ) were taken from the same frost boil but at different depths; both have Cu contents within the 95th percentile (41–58 ppm Cu). Samples 10-PTA-121, -124, -112, and -103 have 27 to 41 ppm Cu; samples 10-PTA-121, -124 and -112 were collected 150, 200, and 500 m from the KMZ, respectively. Similar to Ag and Au, Cu is elevated in the samples collected proximal to Sleek Lake. Although these samples are not classified as anomalous, they were found to contain 22–27 ppm Cu, i.e., the 75–90th percentile. In additional, sample 10-PTA-086 has elevated Cu (26.8 ppm Cu) as well as elevated Ag contents. Sample 10-PTA-074 (10 km southwest of KMZ) has an elevated signature with 27.1 ppm Cu. The up-ice samples do not have anomalous Ag or Cu values, all placing in the 50th percentile (<14 ppm Cu). The Cu contents in till is related to the distance from the Kiggavik deposit, similarly for U, Bi, and Ag. Copper contents in till display significant positive correlations with Ag, Zn, Li, Bi, Fe, Tl, Na, Mo, Ga, and Cs, and moderate positive correlations with Rb, Mg, U, V, Ni, Te, Sc, Al, W, Mn, K, Ti, Be, Cr, and Y (Table 3).

Cobalt and nickel

The contents of Co and Ni in till samples, as determined by aqua regia (30 g) ICP-MS, ranged from 2.5 to 14.2 ppm Co and 6.8 to 44.4 ppm Ni, with median values of 6.5 ppm Co and 17.6 ppm Ni. These elements are strongly correlated (R=0.911). Seven samples have anomalous Co or Ni, five of which are anomalous for both (samples 10-PTA-074, 086, 112, 115, and 116). Cobalt contents are highest to the west-northwest of the deposit (sample 10-PTA-116) and Ni has the highest concentrations also to the north-northwest but further from the deposit (sample 10-PTA-086). Similar to what was observed with Cu and Ag, Ni and Co contents are relatively high in sample 10-PTA-074, which was collected 10 km southwest of the KMZ. This observation is intriguing as till samples collected more than 2 km from the KMZ typically have lower contents (Appendix J). The distribution of samples with elevated Ni is more random than those with elevated Co; five of the seven anomalous Co samples were collected within 500 m of the KMZ. Cobalt has a moderate positive correlation with U (R =0.450) whereas Ni has a weak positive correlation (R = 0.27) with U; moreover, Co displays a stronger positive correlation with Ag, Cu, Bi, Mo, W, and Ti than Ni.

Tungsten and titanium

Tungsten and Ti in till samples, as determined by aqua regia (30 g) ICP-MS, ranged from 0.021 to 0.06% Ti and 0.3 to 3.8 ppm W, with median values of 0.039% Ti and 0.71 ppm W. Samples with anomalous Ti were all collected within 250 m of the KMZ (with the exception of sample 10-PTA-048, which was collected 17 km to the southeast) and those with anomalous W from within 500 m (Appendix J). Samples 10-PTA-116, -115, and -128 all have a Ti content of 0.06% (>98th percentile) and samples 10-PTA-131, -114, -124, and -129 all have contents >0.051% Ti (>90th percentile). Samples with anomalous W or Ti contents were all collected within close proximity of the KMZ. As observed with Ti, sample 10-PTA-116 has the highest content of W (3.8 ppm) and samples 10-PTA-121, -131, -132, -115, and -093 have contents of >0.05% (>90th percentile). It is observed that samples with elevated W (75–90th percentile) were all collected within 3 km of the KMZ, the majority of which occur within 1 km of the deposit. Titanium and W have a significant correlation (R=0.61), and both of these elements have moderate positive correlations with U (R=0.56 and 0.46, respectively). Titanium and W both have strong to moderately high positive correlations with Mo, Bi, and

Ag (Table 3).

Lead and cesium

Lead and Cs in till samples analyzed by ICP-MS (30 g) after an aqua regia digestion, ranged from 5.61 to 63.95 Pb and 0.26 to 1.98 ppm Cs and have median values of 12.1 ppm Pb and 0.91 ppm Cs. The sample with the highest Pb content is sample 10-PTA-048, collected ~17 km to the southeast of the KMZ (Appendix J3). With the exception of sample 10-PTA-048, all of the samples with anomalous Pb contents (>90th percentile, 21 ppm) were collected <500 m down-ice from the KMZ (Appendix J1).

The locations of samples with anomalous Cs contents were a bit more dispersed than for the other observed mineral trends (Appendix J2). Sample 10-PTA-112, collected 450 m down-ice of the deposit, had the highest Cs content (1.98 ppm). Of the seven anomalous samples, five occur within 1 km down ice of the KMZ and four of these are from <500 m west of the deposit. Samples 10-PTA-074 (1.52 ppm Cs) and 10-PTA-086 (1.79 ppm Cs) have anomalous Cs concentrations and are located 9.8 km and 4.7 km down-ice of the KMZ. Lead and Cs have variable correlations with U (R=0.24 and 0.46, respectively) but do not display common correlations with other elements (Table 3). Lead is shown to have significant correlations with Ce, Sr, La, S, and Ba and moderate correlations with Ti, Y, P, Ge, Ca and Nb. Interestingly, Cs displays strong positive correlations with Rb, Ga, Tl, Al, Li, K, Sc, Mg, Zn, V, Fe, Ni, and Co. Significant and moderate elemental correlations with Cs are outlined in Table 3.

Till matrix geochemistry (<0.002 mm fraction)

Proportional dot maps have been created at regional and deposit scale for selected elements determined by aqua regia ICP-MS on 0.5 g aliquot (Appendix K).

Sample 10-PTA-117

This sample was excluded in statistical analysis and data plotting, as many of the elements are an order of magnitude more concentrated in this sample (analyzed by ICP-MS after an aqua regia digestion: Table 5). Sample 10-PTA-117 is particularly enriched in U, Au, Pt, Pd, Re, Te, and B (>10 times the mean concentration of the 71 samples) and is moderately enriched (>2 times the mean concentration of the 71 samples) in Ag, Bi, V, K, Tl, Hg, Se, Rb, Y, Be, Pb, and Mo. In contrast, elements Nb, Ge, Sb, and As are relatively depleted. The relationships and correlations of elements are significantly altered when sample 10-PTA-117 is including or excluding. In addition, the U content in sample 10-PTA-117 is 15.68 ppm U (weak acid leach digestion), which is significantly higher than the 71 sample mean of 0.53 ppm U (Table 6).

Uranium

Uranium contents in the clay fraction (ICP-MS after an aqua regia digestion (0.5 g)) ranged from 1 to 9.3 ppm with a median value of 2.1 ppm. Samples considered to be anomalous contain >4.3 ppm U, and the highest content came from sample 10-PTA-115, located 75 m west of the KMZ. All the samples with U content in the >90th percentile were collected within 900 m of the deposit (Appendix K1), with the exception of sample 10-PTA-089 (4.4 ppm U, 90–95th percentile), which was collected 4.8 km southwest of the KMZ. The location of samples with elevated U values (2.6–4.32 ppm) is randomly distributed (Appendix K2), vary from 4 km up-ice to 9.6 km down-ice. Overall, U contents do not strongly correlate with any elements, however U does display a significant positive correlation with Mo (R=0.75). Furthermore, Au, Bi, V, S, Co, Se, W, Fe, Cu, and Ag all have moderate positive correlations with U (Table 5).

Additional analysis for U was conducted on the clay fraction using a weak acid leach digestion (HNO_3) on a 0.5 g aliquot. The U contents in till after a HNO_3 digestion ranged from 0.0003 to 1.0394 ppm with a median value of 0.2118 ppm U. Anomalous samples contain >0.48 ppm U. The sample with the highest concentration of U is sample 10-PTA-115, which is identical to value obtained by aqua regia digestion. Uranium content in samples 10-PTA-116 and 10-PTA-124 are both within the 95–98th percentile and both were collected proximal to the KMZ (75 and 200 m west, respectively; Appendix K2). Samples with U content in the 90–95th percentile are different than those determined by aqua regia digestion. Samples 10-PTA-134 (4 km up-ice) and 10-PTA-103 (3 km north) have high U content when analyzed by HNO_3 digestion. Samples 10-PTA-114 and 10-PTA-128 were collected <500 m from the KMZ. Uranium contents determined by HNO_3 digestion display a strong correlation (R=0.88) with U contents determined by aqua regia digestion (Fig. 14).

Molybdenum

Till samples contain between 0.27 and 23.29 ppm Mo, as determined by aqua regia (0.5 g aliquot). The median value is 1.48 ppm Mo and the highest Mo content occurs in sample 10-PTA-116, 75 m west of the KMZ. All anomalous samples (>13.4 ppm Mo) occur less than 900 m down-ice of the deposit (Appendix K2). Samples 10-PTA-115 and 10-PTA-131, which have Mo content of 22.4 and 19.4 ppm, respectively (Appendix K1), were both collected less than 250 m from the KMZ. Samples with elevated Mo contents (5.4–13.4 ppm Mo) were collected less than 3 km from the deposit. Samples collected greater than 3 km down-ice of the KMZ were found to contain <5.4 ppm Mo and are not

Table 5. Correlation matrix for selected elements in the <0.002 mm fraction.

	Mo	Cu	Pb	Zn	Ag	Ni	Co	Mn	Fe	Al	U	Au	Th	Sr	Cd	Sb	Bi	V	Ca	P	La	C	Mg	Ba	Ti	B	Al	Na	K	W	Sc	Tl	S	Hg	Se	Te	Ga	Cs	Ge	Hf	Nb	Rb	Sn	Zr	Y	Li	Pd	Pt
Mo	1																																																
Cu	0.43	1																																															
Pb	0.00	0.04	1																																														
Zn	0.24	0.86	0.05	1																																													
Ag	0.38	0.45	0.16	0.48	1																																											
Ni	0.29	0.79	0.08	0.85	0.53	1																																										
Co	0.44	0.47	0.17	0.48	0.84	0.61	1																																										
Mn	0.25	0.17	0.11	0.18	0.64	0.24	0.85	1																																									
Fe	0.42	0.69	0.08	0.78	0.71	0.78	0.77	0.55	1																																								
Al	-0.03	0.35	0.06	0.52	0.47	0.65	0.53	0.4	0.66	1																																							
U	0.75	0.40	0.18	0.25	0.40	0.31	0.46	0.27	0.41	-0.06	1																																						
Au	0.42	0.41	0.11	0.43	0.51	0.43	0.65	0.64	0.54	0.28	0.56	1																																					
Th	-0.15	0.12	0.12	0.21	0.08	-0.02	-0.13	-0.21	-0.06	-0.15	-0	-0.06	1																																				
S	0.04	-0.31	0.02	-0.33	-0.17	-0.53	-0.28	-0.09	-0.30	-0.45	0.06	-0.1	0.37	1																																			
Cd	0.14	0.06	0.53	0.09	0.38	0.15	0.40	0.29	0.21	0.17	0.25	0.32	0.02	-0.03	1																																			
Sb	0.17	-0.27	0.09	-0.28	0.25	-0.21	0.27	0.36	0.07	0.10	0.19	0.28	-0.06	0.34	0.28	1																																		
Bi	0.74	0.48	0.13	0.36	0.70	0.43	0.74	0.53	0.53	0.17	0.53	0.47	-0.02	-0.12	0.29	0.14	1																																	
V	0.49	0.52	0.19	0.59	0.74	0.63	0.80	0.55	0.86	0.52	0.51	0.58	-0.11	-0.16	0.47	0.28	0.63	1																																
Ca	0.25	0.18	-0.01	0.12	-0.04	-0.04	-0.08	-0.04	0.07	-0.18	0.20	0.10	0.35	0.59	-0.09	0.11	0.08	0.04	1																																
P	0.27	-0.10	0.27	-0.08	0.52	0.02	0.58	0.68	0.34	0.30	0.35	0.61	-0.29	0.06	0.59	0.55	0.36	0.54	-0.11	1																														
La	0.19	-0.11	0.25	-0.17	0.24	-0.25	0.16	0.21	0.04	-0.23	0.38	0.25	0.33	0.66	0.34	0.66	0.16	0.25	0.47	0.38	1																												
C	0.28	0.65	0.08	0.74	0.54	0.92	0.61	0.27	0.82	0.74	0.28	0.39	-0.14	-0.51	0.17	-0.04	0.39	0.72	-0.08	0.16	-0.20	1																											
Mg	0.34	0.81	0.00	0.91	0.39	0.89	0.43	0.09	0.75	0.52	0.27	0.33	0.07	-0.39	-0.04	-0.34	0.34	0.53	0.15	-0.18	-0.31	0.81	1																										
Ba	0.10	-0.04	0.11	0.05	0.23	0.17	0.21	0.22	0.23	0.35	0.19	0.34	-0.10	0.20	0.13	0.31	-0.01	0.26	-0.01	0.50	0.17	0.31	0.12	1																									
Ti	0.44	0.02	0.06	-0.10	0.20	-0.22	0.27	0.36	0.12	-0.21	0.32	0.19	0.07	0.55	0.24	0.50	0.38	0.36	0.46	0.33	0.68	-0.20	-0.22	-0.07	1																							
B	0.35	0.37	-0.02	0.44	0.44	0.30	0.31	0.28	0.44	0.20	0.37	0.57	0.03	0.03	0.12	0.02	0.25	0.39	0.09	0.35	0.05	0.28	0.36	0.26	0.07	1																						
Al	0.14	0.69	0.03	0.85	0.46	0.84	0.44	0.16	0.73	0.62	0.18	0.37	0.02	-0.53	0.06	-0.38	0.25	0.50	-0.10	0.03	-0.42	0.78	0.88	0.22	-0.43	0.45	1																				
Na	0.21	0.13	0.27	0.17	0.61	0.31	0.66	0.64	0.51	0.47	0.33	0.63	-0.31	-0.29	0.52	0.29	0.35	0.55	-0.38	0.86	0.05	0.40	0.12	0.52	-0.04	0.43	0.4	1																		
K	0.03	0.63	-0.02	0.80	0.29	0.70	0.19	-0.06	0.54	0.46	0.05	0.21	0.22	-0.41	-0.04	-0.51	0.10	0.28	-0.02	-0.16	-0.45	0.59	0.81	0.12	-0.49	0.44	0.94	0.21	1																	
W	0.64	0.03	0.16	-0.08	0.56	0.02	0.53	0.47	0.33	0.07	0.42	0.31	-0.16	0.13	0.39	0.60	0.69	0.55	0.04	0.60	0.48	0.15	-0.10	0.14	0.63	0.16	-0.16	0.42	-0.32	1																
Sc	-0.01	0.63	-0.01	0.78	0.24	0.75	0.21	-0.06	0.53	0.54	-0.03	0.18	0.25	-0.45	-0.14	-0.39	0.05	0.26	0.08	-0.30	-0.43	0.68	0.85	0.11	-0.48	0.24	0.85	0.04	0.85	-0.33	1														
Tl	0.26	0.74	0.08	0.88	0.61	0.87	0.55	0.22	0.80	0.61	0.31	0.47	0.09	-0.45	0.11	-0.23	0.39	0.61	-0.03	0.10	-0.24	0.80	0.88	0.26	-0.28	0.51	0.95	0.43	0.87	0.02	0.8	1												
S	0.36	0.01	0.10	-0.01	0.53	0.09	0.57	0.65	0.39	0.26	0.51	0.54	-0.24	0.11	0.18	0.39	0.42	0.49	-0.05	0.72	0.27	0.21	-0.04	0.56	0.21	0.32	0.09	0.65	-0.11	0.46	-0.16	0.19	1											
Hg	0.15	0.00	0.53	0.01	0.37	0.11	0.40	0.33	0.20	0.17	0.27	0.32	-0.08	-0.03	0.98	0.29	0.29	0.46	-0.12	0.67	0.32	0.16	-0.09	0.21	0.22	0.11	0.03	0.59	-0.09	0.43	-0.20	0.08	0.29	1										
Se	0.49	0.51	-0.08	0.51	0.41	0.45	0.42	0.21	0.62	0.32	0.44	0.25	-0.08	-0.02	0.07	0.04	0.38	0.55	0.24	0.16	0.10	0.45	0.54	0.14	0.17	0.24	0.46	0.22	0.35	0.22	0.28	0.47	0.22	0.05	1									
Te	0.48	0.73	0.07	0.71	0.61	0.65	0.56	0.22	0.72	0.42	0.34	0.31	0.07	-0.21	0.23	0.00	0.61	0.70	0.02	0.16	0.01	0.64	0.66	0.10	0.18	0.42	0.61	0.30	0.52	0.38	0.46	0.71	0.17	0.18	0.47	1								
Ga	0.28	0.74	0.05	0.89	0.53	0.84	0.49	0.17	0.81	0.59	0.30	0.40	0.04	-0.42	0.08	-0.29	0.35	0.63	-0.03	0.07	-0.28	0.80	0.91	0.25	-0.28	0.47	0.97	0.39	0.89	-0.02	0.80	0.96	0.14	0.06	0.58	0.72	1							
Cs	0.46	0.75	0.00	0.87	0.56	0.76	0.56	0.29	0.81	0.53	0.37	0.52	0.08	-0.17	0.05	-0.08	0.46	0.67	0.18	0.12	-0.09	0.70	0.88	0.27	0.04	0.59	0.80	0.31	0.72	0.13	0.70	0.87	0.22	0.00	0.60	0.78	0.88	1						
Ge	0.09	0.04	0.14	-0.02	0.45	-0.01	0.36	0.35	0.19	0.17	0.18	0.16	0.20	0.22	0.26	0.48	0.31	0.31	0.07	0.43	0.50	0.07	-0.18	0.18	0.34	0.04	-0.11	0.28	-0.17	0.42	-0.19	0.00	0.36	0.26	0.10	0.19	-0.04	0.02	1						
H	0.05	0.27	0.18	0.27	0.24	0.29	0.22	0.11	0.21	0.07	0.12	0.21	0.25	-0.05	0.05	-0.01	0.21	0.14	0.24	-0.03	0.12	0.22	0.30	0.07	0.00	0.03	0.21	0.08	0.18	0.09	0.35	0.29	0.02	0.01	-0.01	0.09	0.20	0.19	-0.04	1				
Nb	0.22	-0.19	0.29	-0.23	0.49	-0.13	0.54	0.63	0.22	0.10	0.33	0.36	-0.28	0.20	0.48	0.61	0.36	0.47	-0.13	0.83	0.51	0.00	-0.33	0.40	0.49	0.11	-0.22	0.65	-0.43	0.68	-0.49	-0.08	0.70	0.56	0.05	0.09	-0.14	-0.05	0.51	0.06	1			
Rb	0.29	0.72	0.03	0.87	0.54	0.81	0.47	0.18	0.77	0.55	0.32	0.48	0.08	-0.36	0.10	-0.26	0.33	0.59	0.03	0.11	-0.23	0.74	0.88	0.28	-0.26	0.56	0.96	0.42	0.89	-0.02	0.78	0.97	0.17	0.07	0.54	0.69	0.98	0.90	-0.06	0.21	-0.13	1		
Sn	-0.05	0.04	0.15	0.07	0.15	0.08	0.13	-0.04	-0.01	-0.02	0.09	0.08	0.08	-0.09	0.45	0.09	0.07	0.24	-0.18	0.07	0.16	0.05	-0.01	-0.07	0.07	-0.06	-0.03	0.05	-0.08	0.06	-0.07	0.01	-0.04	0.40	-0.04	0.01	0.00	-0.05	0.07	0.06	0.17	0	1		
Zr	0.06	0.26	0.13	0.35	0.19	0.23	0.10	-0.02	0.19	0.03	0.06	0.12	0.50	0.15	-0.03	-0.01	0.17	0.12	0.36	-0.18	0.18	0.15	0.32	0.01	0.14	0.07	0.16	-0.13	0.20	0.08	0.37	0.25	-0.10	-0.10	0.05	0.19	0.19	0.26	-0.02	0.84	-0.11	0.20	0.03	1		
Y	0.08	0.51	0.15	0.58	0.27	0.50	0.21	0.07	0.49	0.28	0.29	0.38	0.39	0.02	-0.01	0.03	0.06	0.29	0.48	-0.06	0.29	0.45	0.55	0.22	-0.08	0.22	0.49	0.04	0.46	-0.14	0.60	0.55	0.07	-0.05	0.35	0.26	0.51	0.49	0.04	0.51	-0.17	0.54	-0.10	0.47	1		
Li	0.27	0.80	0.01	0.90	0.47	0.89	0.50	0.19	0.76	0.55	0.24	0.37	0.08	-0.42	0.00	-0.36	0.38	0.54	0.09	-0.09	-0.33	0.79	0.96	0.15	-0.26	0.36	0.93	0.23	0.86	-0.10	0.85	0.92	0.04	-0.05	0.53	0.66	0.94	0.86	-0.09	0.31	-0.25	0.92	-0.04	0.29	0.55	1		
Pd	0.00	0.09	0.05	0.10	0.28	0.29	0.28	0.05	0.05	0.18	0.03	0.14	0.12	-0.26	0.34	0.23	0.29	0.24	-0.14	0.10	0.08	0.26	0.08	-0.09	-0.03	-0.14	0.07	0.11	-0.01	0.20	0.13	0.14	-0.05	0.27	-0.11	0.15	0.06	0.03	0.36	0.27	0.15	0.04	0.36	0.15	0.06	0.11	1	
Pt	0.03	-0.20	0.01	-0.21	-0.03	-0.31	-0.18	-0.12	-0.25	-0.34	0.08	-0.10	0.25	0.42	-0.14	0.16	0.05	-0.17	0.29	-0.07	0.31	-0.31	-0.23	0.11	0.27	-0.03	-0.30	-0.23	-0.25	0.12	-0.22	-0.19	0.12	-0.13	-0.16	-0.12	-0.27	-0.13	-0.10	0.23	0.14	-0.20	0.00	0.28	0.07	-0.23	-0.14	1

Table 6. Element contents in the <0.002 mm fraction of sample 10-PTA-117 in comparison to the remainder of the samples.

<0.002 mm Fraction by Aqua Regia ICP-MS									
Element	Sample Suite Average (n=71)	Sample 10-PTA-117	Difference	Ratio of Element Content in Sample 10-PTA-117 to Sample Suite Average	Element	Sample Suite Average (n=71)	Sample 10-PTA-117	Difference	Ratio of Element Content in Sample 10-PTA-117 to Sample Suite Average
Mo (ppm)	4.24	9.53	5.29	2.24:1	**Al** (%)	2.51	4.38	1.87	1.74
Cu (ppm)	80.3	104.17	23.87	1.29:1	**Na** (%)	0.59	0.48	0.11	0.81
Pb (ppm)	49.78	167.8	118.02	3.37:1	**K** (ppm)	0.47	1.40	0.93	2.99
Zn (ppm)	74.61	62	12.61	0.83:1	**W** (ppm)	0.6	0.5	0.1	0.83
Ag (ppb)	179.83	1031	851.17	5.73:1	**Sc** (ppm)	6.01	9.1	3.09	1.51
Ni (ppm)	48.59	53	4.41	1.09:1	**Tl** (ppm)	0.3	1.6	1.3	5.32
Co (ppm)	15.6	19.3	3.7	1.23:1	**S** (ppm)	0.01	0.01	0	0.74
Mn (ppm)	487.31	335	152.31	0.68:1	**Hg** (ppm)	96.25	592	495.75	6.15
Fe (%)	4.02	3.15	0.87	0.78:1	**Se** (ppm)	0.28	1.2	0.92	4.36
As (ppm)	21.66	10.2	11.46	0.47:1	**Te** (ppm)	0.1	2.31	2.21	22.25
U (ppm)	3.93	105.7	101.77	27.5:1	**Ga** (ppm)	8.66	14.5	5.84	1.67
Au (ppb)	10.28	231.2	220.92	22.5:1	**Cs** (ppm)	2.17	5.12	2.95	2.36
Th (ppm)	16.85	13.6	3.25	0.80:1	**Ge** (ppm)	0.10	0.05	0.05	0.48
Sr (ppm)	88.76	51.9	36.86	0.58:1	**Hf** (ppm)	0.12	0.11	0.01	0.92
Cd (ppm)	0.46	1.59	1.13	3.45:1	**Nb** (ppm)	0.64	0.04	0.6	0.06
Sb (ppm)	0.14	0.01	0.13	0.07:1	**Rb** (ppm)	27.72	62.4	34.68	2.25
Bi (ppm)	1.97	8.61	6.64	4.37:1	**Sn** (ppm)	1.46	0.9	0.56	0.62
V (ppm)	58.06	282	223.94	4.86:1	**Zr** (ppm)	8.28	9.5	1.22	1.15
Ca (%)	0.28	0.32	0.04	1.16:1	**Y** (ppm)	12.33	30.58	18.25	2.48
P (%)	0.21	0.17	0.04	0.82:1	**Ce** (ppm)	109.67	56.6	53.07	0.52
La (ppm)	60.83	36.7	24.13	0.60:1	**In** (ppm)	0.04	0.05	0.01	1.35
Cr (ppm)	72.4	69.5	2.9	0.96:1	**Re** (ppm)	0.86	12	11.14	13.97
Mg (%)	1.01	1.13	0.12	1.12:1	**Be** (ppm)	1.89	5.9	4.01	3.12
Ba (ppm)	696.4	402	294.4	0.58:1	**Li** (ppm)	33.07	62.3	29.23	1.88
Ti (%)	0.04	0.05	0.01	0.28:1	**Pd** (ppb)	8.92	114	105.08	12.79
B (ppm)	14.35	159	144.65	11.1:1	**Pt** (ppb)	9.20	525.00	515.80	57.08

<0.002 mm Fraction by HNO_3				
Element	Sample Suite Average (n=71)	Sample 10-PTA-117	Difference	Ratio of Element Content in Sample 10-PTA-117 to Sample Suite Average
U (ppm)	0.53	15.68	15.15	29.7:1

Legend
>10
>2–10
<0.5

Samples collected greater than 3 km down-ice of the KMZ were found to contain <5.4 ppm Mo and are not considered to be elevated. Furthermore, Mo content is <5 ppm in samples up-ice of the KMZ. Molybdenum contents show significant positive correlations with U, Bi, and W and moderate positive correlations with V, Se, Te, Cs, Co, Ti, Cu, Au, and Fe (Table 5).

Bismuth

After an aqua regia digestion (0.5 g aliquot), Bi content in till ranged from 0.41 to 7.34 ppm, with a median value of 1.12 ppm. Anomalous samples contain >4.5 ppm Bi. The sample with the highest Bi content (sample 10-PTA-035) was collected 6.3 km west-southwest of the KMZ, to the north of Sleek Lake. Sample 10-PTA-094, which was collected 1.5 km west of the KMZ, has Bi content of 6.16 ppm, which is between the 95–98th percentiles. Five samples with >4.3 ppm Bi

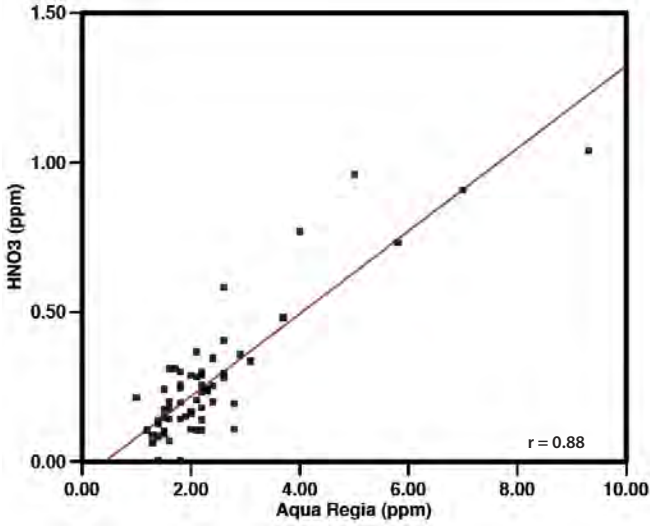

Figure 14. Comparison of U content in the <0.002 mm fraction of the till matrix of each sample (n = 70) determined by aqua regia and weak acid (HNO_3) leach digestion.

occur within 1 km of the deposit (Appendix K1). Sample 10-PTA-089, collected 4.4 km west-southwest of the KMZ, has an elevated Bi value not observed in other samples at this distance. Bismuth content in samples up-ice of the KMZ are not elevated (<2.3 ppm Bi). Bismuth contents show significant positive correlations with Co, Mo, Ag, W, V, and Te and moderate positive correlations with Fe, U, Mn, Cu, Au, Cs, Ni, and S (Table 5).

Gold

The clay fraction of the till samples analyzed by ICP-MS after an aqua regia digestion revealed Au ranging from 2.2 to 35.8 ppb with a median value of 5.9 ppb. Anomalous samples are those with >11.2 ppb Au; the sample with the highest Au content (sample 10-PTA-106) was collected 875 m to the northwest of the KMZ and had Au content of 35.8 ppb (Appendix K2). Other anomalous samples (>11 ppb Au) were collected at varying distances down-ice from the deposit (Appendix K1). Samples 10-PTA-035, collected 6.3 km west-southwest of the Kiggavik deposit, and 10-PTA-089, collected 4.8 km west-southwest of the Kiggavik deposit, near the Sleek Lake and Granite Grid prospects (Fig. 6a). Sample 10-PTA-066 (11.2 ppb Au) occurs 4.4 km to the northeast, up-ice of the KMZ and samples 10-PTA-128, -124, and -093 were all collected in close proximity of the KMZ. Gold contents show significant positive correlations with Co, Mn, Na, and P and moderate positive correlations with V, B, U, Fe, S, Cs, Ag, Rb, Bi, Tl, Be, Ni, Zn, Mo, Cu, and Ga (Table 5).

Silver

Silver in till ranges from 48 to 1014 ppb Ag, as determined by aqua regia (0.5 g aliquot), with a median value of 120 ppb Ag. Anomalous contents are those >301 ppb Ag. Sample 10-PTA-093, which was collected approximately 850 m to the west of the KMZ, had the highest content. Samples 10-PTA-035 and 10-PTA-089, collected to the north of Sleek Lake (6.3 and 4.4 km west-southwest of the KMZ, respectively) have anomalous values of 522 and 456 ppb Ag, respectively. Several samples close to the KMZ (Appendix K1) have elevated Ag contents, however only two (samples 10-PTA-124 and -128) of the 7 anomalous samples in the sample suite are from within 500 m of the KMZ. Samples 10-PTA-091 and 10-PTA-094, which had 413 and 311 ppb Ag, are from 2.6 and 1.5 km down-ice of the KMZ, respectively. All up-ice samples as well as those collected >3 km down-ice, excluding the two samples mentioned above (10-PTA-035 and -089), contain background levels of Ag (<120 ppb). Silver concentrations show a strong positive correlation with Co and significant positive correlations with V, Fe, Bi, Mn, Tl, Te, and Na (Table 5).

Copper

Till samples contain between 15.5 and 425 ppm Cu, as determined by aqua regia (0.5 g aliquot), with a median value of 67.25 ppm Cu. Anomalous samples are considered to be those containing >149 ppm Cu. The highest content (425 ppm Cu) was found in sample 10-PTA-128, collected 500 m northwest of the KMZ. Samples containing the highest Cu concentrations (>90th percentile) are all from within 500 m of the KMZ, with many of these collected within 200 m of the deposit (Appendix K1). Samples distal to the KMZ, and those samples collected up-ice of the deposit, have low to background Cu values except for the three samples proximal to Sleek Lake, which have elevated Cu contents. Samples with elevated Cu have strong positive correlations with Zn, Mg, and Li and have significant positive correlations with Ni, Cs, Ga, Tl, Te, Rb, Al, Fe, Cr, Sc, and K. Copper also shows moderate positive correlations with Be, V, Se, Y, Bi, Co, Ag, Mo, In, Au, and U (Table 5).

Cobalt and nickel

The concentration of Co and Ni in the clay fraction (analyzed by ICP-MS after an aqua regia digestion (0.5 g aliquot)) ranges from 6.8 to 48.3 ppm Co and 21.7 to 84.8 ppm Ni, with median values of 13.9 ppm Co and 46.75 ppm Ni. The highest concentration of Co, 48.3 ppm, is found in sample 10-PTA-035, which was collected to the north of Sleek Lake. Sample 10-PTA-089, which is also within close proximity of Sleek Lake, has an anomalous concentration of 24.6 ppm Co. The remainder of the samples with anomalous Co contents was collected within 2 km to the KMZ. Samples with contents that occur under the 75–90th percentile and have elevated Co are more numerous within 1 km of the KMZ; however, some samples in this percentile range also occur up to 5 km west of the deposit. None of the samples collected up-ice contains elevated Co contents.

Nickel contents in all of the samples are close to the median value. Overall, the highest Ni content is in sample 10-PTA-128, which was collected 500 m to the northwest of the KMZ (Appendix K1). Four of the seven samples in the <90th percentile or higher are clustered to the north-northwest of the KMZ, no further than 450 m from the deposit. Nickel concentrations decrease with distance from the deposit, with the exception of sample 10-PTA-089 that has of 75 ppm Ni. Sample 10-PTA-037, which was collected to the north of Sleek Lake and 6.7 km to the west of the KMZ, has elevated Ni content similar to that of sample 10-PTA-089. The samples that were collected up-ice of the KMZ do not display elevated Ni contents.

There are strong positive correlations of Co with Mn, Ag, and V as well as significant positive correla-

tions with Fe, Bi, Na, Au, Ni, and Cr. Nickel displays strong positive correlations with Cr, Mg, Li, Tl, Zn, Ga, Al, and Rb in addition to significant positive correlations with Cu, Fe, Cs, Sc, Be, K, Te, As, V, In, and Co. Both Co and Ni have extended lists of elements that exhibit moderately positive correlations (Table 5).

Tungsten and titanium

Tungsten and titanium in the <0.002 mm fraction range from 0.2 to 2.2 ppm W and 100 to 1000 ppm Ti, with median values of 0.55 ppm W and 300 ppm Ti. Till samples are considered anomalous at >1.3 ppm W and/or >800 ppm W and were all collected proximal to the Kiggavik deposit. Sample 10-PTA-093, which has the highest W content, was collected 850 m west of the KMZ. Samples with W content in the 90th percentile or higher and elevated Ti contents were all collected within 2.5 km of the KMZ. Sample 10-PTA-035, which was collected to the north of Sleek Lake, is the sole sample with elevated Ti and W from further than 2.5 km from the KMZ. Samples collected up-ice of the KMZ do not contain elevated W.

Samples with elevated Ti occur within relative proximity of the KMZ. Samples 10-PTA-132 and 10-PTA-128 (Fig. 6b) share the highest Ti content of 1000 ppm and are from <500 m of the deposit (Appendix K1). Titanium contents are also high in samples 10-PTA-114, -120, -131, and -122, all of which were collected <250 m from the KMZ. Sample 10-PTA-136 (Fig. 6c) is the only sample with anomalous Ti values that is from a distance of more 500 m from the KMZ. Samples 10-PTA-076 and 10-PTA-075 are both from ~10 km of the deposit and both have elevated Ti. Furthermore, as seen with W and several other elements, sample 10-PTA-035 also contains elevated Ti contents.

Tungsten exhibits significant positive correlations with Bi, Nb, Mo, Ti, P, Sb, and Ag. There are moderate positive correlations of W with Ce, V, Co, La, Mn, S, Hg, Na, Ge, and U. Titanium contents in the <0.002 mm fraction show significant positive correlations with Ce, La, and W and moderate positive correlations with Sr, Sb, Nb, Ca, and Mo (Table 5).

Lead and cesium

Till samples contain between 12.4 to 710 ppm Pb and 0.62 to 4.93 ppm Cs, with median values of 32.6 ppm Pb and 1.8 ppm Cs. Anomalous values for Pb and Cs are >68 ppm and >4 ppm, respectively. The sample containing the highest Pb content is sample 10-PTA-079, which is rather unique from the other enriched samples in that it is from 10 km northwest of the KMZ and is significantly elevated relative to all other samples. Sample 10-PTA-048, which also displays high Pb content (Appendix K3), was collected 16.8 km to the southeast of the KMZ. Two of the samples proximal to Sleek Lake contain high concentrations of Pb. Three of the seven anomalous samples are located within 1.5 km of the KMZ, with sample 10-PTA-122 collected 150 m to the west. Although not considered to be anomalous, the majority of elevated samples (75–90th percentile, Appendix K2) are from <1 km to the west and northwest of the KMZ.

Till samples with high Cs contents were collected relatively close to the Kiggavik deposit. All of the seven samples whose Cs content was within the 90th percentile or greater are found within 850 m of the KMZ. Samples 10-PTA-118 and 10-PTA-119 (field duplicates), which have the highest Cs contents, were collected 180 m to the north of the KMZ. The majority of samples collected <1 km from the KMZ have slightly elevated Cs signatures (Appendix K1).

Lead contents in the clay fraction do not display strong or significant correlations with other elements; a likely consequence of the Pb outlier in sample10-PTA-079. Lead does exhibit positive moderate correlations with Cd and Hg. Comparatively, Cs exhibits strong positive correlations with multiple elements: Rb, Ga, Mg, Tl, Zn, Li, Fe and A. Cesium also displays significant positive correlations with Ni, Cu, K, Be, Cr, Sc, U, V, In, and Se (Table 5).

Lead isotope ratios (<0.002 mm fraction)

The application of isotopic ratios as tracers of Pb is based on the radioactive decay of the isotopes ^{235}U, ^{238}U, and ^{232}Th that produce the stable daughter isotopes ^{207}Pb, ^{206}Pb and ^{208}Pb, respectively. The isotope ^{204}Pb is non-radiogenic (common lead), thus its abundance does not change with time, which facilitates Pb isotope-ratios to be used as geochemical indicators (Russell and Allan, 1955; Cumming and Richards, 1975). Rocks that contain U and Th produce radiogenic Pb, which leads to increasing ^{206}Pb/^{204}Pb, ^{207}Pb/^{204}Pb and ^{208}Pb/^{204}Pb values over time (Gulson, 1986).

^{206}Pb/^{204}Pb ratio

The ^{206}Pb/^{204}Pb ratio of sample 10-PTA-117, which was collected <25 m from the KMZ, exhibits the highest ratio of 215. This ratio is well above the next highest ratio of 23.1 in sample 10-PTA-124 (collected 250 m west of the KMZ). Samples 10-PTA-115 and 10-PTA-116 also have elevated ratios of 20.5 and 20.1 (Fig. 15), however these are below the ^{206}Pb/^{204}Pb ratio of 30 that Holk et al. (2003) suggest is the barrier for anomalous concentrations in rocks of similar age. Furthermore, the median ^{206}Pb/^{204}Pb ratio for the entire sample suite is 18.3, which is close to the average crustal ratio of 19.0 (Pagel et al., 1993). Sample 10-PTA-047 also has an elevated ^{206}Pb/^{204}Pb ratio, however this sample was collected 28 km to the south

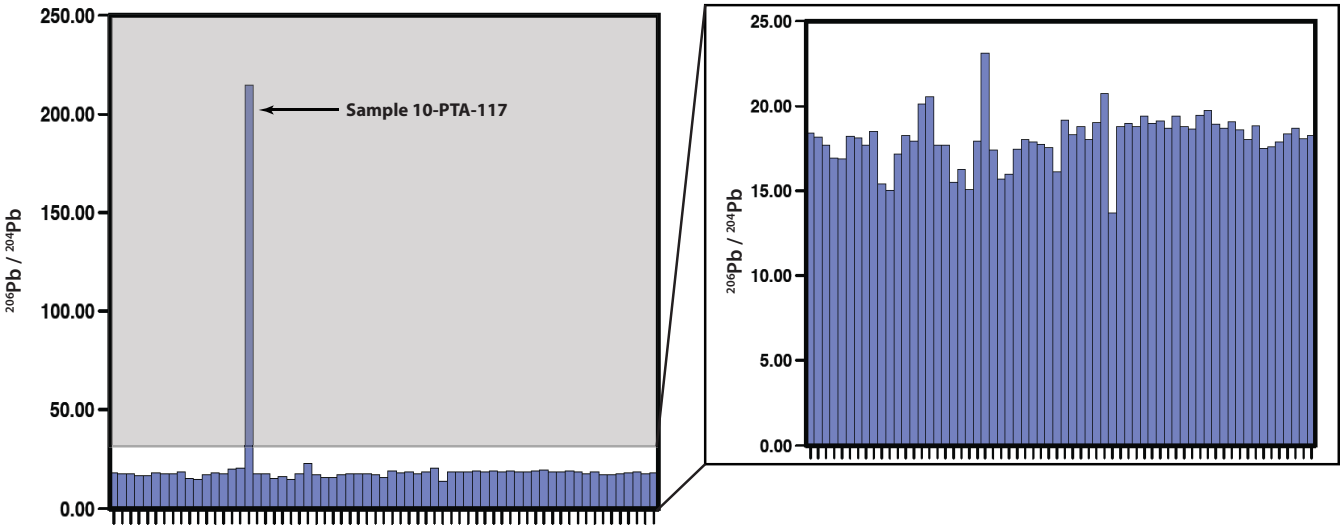

Figure 15. $^{206}Pb/^{204}Pb$ ratio of the complete sample suite (n=71). The grey area of the graph denotes anomalously high $^{206}Pb/^{204}Pb$ values of >30 (after Holk et al., 2003), the inset shows lower ratio values.

of the KMZ and this elevated value likely attributable to local granitoid rocks.

$^{207}Pb/^{204}Pb$ ratio

The $^{207}Pb/^{204}Pb$ ratio in the clay fraction has a very similar trend and distribution to that of $^{206}Pb/^{204}Pb$. The $^{207}Pb/^{204}Pb$ ratio is highest in sample 10-PTA-117 at 28 and is well above the median and mean of 16. More evident than with the $^{206}Pb/^{204}Pb$ ratios, samples that were collected >3 km from the deposit have low $^{207}Pb/^{204}Pb$ ratios, with all the elevated samples collected proximal to the deposit. Sample 10-PTA-134 is the sole elevated sample that does not occur immediately down-ice of the deposit; it was collected 4 km to the southeast of the KMZ.

$^{207}Pb/^{206}Pb$ ratio

The distribution of $^{207}Pb/^{206}Pb$ ratios in the <0.002 mm fraction of till is sporadic and does not exhibit any trends. Sample 10-PTA-117, collected directly above the deposit, has a ratio of 0.13, which can be considered to be highly anomalous. Samples 10-PTA-124, 10-PTA-115, 10-PTA-116, and 10-PTA-047 all report lower than median ratios and are considered to be depleted as a result of ^{206}Pb enrichment.

$^{208}Pb/^{204}Pb$ ratio

The $^{208}Pb/^{204}Pb$ ratio illustrates the abundance of Pb derived from the decay of Th as opposed to common Pb. This ratio ranged from 31.2 to 41.7, with the highest ratios in samples collected 10 km from the KMZ. $^{208}Pb/^{204}Pb$ ratios are relatively consistent over the study area with samples collected closer to the deposit being slightly lower.

Clay mineralogy (X-ray diffraction)

Fifteen till samples were selected from proximal, distal, and up-ice locations from the KMZ to observe clay mineralogical variability. Results show that quartz is the most abundant phase in all samples, ranging from 27–47 wt.% (Table 7). Plagioclase feldspar, K-feldspar, amphibole-group minerals, chlorite-group minerals, illite, kaolinite, and hematite minerals occur in minor amounts. Plagioclase feldspar and K-feldspar have relatively consistent abundances, ranging from 7–11 wt.% and 6–13 wt.%, respectively. Amphibole-group minerals occur in trace amounts in about half the samples. Chlorite-group minerals, confirmed by heat treatment, range from 6 to 16 wt.%. Illite varies between 8 and 20

Table 7. Semi-quantitative (wt.%) mineralogy of the till samples based on X-ray diffraction.

Sample No.	Qtz	Pl	Kfs	Amp	Chl	Ill	Kln	Sm	ML	Hem	GoF
10-PTA-047	39	8	9		11	18	10			5	3.28
10-PTA-074	38	7	10		12	18	9			5	3.38
10-PTA-078	42	9	13		14	13	6			4	4.52
10-PTA-082	40	8	12		6	20	11			3	3.87
10-PTA-083	44	10	11	tr	8	12	6			8	3.33
10-PTA-097	40	10	9		11	19	7			4	3.15
10-PTA-111	47	9	11	tr	8	13	8			4	3.82
10-PTA-115	34	10	12	tr	12	17	14		tr	2	3.39
10-PTA-116	41	9	8	tr	12	8	11	5		5	3.41
10-PTA-117	27	9	6		16	20	18			2	4.26
10-PTA-118	33	11	11	tr	13	17	11			3	3.43
10-PTA-119	28	10	13		16	19	10			3	3.65
10-PTA-130	38	10	11	tr	14	11	9			6	3.56
10-PTA-134	37	7	9		10	15	19		tr	3	3.76
10-PTA-135	40	7	8		10	17	13			4	3.21

Qtz=quartz; Pl=plagioclase feldspar; Kfs=K-feldspar; Amp=Amphibole-group mineral; Chl= chlorite-group mineral; Ill=illite(muscovite); Kln=kaolinite-group mineral; Sm=smectite; ML=mixed-layer clay mineral; Hem=hematite; GoF=Goodness of Fit; tr=trace

wt.%. Kaolinite-group minerals vary from 7 to 14 wt.% and hematite between 3 to 8 wt.%. One sample, 10-PTA-116, contains minor amounts of smectite (~5 wt.%). Mixed-layer clay minerals (illite-smectite) were observed in two samples in trace amounts. The results are considered semi-quantitative rather than quantitative due to the presence of smectite, the lack of matching or valid mineral structures in the software database, as well as peak overlap with chlorite in the air-dried samples. Mixed-layer clay minerals occur in very trace amounts. Quartz contents are lowest in the highly mineralized sample 10-PTA-117, which also contains higher chlorite, illite, and kaolinite contents. To a reduced extent, this observation is also present in samples proximal to the deposit (samples 10-PTA-115, -116, -118, and -119). Uranium in the <0.002 mm fraction (aqua regia digestion) exhibits correlations with kaolinite (R=0.54), illite (R=0.29), and quartz (R=-0.56).

Laboratory gamma-ray spectrometry

Proportionally scaled symbol plots of the laboratory gamma ray spectrometry (LGRS) analysis for potassium "K", eU, and eTh are presented in Appendix G. Potassium contents range from 1 to 2.9 wt.%, with a median value of 2 wt.%. Equivalent U values range from 1.3 to 677 ppm, with a median value of 2.2 ppm. Data for eTh display a range of 4.3 to 15.5 ppm, with a median value of 10 ppm. LGRS analysis reveals that sample 10-PTA-117 is an extreme outlier at 677 ppm eU, which is over 600 ppm higher than the second highest sample. For this reason, sample 10-PTA-117 was excluded from the data plots and analysis.

The highest K, eU, and eTh contents determined by LGRS are in samples from within 1 km of the KMZ (Appendix G2). Samples with elevated eU and K have a linear distribution from the KMZ to the west, with a slight offset to the west-northwest. Although K and eTh contents are mostly elevated in samples collected at <1 km from the KMZ, these elements are not elevated in samples 10-PTA-115, -116, -118, and -119, which are from directly down-ice of the KMZ suggesting that the K and eTh enrichments are more likely derived from intrusive bodies, rather than the mineralization itself. However, samples 10-PTA-115 and 10-PTA-116 have elevated eU and eU/eTh ratios at 0.46 and 0.56, which are above average crustal values of 0.25 (Cuney, 2010). The elevated eU and eU/eTh ratios would suggest that these samples likely contain traces of hydrothermal U mineralization derived from Kiggavik.

Similarities and differences were observed when comparing the LGRS data of the sand fraction with K and eTh concentrations in the <0.063 mm fraction analyzed by ICP after an aqua regia digestion. When examining the ICP-MS data, several samples distal from the deposit have elevated K and Th concentrations, whereas this is not observed in the LGRS data. Overall, both methods illustrate generally elevated concentrations of both K and Th in samples proximal to the deposit. A significant difference is that K, on average, has contents 18 times higher when analyzed by LGRS than by ICP-MS, and the two analytical methods have a correlation coefficient of 0.48. This variability could potentially be a result of K being concentrated in the coarser fraction of the samples. Conversely, Th values are about the same in both data sets with both eTh and Th determined by ICP-MS having averages of 9.8 ppm and 9.3 ppm, respectively, and a correlation of 0.68. Equivalent U and U content determined by aqua regia digestion on the <0.063 mm fraction of the till samples as have very similar trends to that of eTh and Th. This similarity is also true for eTh and U values determined by other digestion methods and using different size fractions (Fig. 16).

Pebble lithological analysis

Pebble lithology of the >5.6 mm fraction of the till samples, which is summarized in Table 8, is composed of 1) metasedimentary and metavolcanic rocks average 42.5% in total abundance and ranges from 21.9 to 69.6% per sample; 2) Thelon sandstone averages 22% and ranges from 5.1 to 39.2%; 3) Pitz Formation volcanic rocks average 12.4% and ranges from 4.6 to 22.8%; 4) intrusive rocks average 11.5% and ranges from 3.0 to 27.8%; 5) granitoid gneiss averages 4.6% and ranges from 1.3 to 21%; and 6) Paleoproterozoic quartzite averages 4% and ranges from 1.6 to 14.7%. The remaining categories (iron formation, vein quartz, and Pitz Formation with quartz veins) comprise on average <3% of the total abundance. Total pebble counts are listed in Appendix H.

The abundance of metasedimentary clasts reflects the predominance of the Neoarchean arkosic metagreywacke in the Kiggavik Camp. Till samples collected close to, or directly above the metagreywacke bedrock, such as proximal to the KMZ, are dominated by metagreywacke and have low abundances of Thelon sandstone clasts that are interpreted to have been derived from the Baker Lake Basin some 50 km to the southeast. Conversely, Thelon-derived sandstone pebbles are more abundant in samples to the northwest of Kiggavik, on the northwest side of the Thelon Fault where the immediate bedrock is Thelon Formation sandstone. Paleoproterozoic quartzite flanking the southeast side of the Thelon Fault and silicification along the fault zone have made the Thelon Fault zone resistant to erosion, resulting in a linear ridge, behind which some crag-and-tail features were developed. Till in these tails is also rich in Thelon sandstone, and boulders of sandstone are prominent at surface. The Judge Sissons fault also forms a ridge but with no Thelon

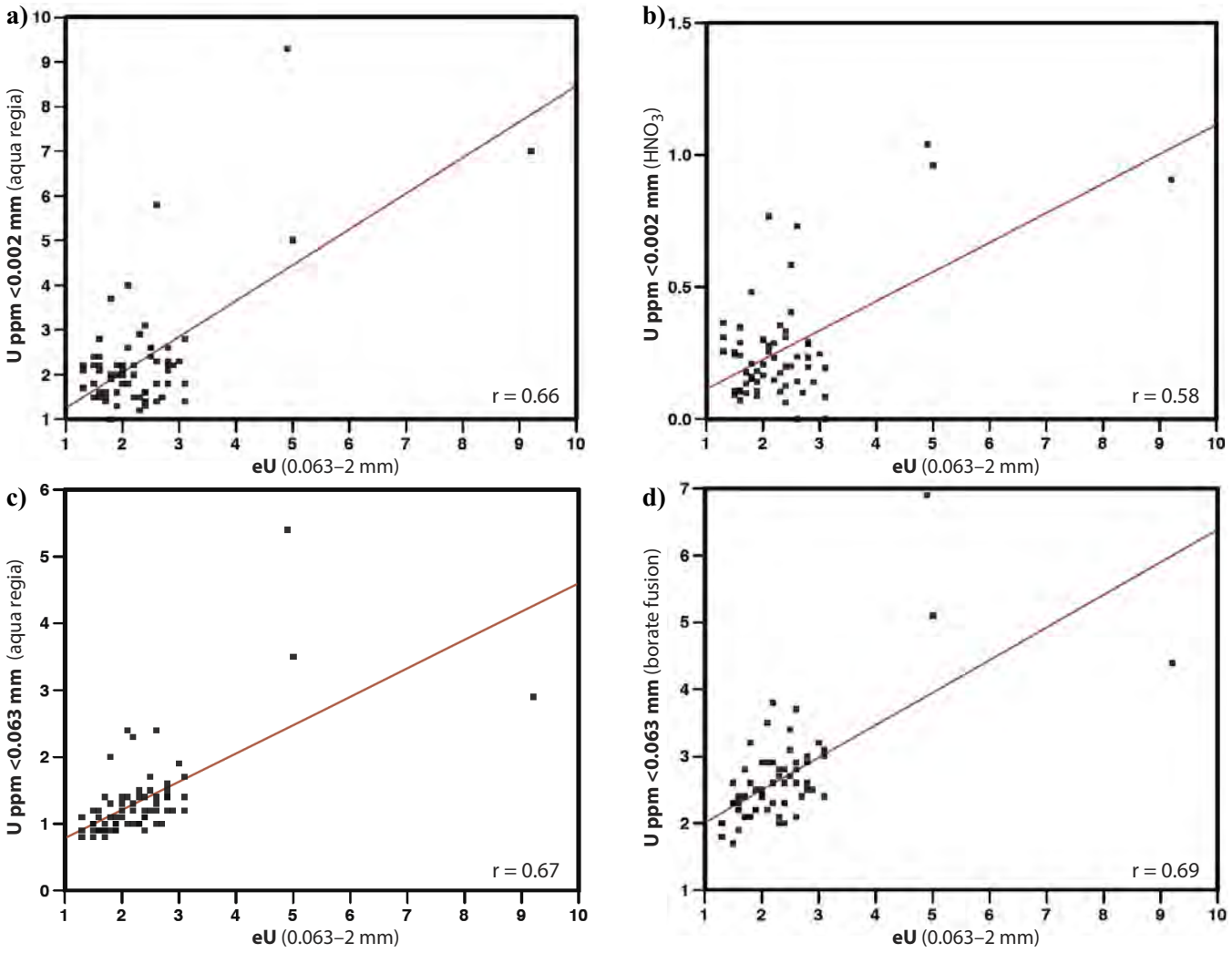

Figure 16. Equivalent U (eU) value in the 0.063–2.0 mm fraction of the till matrix): eU value compared to the U content in the <0.002 mm fraction of the till matrix determined by **(a)** aqua regia digestion and **(b)** weak acid leach digestion; eU value compared to U content in the <0.063 mm fraction of the till matrix determined by **(c)** aqua regia and **(d)** borate fusion digestion.

Formation nearby, tills in this area are dominated by metagreywacke.

The abundance of Pitz Formation porphyritic rhyolite clasts demonstrates a more random spatial distribution. This is likely attributed to the exotic nature of this lithology as the nearest bedrock source is >30 km to south-southeast of the KMZ. Sample 10-PTA-048, which was collected 18 km to the southeast of the Kiggavik deposits, has the highest abundance of Pitz Formation clasts (21%). The presence of Pitz Formation clasts in the tills of the study area is clear evidence of a strong northwest ice-flow that transported these pebbles from a moderately distant bedrock source.

The distribution of intrusive rock pebbles is instructive for new geological mapping (Fig. 3). The two till samples with the highest total abundance of granitoid intrusive rocks are located proximal to and distal from the KMZ (samples 10-PTA-112 and 10-PTA-048, respectively). The great quantity of intrusive rock pebbles in sample 10-PTA-112, which was collected near the KMZ, may be attributed to abundant outcrop of Hudson granitoid sills in the area (Fig. 3). Sample 10-PTA-048 was collected down-ice of the 2.6 Ga granodiorite to monzogranite Judge Sissons pluton and also down-ice of the Nutaaq syenite. The Nutaaq syenite is tentatively considered to be part of the 1.75 Ga Kivalliq Igneous Suite (Fig. 3; Peterson et al., in prep) and consists of distinctive plugs of Hudson monzogranite in the Granite Grid area (Scott, 2012) and characterized by abundant gossanous pyrite. Till samples collected over the Thelon Formation have relatively low numbers of intrusive pebbles, however the persistence of such phases in sandstone-dominated till is a strong indicator of the magnitude of the northwest-trending ice flow.

Granitoid gneiss clasts have a relatively uniform distribution in till across the study area, with the highest abundance being in sample 10-PTA-120 (Appendix

Table 8. Pebble lithological analysis of 21 till samples, listed by % abundance. Total counts are listed in Appendix H.

Sample	Granitoid Gneiss	Intrusive (no meta fabric; includes diabase)	Metasediment (greenstone / metavolcanic)	Thelon Sandstone	Paleo Pro Quartzite	Quartz Vein	Pitz Volcanic	Pitz with Quartz Veins	Fe Fm	Other
10-PTA-037	1.9	7.4	61.3	11.0	6.0	3.8	8.5	0.0	0.0	0.0
10-PTA-048	5.8	27.1	24.5	17.1	1.9	2.3	21.3	0.0	0.0	0.0
10-PTA-066	1.7	10.1	43.1	27.7	6.4	2.3	8.7	0.0	0.0	0.0
10-PTA-074	5.1	9.9	39.8	23.2	2.7	3.3	16.0	0.0	0.0	0.0
10-PTA-079	5.2	12.2	35.4	25.9	2.4	2.4	16.5	0.0	0.0	0.0
10-PTA-083	1.7	9.2	29.4	28.7	4.3	4.0	22.8	0.0	0.0	0.0
10-PTA-085	8.0	14.1	34.8	21.0	6.9	2.8	12.2	0.0	0.3	0.0
10-PTA-087	1.3	7.7	51.0	24.3	5.3	2.3	7.7	0.0	0.0	0.3
10-PTA-093	2.4	11.7	45.5	22.1	3.4	1.6	13.2	0.0	0.0	0.0
10-PTA-095	2.9	7.5	45.6	34.3	2.1	1.9	5.6	0.0	0.0	0.0
10-PTA-096	2.9	13.6	39.6	19.8	2.9	3.1	18.1	0.0	0.0	0.0
10-PTA-108	3.0	12.8	41.0	24.6	1.6	5.2	11.8	0.0	0.0	0.0
10-PTA-109	2.1	3.0	41.9	39.2	4.3	4.9	4.6	0.0	0.0	0.0
10-PTA-112	2.0	27.7	36.7	23.1	2.9	1.4	6.1	0.0	0.0	0.0
10-PTA-113	3.1	8.9	37.6	28.7	2.1	2.1	17.1	0.0	0.3	0.0
10-PTA-115	11.3	7.4	53.3	5.6	2.2	1.9	18.3	0.0	0.0	0.0
10-PTA-116	4.2	16.2	64.5	5.1	2.2	1.7	6.1	0.0	0.0	0.0
10-PTA-117	4.0	7.5	69.6	10.2	1.9	0.5	5.4	0.0	0.0	0.8
10-PTA-120	21.0	5.6	21.9	20.3	14.7	1.9	13.3	0.5	0.9	0.0
10-PTA-134	3.7	13.4	27.8	29.2	4.3	3.4	17.8	0.4	0.0	0.0
10-PTA-135	4.1	8.5	47.5	21.6	3.8	4.6	9.6	0.3	0.0	0.0

Note: Paleo Pro = Paleoproterozoic; Fe Fm = iron formation.

H1). The location of sample 10-PTA-120 is distal from any high-grade metamorphic source, thus the high gneiss content of this sample can likely be attributed to strong northwest-trending ice flow. Quartzite clast distribution also illustrates the dominance of northwest-trending flow as till samples from northwest of the ridges of quartzite bedrock have higher abundances than those collected to the southeast.

DISCUSSION

The geochemistry of till sampled directly overlying, down-ice, and up-ice of the Kiggavik U deposit incorporates the geochemical signatures of multiple bedrock types. This variability in geochemistry can be attributed to the complex bedrock geology of the study area. Another contributing factor is the impact of the migration of the Keewatin Ice Divide, which was prominent within the Schultz Lake map area during the last glaciation (Aylsworth and Shilts, 1989; McMartin et al., 2006). The texture of till at Kiggavik is variable: 43–80% sand, 20–54% silt, and 0.2–6.9% clay. This wide range in texture was also observed by McMartin et al. (2006), yet the samples collected over the Schultz Lake survey area were considerably finer, with an average composition of 48% sand, 47% silt, and 5% clay. Inorganic carbon contents of the till matrix was reported as 0 wt.% C with Ca values below 0.45 wt.% Ca. This reflects the paucity of carbonate bedrock units in the Kiggavik camp and indeed within the Schultz Lake map area (Figs. 2, 3).

Comparing the LGRS data of the sand fraction with K and Th content in the <0.063 mm fraction as analyzed ICP–MS after an aqua regia digestion reveals both similarities and differences. Overall, both methods illustrate a generally elevated K and Th content in proximity to the Kiggavik deposit. Of significance is that K values, on average, are 18 times higher when determined by LGRS, and have a correlation coefficient of 0.48 between the two methods. This variability could potentially be a result of K being concentrated in the coarser fraction of the till. Conversely, Th values are about the same in both data sets as both eTh and Th (ICP-MS aqua regia) have average content of 9.8 and 9.3 ppm, respectively, with a correlation coefficient of 0.68. Equivalent uranium and U contents in the <0.063 mm fraction of till analyzed by aqua regia digestion have very similar distribution trends as eTh and Th. eTh values and U, determined by varying digestion methods and size fractions, show similar trends (Fig 16). However, some local differences are also apparent. For example, the aqua regia ICP-MS data for several samples distal from the deposit have elevated K and Th that are not apparent in the LGRS data.

Till colour

The most prominent colour of surface till within this

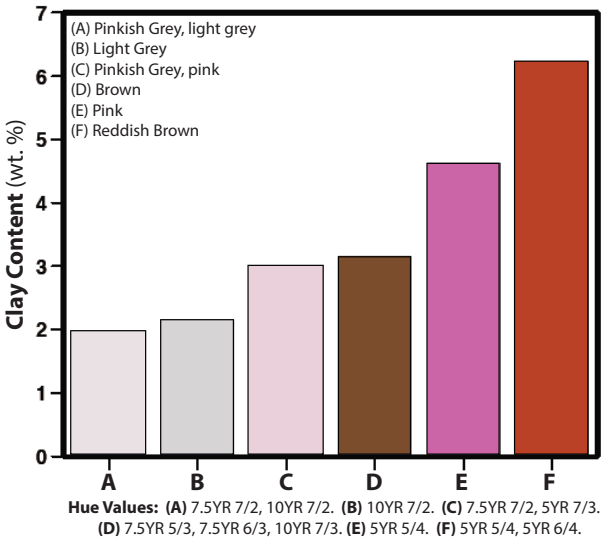

Figure 17. Dry till matrix Munsell hue colour versus clay content (wt.%) illustrating that tills with a red or pink hue are, in general, more clay-rich.

study area is a pink-grey to light grey (Munsell hue of 7.5YR to 10YR, Fig 6). Till sampled in topographic lows or areas of thicker drift typically has a red hue in comparison to samples collected in areas of thin till veneer. In general, tills displaying a pink to reddish hue (5YR 7/3, 5YR 6/3, 2.5YR 5/4) have higher clay content (Fig. 17). Till with a reddish hue was reported by Kaszycki and Shilts (1980) over the Keewatin region and contained clasts of Dubawnt Supergroup. Similar observations were made by McMartin et al. (2006), who reported that till to the southwest of the Thelon River and northwest of Schultz Lake commonly had a reddish to pinkish matrix, reflecting the incorporation of red Dubawnt Supergroup clasts. Pebble counts for this project reveal similar trends to those noted by Kaszycki and Shilts (1980) and McMartin et al. (2006): samples having a reddish hue also had, on average, a higher content of red Pitz volcanic rocks and Thelon Formation clasts. Furthermore, McMartin et al. (2006) noted that till in the Schultz Lake map area with an olive-brown to grey-brown colour was more dominant beyond the margins of the Dubawnt Supergroup dispersal trains and likely reflects supracrustal and/or intrusive rocks. The dominant colour of the majority of surface till samples collected in this study around the Kiggavik deposit is light grey, a result of Neoarchean supracrustal rocks of the Woodburn Group located to the west and northwest of the study area (Fig 6).

Till geochemistry

The Kiggavik U deposits are dominated by primary uraninite and coffinite, with an extensive list of accessory minerals and secondary uranophane (Table 1). This mineralogy is reflected in the geochemistry of the till around Kiggavik in both the <0.063 mm and <0.002 mm size fractions. Based on the geochemical correlations, the till pathfinder elements for the Kiggavik U deposit include U, Au, Mo, Ag, Bi, Cu, Co, W, Pb, and Cs. These elements show a dispersal pattern of at least 1 km, trending to the west and northwest of the KMZ. The highest abundances of these pathfinder elements are in sample 10-PTA-117, which was collected immediately over the KMZ where element contents are one to two orders of magnitude greater than the median. Platinum, Pd, B, Hg, and Te contents are high in sample 10-PTA-117, yet are at background or below detection in all other till samples. Due to the point-source nature of Pt, Pd, B, Hg, and Te, and because these elements are not elevated in distal till samples, they cannot be considered effective exploration pathfinder elements.

Gold, Ag, and Bi have similar spatial distribution trends as U. These elements have higher concentrations in proximity to the deposit and are also elevated in samples 10-PTA-089, 10-PTA-035, 10-PTA-036, and 10-PTA-037, which were collected to the west of the KMZ (Figs. 3, 6a). Copper, Cs, and Mo show higher contents at distances of <1 km from the KMZ, and are background to only slightly elevated at distances of >1 km. Cobalt and Pb also have trends similar to U, i.e., their contents are elevated close to the KMZ and close to the Granite Grid prospect. The dispersal pattern of Co extends beyond 1 km west of the KMZ to approximately 2.5 km to the west. No Ni-bearing minerals have been reported from Kiggavik (e.g. Reyx, 1994; Weyer et al., 1987); however, Ni has been reported as a common pathfinder element in the Athabasca Basin and Co-Ni sulphur arsenide occurs in the polymetallic ores (Jefferson et al., 2007; Campbell, 2009). Nickel is relatively elevated near the Kiggavik deposit and in sample 10-PTA-089; however, the cumulative probability statistics for Ni show a regular distribution, with no samples being truly anomalous. While elevated Ti contents reflect the high amount of rutile at the Kiggavik deposit, its genetic association with the ore at Kiggavik cannot be proven (Table 1). Rutile has been dated as Nueltin (Scott et al., 2010, in prep.) and should not be utilized as a pathfinder element except as a possible indicator of earlier metasomatism associated with the 1.75 Ga Kivalliq Igneous Suite (Peterson et al., in prep.).

Samples 10-PTA-035, -036, -037, and -089

Anomalously high (>90th percentile) and elevated (75–90th percentile) metal contents occur in samples 10-PTA-035, -036, -037, and -089. These tills samples were collected 50 m apart in a northwest-southeast line, proximal to a small outcrop of metagreywacke that had been reported as having elevated counts per second (CPS) of gamma-ray radiation using a handheld gamma-ray detector (P. Wollenberg, pers. comm., 2010). Geochemical analysis revealed that these till

samples have elevated metal trends similar to samples collected close to the KMZ. These samples (10-PTA-035, -036, -037, and -089) are from within 400 m west of the Granite Grid U prospect (Fig. 6a), which is likely the provenance of their metal content and not the KMZ, which is ~6.5 km up-ice to the east. Sample 10-PTA-089, collected ~1.4 km to the east of Granite Grid prospect and 2.2 km to the northwest of the Bong deposit, has elevated and even anomalous contents of U and pathfinder elements (Fig. 3).

Geochemical variability with grain size

To determine if elemental content varies with size fractions of the till at the KMZ, both the <0.063 and <0.002 mm fractions were chemically analyzed. Seventy samples (sample 10-PTA-117 excluded) analyzed by ICP-MS after an aqua regia digestion (30 g for <0.063 mm, 0.5 g for <0.002 mm) had U content 1.9x higher in the <0.002 mm fraction than in the <0.063 mm fraction. Elements of interest, such as Au, Ag, Bi, Cu, Co, Cs, Mo, Ni, Pb, and Ti, also have greater content in the <0.002 mm fraction; only W has greater content in the <0.063 mm fraction (Figs. 18, 19).

Previous studies of U in sediment in the District of Keewatin (Klassen and Shilts, 1977a; Dilabio, 1979; Klassen, 1995) also reported U content was greater in the <0.002 mm fraction. Similar findings were also reported in several studies in Finland. Bjorklund (1975), noted that the U content in till was 20% higher in the <0.006 mm fraction compared to the 0.025 mm fraction. Simpson and Sopuck (1983) also reported that U had preferentially partitioned to the clay fraction by a ratio of 10:1. Unlike the studies conducted around Kiggavik, the sediment tested from Finland had been exposed to constant interaction with water and surficial weathering and the higher U content in the finer fractions can be largely attributed to metal adsorption onto phyllosilicates and/or absorption into the structure of phyllosilicates (Klassen and Shilts, 1977b; Shilts, 1995) as a consequence of the high cation exchange capacity of clays (Brady and Weil, 2008). However, at the Kiggavik camp, U does not have a correlation (R=0.12) with the amount of clay in the till sample, illustrating that elevated U values in the <0.002 mm fraction reflect the overall fine-grained nature of the ore and greater concentrations are not created by the scavenging of remobilized U onto phyllosilicates in clay.

The contents of Cs, Co, Ni, and Ag in the <0.063 mm till fraction are strongly correlated with the total clay content. After normalization to the <0.063 mm data set (aqua regia, ICP-MS), some samples are no longer anomalous or even elevated. For example, till samples 10-PTA-074 and 10-PTA-086 have the highest clay contents of the sample suite at 6.9 and 6.6 wt.%, respectively (mean clay content is 2.5 wt %), and both have anomalous to elevated contents of elements with high clay correlation coefficients. These two samples are distal from the KMZ and all other known occurrences and therefore likely do not represent true till geochemical anomalies.

Lead isotope ratios in till

Pb contents coupled with Pb isotopic ratios can be used to document glacial dispersal from mineral deposits and to delineate till provenance. Previously, Pb isotope ratios in till have been used to explore for base metals, particularly volcanogenic massive sulfide (VMS) deposits (Bell and Franklin, 1993; Bell and Murton 1995; Hussein et al., 2003). These authors noted that glaciogenic material proximal to and down-ice of VMS deposits was characterized by $^{206}Pb/^{204}Pb$ ratios lower than material up-ice or distal from the VMS deposits. VMS deposits are characterized by very low U contents, and thus are depleted in radiogenic ^{206}Pb compared to common ^{204}Pb. The Pb isotopic signature for uranium deposits is different from that for VMS, as U in large quantities decays to enrich ^{206}Pb and ^{207}Pb relative to ^{204}Pb (Gulson, 1986). Therefore, the analysis of the $^{206}Pb/^{204}Pb$ ratio is applicable to the Kiggavik camp because till samples with high $^{206}Pb/^{204}Pb$ ratios signify that the Pb is radiogenic.

Sample 10-PTA-117 displays exponentially high $^{206}Pb/^{204}Pb$ and $^{207}Pb/^{204}Pb$ as well as low $^{207}Pb/^{206}Pb$ ratios relative to the remainder of the sample suite. Excluding sample 10-PTA-117 as a statistical outlier, samples 10-PTA-115, -116, and -047 all have $^{206}Pb/^{204}Pb$ ratios >20 and can be considered elevated for the Proterozoic host rocks at Kiggavik. Sample 10-PTA-124, with a $^{206}Pb/^{204}Pb$ ratio of 23.1, is considered to be anomalously high, given that the host rocks and U mineralization at Kiggavik are comparable in age to the Athabasca Basin systems. Anomalously high $^{206}Pb/^{204}Pb$ ratios for rocks of similar age are generally attributed to be >30 (Holk et al., 2003); only sample (10-PTA-117: $^{206}Pb/^{204}Pb$=215) had a value above this threshold. However, when taking in to consideration the cumulative probability plots, the samples listed above are classified as elevated to anomalous. All of these samples are elevated relative to the average present-day $^{206}Pb/^{204}Pb$ ratios for continental crust of similar age (source rock), which have ratio values between 18.6 and 18.9 (Allegre et al., 1988). Samples with elevated or anomalous $^{206}Pb/^{204}Pb$ ratios are also represented by low $^{207}Pb/^{206}Pb$ ratios.

To determine if the till has undergone mixing, an isotopic ratio can be plotted against the abundance of any element, oxide, or nuclide (Hussein et al., 2003). If till was mixed, samples with higher Pb contents would have lower ^{206}Pb values (Bell and Murton, 1995; Hussein et al., 2003). On the other hand, if no mixing

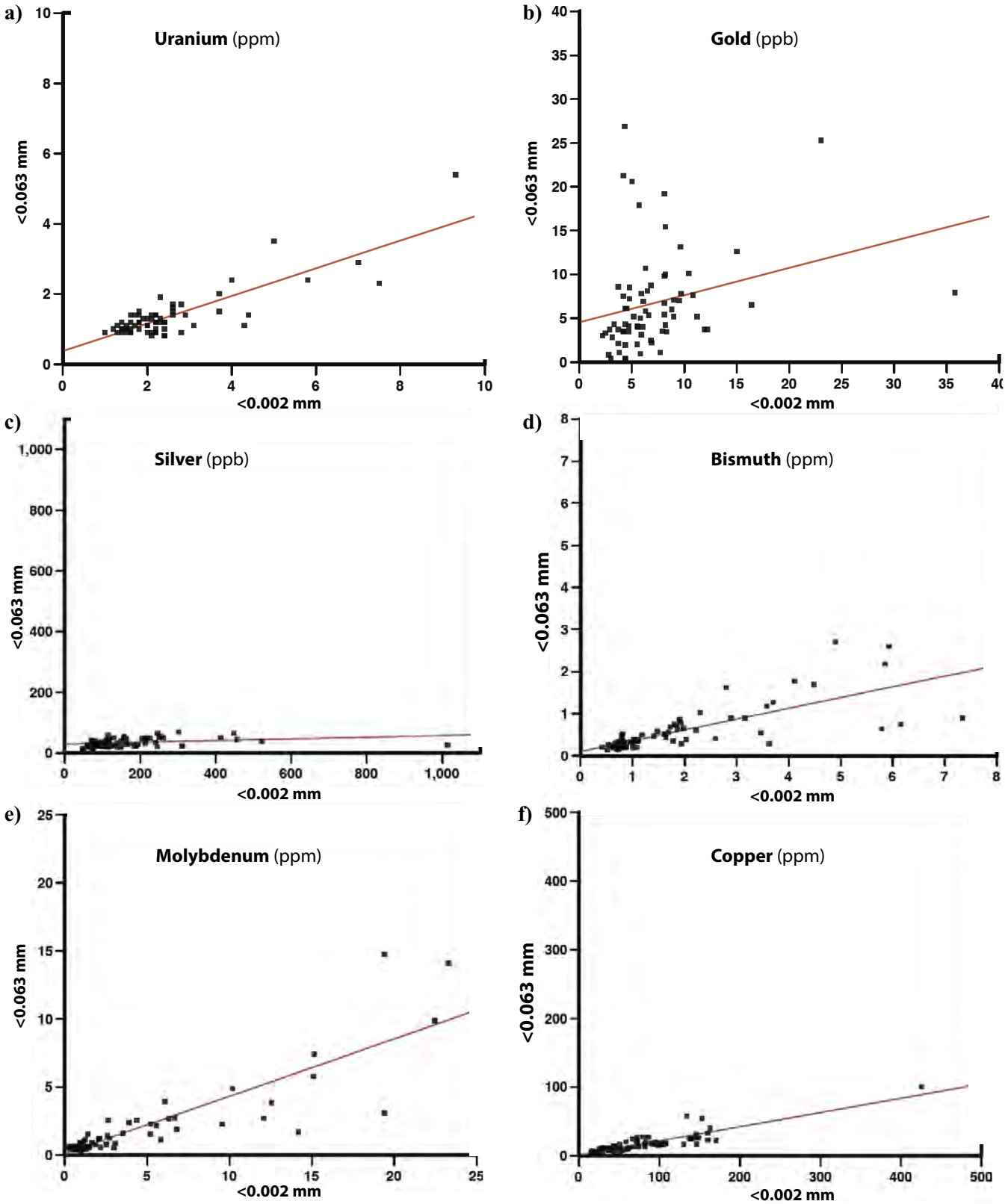

Figure 18. Geochemical relationship between the <0.063 and <0.002 mm fractions of the till matrix for **(a)** U, **(b)** Au, **(c)** Ag, **(d)** Bi, **(e)** Mo, and **(f)** Cu. In general, the <0.002 mm fraction contains higher contents of these elements.

of till took place and only one provenance possible, samples would display similar isotopic Pb to total Pb values. Figure 20 does show a moderate negative correlation (R=-0.68) between the $^{206}Pb/^{204}Pb$ ratio and total Pb, suggesting that the dominant lead source was not radiogenic and, despite the fact that the Kiggavik

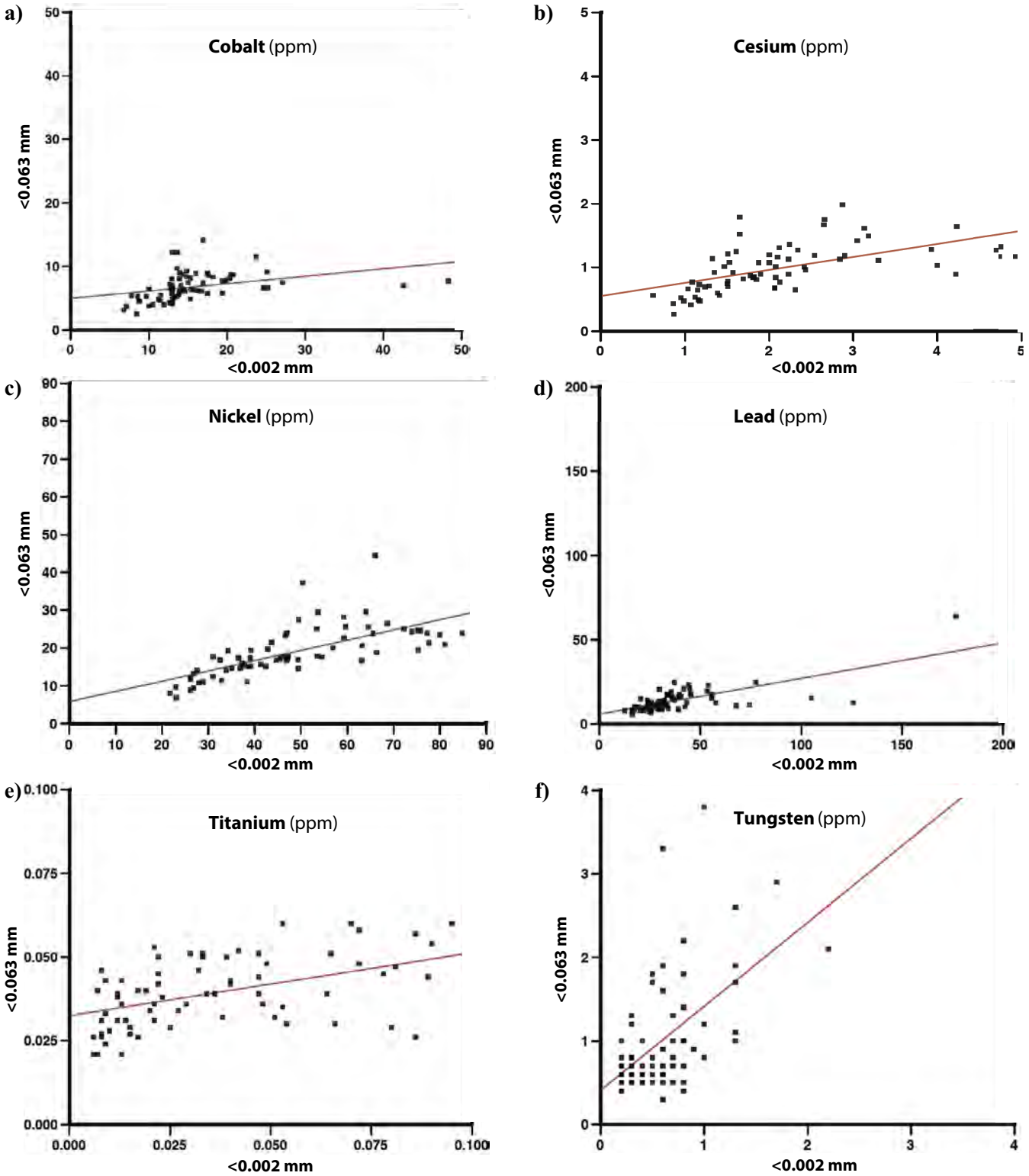

Figure 19. Geochemical relationship between the <0.063 and <0.002 mm fractions of the till matrix for **(a)** Co, **(b)** Cs, **(c)** Ni, **(d)** Pb, **(e)** Ti, and **(f)** W. In general, the <0.002 mm fraction contains greater concentrations of these elements, with the exception of W.

deposits have experienced multiple ice-flow trajectories, there is no measurable effect of provenance mixing.

Thorium is strongly depleted in unconformity-associated uranium deposits because it is not easily transported by hydrothermal fluids with the chemistry and temperature proposed for creation of these deposits. In contrast, paleoplacer U deposits can contain elevated Th content, since the magmatic Th was transported along with U as detrital minerals (Cuney and Kyser,

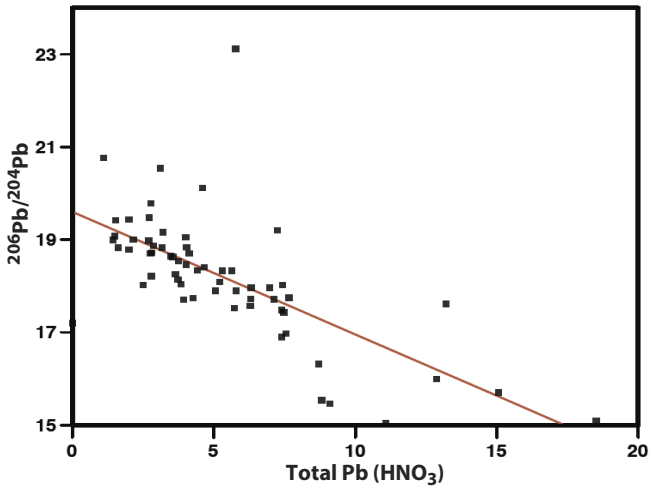

Figure 20. $^{206}Pb/^{204}Pb$ ratio versus Pb concentration of the till matrix determined by weak acid leach digestion (0.5 g HNO_3).

2009). To recognize this depletion, Pb isotopes, derived from Th and U, are compared by plotting $^{208}Pb/^{204}Pb$ versus $^{206}Pb/^{204}Pb$ (Fig. 21). As high levels of ^{206}Pb suggest elevated U content, a lower $^{206}Pb/^{204}Pb$ ratio and a higher $^{208}Pb/^{204}Pb$ ratio would suggest that the material is either distal from the unconformity-associated ore deposit and/or includes detritus from a magmatic source rock that includes Th. In this study, a cluster of samples with higher $^{208}Pb/^{204}Pb$ ratios were collected on average 5 km further from the KMZ than a cluster with the inverse. Gulson and Mizon (1980) observed higher $^{206}Pb/^{204}Pb$ ratios proximal to the unconformity-associated U Jabiluka orebodies in the Northern Territory of Australia. The authors also found that $^{208}Pb/^{206}Pb$ ratios did not increase with increasing $^{206}Pb/^{204}Pb$ ratios. The present study does show a positive correlation between $^{208}Pb/^{206}Pb$ and $^{206}Pb/^{204}Pb$. Therefore, two different isotopic sources of U and Th are recorded in till samples of the Kiggavik camp. The cluster of samples with high $^{208}Pb/^{204}Pb$ ratios is on average from much further from the deposit and is located on the Thelon Formation bedrock map unit (red group, Fig. 21). These samples also incorporate higher proportions of Thelon Formation sandstone relative to the cluster of samples that are from closer to the deposit (blue group, Fig. 21). The proximal cluster contains a greater abundance of Neoarchean metagreywacke clasts. Sample 10-PTA-116 is particularly interesting because it was collected within 100 m of the KMZ, yet is isotopically similar to the distal samples. Samples 10-PTA-115 and 10-PTA-116 were collected from the same frost boil; however, sample 10-PTA-115 was taken closer to surface than sample 10-PTA-116. The $^{206/204}$ Pb ratio for these two samples is identical, as are their anomalous U contents. However, sample 10-PTA-116 has a higher $^{208}Pb/^{206}Pb$ ratio, which likely reflects the regional till signature as the sample was collected deeper within the frost boil.

Glacial transport

The Kiggavik area was affected by four major stages of ice flow, the net effect of each playing a significant cumulative role on the dispersal of the geochemical signature of the deposit. Samples with elevated U and its associated pathfinder elements occur to the west, northwest, and north-northwest of the KMZ. A distinct dispersal pattern of metallic elements was not defined by this study. The highest concentrations of all pathfinder elements are located within 250 m of the KMZ, with weaker concentrations (slightly elevated) being found up to 1 km down-ice from the deposit. A previous regional till sample survey, with a sample interval of 10 km in the Schultz Lake region did not show any samples with anomalous U concentrations (McMartin et al., 2006). Dilabio (1979) reported that U and its associated pathfinder elements, which might have formed a dispersal train, were not detected at 1.6 km sample spacing.

Samples containing elevated pathfinder elements occur to the west, northwest, and north-northwest of the KMZ. However, the highest pathfinder element concentrations were in samples proximal (<250 m) to and just west of the KMZ. These samples also have elevated to anomalously high $^{206}Pb/^{204}Pb$ and $^{207}Pb/^{204}Pb$ values. Furthermore, the highest eU values were also in till samples collected directly west of the deposit. Although landforms and striae show that the northwest ice-flow was the most dominant in the

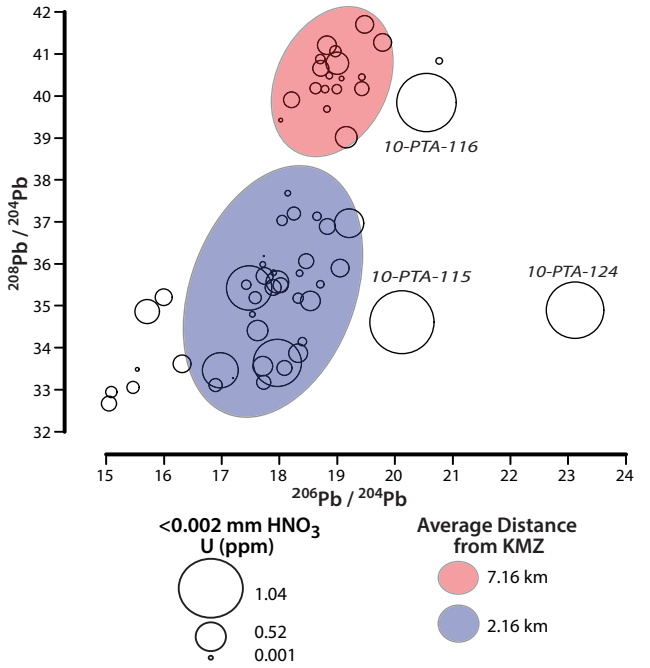

Figure 21. $^{208}Pb/^{204}Pb$ versus $^{206}Pb/^{204}Pb$ showing related U contents determined by weak acid leach digestion (0.5 g HNO_3). Two clusters separate distal and proximal samples suggesting different till provenances. The samples highlighted in blue are on average closer to the deposit and have greater U contents.

Table 9. Comparison of pathfinder element signatures and dispersal extent from a number of studies that reported till geochemical patterns for U deposits and associated showings.

Study	Pathfinder Elements	Dispersal Extent
Kiggavik[1]	U, Au, Ag, Bi, Cu, Mo, Co, Cs, Pb, W	1 km
Granite Grid[1]	U, Au, Ag, Bi, Cu, Mo, Co, V	300 m
Paukkanjanvaara[2]	U	900 m
Duddridge Lake[3]	U, Cu, Ni	1 km
Keewatin[4]	U, Mo, Pb, Cu	1–1.5 km
Midwest[5]	U	1800 m
Cluff Lake[6]	U, As, B, V	250 m

[1]This study; [2]Bjorklund, 1975; [3]Haughton, 1976; [4]DiLabio, 1979; [5]Simpson and Sopuck, 1983; [6]Wilson, 1985.

region (Aylsworth and Shilts, 1989; McMartin et al., 2006), the surface till proximal to the KMZ is composed predominantly of a grey till derived from the Woodburn Group supracrustal rocks to the east of the KMZ and was deposited by west-trending ice-flow. Samples that were taken immediately to the northwest and north-northwest of the KMZ are not as metal-rich as those west of the KMZ, as the earlier and possibly a later ice-flow event likely diluted or masked the westerly transported till geochemical signature. The colour of the till samples is a strong indicator of provenance, with red tills being of an exotic nature, reflecting derivation from the Baker Lake Basin at least 50 km to the southeast. The high abundance of Dubawnt Supergroup clasts that were deposited by the earlier southeast, northwest, and north-northwest ice-flows diluted the metal concentrations (Klassen, 1995; McMartin et al., 2006). As a consequence, these exotic tills are not the ideal sample medium to retrieve geochemical signatures of U deposits like Kiggavik.

Till geochemical signatures and comparison to other studies

Drift prospecting for U deposits has been documented in many studies of boulder train prospecting (e.g. Earle, 2001). While detailed studies observing till geochemistry adjacent to U deposits are not widely available, previous till geochemical studies have reported patterns from U showings and their geochemical signatures (e.g. Bjorklund, 1975; Haughton, 1976; Dilabio, 1979; Simpson and Sopuck, 1983; Wilson, 1985; Campbell, 2009). Table 9 compares pathfinder elements reported by previous studies to those observed in the Kiggavik camp. Uranium is the best element for detecting bedrock with U mineralization and Cu, Mo, Ni, Pb, B, and V are also pathfinder elements but to a lesser degree. These pathfinder elements are similar to those listed by Campbell (2009), who comments that U is the best pathfinder element as well as Ni, Cu, Pb, Co, As, V, and REEs. Elements not discussed in other studies but of interest at Kiggavik are Au, Ag, and Bi, which are shown to have high correlations with U in till at both the KMZ and near the Granite Grid. Combined, these elements reflect the mineralogy of the Kiggavik deposits as we know it, likely related to the interaction of the mineralizing fluids with the Neoarchean metagreywacke and the Nueltin Granite (Scott, in prep.). This mineralogical association or parts of it may or may not be applicable to U deposits outside of the Kiggavik camp; such applications would require site-specific studies such as this.

CONCLUSIONS

The Kiggavik region has experienced four different phases of ice-flow, two of which were the dominant erosion and transport events. The older northwest- and younger west-trending ice-flows have dispersed the geochemical signature of the Kiggavik Main Zone (KMZ) 1 km down-ice. The geochemical signature of the KMZ is strongest within 250 m of the deposit, forming an irregular dispersal fan. Samples that contain the highest metal values were collected directly west of the deposit and are characterized by locally derived grey till that visibly contrasts with, and stratigraphically overlies, the regional red till that was derived from the Dubawnt Supergroup in the Baker Lake Basin, 50 km to the southeast.

This study has found that till at the Kiggavik U deposit has a polymetallic geochemical signature. The useful pathfinder elements for exploring for U in this region are U, Bi, Mo, Ag, Au, Cs, Co, and W, as determined using both 30 g and 0.5 g aliquots by aqua regia on both the <0.063 mm and <0.002 mm fractions, respectively. These pathfinder elements are also present in samples taken down-ice of other U showings within the Kiggavik camp, demonstrating their applicability for exploration of basement-hosted U deposits around the Thelon Basin. Several elements (Te, Re, Pd, Pt, and B), although highly anomalous in sample 10-PTA-117 collected immediately above the KMZ, have low content or are below detection limit in samples collected further away, limiting their use as pathfinder elements. There is a possibility that material entrained from both the CZ and EZ deposits, located up-ice, could be mixing with the geochemical signature of the KMZ, however this is unlikely as they are located >600 m from the KMZ.

Pathfinder elements in the Kiggavik camp show strong positive correlations between the <0.063 mm and <0.002 mm fractions of the till matrix. However,

elemental contents are significantly greater in the finer fraction of material, indicating their occurrence in the fine fraction of metal-rich bedrock. Analyzing the <0.002 mm fraction is recommended because it is more useful for detecting subtle geochemical trends.

Laboratory gamma-ray spectrometry and Pb isotope ratios in the till matrix are shown to be successful exploration tools because elevated eU and $^{206}Pb/^{204}Pb$ ratios are both strongly correlated with geochemically determined elemental U contents in till. It was also observed that the clay mineralogy of samples with elevated to anomalous U is enriched in illite and kaolinite relative to quartz.

The till geochemical dispersal train from the KMZ does not exceed 1 km and could be easily missed in a regional-scale till sampling survey. It is essential to preface a regional till geochemical survey for U exploration with a smaller 25–100 m scale orientation survey to calibrate and characterize dispersal trains around individual known deposits.

ACKNOWLEDGEMENTS

Funding for this project was provided under the Geomapping for Energy and Minerals (GEM) Program (2008-2013) as part of the Tri-Territorial Indicator Mineral Project (M.B. McClenaghan and R.C. Paulen), and this study was closely coordinated with the GEM Uranium Project (C. Jefferson). AREVA Resources Canada is thanked for providing access, logistical support, confidential geological information, and rock samples from the Kiggavik deposits. The authors would also like to express our thanks to Matthew Pyne (GSC) for his help in the collection of till samples at the Kiggavik deposit. Isabelle McMartin (GSC) is also thanked for her input and regional knowledge with the Schultz Lake surficial geology and for access to literature that was helpful to this project. Anna Hicken (Queen's University) is also thanked for her help with ARCMAP GIS and geochemical discussions. Lastly, the authors would like to thank Eric Potter for his review and edits of this report.

REFERENCES

Allegre, C.J., Lewin, E., and Dupre, B., 1988. A coherent crust-mantle model for the uranium-thorium-lead isotopic system; Chemical Geology, v. 70, p. 211–234.

Anand, A., Jefferson, C.W., Chorlton, L.B., and Buenviaje, R., in prep. Structural geology of faults and shear zones in the region around the Kiggavik uranium camp, Nunavut; Geological Survey of Canada, Preliminary Canadian Geoscience Map, scale 1:50,000, 1 sheet.

Averill, S.A., 1988. Regional variations in the gold content of till in Canada, *In* Prospecting in Areas of Glaciated Terrain – 1988, (eds.) D.R. MacDonald and K.A. Mills; Canadian Institute of Mining and Metallurgy, p. 271–284.

Aylsworth, J.M. and Shilts, W.W., 1989. Glacial features around the Keewatin Ice Divide: Districts of Mackenzie and Keewatin; Geological Survey of Canada, Paper 88-24, 21 p.

Aylsworth, J.M., Cunningham, C.M., and Shilts, W.W., 1990. Surficial geology, Schultz Lake, District of Keewatin, Northwest Territories; Geological Survey of Canada, Map 43-1989, scale 1:125 000.

Beak Consultants Limited, 1988. Project concept description of the Kiggavik (Lone Gull) Uranium mine, Summary Report; Urangesellschaft Canada Limited, Beak Reference 2305.3, 43 p.

Bell, K. and Franklin, J.M., 1993. Application of lead isotopes to mineral exploration in glaciated terrains; Geology, v. 21, p. 1143–1146.

Bell, K. and Murton, J.B., 1995. A new indicator of glacial dispersal: lead isotopes; Quaternary Science Reviews, v. 14, p. 275–287.

Berthet, L., 2011. Technical report on resource estimation Andrew Lake Deposit Kiggavik Area, Nunavut; AREVA report number BGM/DS/SER RT 11/015, 78 p. plus appendix.

Berthet, L. and Osorio, J-C., 2011a. Technical report on resources Main Zone Deposit Kiggavik area, Nunavut; AREVA report number BGM/DS/SER RT 11/016, 73 p. plus appendices.

Berthet, L. and Osorio, J-C., 2011b. Technical report on resources Centre Zone Deposit Kiggavik area, Nunavut; AREVA report number BGM/DS/SER RT 11/017, 63 p. plus appendices.

Bjorklund, A., 1975. The use of till in geochemical uranium exploration, *In* Exploration for Uranium Ore Deposits - 1976; International Atomic Energy Agency, Vienna, p. 241–266.

Bostock, H.S., 1970. Physiographic regions of Canada; Geological Survey of Canada, Map 1254A, scale 1:5,000,000.

Brady, N.C. and Weil, R.R., 2008. The Nature and Properties of Soils, 14th edition; Pearson Education Incorporated, Upper Saddle River, N.J.

Campbell, J.E., 2009. Drift prospecting for uranium in the Athabasca Basin, Saskatchewan, *In* Application of Till and Stream Sediment Heavy Mineral and Geochemical Methods to Mineral Exploration in Western and Northern Canada, (eds.) R.C. Paulen and I. McMartin; Geological Association of Canada, GAC Short Course Notes 18, p. 207–214.

Campbell, R. and Clark, M., 2009. Kiggavik-Sissons updated technical report 2007/2008, prepared for AREVA Resources Canada; SRK Consulting Canada Incorporated, SRK Project Number 1CA015.003.

Cumming, G.L. and Richards, J.R., 1975. Ore lead isotope ratios in a continuously changing earth; Earth and Planetary Science Letters, v. 28, p. 155–171.

Cunningham, C.M. and Shilts, W.W., 1977. Surficial geology of the Baker Lake area, District of Keewatin; Geological Survey of Canada, Report on Activities, Paper 77-1B, p. 311–314.

Cuney, M. and Kyser, K. (eds.), 2009. Recent and Not-So-Recent Developments in Uranium Deposits and Implications for Exploration; Mineralogical Association of Canada, Short Course Series 39, 257 p.

Cuney, M., 2010. Evolution of uranium fractionation processes through time: driving the secular variation of uranium deposit types; Economic Geology, v. 105, p. 553–569.

Dilabio, R.N.W., 1979. Drift prospecting in uranium and base-metal mineralization sites, District of Keewatin, Northwest Territories, Canada, *In* Prospecting in Areas of Glaciated Terrain – 1979, (ed.) M.J. Jones; The Institution of Mining and Metallurgy, Dublin, Ireland, p. 91–100.

Donaldson, J.A., 1965. The Dubawnt Group, districts of Keewatin and Mackenzie; Geological Survey of Canada, Paper 64-20, p. 11.

Dredge, L.A., McMartin, I., and Ford, K., 2005. Till geochemistry, gamma ray spectrometry and gold grain counts, Wager Bay,

Mainland Nunavut (NTS 56G); Geological Survey of Canada, Open File 5014, 184 p.

Dyke, A.S., 2004. An outline of North American deglaciation with emphasis on central and northern Canada, *In* Quaternary Glaciations; Extent and Chronology Part II – 2004, (eds.) K. Ehlers and P.L. Gibbard; Elsevier, Amsterdam, p. 373–424.

Dyke, A.S. and Prest, V.K., 1987. Late Wisconsinan and Holocene history of the Laurentide Ice Sheet; Géographie physique et Quaternaire, v. 41, p. 237–263.

Dyke, A.S., Andrews, J.T., Clark, P.U., England, J.H., Miller, G.H., Shaw, J., and Veillette, J.J., 2002. The Laurentide and Innuitian ice sheets during the last glacial maximum; Quaternary Science Reviews, v. 21, p. 9–31.

Earle, S., 2001. Application of composite glacial boulder geochemistry to exploration for unconformity-type uranium deposits in the Athabasca Basin, Saskatchewan, Canada, *In* Drift Exploration in Glaciated Terrain, (eds.) M.B. McClenaghan, P.T. Bobrowsky, G.E.M. Hall, and S.J. Cook; Geological Society, London, Special Publication 185, p. 225–235.

Ford, K., Harris, J.R., Shives, R., Carson, J., and Buckle, J., 2008. Gamma-ray spectrometry, Chapter 4 *In* Remote Predictive Mapping: An Aid for Northern Mapping, (eds.) J. R. Harris; Geological Survey of Canada, Open File 5643, p. 53–97.

Friske, P.W.B., Ford, K.L., Kettles, I.M., McCurdy, M.W., McNeil, R.J., and Harvey, B.A., 2010. North America Soil Geochemical Landscape Project: Canadian field protocols for collecting mineral soils and measuring soil gas radon and natural radioactivity; Geological Survey of Canada, Open File 6282, 175 p.

Friske, P.W.B., Ford, K.L., and McNeil, R.J., 2012. Soil geochemical, mineralogical, radon and gamma ray spectrometric radiometric data from the 2007 North American Soil Geochemical Landscapes Project in New Brunswick, Nova Scotia and Prince Edward Island; Geological Survey of Canada, Open File 6433.

Fuchs, H.D. and Hilger, W., 1989. Kiggavik (Lone Gull): An unconformity related uranium deposit in the Thelon Basin, Northwest Territories, Canada, *In* Uranium Resources and Geology of North America, (ed.) E. Muller-Kahle; International Atomic Energy Agency-TECDOC-500, p. 429–454.

Fuchs, H.D., Hilger, W., and Prosser, E., 1985. Geology and exploration history of the Lone Gull property, *In* Uranium Deposits of Canada, (ed.) E.L. Evans; Canadian Institute of Mining and Metallurgy, Special Volume 33, p. 286–292.

Girard, I., Klassen, R.A., and Laframboise, R.R., 2004. Sedimentology laboratory manual, Terrain Sciences Division; Geological Survey of Canada, Open File 4823, 134 p.

Griep J., 1978. Final report on diamond drilling programme, Lone Gull Lake: NTS area 66-A-5; Urangellschaft Assessment Report.

Griep, J., Hesse, B.P., Hilger, W., and Prosser, E., 1980. Annual report on exploration and drilling, Baker Lake area, Lone Gull Project; Urangesellschaft Canada Limited, 127 p.

Gulson, B.L., 1986. Lead isotopes in mineral exploration; Elsevier, Developments in Economic Geology, v. 23.

Gulson, B.L. and Mizon, K.J., 1980. Lead isotope studies at Jabiluka, *In* Uranium in the Pine Creek Geosyncline: Proceedings of the International Uranium Symposium on the Pine Creek Geosyncline, (eds.) J. Ferguson, A.B. Golby, and J.C. Rowntree; Institute of Earth Resources (Australia), *In*ternational Atomic Energy Agency, p. 439–455.

Haughton, D.R., 1976. A multiple media geochemical survey of a boulder train associated with the Duddridge Lake uranium deposit, Saskatchewan, *In* Uranium in Saskatchewan: Proceedings, (ed.) C.E. Dunn; Saskatchewan Geological Society, Special Publication No. 3, p. 256–295.

Holk G., Kyser, T.K., Chipley, D., Hiatt, E., and Marlatt, J., 2003. Mobile Pb-isotopes in Proterozoic sedimentary basins as guides for exploration of uranium deposits; Journal of Geochemical Exploration, v. 80, p. 297–320.

Hussein, A.A., Lochner, C., and Bell, K., 2003. Application of Pb isotopes to mineral exploration in the Halfmile Lake area, Bathurst, New Brunswick; Economic Geology, v. 11. p. 679–688.

Jefferson, C.W., Thomas, D.J., Gandhi, S.S., Ramaekers, P., Delaney, G., Brisbin, D., Cutts, C., Quirt, D., Portella, P., and Olson, R.A., 2007. Unconformity-associated uranium deposits of the Athabasca Basin, Saskatchewan and Alberta, *In* Mineral Deposits of Canada: A Synthesis of Major Deposit Types, District Metallogeny, the Evolution of Geological Provinces, and Exploration Methods, (ed.) W.D. Goodfellow; Geological Association of Canada, Mineral Deposits Division, Special Publication No. 5, p. 273–305.

Jefferson, C.W., Chorlton, L.B., Pehrsson, S.J., Peterson, T., Wollenberg, P., Scott, J., Tschirhart, V., McEwan, B., Bethune, K., Calhoun, L., White, J.C., Leblon, B., LaRocque, A., Shelat, Y., Lentz, D., Patterson, J., Riegler, T., Skulski, T., Robinson, S., Paulen, R., McClenaghan, B., Layton-Matthews, D., MacIsaac, D., Riemer, W., Stieber, C., and Tschirhart, P., 2011a. Northeast Thelon Region: geomapping for uranium in Nunavut; Geological Survey of Canada, Open File 6862, Power Point Presentation, 38 slides. doi:10.4095/289037

Jefferson, C.W., Hunter, R., McLaren, M., Peterson, T., Skulski, T., Rainbird, R., Young, G.M., Gandhi, S.S., and Costello, K., 2011b. Northeastern Thelon Basin uranium region: geological compilation for geophysical consortium planning; Geological Survey of Canada, Open File 6950. doi:10.4095/288801

Jefferson, C.W., Pehrsson, S., Peterson, T., Chorlton, L., Davis, W., Keating, P., Gandhi, S., Fortin, R., Buckle, J., Miles, W., Rainbird, R., LeCheminant, A., Tschirhart, V., Tschirhart, P., Morris, W., Scott, J., Cousens, B., McEwan, B., Bethune, K., Riemer, W., Calhoun, L., White, J., MacIsaac, D., Leblon, B., Lentz, D., LaRocque, A., Shelat, Y., Patterson, J., Enright, A., Stieber, C., Riegler, T., 2011c. Northeast Thelon region geoscience framework - new maps and data for uranium in Nunavut; Geological Survey of Canada, Open File 6949. doi:10.4095/288791

Jefferson, C.W., Peterson, T., Tschirhart, V., Davis, W., Scott, J.M.J., Reid, K., Ramaekers, P., Gandhi, S.S., Bleeker, W., Pehrsson, S., Morris, W.A., Fayek, M., Potter, E., Bridge, N., Grunsky, E., Keating, P., Ansdell, K., and Banerjee, N., 2013a. LIPs and Proterozoic uranium (U) deposits of the Canadian Shield; Geological Survey of Canada, Open File 7352, 56 pages + spread sheet. doi:10.4095/292377

Jefferson, C.W., Pehrsson, S., Peterson, T., Wollenberg, P., Riegler, T., McEwan, B., Tschirhart, V., Tschirhart, P., Scott, J., Chorlton, L., Davis, W., Bethune, K., Anand, A., Riemer, W., White, J.C., Patterson, J., and Stieber, C., 2013b. Bedrock geology of the western Marjorie-Tehek supracrustal belt and Northeast Thelon Basin margin in parts of NTS 66A and 66B, Nunavut; Geological Survey of Canada, Open File 7241.

Kaszycki, C.A. and Shilts, W.W., 1980. Glacial erosion of the Canadian Shield – calculation of average depths; Atomic Energy of Canada Limited, Technical Record TR-106.

Kaszycki, C.A., Neilsen, E., and Gobart, G., 1996. Surficial geochemistry and response to volcanic-hosted massive sulphide mineralization in the snow lake region, *In* EXTECH 1: A Multidisciplinary Approach to Massive Sulphide Research in the Rusty Lake-Snow Lake Greenstone Belts, Manitoba, (eds.) G.F. Bonham-Carter, A.G. Galley, and G.E.M. Hall; Geological Survey of Canada, Bulletin 426, p. 139–154.

Klassen, R.A., 1995. Drift composition and glacial dispersal trains, Baker Lake area, District of Keewatin, Northwest Territories; Geological Survey of Canada, Bulletin 485, 68 p.

Klassen, R.A. and Shilts W.W., 1977a. Uranium exploration using till, District of Keewatin; Geological Survey of Canada, Report of Activities, Paper 77-1A, p. 471–477.

Klassen, R.A. and Shilts, W.W., 1977b. Glacial dispersal of uranium in the District of Keewatin, Canada, *In* Prospecting in Areas of Glaciated Terrain - 1977, (eds.) M.J. Jones; The Institution of Mining and Metallurgy, Espoo, Finland, p. 80–88.

Lundqvist, J., 1990. Glacial morphology as an indicator of the direction of glacial transport, *In* Glacial Indicator Tracing, (eds.) R. Kujansuu and M. Saarnisto; A.A. Balkema, Rotterdam, p. 61–70.

Lydon, J.W., 2007. An overview of the economic and geological contexts of Canada's major mineral deposit types, *In* Mineral Deposits of Canada: A Synthesis of Major Deposit Types, District Metallogeny, the Evolution of Geological Provinces, and Exploration Methods, (ed.) W.D. Goodfellow; Geological Association of Canada, Mineral Deposits Division, Special Publication No. 5, p. 3–48.

McClenaghan, M.B., 2001. Regional and local-scale gold grain and till geochemical signatures of the lode Au deposits in the western Abitibi Greenstone Belt, central Canada, *In* Drift Exploration in Glaciated Terrain, (eds.) M.B. McClenaghan, P.T. Bobrowsky, G.E.M. Hall, and S.J. Cook; Geological Society, London, Special Publication 185, p. 201–224.

McConnell, J.W. and Batterson, M.J., 1987. The Strange Lake Zr-Y-Nb-Be-REE deposit, Labrador: a geochemical profile in till, lake and stream sediment, and water; Journal of Geochemical Exploration, v. 29, p. 105–127.

McEwan, B., Bethune, K.M., Riemer, W., and Jefferson, C.W., 2011. Structural style and regional correlation of the Ketyet River and Woodburn Lake groups in the Baker Lake area, Nunavut: New insights into the age and stratigraphic / structural relationships between complexly interfolded Archean and Paleoproterozoic supracrustal sequences of the central Rae Province; NE Thelon Consortium Workshop, McMaster University, Hamilton, Ontario, March 10, 2011 (extended abstract).

McMartin, I. and Campbell, J.E., 2009. Near-surface till sampling protocols in Shield terrain, with examples from western and northern Canada, *In* Application of Till and Stream Sediment Heavy Mineral and Geochemical Methods to Mineral Exploration in Western and Northern Canada, (eds.) R.C. Paulen and I. McMartin; Geological Association of Canada, Short Course Notes 18, p. 75–95.

McMartin, I. and Dredge, L.A., 2005. History of ice flow in the Schultz Lake (NTS 66a) and Wager Bay (NTS 56G) areas, Kivalliq Region, Nunavut; Geological Survey of Canada, Current Research, 2005-B-2, 10 p.

McMartin, I. and Henderson, P.J., 2004. Evidence from Keewatin (central Nunavut) for paleo-ice divide migration; Géographie physique et Quaternaire, v. 58, p. 163–186.

McMartin, I. and McClenaghan, M.B., 2001. Till geochemistry and sampling techniques in glaciated terrain: a review, *In* Drift Exploration in Glaciated Terrain, (eds.) M.B. McClenaghan, P.T. Bobrowsky, G.E.M. Hall, and S. Cook; Geological Society of London, Special Publication 185, p. 83–123.

McMartin, I. and Paulen, R.C., 2009. Ice-flow indicators and the importance of ice-flow mapping for drift prospecting, *In* Application of Till and Stream Sediment Heavy Mineral and Geochemical Methods to Mineral Exploration in Western and Northern Canada, (eds.) R.C. Paulen and I. McMartin; Geological Association of Canada, Short Course Notes 18, p. 15–34.

McMartin I., Dredge L.A., Ford K.L., and Kjarsgaard, I.M., 2006. Till composition, provenance and stratigraphy beneath the Keewatin Ice Divide, Schultz Lake area (NTS 66A), mainland Nunavut; Geological Survey of Canada, Open File 5312, 81 p.

McMartin, I., Dredge, L.A., and Alysworth, J.M., 2007. Surficial geology, Schultz Lake South, NTS 66A-south; Geological Survey of Canada, A-series map 2038A, scale 1:100,000.

Miller, A.R. and LeCheminant, A.N., 1985. Geology and uranium metallogeny of Proterozoic supracrustal successions, central district of Keewatin, N.W.T with comparisons to northern Saskatchewan, *In* Geology of uranium deposit, (eds.) T.I.I. Sibbald and W. Petruk; Canadian Institute of Mining and Metallurgy, Special Volume 32, p. 167–185.

Morrison, D., 2009. Kiggavik-Sissons Project; AREVA Annual Report 2008, Vol I. Report 08-CND-92-02.

Osorio, J-C., 2011. Technical Report on resources End Grid (North Pod) Deposit Kiggavik area, Nunavut; AREVA report number BGM/DS/SER RT 11/018, 62 p. plus appendices

Pacquet, A., 1993. Kiggavik Main Zone; Urangesellschaft Canada Limited, Report 8493, 38 p.

Pagel, M., Michard, A., Juteau, M., and Turpin, L., 1993. Sm–Nd, Pb–Pb, and Rb–Sr systematics of the basement in the Cigar Lake area, Saskatchewan, Canada; Canadian Journal of Earth Sciences, v. 30, p. 731–742.

Parkhill, M. and Doiron, A., 2003. Quaternary geology of the Bathurst Mining Camp and implications for base metal exploration using drift prospecting, *In* Massive Sulfide Deposits of the Bathurst. Mining Camp, New Brunswick, and Northern Maine, (eds.) W.D. Goodfellow, S.R. McCutcheon, and J.M. Peter; Economic Geology, Monograph 11, p. 631–660.

Pehrsson, S., Jefferson, C.W., Peterson, T., Scott, J., Chorlton, L., and Hillary, B., 2010. Basement to the Thelon Basin, Nunavut – revisited; GeoCanada 2010, Calgary, Alberta, May 10–14, 4 p. (extended abstract).

Peterson, T.D., van Breemen, O., Sandeman, H., and Cousens, B., 2002. Proterozoic (1.85–1.75 Ga) igneous suites of the Western Churchill Province: granitoid and ultrapotassic magmatism in a reworked Archean hinterland; Precambrian Research, v. 119, p. 73–100.

Peterson, T.D., Scott, J.M.J., LeCheminant, A.N., Jefferson, C., and Pehrsson, S.J., in prep. The Kivalliq Igneous Suite: anorogenic bimodal magmatism of central Nunavut at 1.75 Ga; Precambrian Research.

Rainbird, R.H., Hadlari, T., Aspler, L.B., Donaldson, J.A., LeCheminant, A.N., and Peterson, T.D., 2003. Sequence stratigraphy and evolution of the Paleoproterozoic intracontinental Baker Lake and Thelon basins, western Churchill Province, Nunavut, Canada; Precambrian Research, v. 125, p. 21–53.

Reilly, B., 1997. Assessment Report for Uranium exploration Activities: 1996 Field Season Diamond Drilling. Cogema Resources Incorporated; Nunavut Assessment Report 083829, 26 p.

Reyx, J., 1994. Petrographic report 8634, Canada, Kiggavik Project; Cogema, unpublished internal report, No. 94-UGC-92-01, 33 p.

Robinson, S.V.J., Paulen, R.C., Jefferson, C.W., Layton-Matthews, D., McClenaghan, M.B., and Joy, B., in prep. Indicator Mineral Signature of the Kiggavik Uranium Deposit, Nunavut.

Russell, R.D. and Allan, D.W., 1955. The age of the earth from lead isotope abundances. Monthly Notices; Royal Astronomical Society, Geophysical Supplement, v. 7, p. 80–101.

Scott, J.M.J., 2012. Paleoproterozoic (1.75 Ga) Granitoid Rocks and Uranium Mineralization in the Baker Lake—Thelon Basin region, Nunavut. M.Sc. thesis, Carleton University, Canada, 136 p.

Scott, J., Peterson, T.D., Jefferson, C.W., and Cousens, B., 2010. Proterozoic (1.85–1.7 Ga) granitoid rocks and uranium in Baker Lake – Thelon Basin region, Nunavut; GeoCanada 2010, Calgary, Alberta, May 10–14, 4 p. (extended abstract).

Scott, J.M.J., Davis, W.J., Peterson, T.D., Jefferson, C.W., and Cousens, B.L., in prep. Petrography, geochemistry and U-Pb (zircon) ages of Paleoproterozoic intrusive rocks, Kiggavik uranium camp, Nunavut.

Shilts, W.W., 1973. Drift Prospecting: Geochemistry of Eskers and Till in Permanently Frozen Terrain, District of Keewatin, Northwest Territories; Geological Survey of Canada, Paper 72-45.

Shilts, W.W., 1978. Nature and genesis of mudboils, central Keewatin, Canada; Canadian Journal of Earth Sciences, v. 15, p. 1053–1068.

Shilts, W.W., 1995. Geochemical partitioning in till, *In* Drift exploration in the Canadian Cordillera, (ed.) P.T. Bobrowsky, S.J. Stibbick, J.M. Newell, and P.F. Matysek; British Columbia Ministry of Energy, Mines, and Petroleum Resources, Paper 1995-2, p. 149–163.

Shilts, W.W. and Cunningham, C.M., 1977. Anomalous uranium concentrations in till north of Baker Lake, District of Keewatin, *In* Report of Activities; Geological Survey of Canada, Paper 77-1B, p. 291–292.

Shilts, W.W. and Klassen, R.A., 1976. Drift prospecting in the District of Keewatin – uranium and base metals, *In* Report of Activities; Geological Survey of Canada, Paper 76-1A, p. 255–257.

Shilts, W.W., Cunningham, C.M., and Kaszycki, C.A., 1979. Keewatin Ice Sheet – Re-evaluation of the traditional concepts of the Laurentide Ice Sheet; Geology, v. 7, p. 537–541.

Simpson, M.A. and Sopuck, V.J., 1983. Till geochemistry near the Midwest uranium deposit, *In* Uranium Exploration in the Athabasca Basin, Saskatchewan, Canada, (ed.) E.M. Cameron; Geological Survey of Canada, Paper 82-11, p. 207–214.

Stea, R.R., Johnson, M., and Hanchar, D., 2009. The geometry of kimberlite indicator mineral dispersal fans in Nunavut, Canada, *In* Application of Till and Stream Sediment Heavy Mineral and Geochemical Methods to Mineral Exploration in Western and Northern Canada, (eds.) R.C. Paulen and I. McMartin; Geological Association of Canada, Short Course Notes 18, p. 1–13.

Stokes, C.R. and Clark, C.D., 2003. The Dubawnt Lake palaeo–ice stream: evidence for dynamic ice sheet behaviour on the Canadian Shield and insights regarding the controls on ice-stream location and vigour; Boreas, v. 32, p. 263–279.

Tyrrell, J.B., 1897. Report on the Dubawnt, Kazan and Ferguson Rivers, and the northwest coast of Hudson Bay; and on two overland routes from Hudson Bay to Lake Winnipeg; Geological Survey of Canada, Annual Report, v. 9, p. 1–218.

Tyrrell, J.B., 1898. The glaciation of north-central Canada; Journal of Geology, v. 6, p. 147–160.

Weyer, H.J., 1992. The Kiggavik uranium deposit, Northwest Territories, Canada; Ph.D. thesis, Rheinish-Westfaelishe Technishe Hochschule Aachen, Germany.

Weyer, H.J., Friedrich, G., Bechtel, A., and Ballhorn, R.K., 1987. The Lone Gull uranium deposit – new geochemical and petrological data as evidence for the nature of the ore bearing solutions; International Atomic Energy Agency, IAEA-TECDOC-542/19, p 293–306.

Wilson, J.S., 1985. Exploration in the Carswell Structure, *In* The Carswell Structure Uranium Deposits, Saskatchewan, (eds.) D. Alonso and M. Svab; Geological Association of Canada, Special Paper 29, p. 175–188.

Wright, G.M., 1955. Geological Notes on central District of Keewatin, Northwest Territories; Geological Survey of Canada, Paper 55-17, 17 p.

APPENDIX A3. Annotated colour photographs of sample and striation sites.

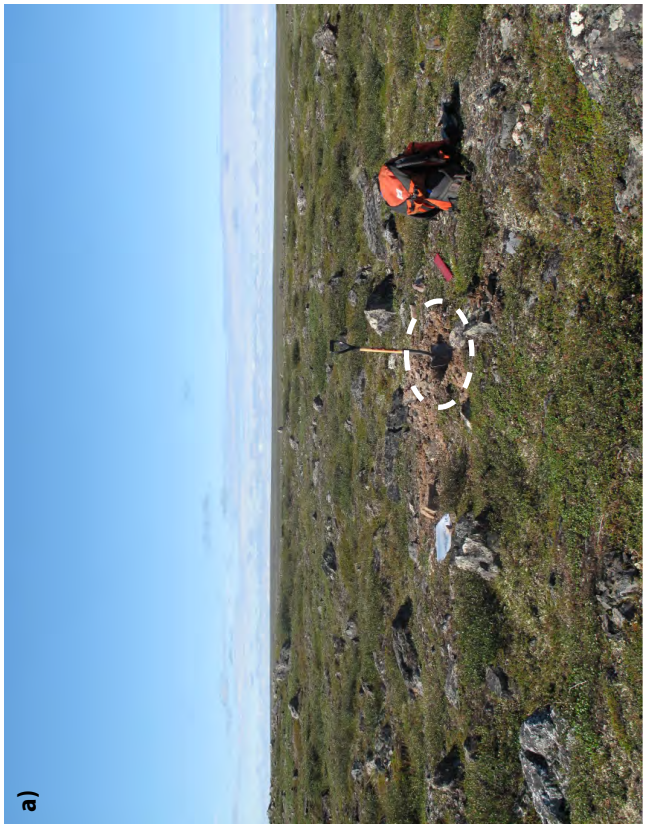

Site 10-PTA-035
a) Overview of the till sample site (shovel for scale).
b) Till sample site, with samples.
c) Overhead view of the sample pit.

APPENDIX A3 continued.

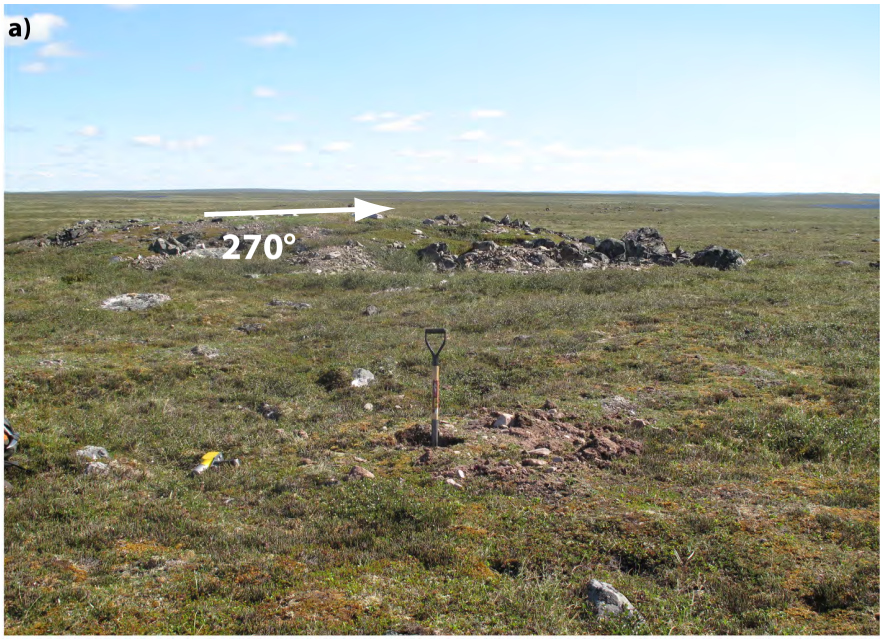

Site 10-PTA-036

a) Overview of till sample site (shovel for scale), with thin till cover and a small bedrock knoll in the background, which has been sculpted to the west.

b) Till sample pit.

c) Striae on exposed bedrock near the sampling site.

APPENDIX A3 continued.

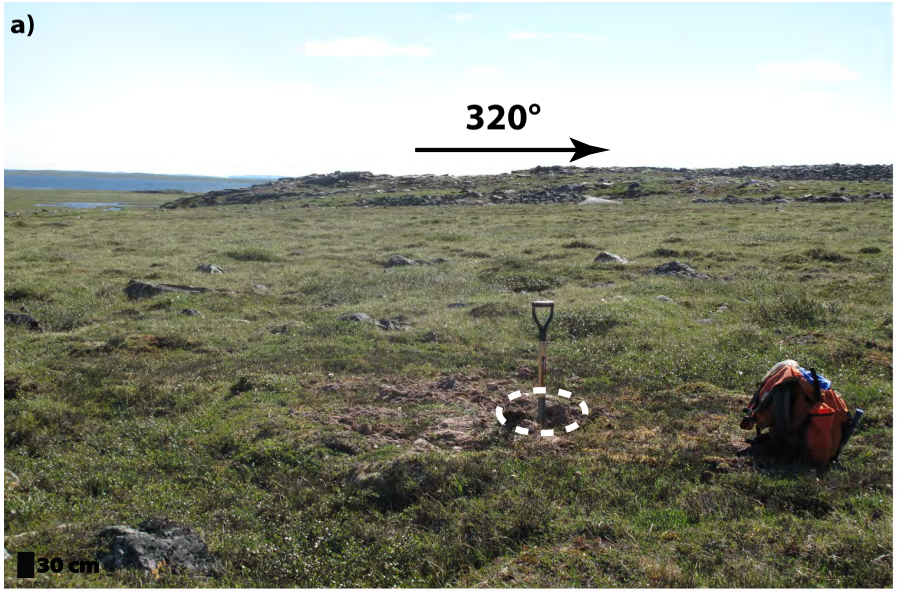

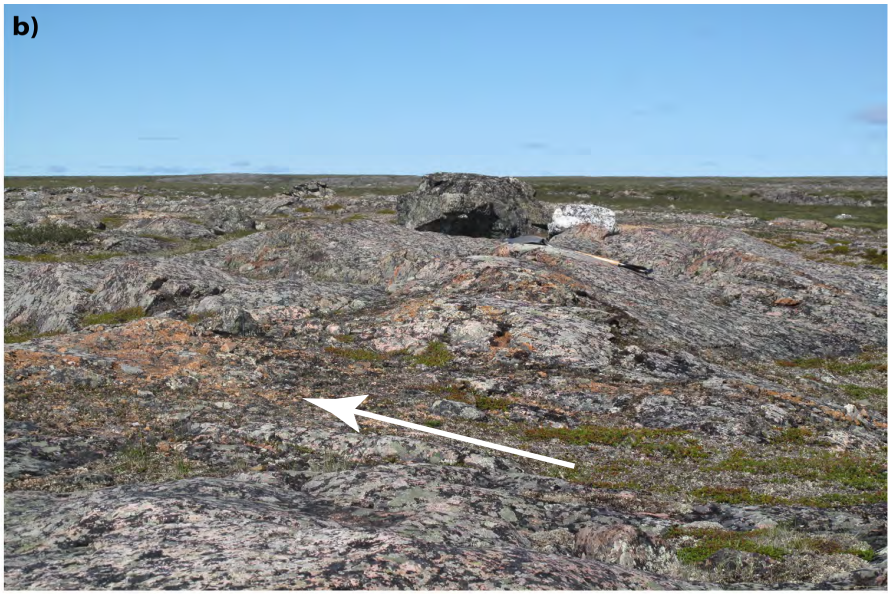

Site 10-PTA-037
a) Overview of the till sample site after the sampling was completed.
b) Scoured granitic bedrock displaying a general ice-flow pattern of 320°, approximately 50 metres west of the sample site.
c) Scoured bedrock displaying glacial grooves oriented 320°.

APPENDIX A3 continued.

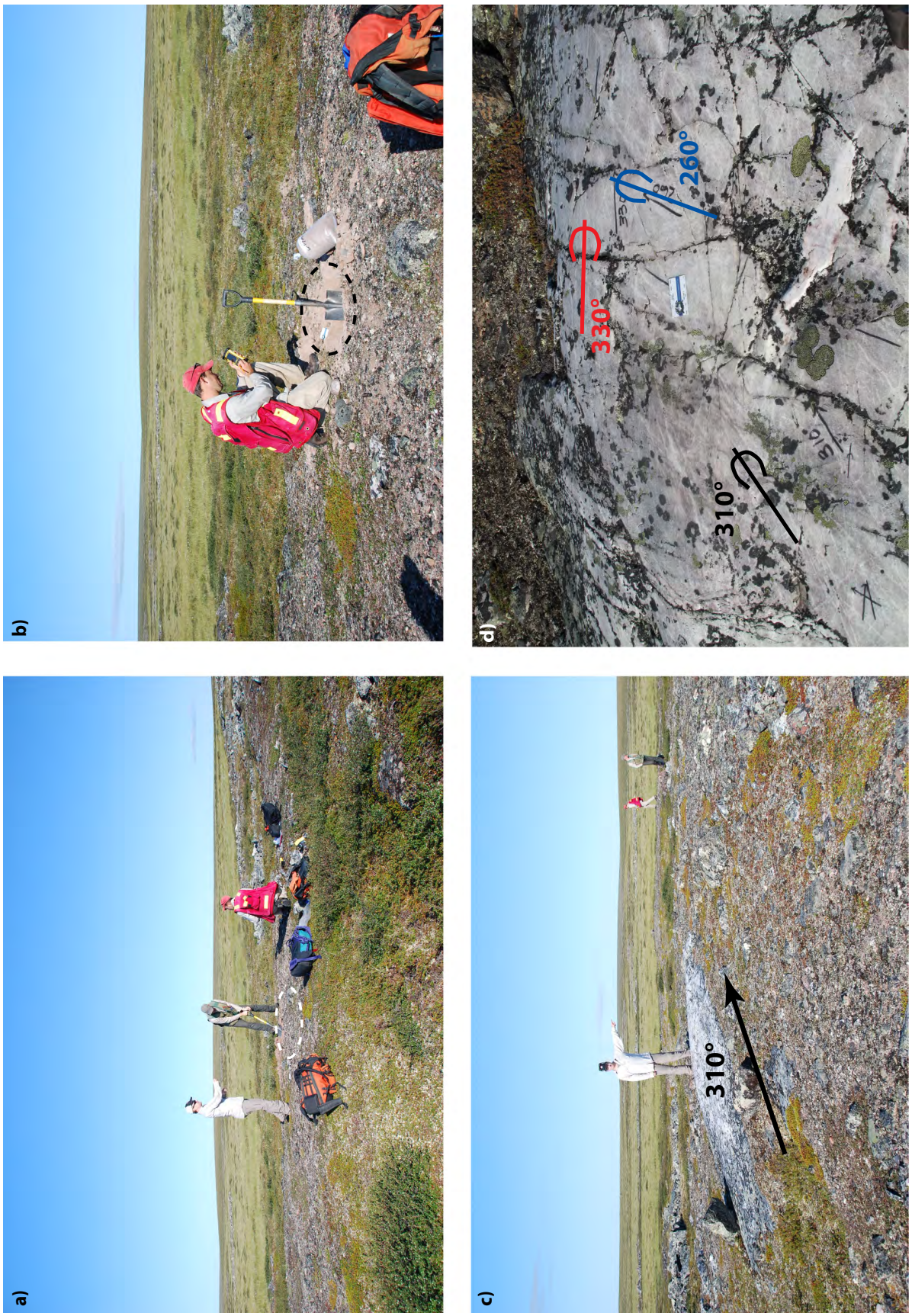

Site 10-PTA-066 a) Overview of the sample site prior to sampling. **b)** Till sample site after sampling was completed. **c)** Scoured quartzite bedrock close to the sampling site showing a dominant ice-flow direction of 310°. **d)** Close-up image of polished quartzite displaying three sets of striae, which trend (from oldest to youngest) 330°, 310°, and 260°.

APPENDIX A3 continued.

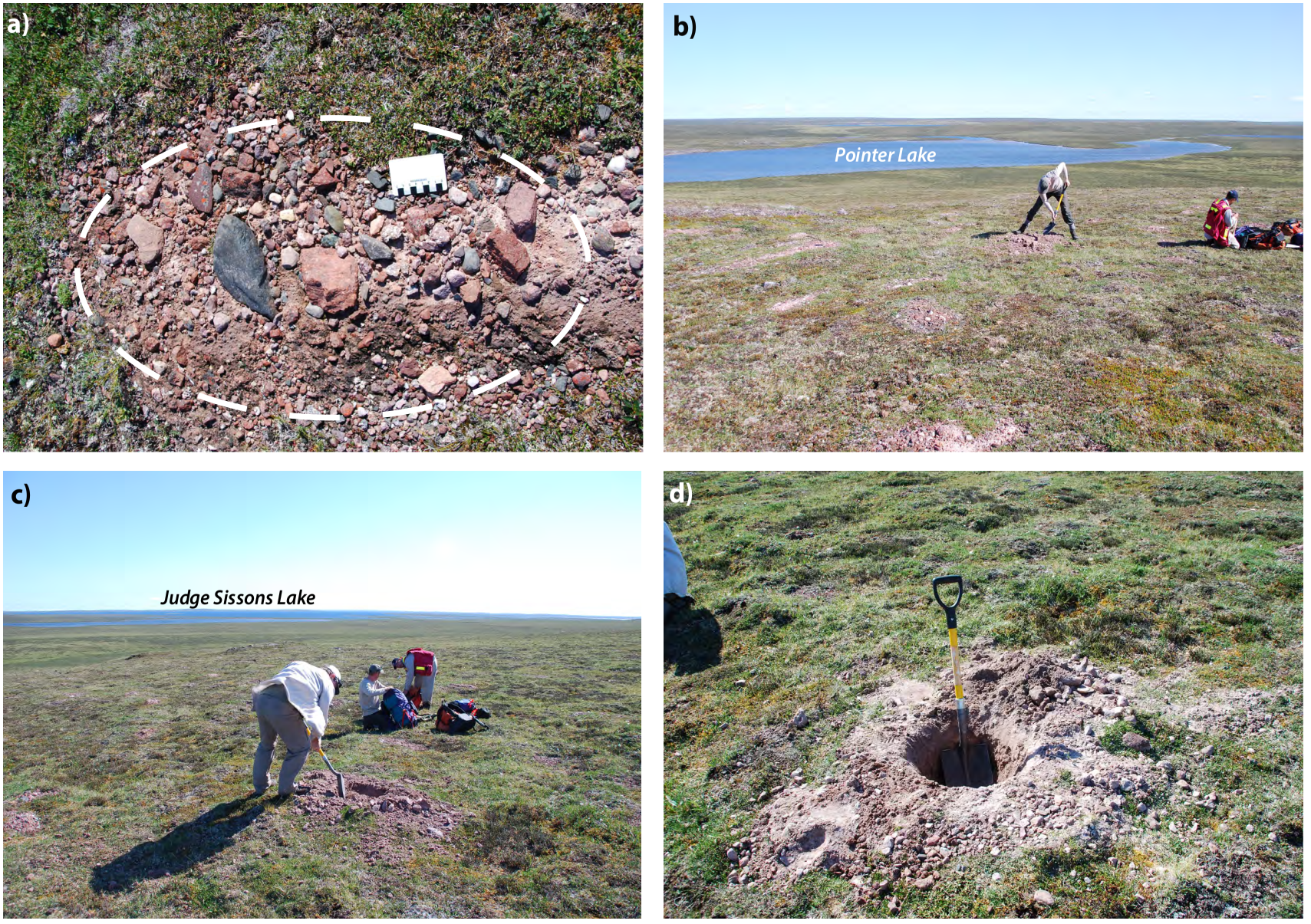

Site 10-PTA-071 a) Close-up of the till sample site prior to sampling (photo card (cm) for scale). Note the abundance of red Pitz Formation clasts. **b)** Overview of the sample site location looking east. **c)** Overview of the sample site location looking south. **d)** Till sample site after the sample was collected (shovel for scale).

APPENDIX A3 continued.

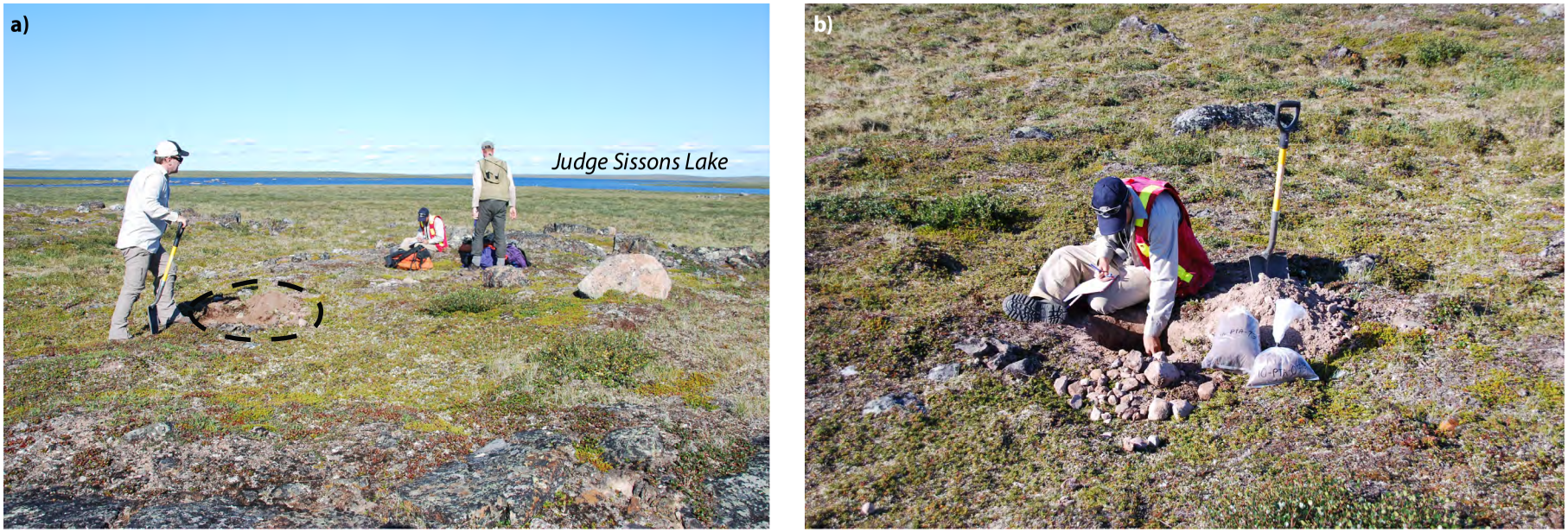

Site 10-PTA-073 a) Overview of the till sample site prior to sampling. **b)** Overview of the till sample site after collecting the sample.

APPENDIX A3 continued.

Site 10-PTA-074

a) Overview of the till sample site prior to sampling (shovel for scale).

b) Bulk (~10 kg) and till geochemistry (~2 kg) samples after completing sampling.

c) View of the side wall of the sample pit and till that was sampled.

APPENDIX A3 continued.

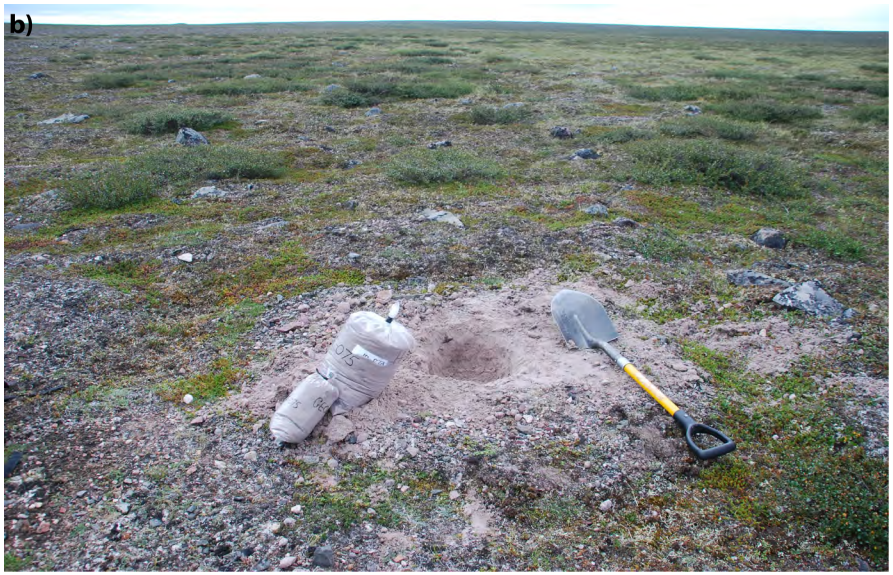

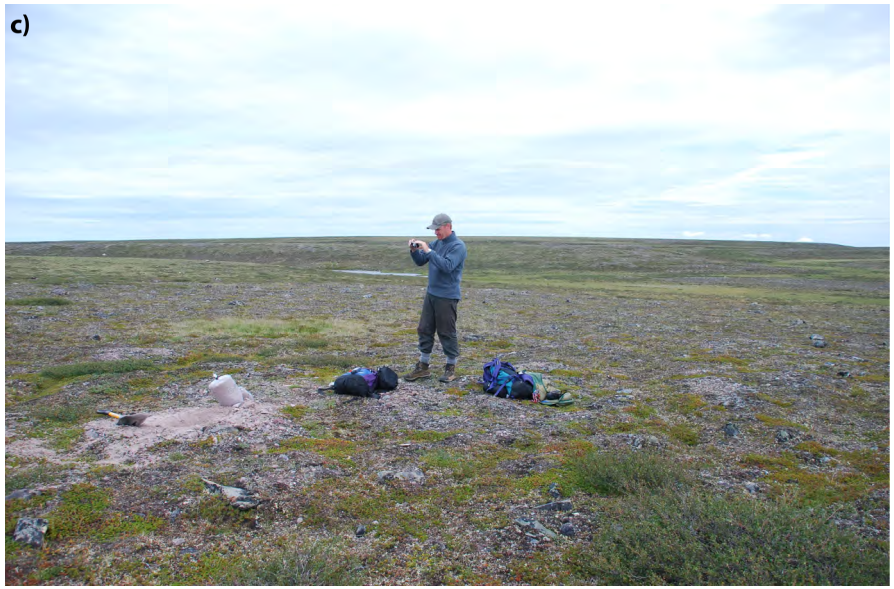

Site-10-PTA-075
a) Overview of the till sample site prior to sampling.
b) Overview of the till sample site after sampling was completed.
c) Till sample location showing tundra environment.

APPENDIX A3 continued.

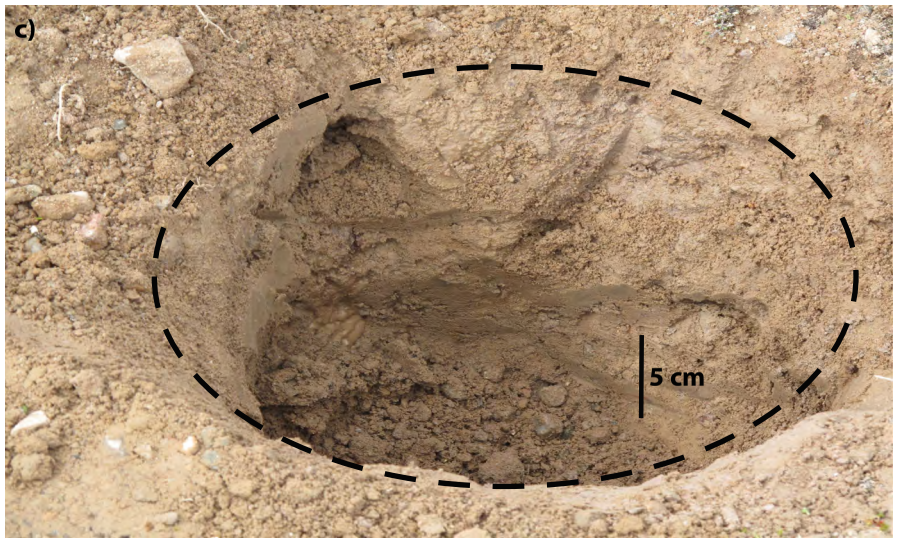

Site 10-PTA-076
a) Overview of the till sample site prior to sampling.
b) Heavy mineral concentrate and till geochemistry samples.
c) Close-up of the beige-brown sandy silty till in the frost boil.

APPENDIX A3 continued.

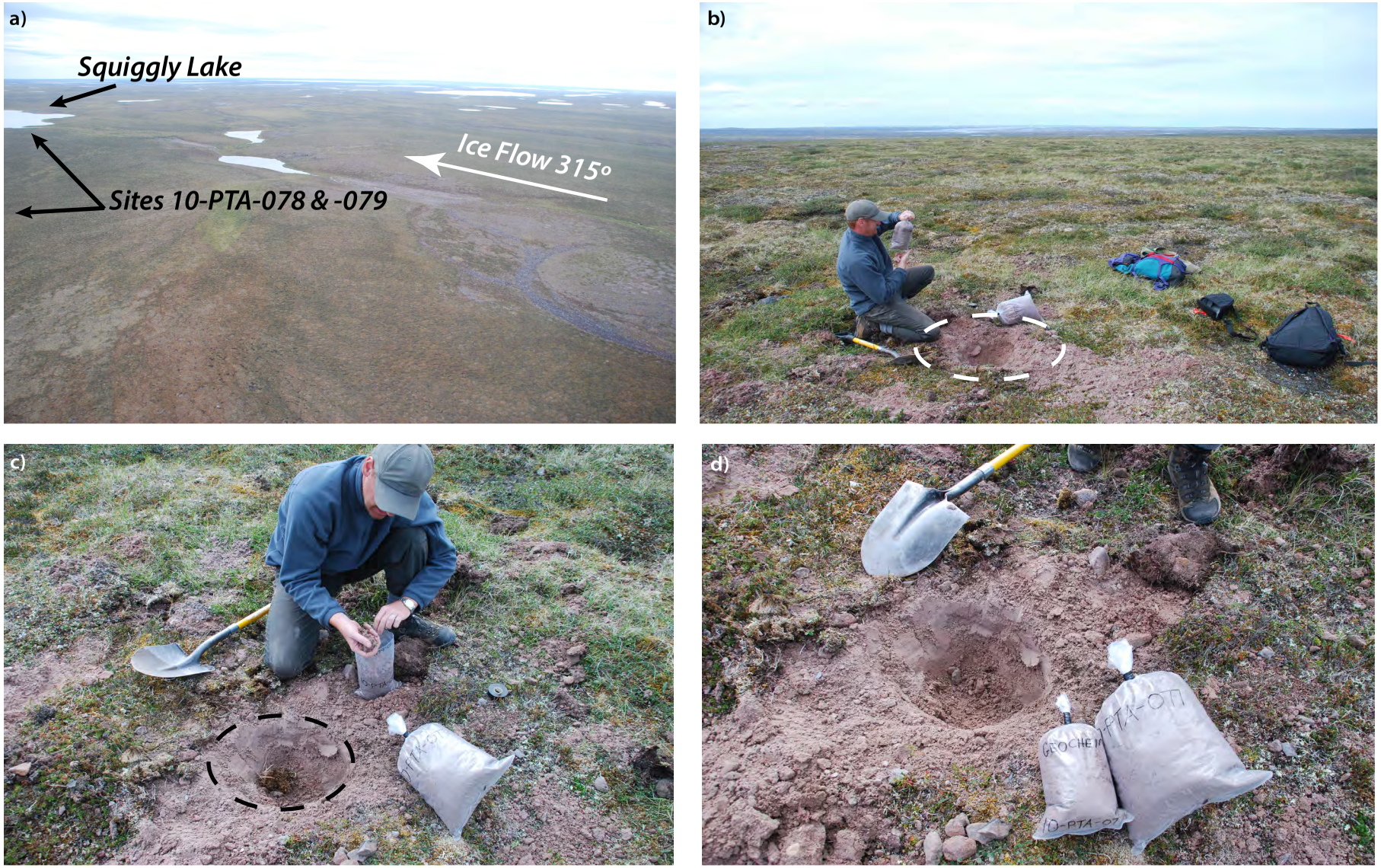

Site 10-PTA-077 a) Aerial view of the 10 km sampling line taken directly prior to sampling 10-PTA-077; view is looking north-northeast. **b)** Overview of the tundra physiography at the sample site. **c)** Collection of the till for heavy mineral concentrate analysis and till geochemistry. **d)** Till sample site overview after sampling was complete.

APPENDIX A3 continued.

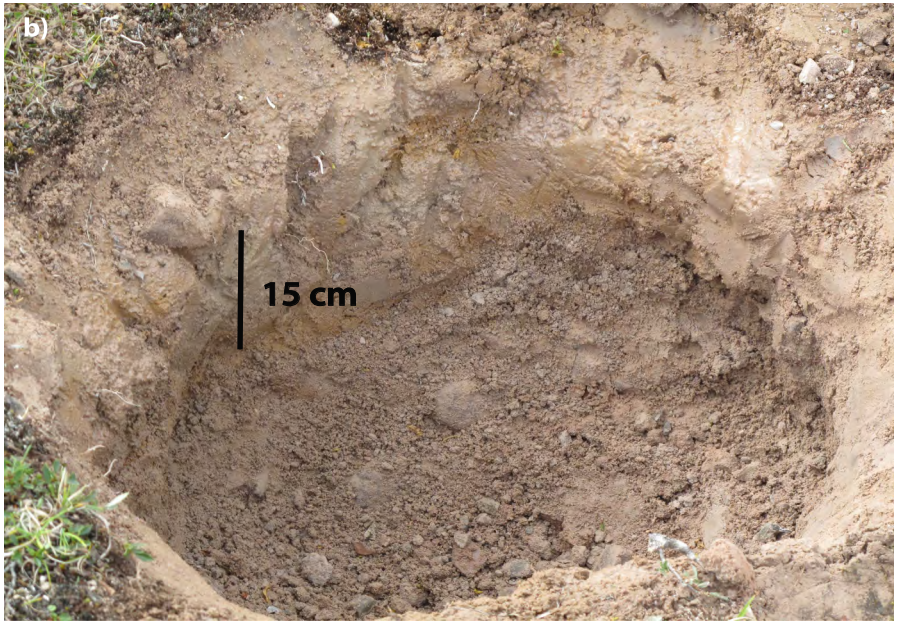

Site 10-PTA-078
a) Overview of the till sample site prior to sampling.
b) Till sample pit.
c) Samples collected for heavy mineral concentrate and till geochemistry.

APPENDIX A3 continued.

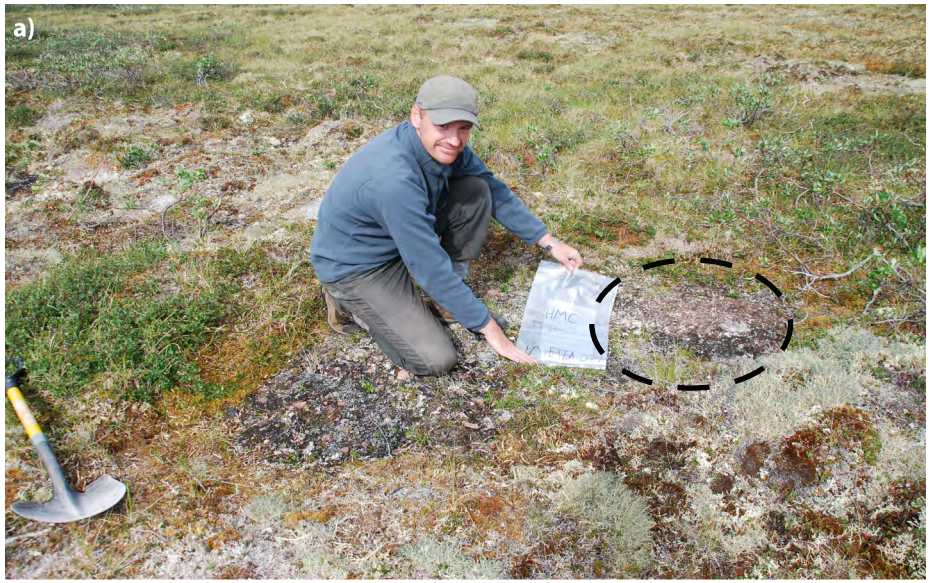

Site 10-PTA-079

a) Overview of the till sample site prior to sampling.
b) Collection of the till for geochemical and heavy mineral concentrate analyses on an island in Squiggly Lake.
c) Overview of sample site after the samples have been collected.

APPENDIX A3 continued.

Site 10-PTA-080
a) Commencement of till collection after scraping off organic matter.
b) Overview of the sample site after collection of the till.
c) Overhead view of the till sample pit.

APPENDIX A3 continued.

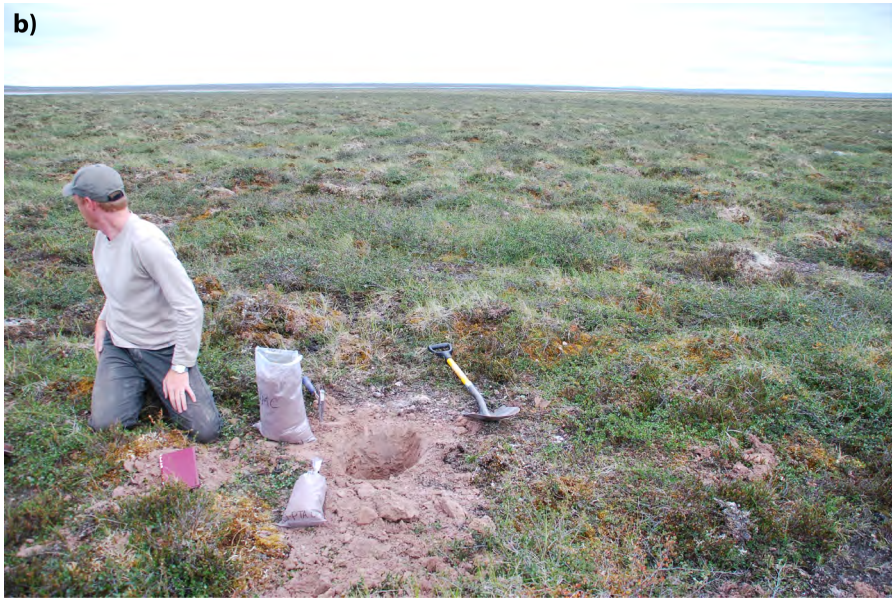

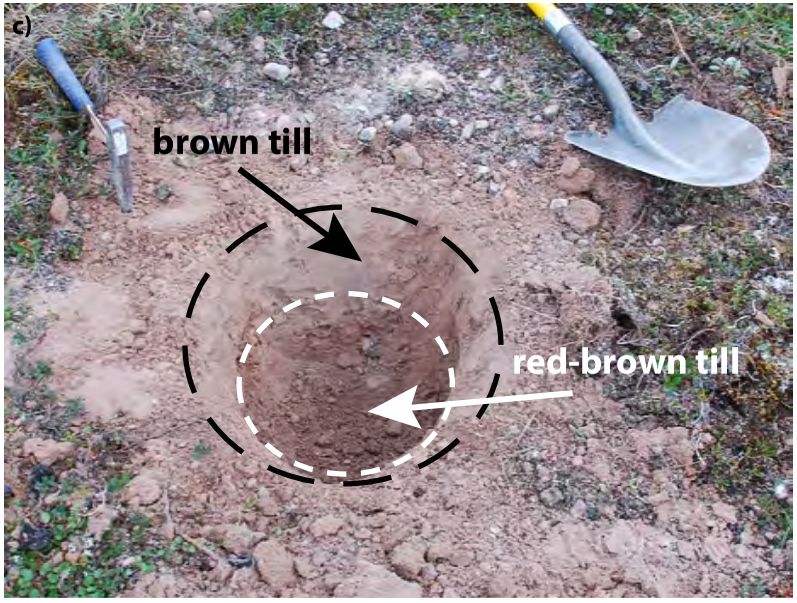

Site 10-PTA-081
a) Overview of the till sample site showing frost boil prior to sampling.
b) Till sample site on tundra during sampling.
c) Overhead view of the sample pit showing upper brown-beige till with a lower reddish-brown till.

APPENDIX A3 continued.

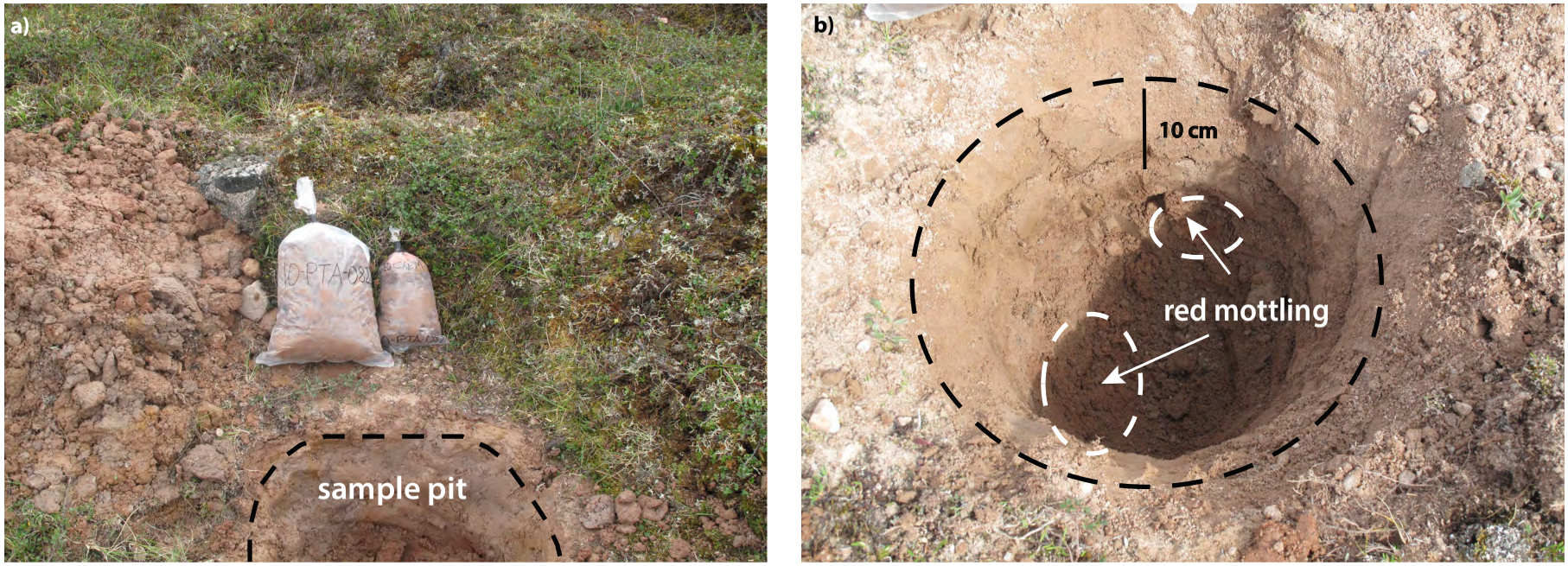

Site 10-PTA-082 a) Heavy mineral concentrate and till geochemistry samples after completion of sampling. **b)** Close-up of an excavated frost boil after sampling. Red mottling is the result of either the mixing of lower redder till or the in situ breakdown of Pitz Formation clasts.

APPENDIX A3 continued.

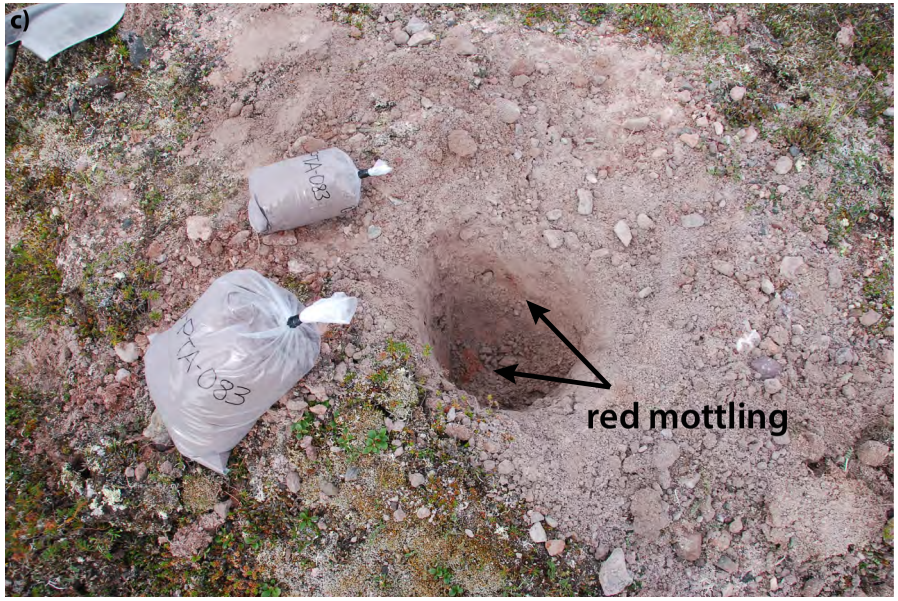

Site 10-PTA-083
a) Overview of the tundra physiography at the till sample site.
b) Till sample site and samples.
c) The excavated frost boil showing beige-brown till with red mottling.

APPENDIX A3 continued.

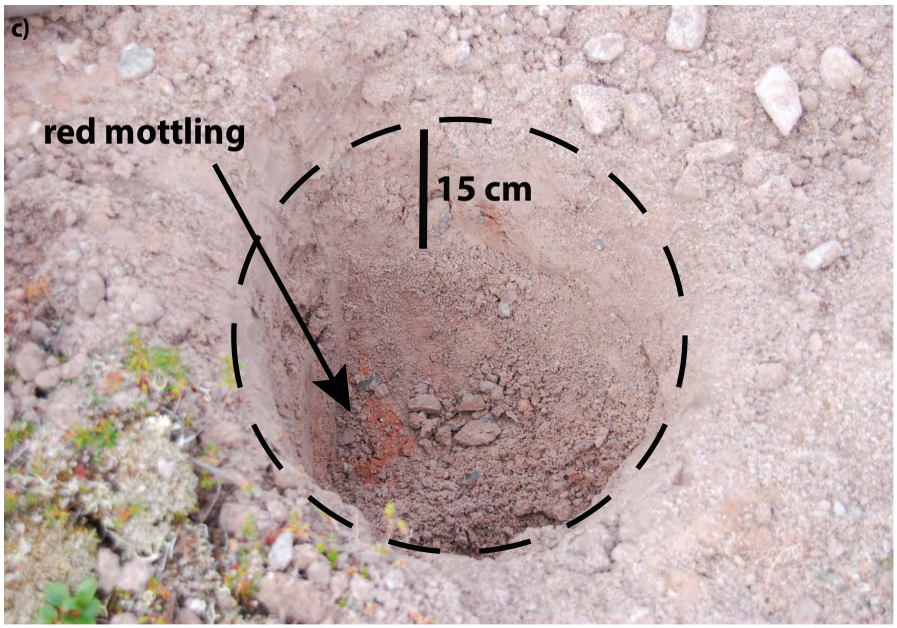

Site 10-PTA-084

a) Overview of the till sample site prior to sampling.

b) Heavy mineral concentrate and till geochemistry samples above the excavated frost boil.

c) Close-up of the excavated frost boil with beige-brown till and minor red mottling.

APPENDIX A3 continued.

Site 10-PTA-085
a) Frost boil and till sample site prior to sampling.
b) Heavy mineral concentrate and till geochemistry samples collected from the reddish brown till of the frost boil.
c) Overview of the till sample site after completion of sampling.

APPENDIX A3 continued.

Site 10-PTA-086

a) Sampling environment adjacent to site 10-PTA-086.

b) Heavy mineral concentrate and till geochemistry samples beside the sampled frost boil. Organic material along the rim of the frost boil.

c) Excavated frost boil showing brown till on top of till that appears to display a mixture of both the beige-brown till and the lower red till.

APPENDIX A3 continued.

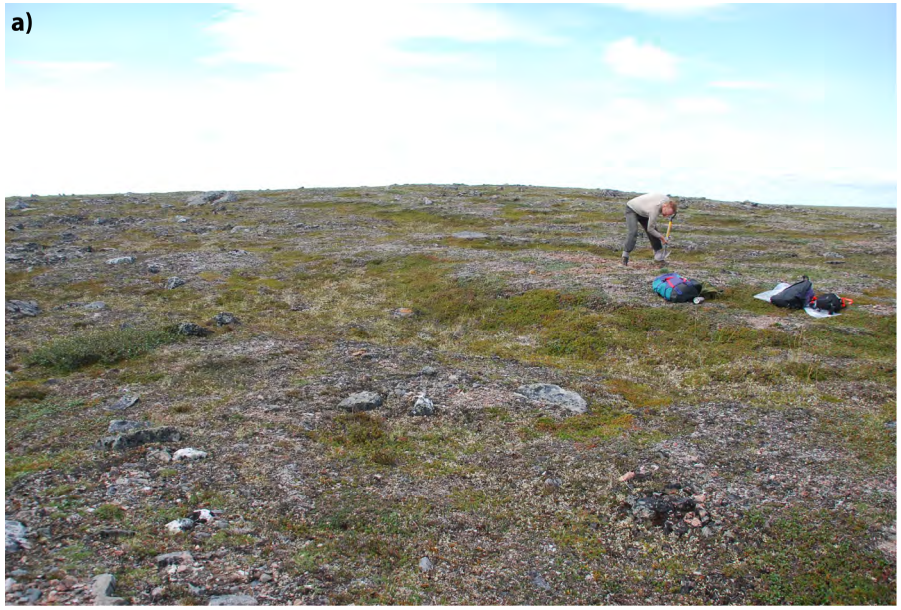

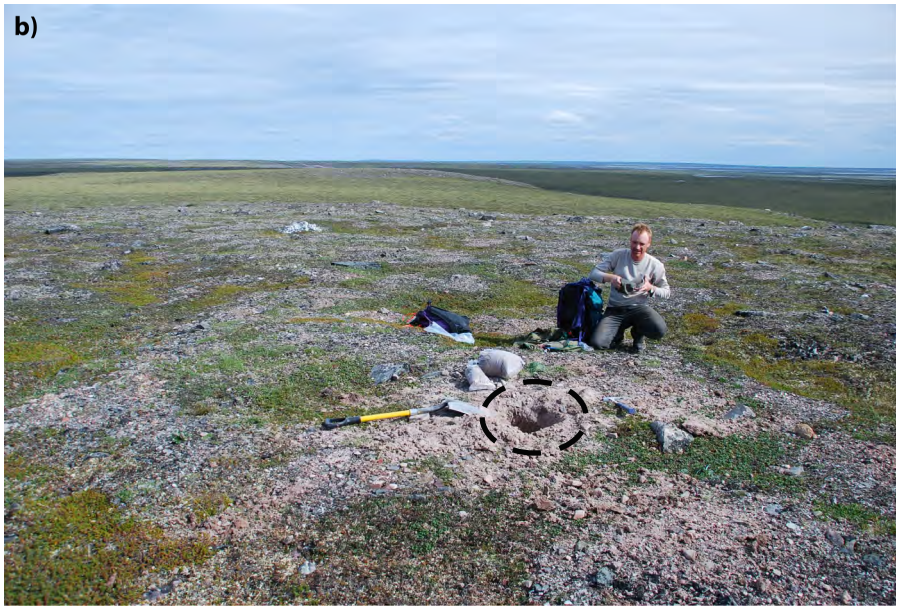

Site 10-PTA-087

a) Overview of the till sample site prior to sampling. Tje site is located on a thin veneer of till with abundant frost boils in the vicinity.

b) Overview of the till sample site after sampling is completed. Photo is oriented northwest.

c) Sample site after the frost boil has been excavated. This sample location is well drained and sand-rich due to its thin cover, relative high elevation, and proximity to both Thelon sandstone and quartzite.

APPENDIX A3 continued.

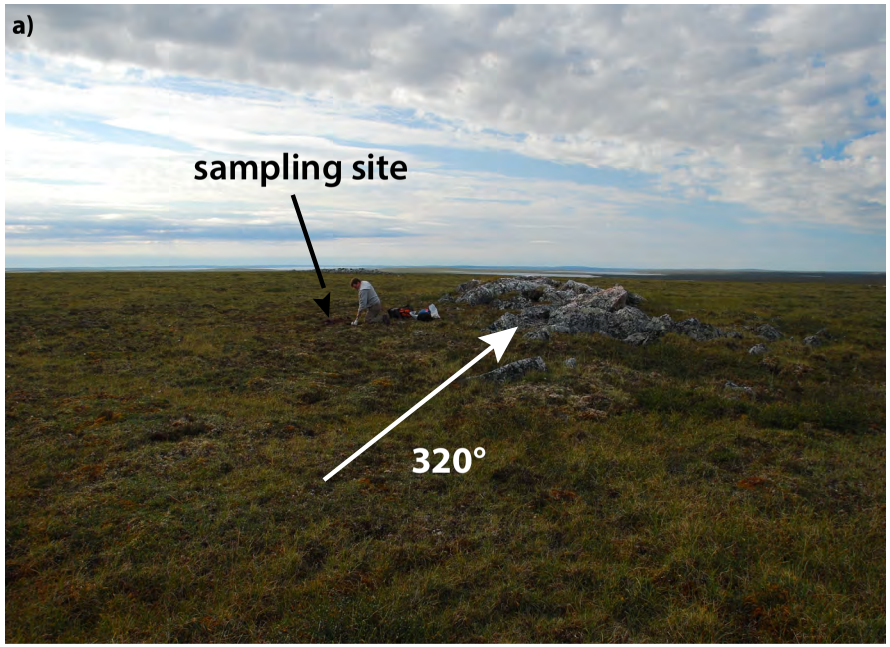

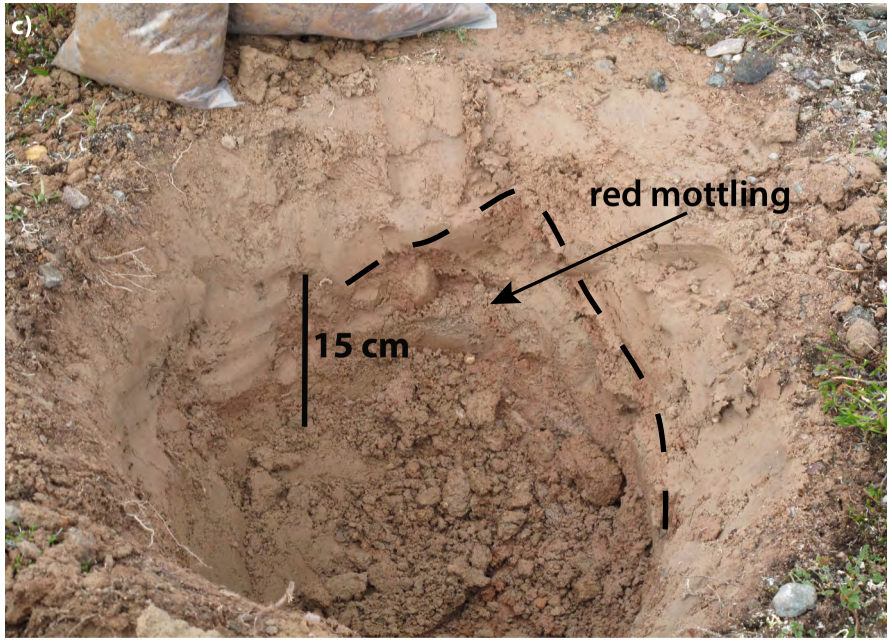

Site 10-PTA-088

a) Overview of the till sample site showing a small quartzite outcrop with glacial striations oriented at 320°.

b) Heavy mineral concentrate and till geochemistry samples next to the excavated frost boil.

c) View of the sample pit showing sandy silty beige-brown till with minor clay-rich red mottling.

APPENDIX A3 continued.

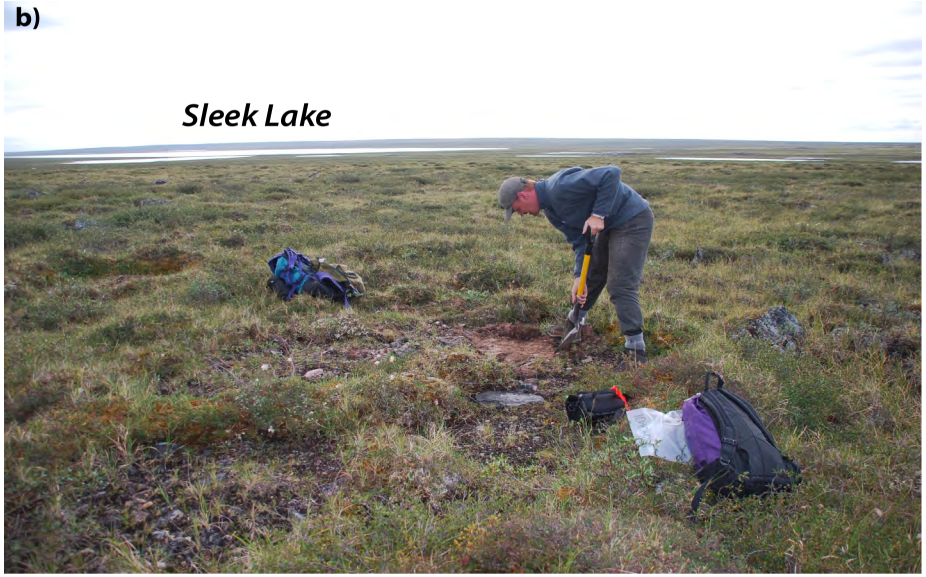

Site 10-PTA-089

a) Overview of the till sample site showing the frost boil after the organic material has been scraped off.

b) Sampling of the frost boil; view is to the southwest.

c) The excavated frost boil prior to sampling, showing an upper oxidized brown till and a lower, unoxidized grey till.

d) Overview of till sample site after completion of the sampling.

APPENDIX A3 continued.

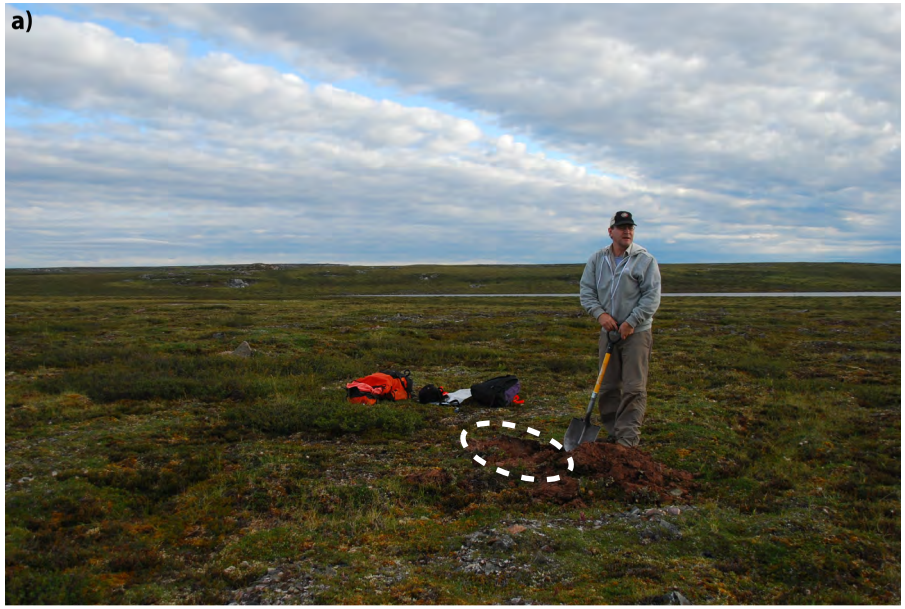

Site 10-PTA-090
a) Overview of the till sample site looking north.
b) The frost boil being sampled is on a flat till plain in tundra.
c) View of the sampled frost boil, showing red oxidized till.

APPENDIX A3 continued.

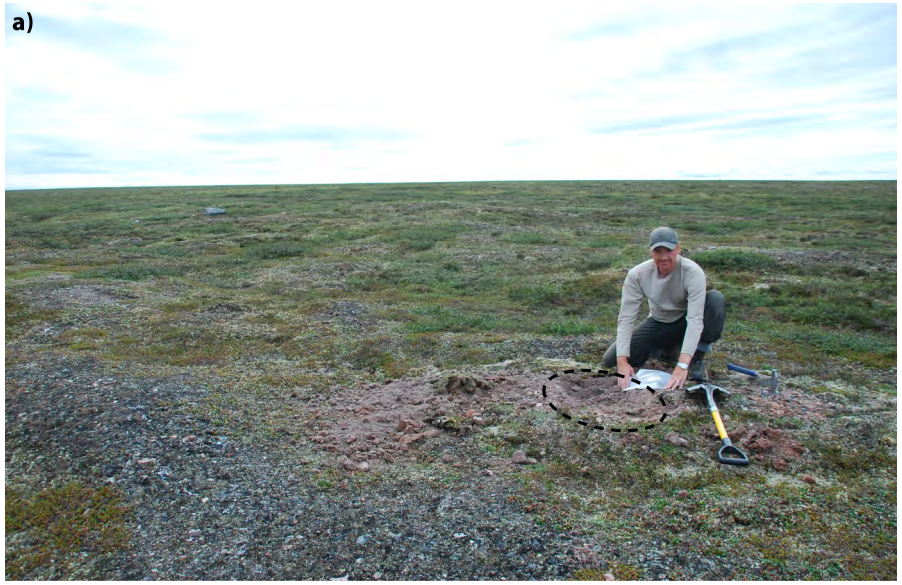

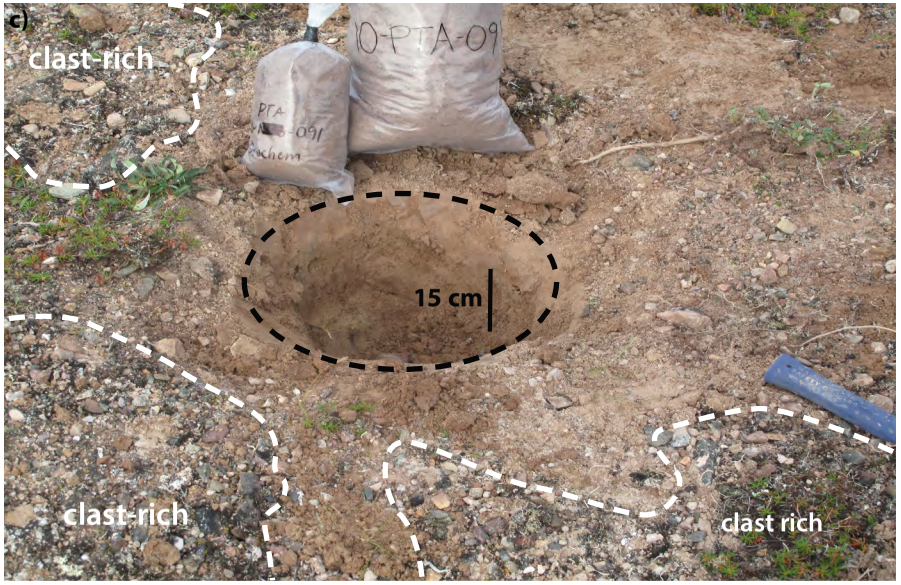

Site 10-PTA-091

a) Overview of the till sample site showing the frost boil with the organic veneer scraped off.

b) Heavy mineral concentrate and till geochemistry samples beside the excavated frost boil.

c) The sampled frost boil surrounded by clast-rich, silty sandy till.

APPENDIX A3 continued.

Site 10-PTA-092

a) Overview of the till sample site looking south.

b) Sample site showing the frost boil being sampled. Till at this location was dry and dominated by sand.

c) Till sample site upon completion of sampling.

APPENDIX A3 continued.

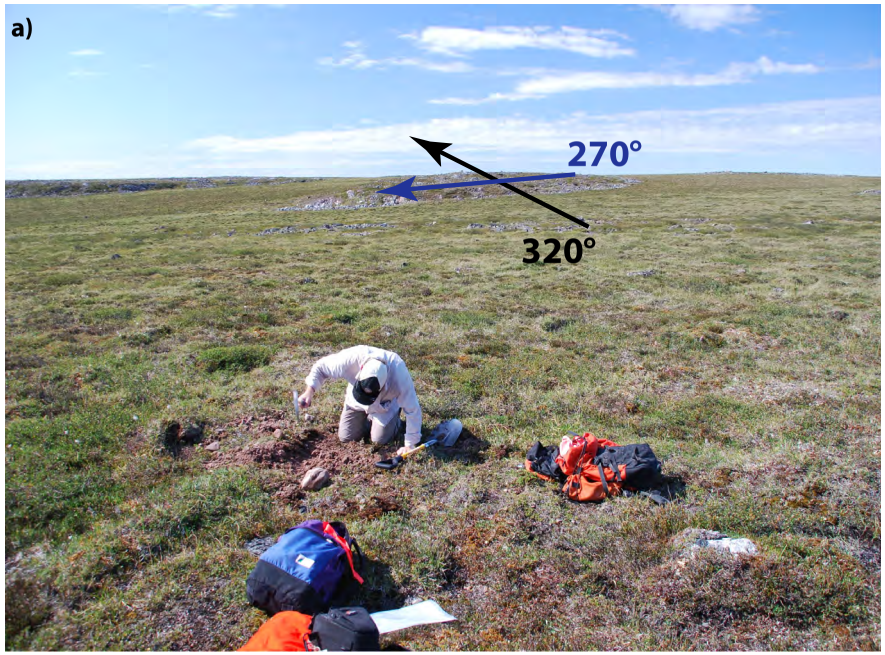

Site 10-PTA-093

a) Overview of the till sample site looking north. Quartzite outcrop with older (320°) and younger (270°) ice-flow indicators in the background.

b) Excavated frost boil after sampling showing the dry silty sandy till.

c) Heavy mineral concentrate and till geochemistry samples after the completion of sampling.

APPENDIX A3 continued.

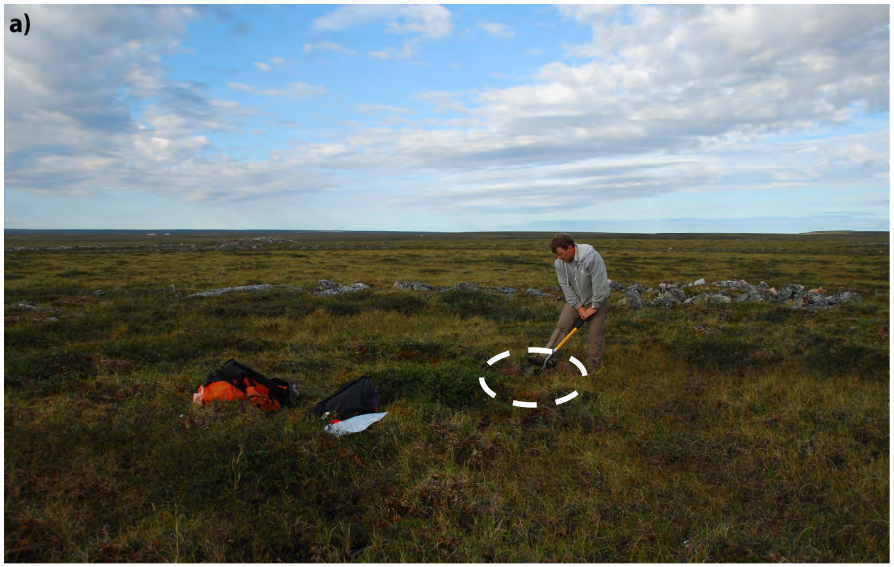

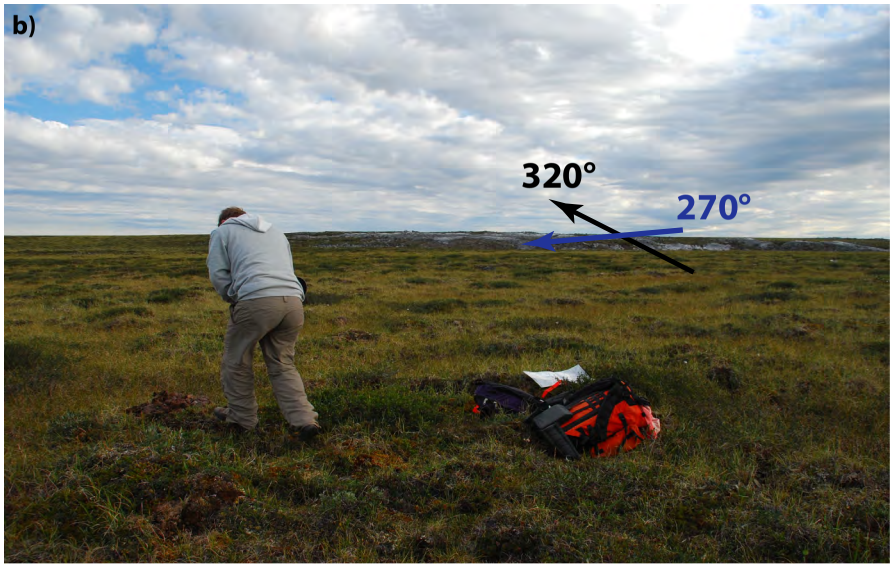

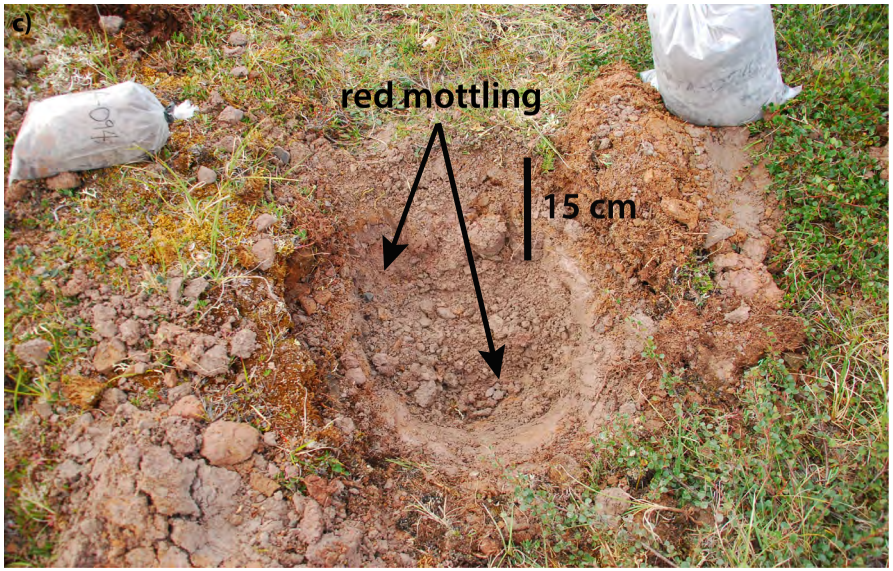

Site 10-PTA-094

a) Overview of the till sample site looking northeast.

b) Overview of the till sample site showing a quartzite outcrop in the background due northwest. Ice-flow indicators on quartzite display an older (320°) and younger (270°) trend.

c) Excavated frost boil showing a predominantly sandy silty brown till with red clay-rich mottling.

APPENDIX A3 continued.

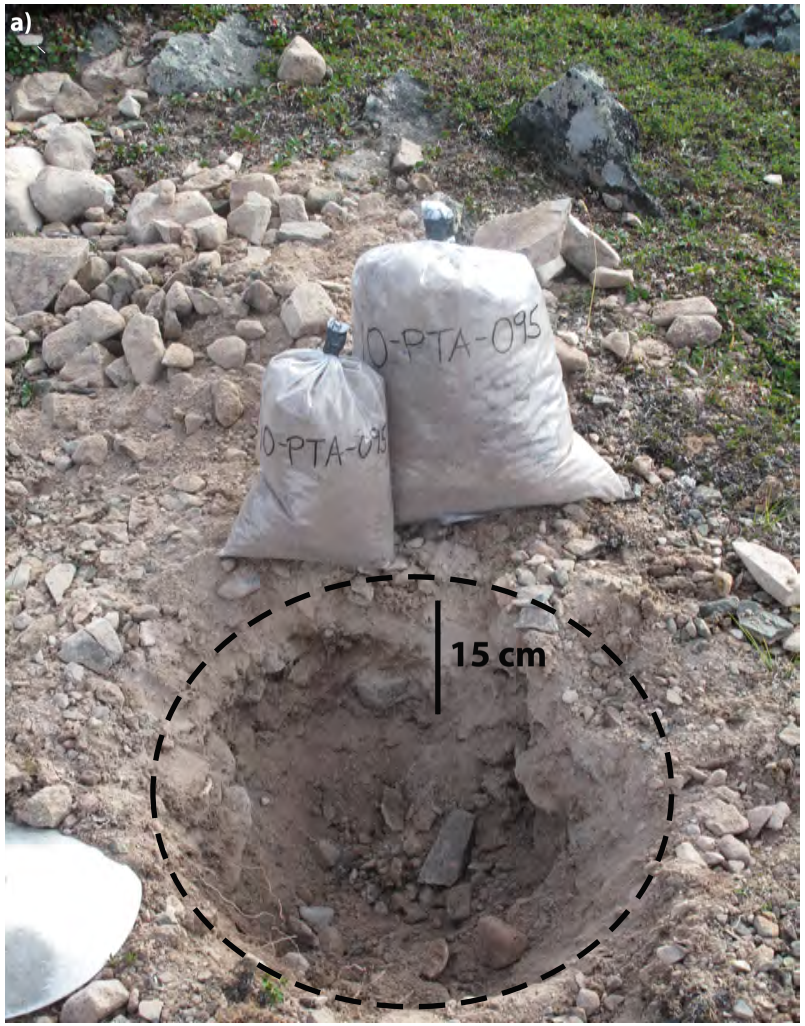

Site 10-PTA-095

a) Till sample site showing the excavated frost boil, composed of 15% clasts, dominated by subangular to angular quartzite and sandstone cobbles / pebbles.

b) Heavy mineral concentrate and till geochemistry samples.

APPENDIX A3 continued.

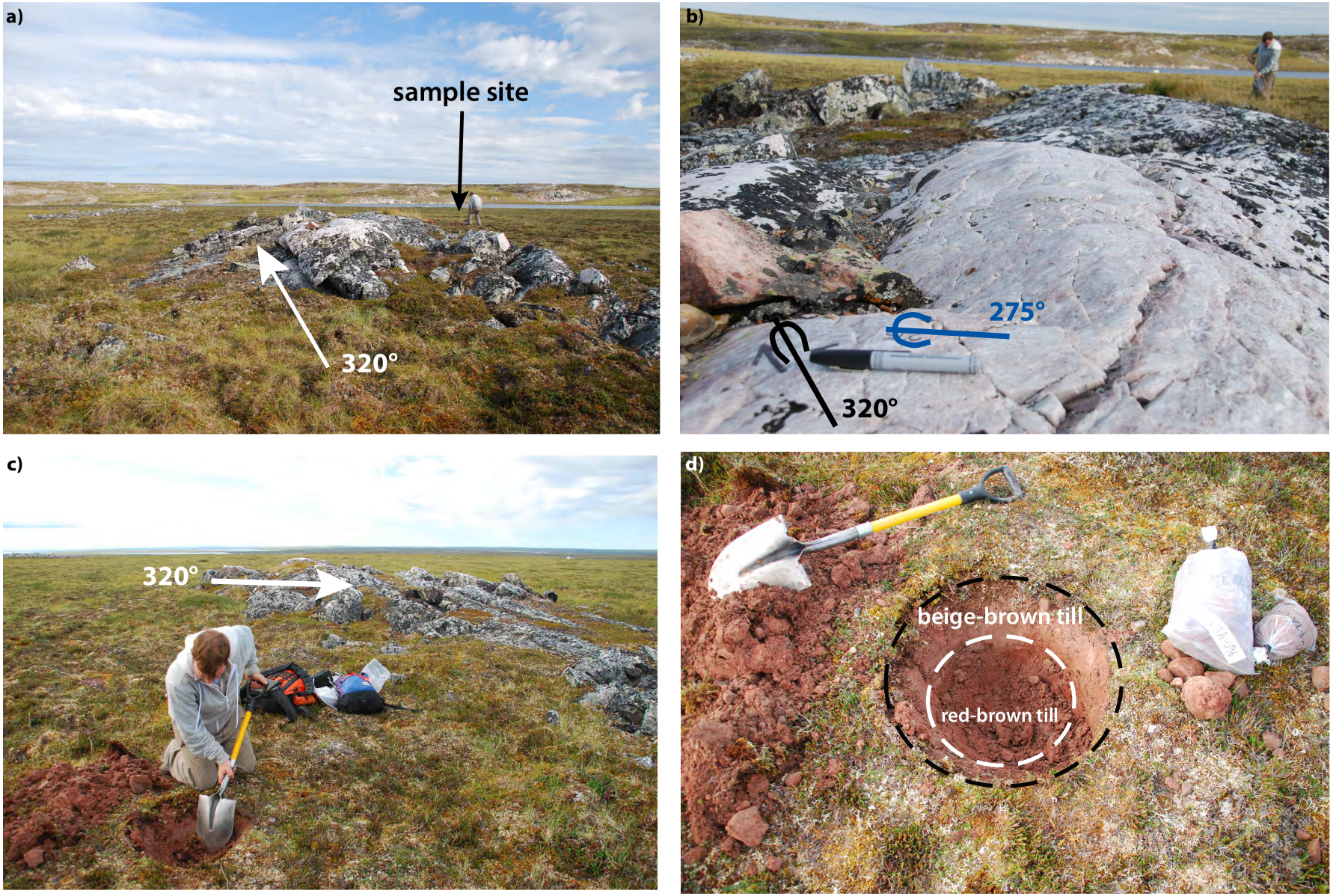

Site 10-PTA-096 a) Till sample site with a quartzite outcrop adjacent to a general ice-flow trend of 320º. **b)** Striations on polished quartzite outcrop trending 320º and 275º. **c)** The frost boil displayed a reddish brown clay-rich sandy silt till. **d)** Upon completion of sampling, the frost boil has two distinct tills: a top beige-brown till with reddish, more clay-rich till beneath.

APPENDIX A3 continued.

Site 10-PTA-097

a) Overview of the till sample site after the completion of sampling. A small quartzite boulder field can be seen in the background.

b) Heavy mineral concentrate and till geochemistry samples. Clasts from the till, which are of various lithologies, are shown on the right: 1) quartzite, 2) metawacke, and 3) Thelon sandstone.

c) The excavated frost boil showing silty sandy till.

APPENDIX A3 continued.

Site 10-PTA-098

a) Overview of the till sample site during the sampling. A quartzite ridge is visible in the background.

b) Excavated frost boil showing a brown-beige silty sandy till with abundant angular clasts.

c) Overview of the sample site showing the heavy mineral concentrate and the till geochemistry samples.

APPENDIX A3 continued.

Site 10-PTA-099
a) Overview of the till sample site looking southwest. The Kiggavik Camp can be seen in the background.
b) The excavated frost boil displaying a sandy, compact till.
c) Heavy mineral concentrate and till geochemistry samples.

APPENDIX A3 continued.

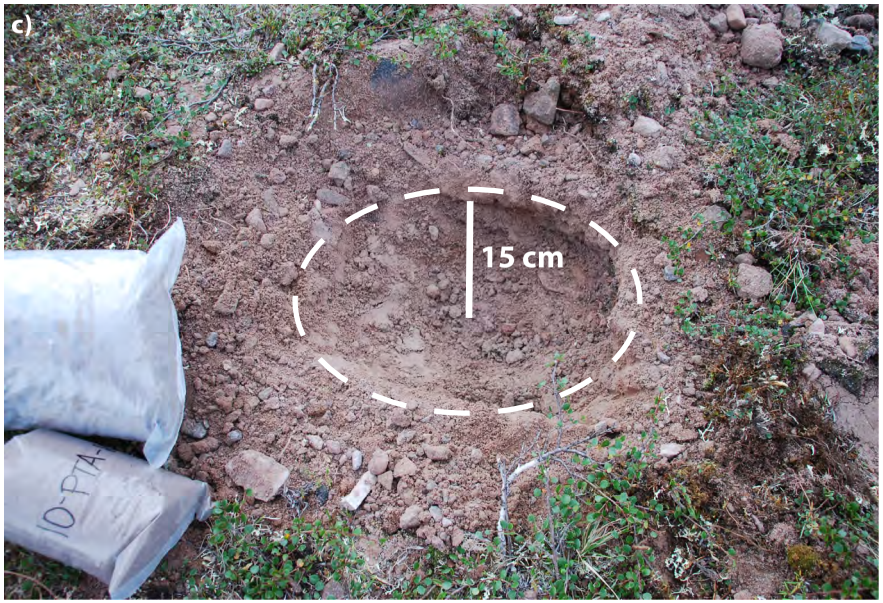

Site 10-PTA-100

a) Overview of the till sample site with quartzite outcrops to the south. Further south, the terrain is low lying due to a change in lithology to metawacke bedrock.

b) Frost boil being excavated; photo is oriented to the northwest.

c) The excavated frost boil contains a homogenous mixture of brown and red-brown till.

APPENDIX A3 continued.

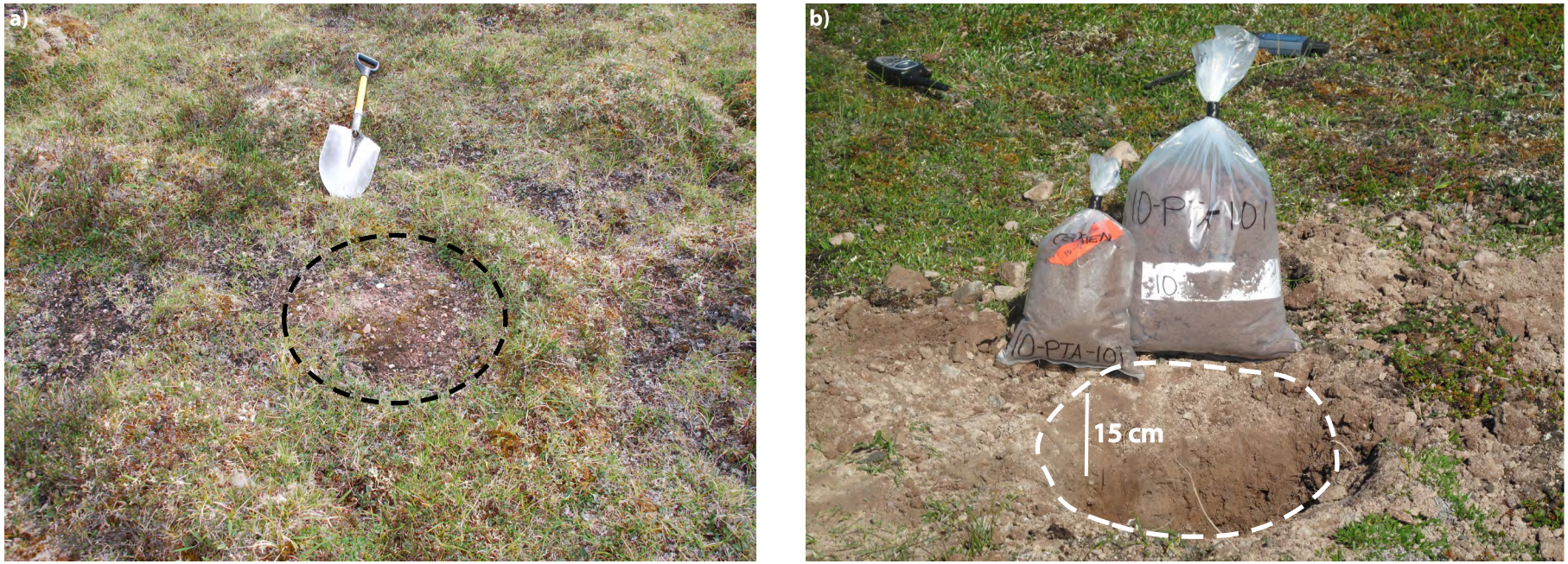

Site 10-PTA-101 a) Overview of the sample site prior to sampling. **b)** Sample site with heavy mineral concentrate and till geochemistry samples taken from the sandy silty till.

APPENDIX A3 continued.

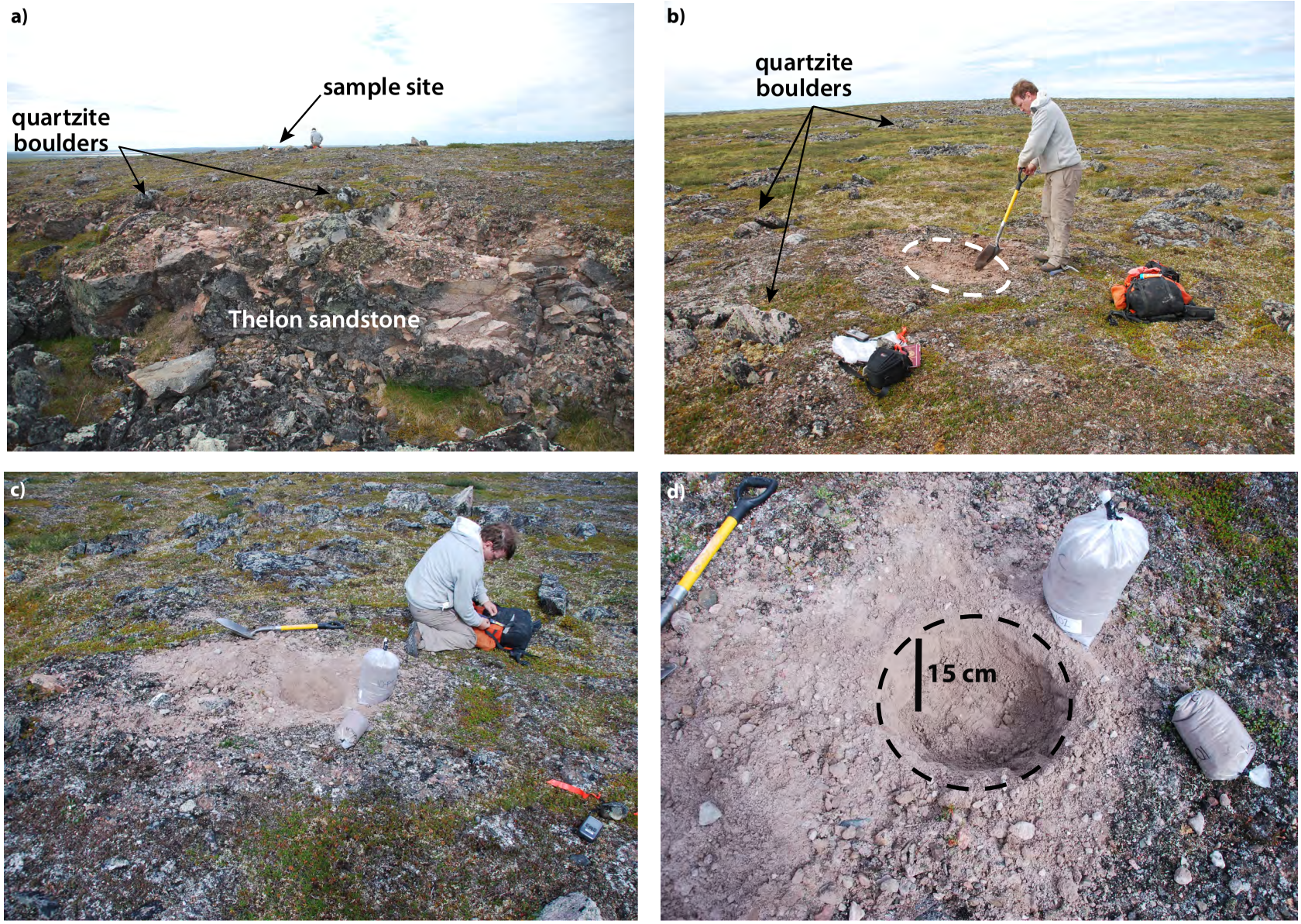

Site 10-PTA-102 a) View of the sample site showing thin till on Thelon sandstone. An abundance of white quartzite boulders were observed 50 m up-ice. **b)** Overview of the sample site looking north, showing an abundance of angular quartzite boulders. **c)** Till sample site after completion of the sampling. **d)** The excavated frost boil showing a predominant silty sandy till.

APPENDIX A3 continued.

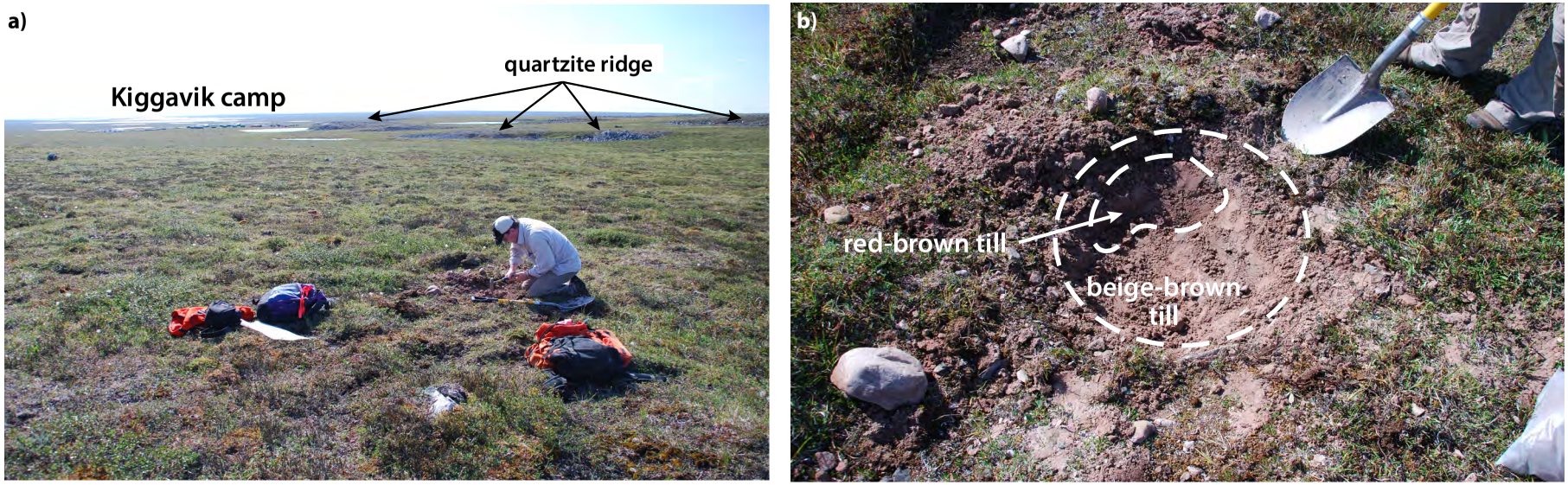

Site 10-PTA-104 a) Overview looking southwest of the till sample site on a till plain with a quartzite ridge and the Kiggavik exploration camp in the background. **b)** The excavated frost boil with a mixture of a silty sandy beige-brown till and a more clay-rich red-brown till.

APPENDIX A3 continued.

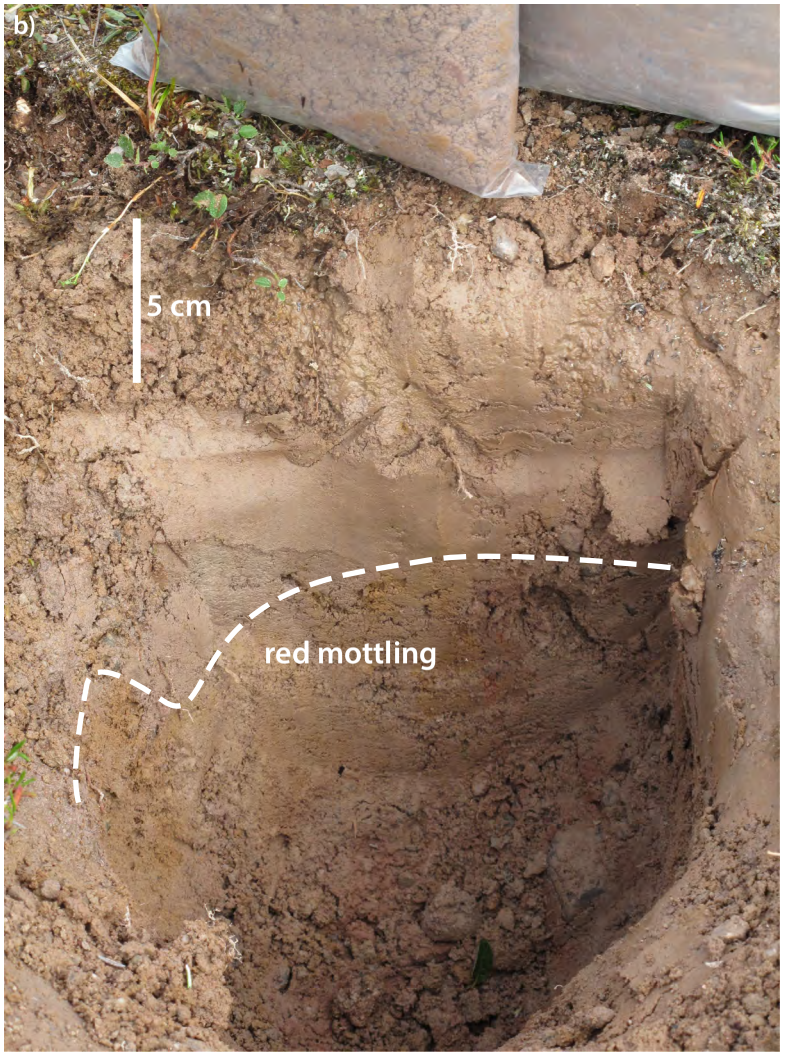

Site 10-PTA-105

a) Overview of the till sample site.

b) Excavated frost boil showing beige-brown, clay-rich silt till with mottles of red-brown clay-rich till.

c) Sampled frost boil with heavy mineral concentrate and till geochemistry samples.

APPENDIX A3 continued.

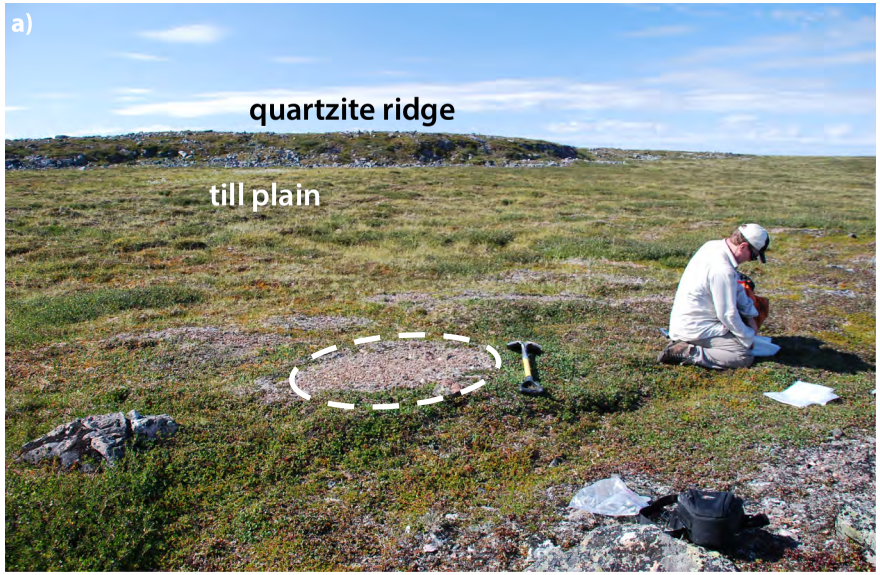

Site 10-PTA-106

a) Till sample site looking north, showing a till plain and a quartzite bedrock ridge.

b) Till sample site looking northeast.

c) Heavy mineral concentrate and geochemistry samples beside the excavated frost boil.

APPENDIX A3 continued.

Site 10-PTA-107 a) Till sample site with heavy mineral concentrate and till geochemistry samples. **b)** Excavated frost boil with clast in poor, silty sand till.

APPENDIX A3 continued.

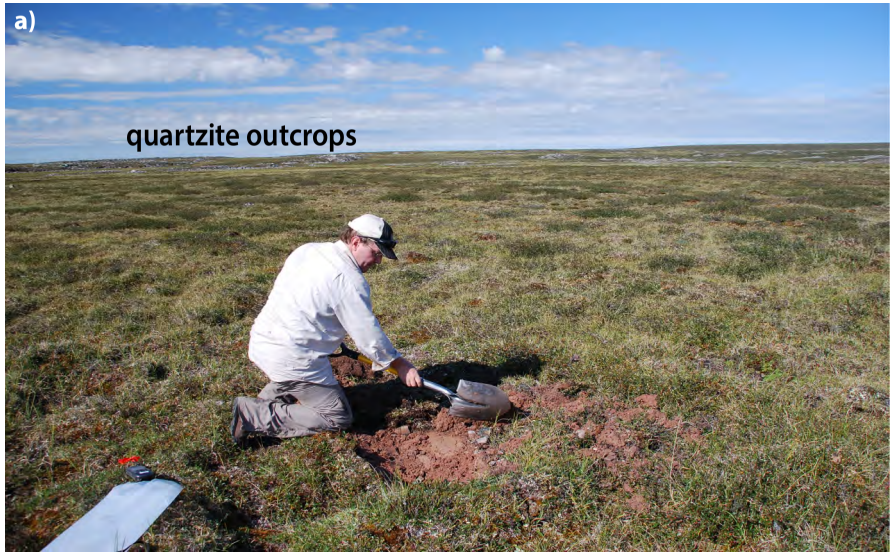

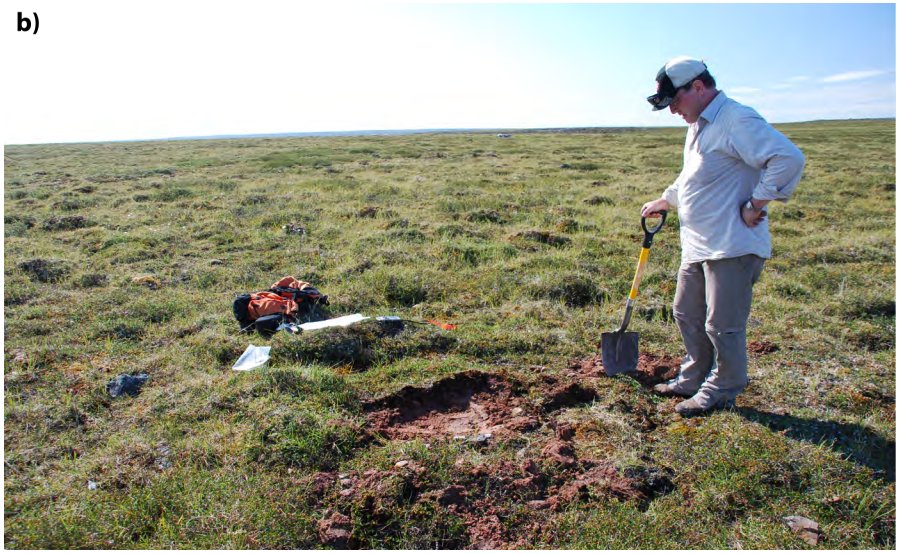

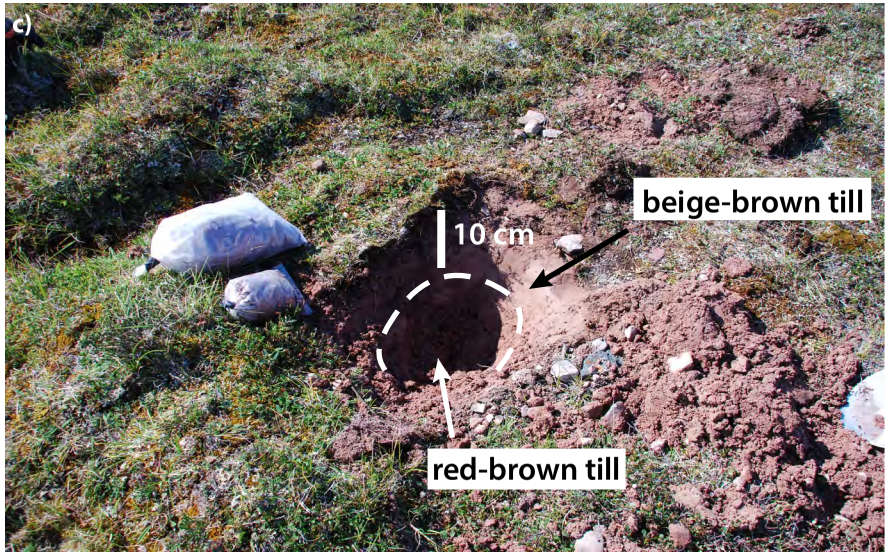

Site 10-PTA-108

a) Overview of the till sample site looking north; a quartzite ridge can be seen to the north.

b) The till sample site with the organic matter removed.

c) The excavated frost boil after being sampled, revealing a mixture of beige-brown and red-brown till.

APPENDIX A3 continued.

Site 10-PTA-109
a) Till sample site with the undisturbed frost boil outlined.
b) The excavated frost boil showing a pebbly sand till.
c) Heavy mineral concentrate and till geochemistry samples.

APPENDIX A3 continued.

Site 10-PTA-110

a) Till sample site aproximately 300 metres north of the Kiggavik exploration camp.

b) Till sample site showing the frost boil after the removal of the organic material.

c) Excavated frost boil containing silty sand till.

APPENDIX A3 continued.

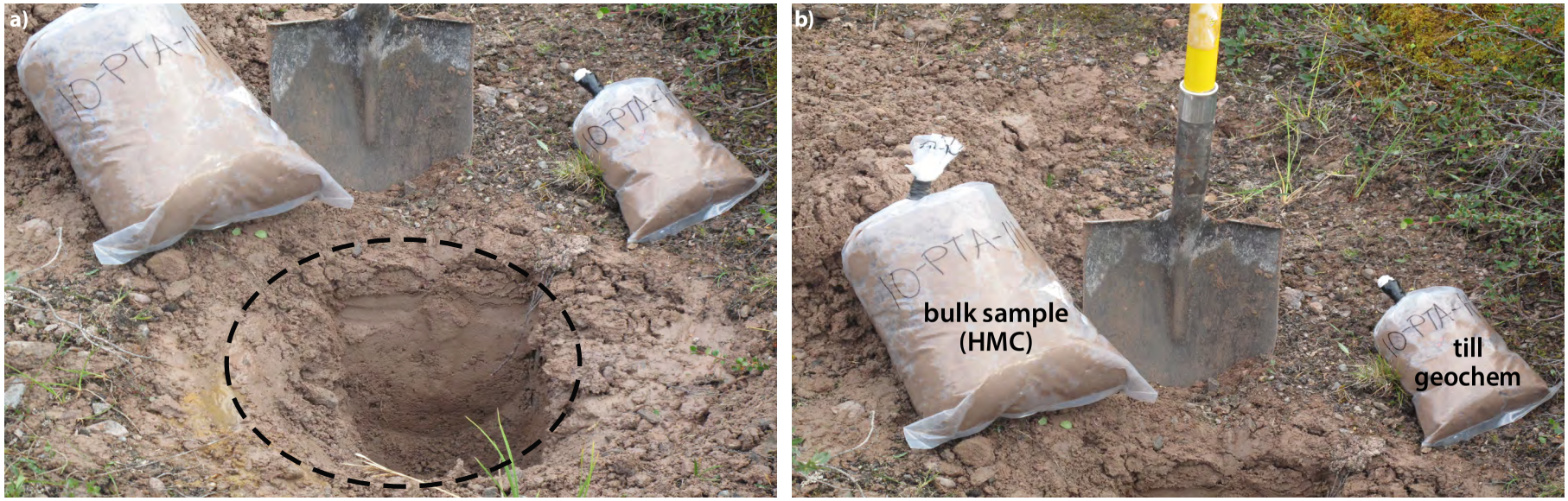

Site 10-PTA-111 a) Till sample site in a frost boil that displayed elevated water content in the silty sand till. **b)** Heavy mineral concentrate and till geochemistry samples.

APPENDIX A3 continued.

Site 10-PTA-113
Till sample site10-PTA-113, which is located approximately 1 metre to the west of sample site 10-PTA-095

APPENDIX A3 continued.

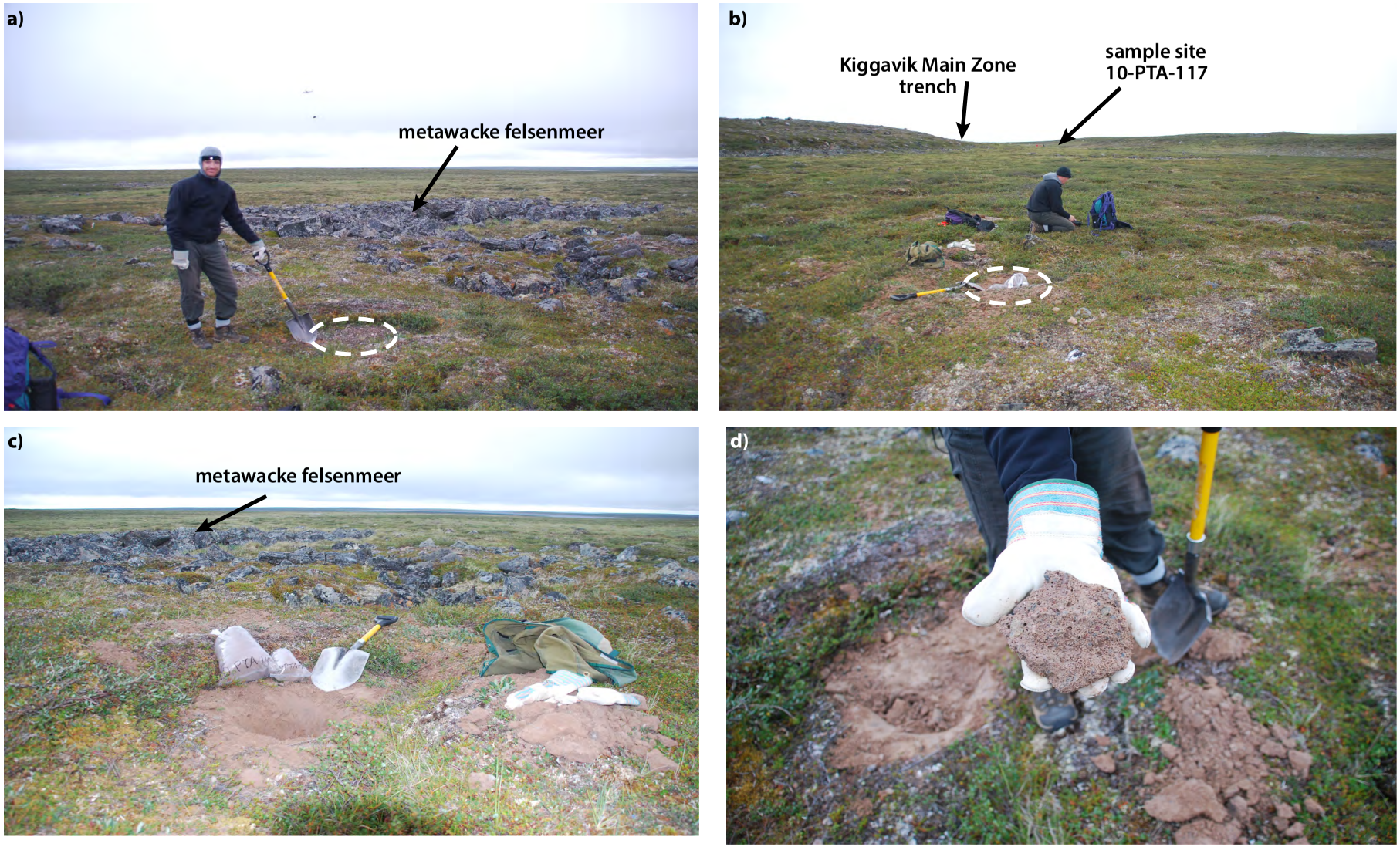

Site 10-PTA-114 a) Till sample site looking east with felsenmeer arkosic metawacke of the Woodburn Group int he background. **b)** Sample site looking northwest. The Main Zone trench at Kiggavik (~150 m to the northwest) can be seen as well as sample site 10-PTA-117. **c)** The excavated frost boil and samples. **d)** Typical cyrosolic till texture with porosity and air bubbles from thawed seasonal frost.

APPENDIX A3 continued.

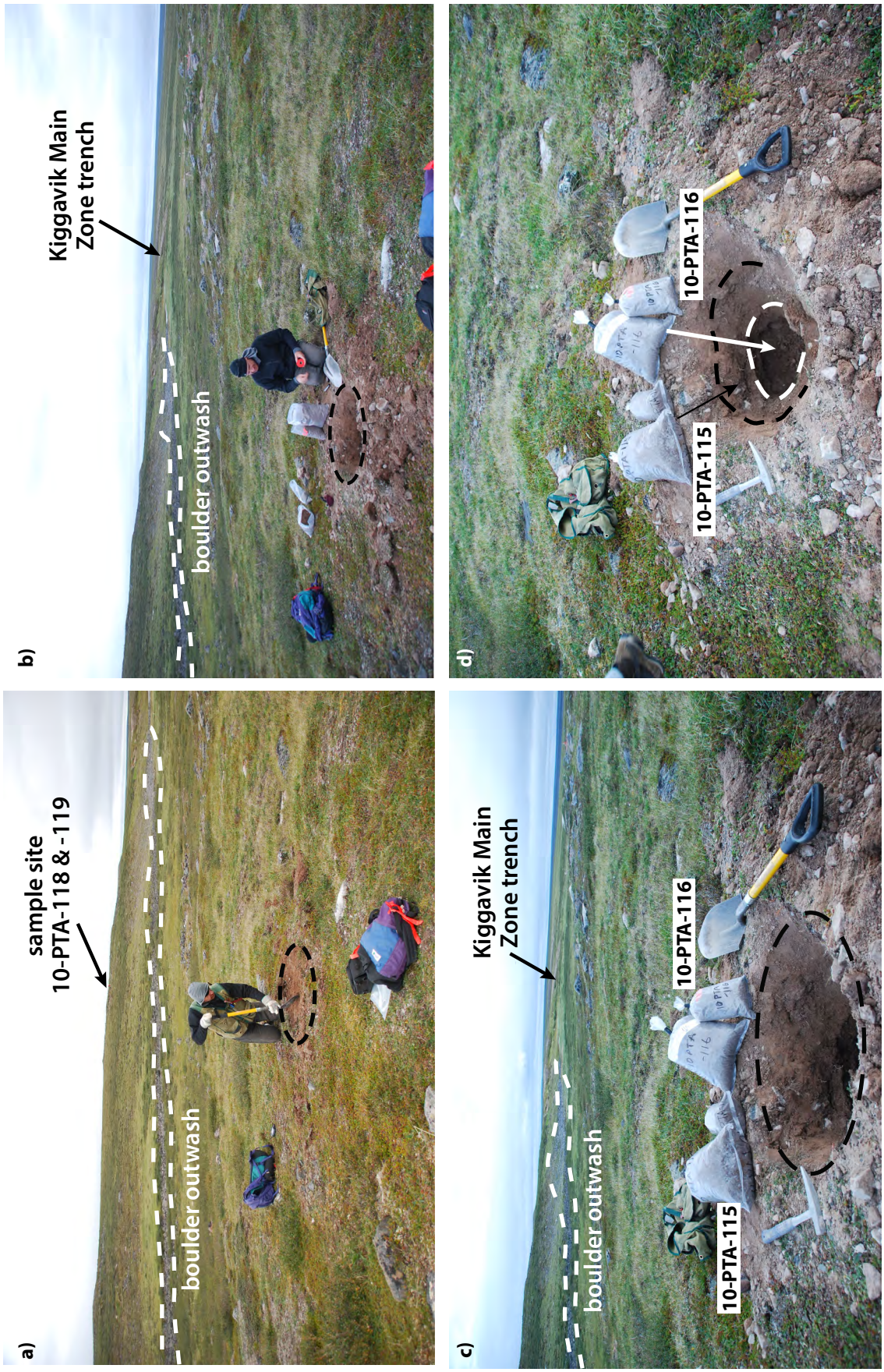

Site 10-PTA-115 & -116 a) Till sample site with boulder outwash in the background, which occurs in a northwest-southeast orientation between two bedrock ridges. Sample site 10-PTA-118 & -119 are collected on the other side of boulder outwash. **b)** Till sample site after completion of sampling, looking towards the Main Zone trench that is 80 m to the east. **c)** Heavy mineral concentrate and till geochemistry samples. **d)** Excavated frost boil showing the upper section where the material for sample 10-PTA-115 was taken and the lower section where sample 10-PTA-116 was collected.

APPENDIX A3 continued.

Site 10-PTA-117 a) Overview of the sample site prior to sampling. The Kiggavik Main Zone trench is located ~50 metres to the west. **b)** The frost boil prior to sampling. **c)** The excavated frost boil contains silty sand till that is clast-rich. The observed clast lithologies include 1) meta-wacke, 2) Thelon sandstone, and 3) Hudsonian granite. **d)** Heavy mineral concentrate and till geochemistry samples.

APPENDIX A3 continued.

Site 10-PTA-118 & -119 a) Duplicate sample site after excavation of the frost boil. **b)** Excavated frost boil showing sandy, clast-poor till.

Site 10-PTA-120 a) The sample site is in a till veneer above Kiggavik granite and has a silty to very fine-sand texture. **b)** Heavy mineral concentrate and till geochemistry samples.

APPENDIX A3 continued.

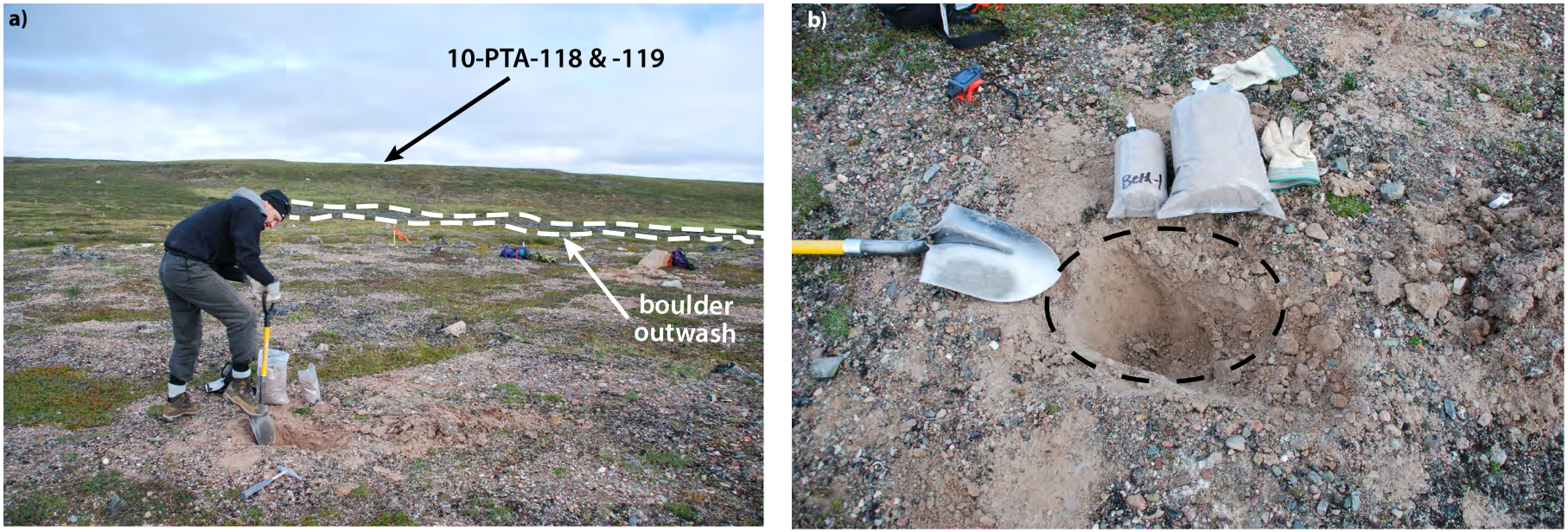

Site 10-PTA-121 a) Overview of the sample site looking northeast. The location of sample site 10-PTA-118 and -119 can be seen in the background. **b)** Excavated frost boil displaying silty to fine-sand texture. Clasts at this sample location were predominantly subrounded pebbles.

APPENDIX A3 continued.

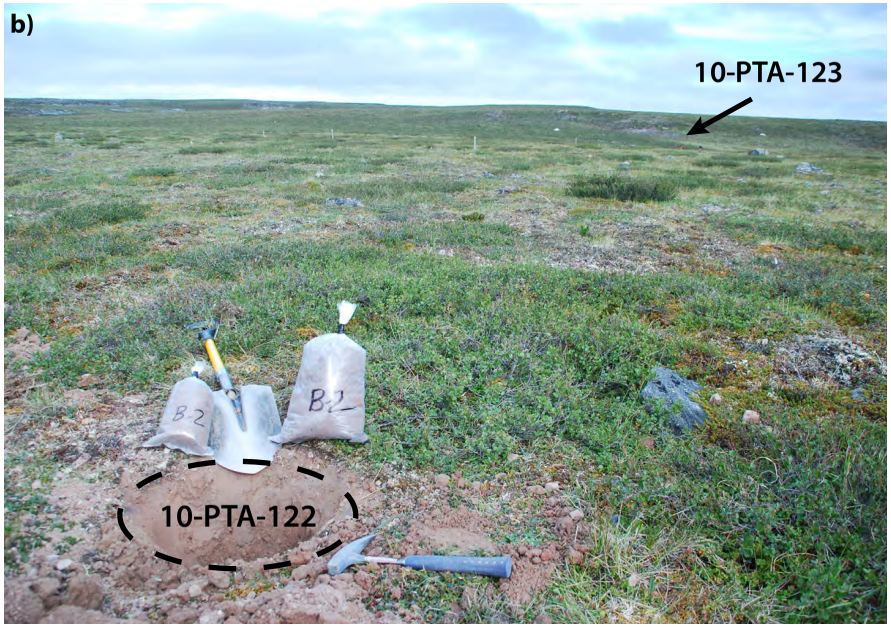

Site 10-PTA-122

a) Till sample site with abundant frost boil.

b) View of the sample site looking north; sample site 10-PTA-123 can be seen in the background.

c) Heavy mineral concentrate and till geochemistry samples; excavated frost boil shows a transition of colour and texture with depth.

APPENDIX A3 continued.

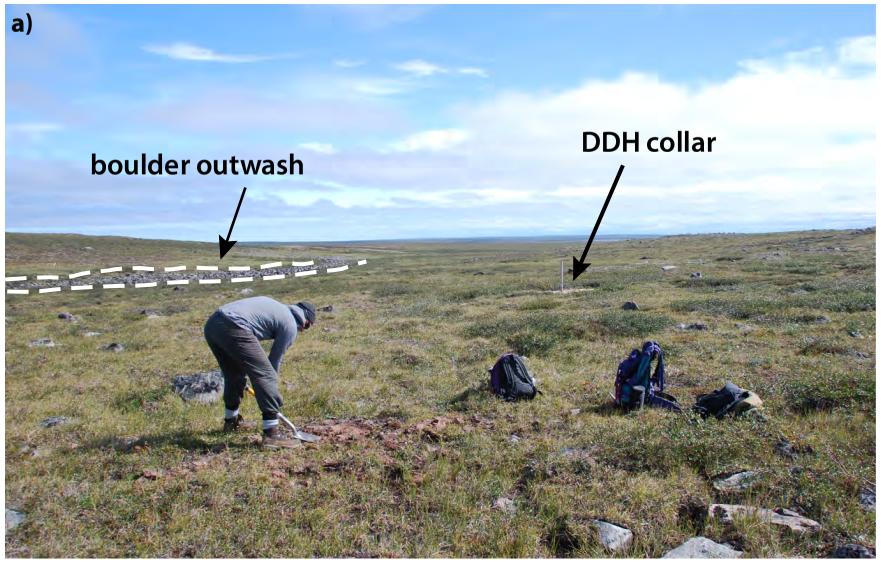

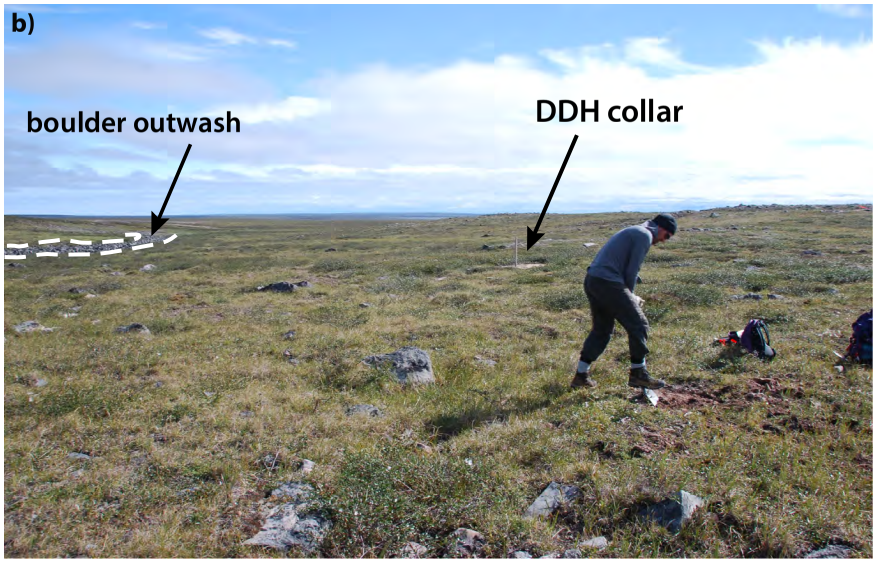

Site 10-PTA-123

a) Overview of the till sample site looking to the northeast. A diamond drill hole (DDH) collar is located proximal to the sample site.

b) The sample site is in a frost boil among frost-heaved boulders.

c) The excavated frost boil shows beige-brown till occurring above red-brown till.

APPENDIX A3 continued.

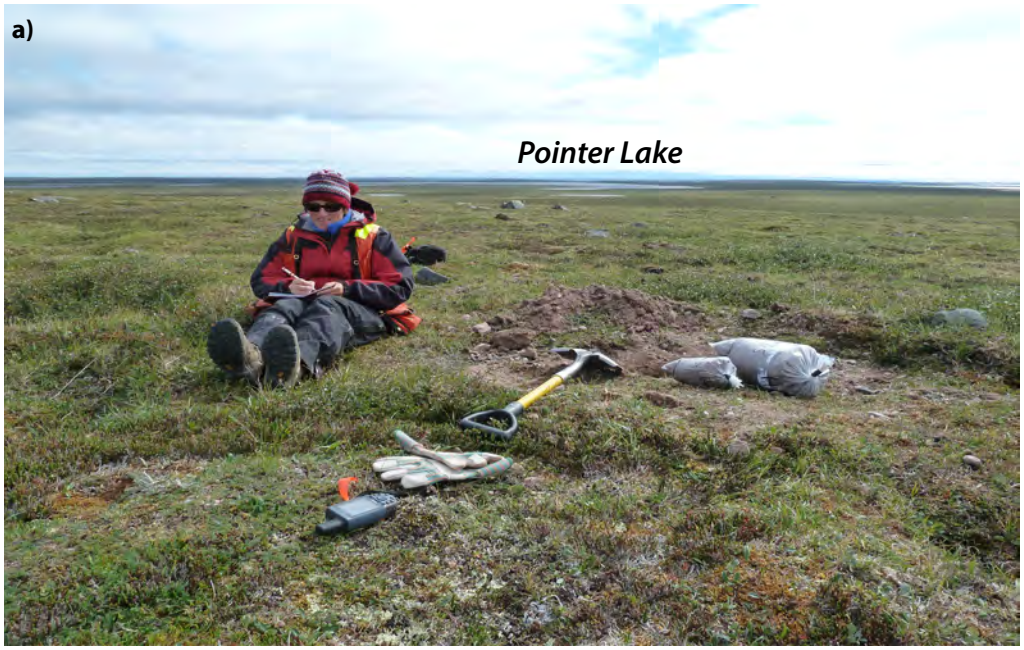

Site 10-PTA-124
a) Till sample location, looking south towards Pointer Lake.
b) Till samples collected from the frost boil.
c) Close-up of the excavated frost boil, which has compact silty sand till.

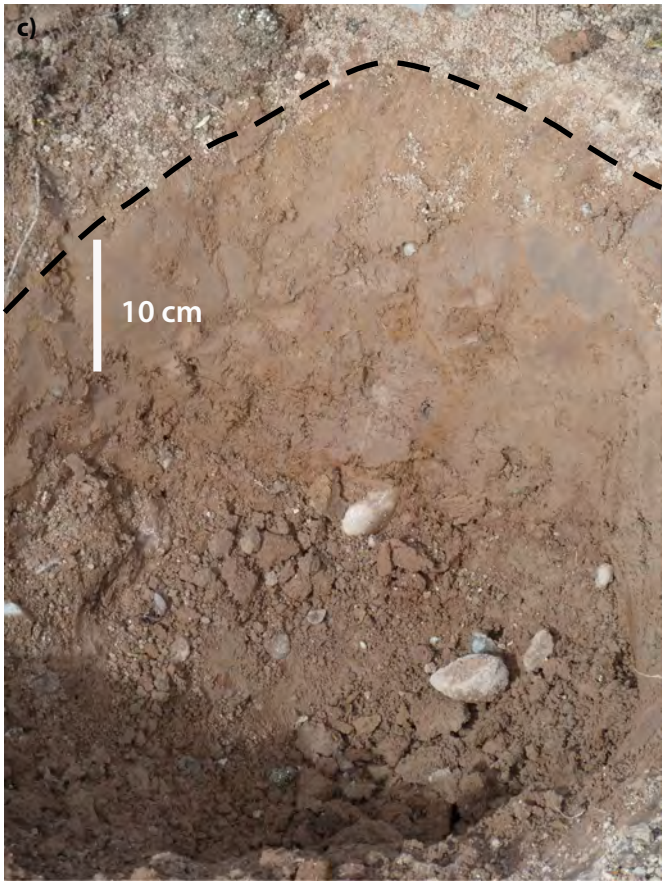

APPENDIX A3 continued.

Site 10-PTA-125 a) Overview of the till sample site. The pebble to cobble fraction was dominated by angular metawacke clasts. **b)** Heavy mineral concentrate and till geochemistry samples alongside the excavated frost boil.

APPENDIX A3 continued.

a)

Site 10-PTA-126 a) Overview of the till sample site looking west to the Kiggavik exploration camp. The sample site occurs between the Kiggavik camp and the Kiggavik Main Zone trench. **b)** Sampled frost boil revealing till with a silty sand texture.

APPENDIX A3 continued.

Site 10-PTA-127

a) Removal of the organic veneer from a frost boil at the sample site.

b) Excavated frost boil, with two dominant types of clasts: angular metawacke and rounded Thelon sandstone.

c) Excavated frost boil, showing brown-beige silty sand till.

APPENDIX A3 continued.

Site-10-PTA-128 & -133

a) Sample site on a till plain occurring above Woodburn Group metawacke. Quartzite bedrock of the Woodburn Group can be seen to the north in the tbackground .

b) Excavated frost boil revealing a silty fine-sand till with red clay-rich silt till.

c) This locality was a field duplicate site with a pair of heavy mineral concentrate and till geochemistry samples.

APPENDIX A3 continued.

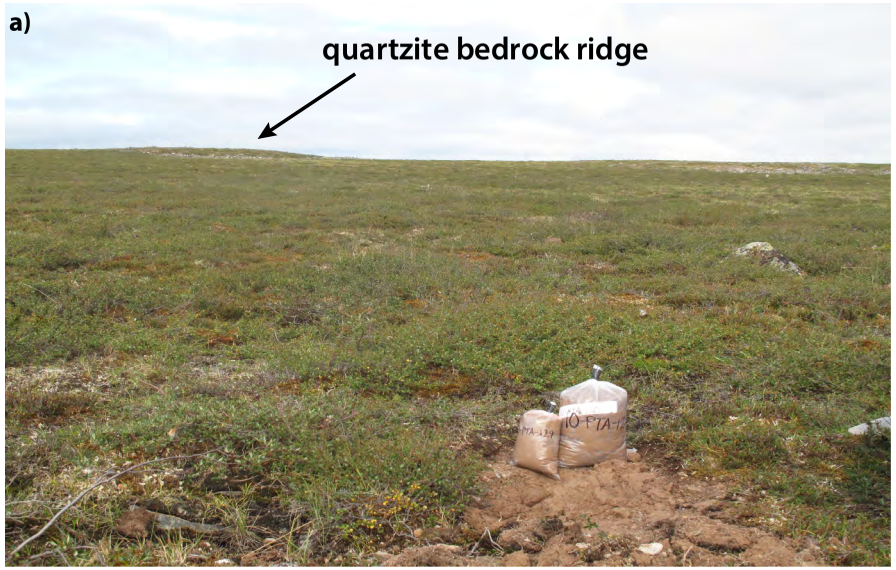

Site 10-PTA-129

a) Till sample site on a till plain 500 m north of the Kiggavik camp.

b) Sampled frost boil with heavy mineral concentrate and till geochemistry samples.

c) Excavated frost boil revealing a beige-brown silty till with small clusters of red-brown clay till.

APPENDIX A3 continued.

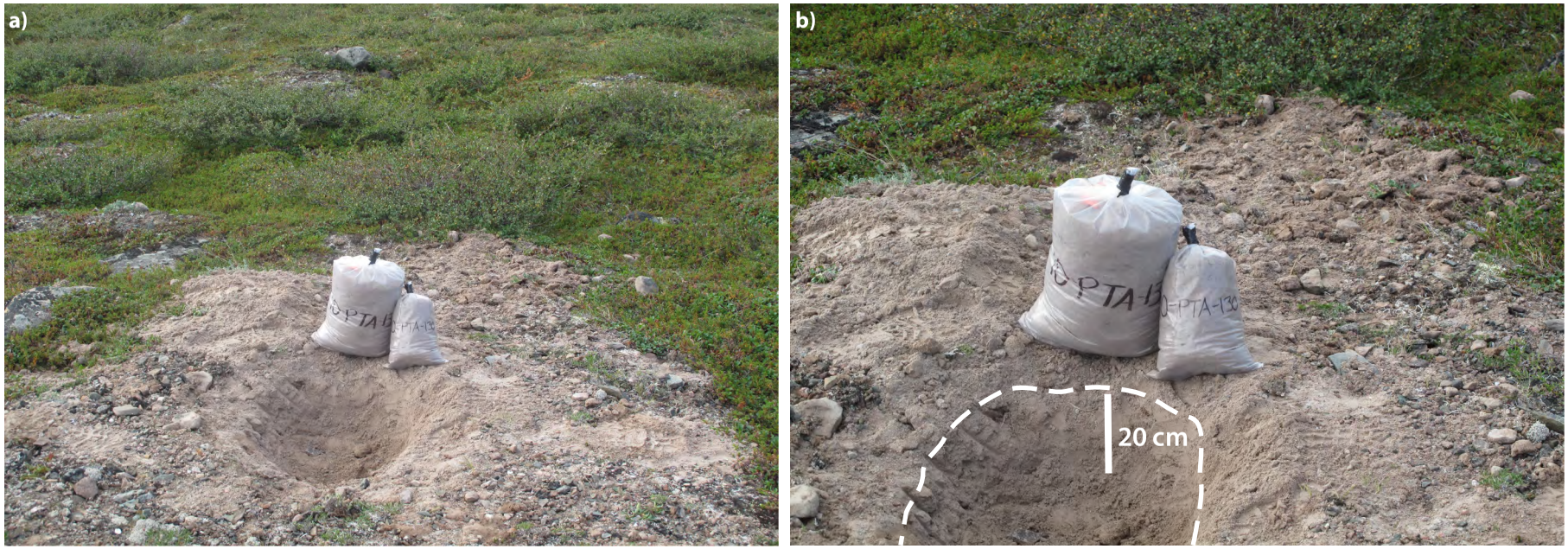

Site 10-PTA-130 a) Overview of the till sample site and samples. **b)** Excavated frost boil showing a beige-brown silty fine-sand till with a cobble and pebble fraction dominated by metawacke.

APPENDIX A3 continued.

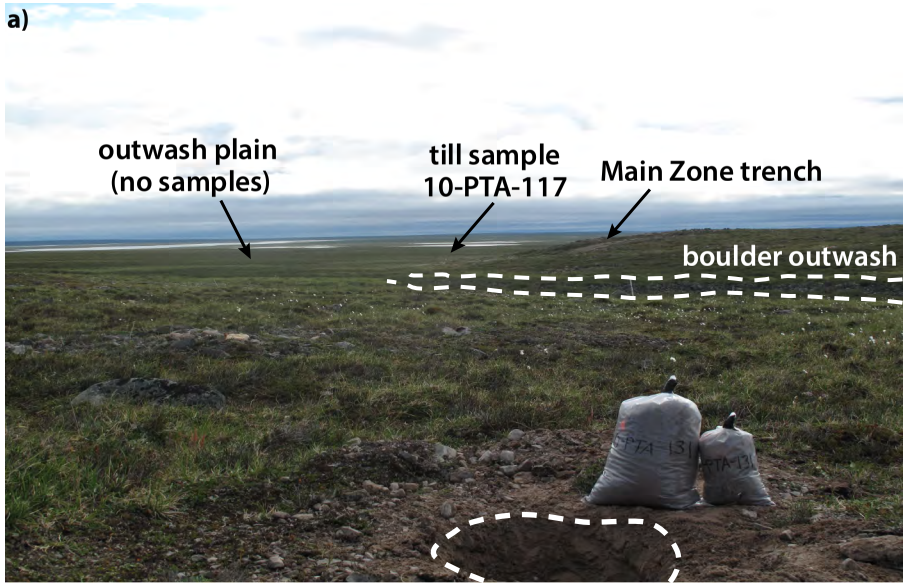

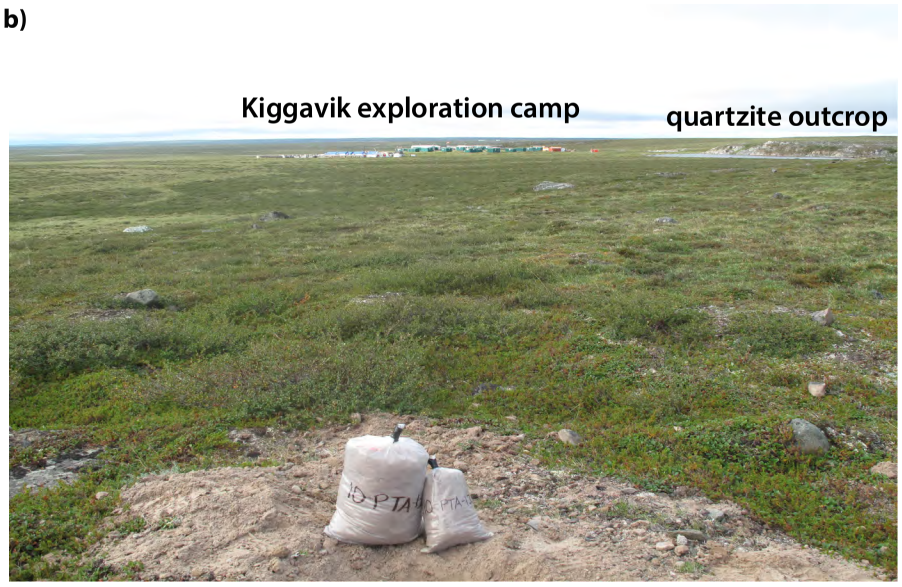

Site 10-PTA-131

a) Sample site10-PTA-131 looking southeast to the outwash plain, where no samples were collected. The Kiggavik Main Zone trench and the location of sample 10-PTA-117 are noted in the background.

b) Looking southwest to the Kiggavik camp from sample site 10-PTA-131.

c) Heavy mineral concentrate and till geochemistry samples taken from the excavated frost boil.

APPENDIX A3 continued.

Site 10-PTA-132

a) Frost boil prior to digging. Note the high clast content, dominated by metawacke and granite.

b) Overview of the till sample site, looking to the west.

c) Excavated frost boil, showing abundant pebbles that were contained in the sandy till.

APPENDIX A3 continued.

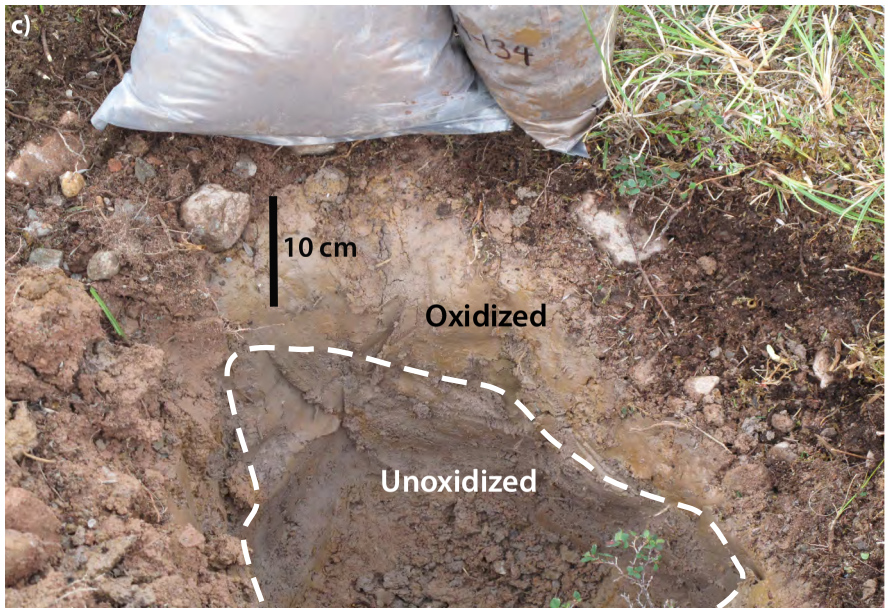

Site 10-PTA-134

a) Overview looking west from the till sample site, which is located in a till plain overlying metawacke bedrock.

b) Heavy mineral concentrate and till geochemistry samples collected from the frost boil with a clay-rich silt texture.

c) Excavated frost boil revealing an upper, brown oxidized till and a lower, grey unoxidized till.

APPENDIX A3 continued.

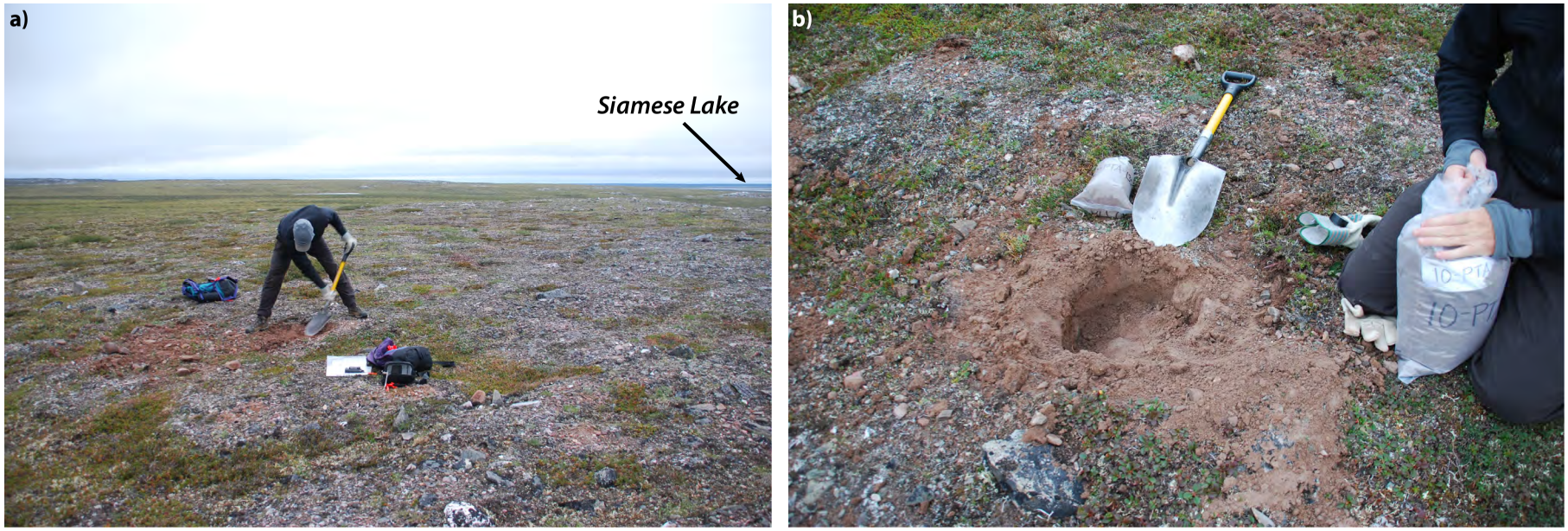

Site 10-PTA-135 a) Till sample site location looking to the southeast where abundant frost boils can be seen. **b)** Sampled frost boil revealing a red-brown silty sand till.

APPENDIX A3 continued.

Site 10-PTA-136
a) Till sample site prior to sampling.
b) Sample being collected from a shallow frost boil.
c) Excavated frost boil revealing a silty sand till with low clast content.

APPENDIX E2 Deposit-scale maps of lead isotope ratio.

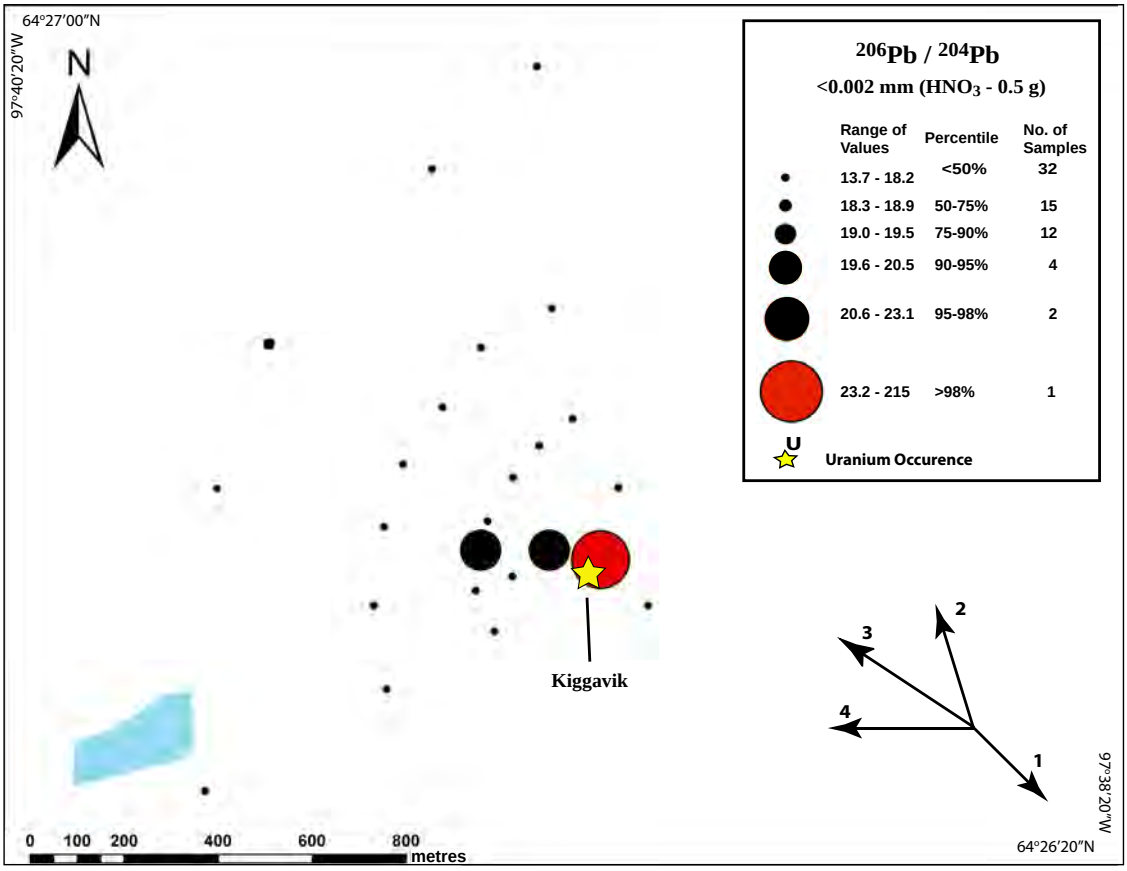

Appendix E2 Map 1. Deposit-scale map of the study area showing the ^{206}Pb /^{204}Pb ratio in the <0.002 mm fraction of the till matrix.

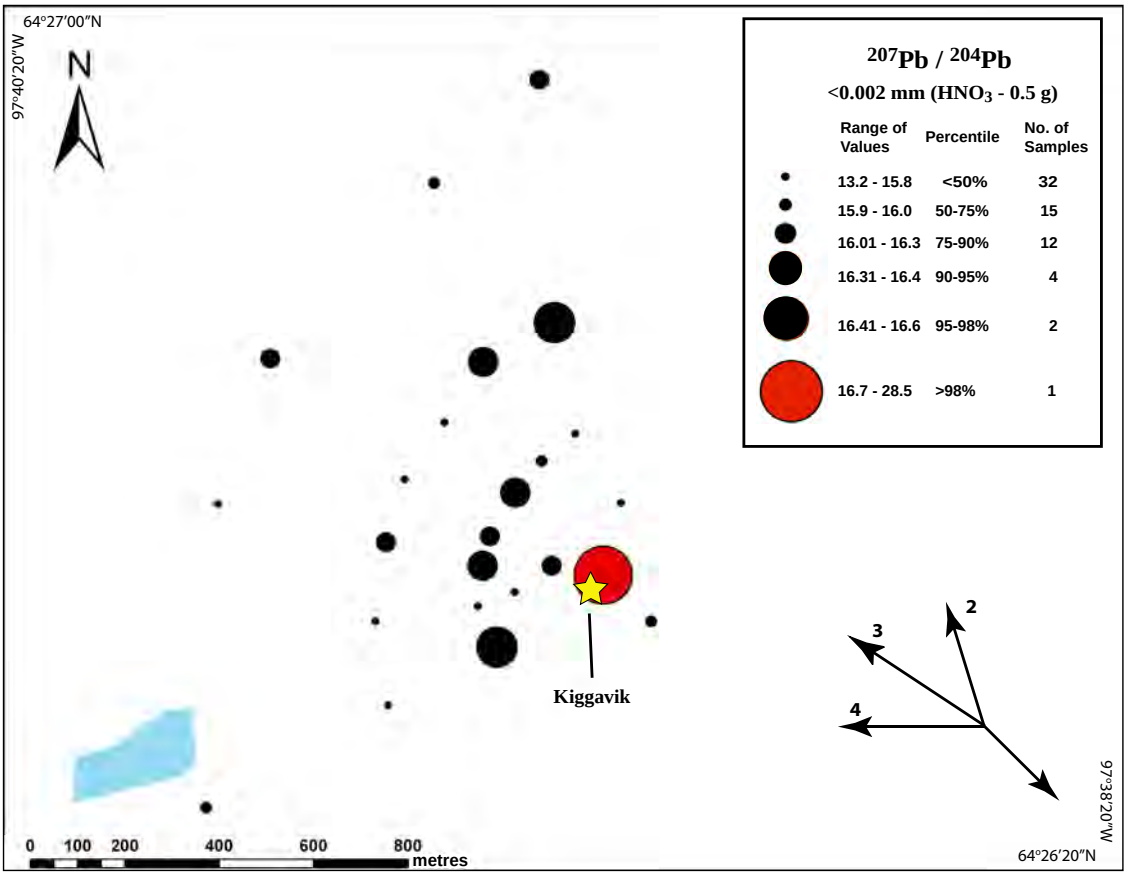

Appendix E2 Map 2. Deposit-scale map of the study area showing the ^{207}Pb /^{204}Pb ratio in the <0.002 mm fraction of the till matrix.

APPENDIX E2 continued.

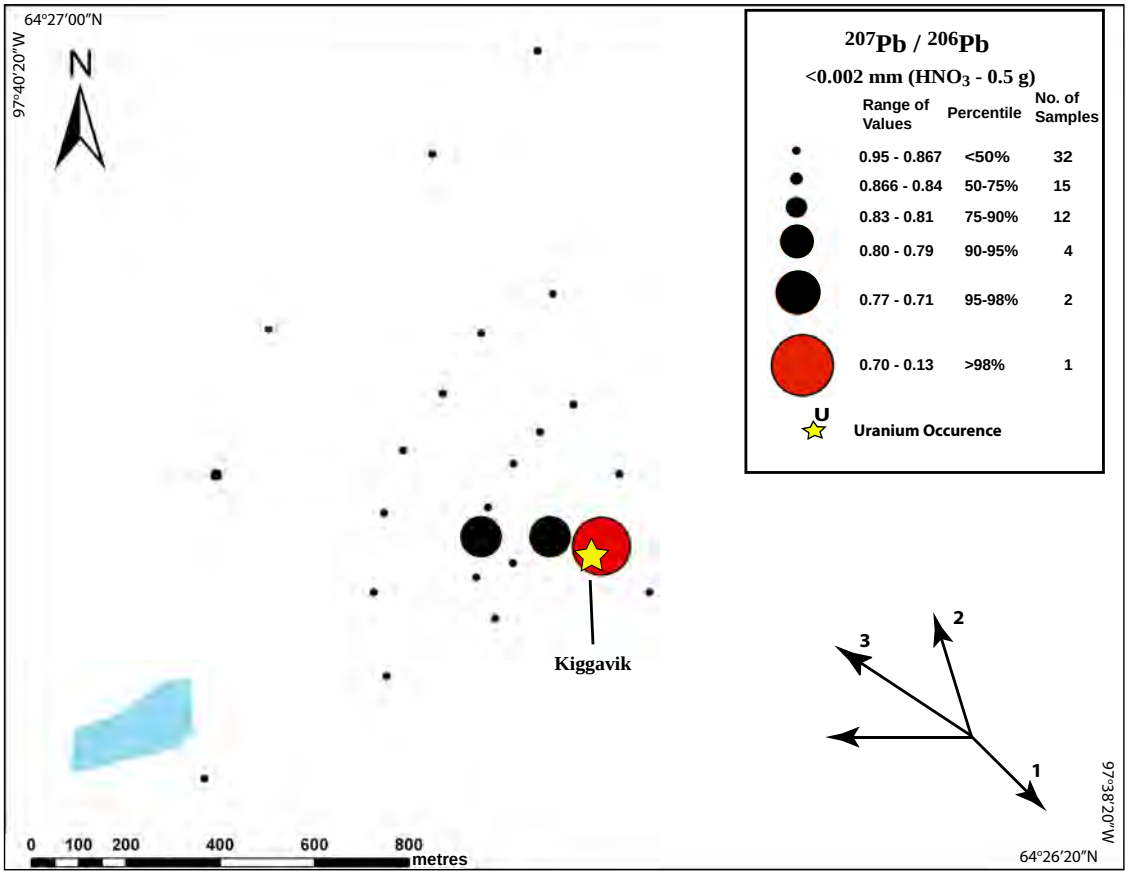

Appendix E2 Map 3. Deposit-scale map of the study area showing the ^{207}Pb /^{206}Pb ratio in the <0.002 mm fraction of the till matrix.

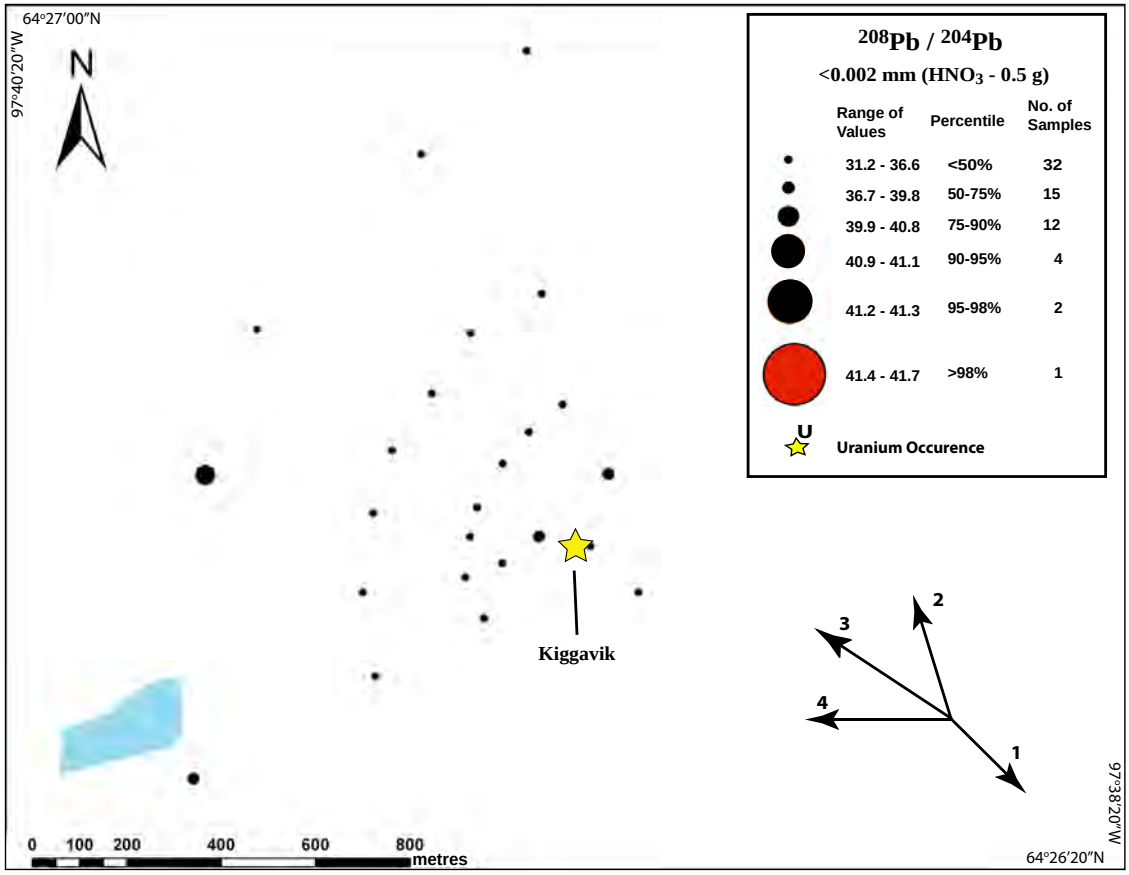

Appendix E2 Map 4. Deposit-scale map of the study area showing the ^{208}Pb /^{204}Pb ratio in the <0.002 mm fraction of the till samples.

APPENDIX E2 continued.

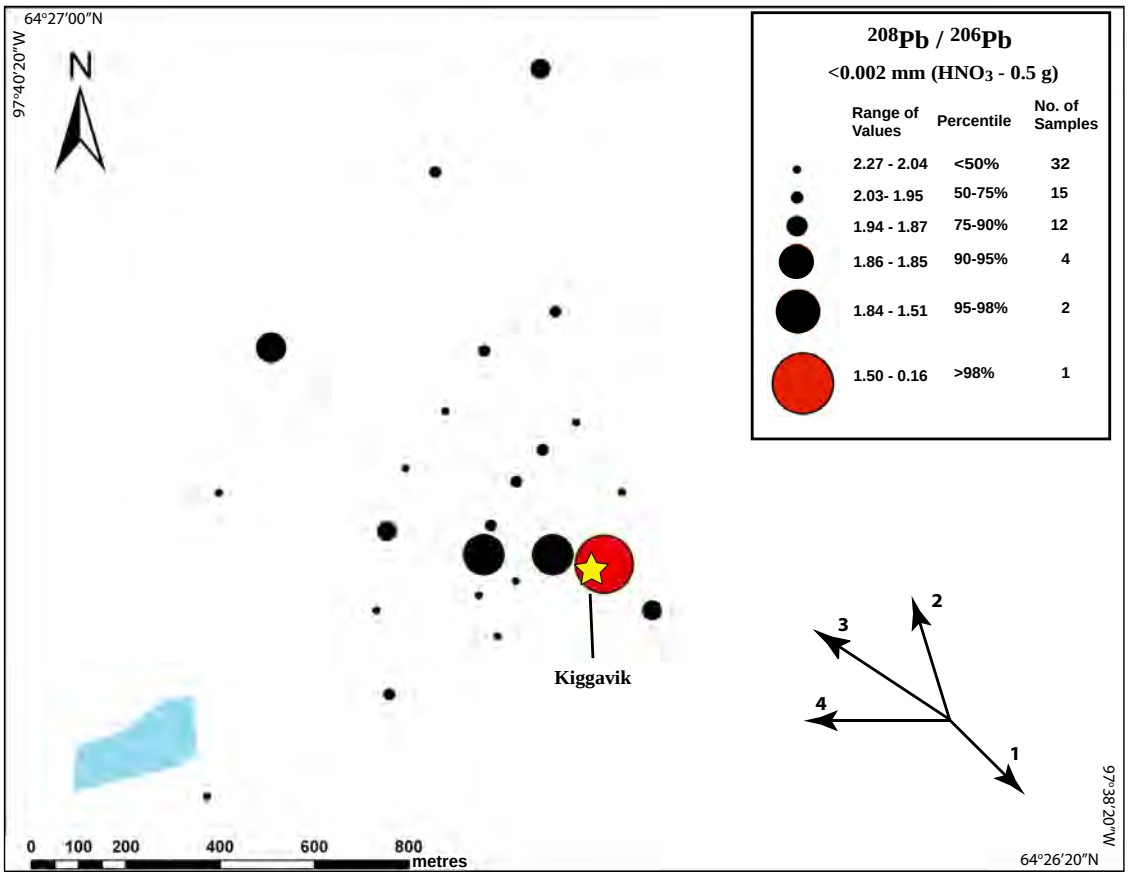

Appendix E2 Map 5. Deposit-scale map of the study area showing the ^{208}Pb /^{206}Pb ratio in the <0.002 mm fraction of the till matrix.

APPENDIX E3 Regional-scale maps of lead isotope ratios.

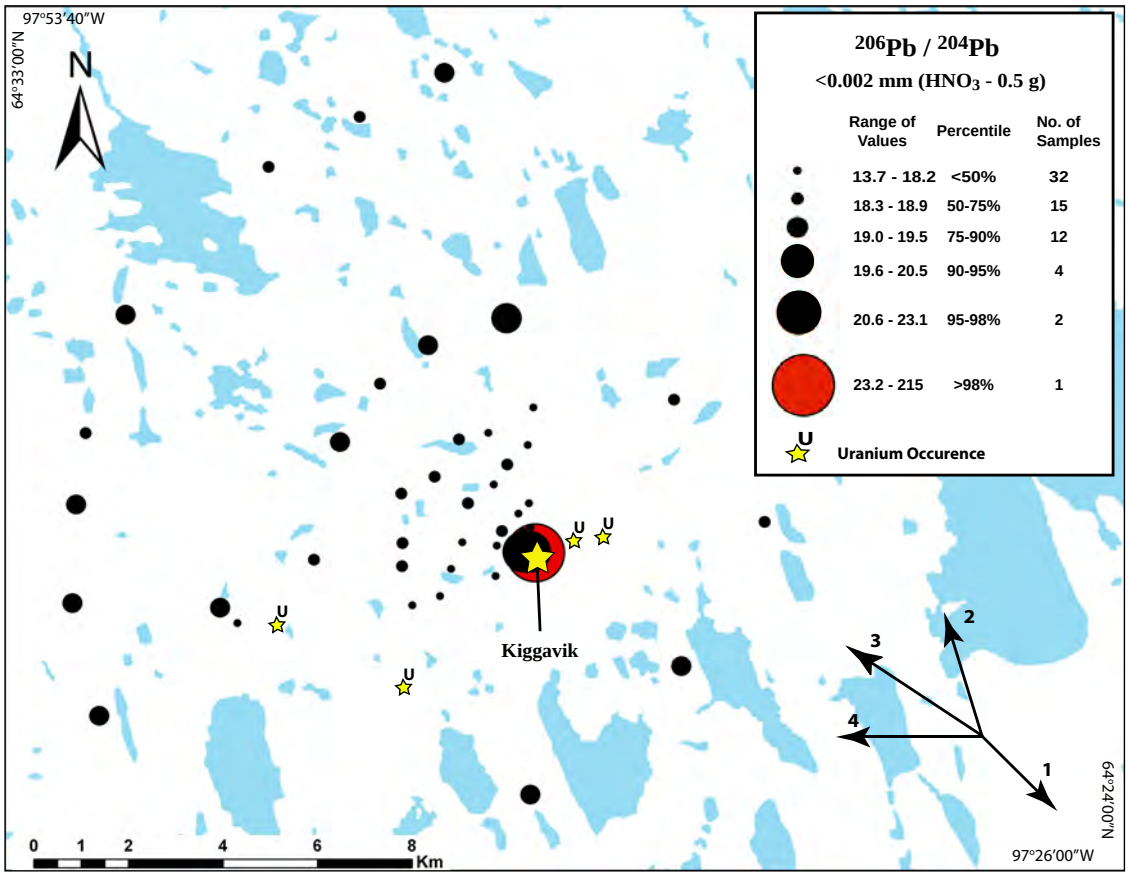

Appendix E3
Map 1. Regional-scale map of the study area showing the ^{206}Pb /^{204}Pb ratio in the <0.002 mm fraction of the till matrix.

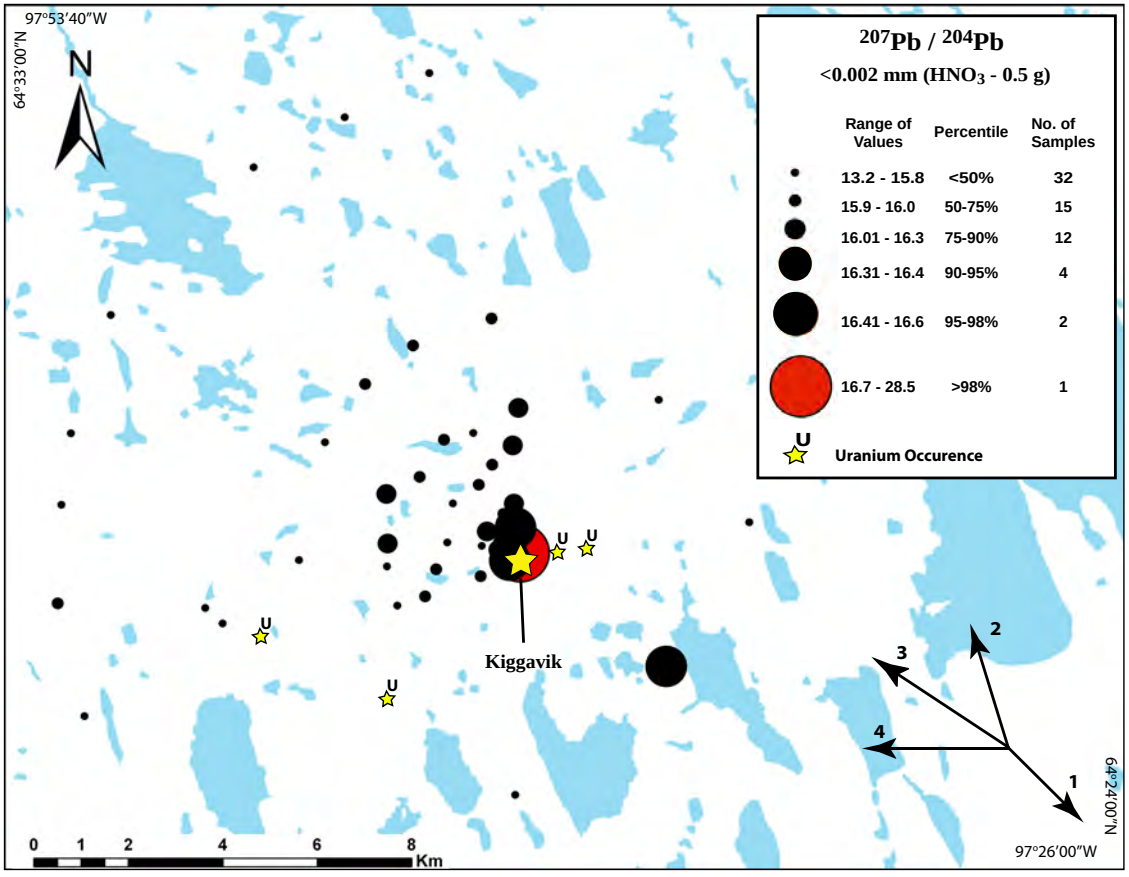

Appendix E2
Map 2. Regional-scale map of the study area showing the ^{207}Pb /^{204}Pb ratio in the <0.002 mm fraction of the till matrix.

APPENDIX E3 continued.

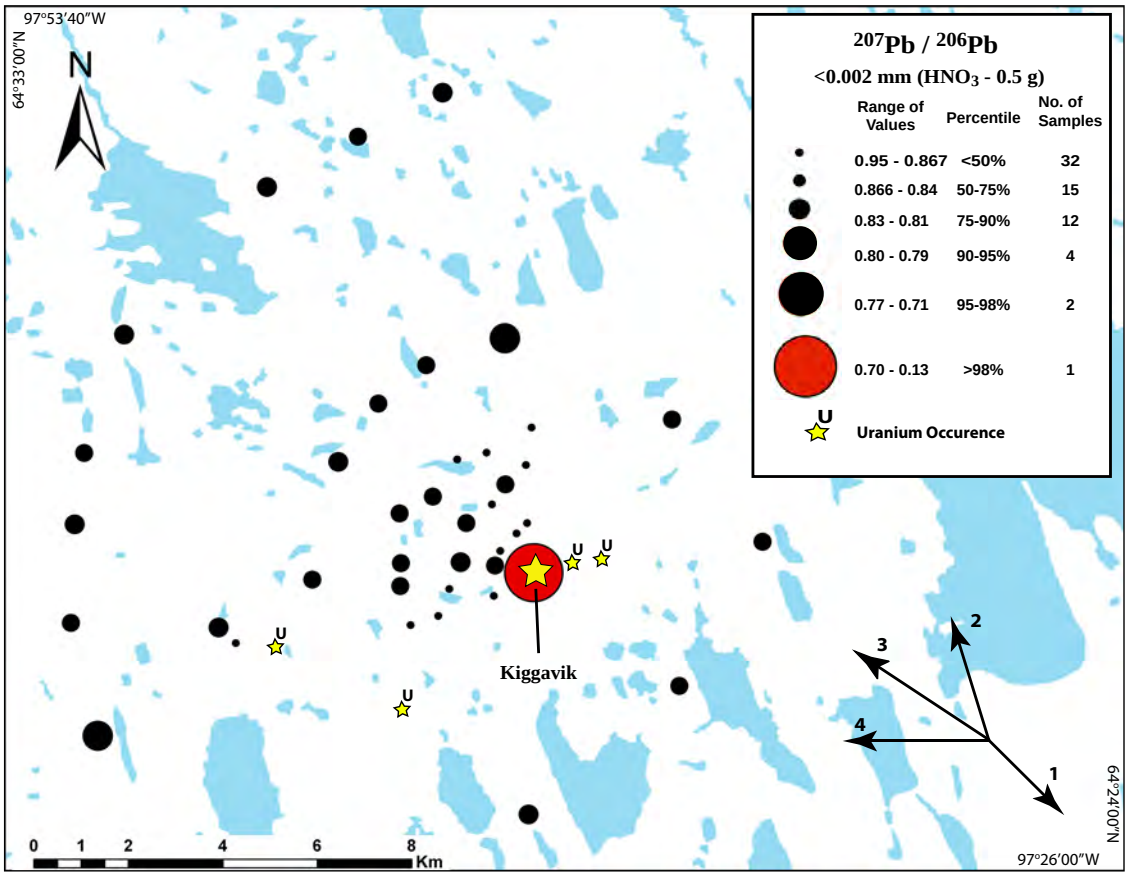

Appendix E3 Map 3. Regional-scale map of the study area showing the ^{207}Pb /^{206}Pb ratio in the <0.002 mm fraction of the till matrix.

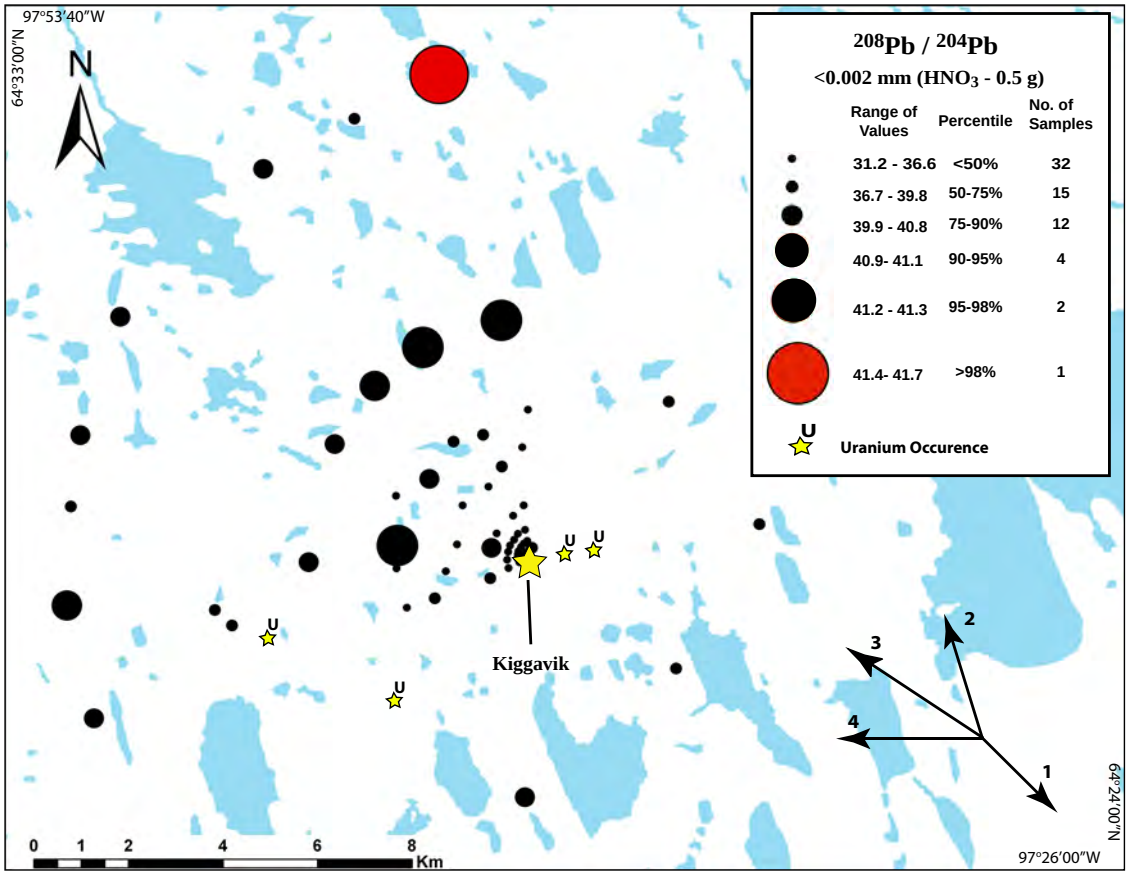

Appendix E3 Map 4. Regional-scale map of the study area showing the ^{208}Pb /^{204}Pb ratio in the <0.002 mm fraction of the till matrix.

APPENDIX E3 continued.

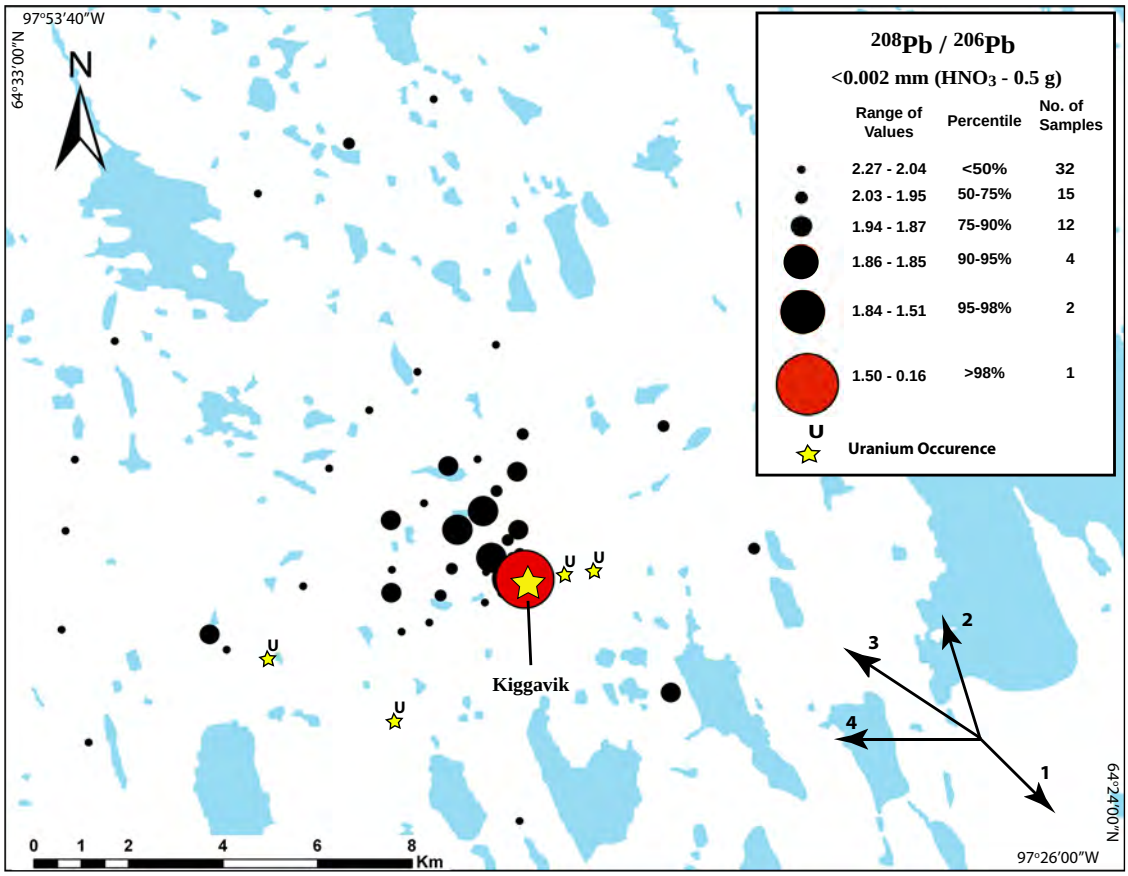

Appendix E3 Map 5. Regional-scale map of the study area showing the $^{208}Pb/^{206}Pb$ ratio in the <0.002 mm fraction of the till matrix.

APPENDIX F

SEMI-QUANTITATIVE X-RAY DIFFRACTION ANALYSES

Alain Grenier and Jeanne B. Percival
Northern and Central Canada Divisions
November, 2011

X-Ray Diffraction Analysis

The mineralogy of bulk materials and clay-size separates is determined by X-ray powder diffraction analysis (XRD). Press-powder mounts are prepared to minimize preferred orientation in specific minerals. Suspensions (in water) of the samples are pipetted onto glass slides and air-dried overnight to produce oriented mounts. X-ray patterns of the press-powder and air-dried samples are recorded on a Bruker D8 Advance Powder Diffractometer equipped with a graphite monochromator, Co Kα radiation set at 40 kV and 40 mA. The samples are also X-rayed following saturation with ethylene glycol and heat treatment (550ºC).

Treatments	
press-powder	2-86 E2θ
air-dried	2-86 E2θ
glycolation	2-86 E2θ
heat treatment (550 EC for 2 hours)	2-35 E2θ

For completeness, all samples were prepared as whole rock mounts (randomly oriented, pressed powder) as well as smear (oriented) mounts.

Mineral Identification and Quantitative Analysis

Initial identification of minerals is made using EVA (Bruker AXS Inc.) software by comparison to reference mineral patterns using Powder Diffraction Files (PDF) of the International Centre for Diffraction Data (ICDD) and other available databases. Quantitative analysis is carried out using TOPAS (Bruker AXS Inc.), a computer-based program that performs Rietveld refinement (RR) of XRD spectra. This is based on a whole pattern fitting algorithm. It relies on having particular mineralogical structure files (.cif) such that the reference minerals are as close a match to the unknown as possible.

Quantitative analyses appear reasonable when minerals in the samples can be matched to the standards. The lower the Goodness of Fit (GoF) value, the closer the standards match the unknowns and the better the results. Difficulty arises when clay minerals of varying composition (e.g. expandable layers, mixed-layers) are encountered, or when mineral species have overlapping X-ray peaks (e.g. kaolinite and chlorite; quartz and graphite). Also, there are a limited number of reference minerals available as structure files; these may not be an exact match to the mineral being analyzed (e.g. using actinolite rather than ferro-hornblende). Differences in estimation will also arise if using a pressed powder (preferable for RR) vs. smear (oriented) samples. Smear samples can be used if insufficient material is available. Occasionally smear mounts are made in order to better identify the clay minerals that are found in minor to trace amounts, as the orientation enhances the *00l* peaks relative to the *hkl* peaks.

Results

Quartz is the most abundant phase in all samples, ranging between 27 and 47 wt.% (Table F1). Chlorite-group, illite, plagioclase feldspar, K-feldspar, kaolinite-group, and hematite minerals occur in minor amounts. Plagioclase feldspar and K-feldspar are relatively consistent with abundance, ranging from 7–1 wt.% and 6–13 wt.%, respectively. Amphibole-group minerals occur in trace amounts in about half the samples. Chlorite-group minerals, confirmed by heat treatment (i.e. disappearance of 7 and 3.54 Δ peaks and increased intensity of 14 Δ peak), range from 6 to 16 wt.%. Illite varies between 8 and 20 wt.%., kaolinite-group minerals vary from 7 to 14 wt.%, and hematite between 3 and 8 wt.%. One sample, 10-PTA-116, contains minor amounts of smectite (~5 wt.%). Mixed-layer clay minerals (illite-smectite) were observed in two samples in trace amounts.

The results are considered semi-quantitative rather than quantitative due to the presence of smectite and the lack of matching or valid mineral structures, as well as the overlap with chlorite in the air-dried sample. At this time, mixed-layer clay minerals were not evaluated because they occur in very trace amounts.

X-ray diffractograms for two samples are presented in Figures F.1 and F.2. Sample 10-PTA-074 (Fig. F.1) is typical of most of the samples. Sample 10-PTA-116 (Fig. F.2) shows the presence of smectite in the glycol-saturated spectrum (red). All X-ray peaks are labeled.

Table F.1. Semi-quantitative (wt.%) analysis based on XRD.

Sample No.	Qtz	Pl	Kfs	Amp	Chl	Ill	Kln	Sm	ML	Hem	GoF
10-PTA-047	39	8	9		11	18	10			5	3.28
10-PTA-074	38	7	10		12	18	9			5	3.38
10-PTA-078	42	9	13		14	13	6			4	4.52
10-PTA-082	40	8	12		6	20	11			3	3.87
10-PTA-083	44	10	11	tr	8	12	6			8	3.33
10-PTA-097	40	10	9		11	19	7			4	3.15
10-PTA-111	47	9	11	tr	8	13	8			4	3.82
10-PTA-115	34	10	12	tr	12	17	14		tr	2	3.39
10-PTA-116	41	9	8	tr	12	8	11	5		5	3.41
10-PTA-117	27	9	6		16	20	18			2	4.26
10-PTA-118	33	11	11	tr	13	17	11			3	3.43
10-PTA-119	28	10	13		16	19	10			3	3.65
10-PTA-130	38	10	11	tr	14	11	9			6	3.56
10-PTA-134	37	7	9		10	15	19		tr	3	3.76
10-PTA-135	40	7	8		10	17	13			4	3.21

Amp=amphibole-group mineral; Chl=chlorite-group mineral; GoF=goodness of fit; Hem=hematite; Ill=illite (muscovite); Kfs=K-feldspar; Kln=kaolinite-group mineral; ML=mixed-layer clay mineral; Pl=plagioclase feldspar; Qtz=quartz; Sm=smectite; tr=trace.

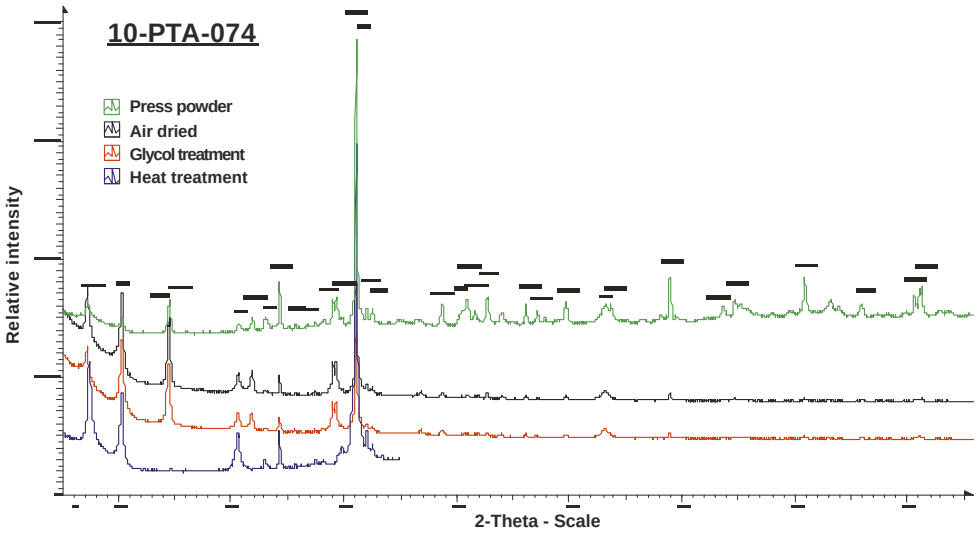

Figure F.1. XRD diffractogram of sample 10-PTA-074.

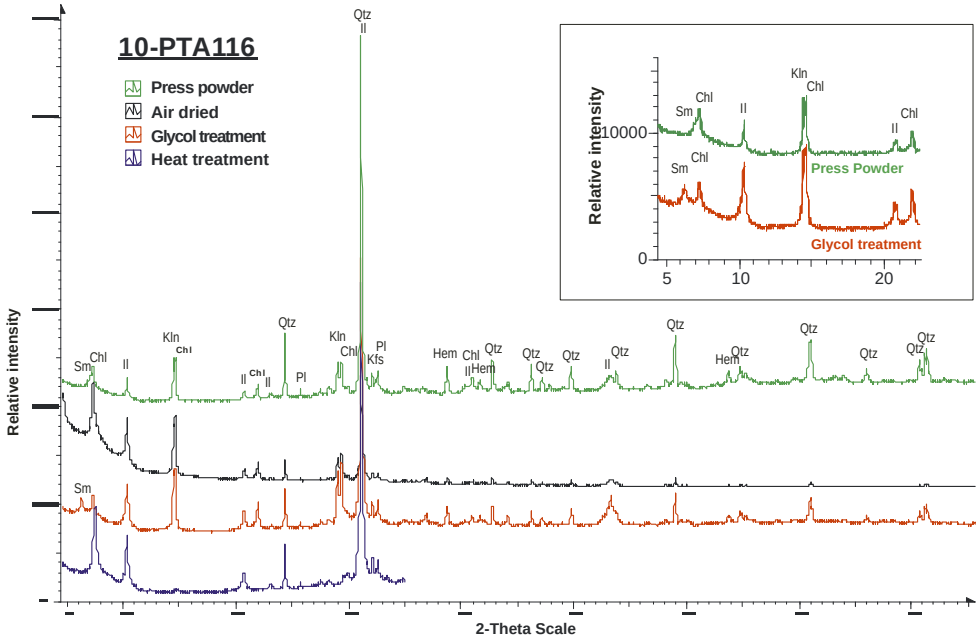

Figure F.2. XRD diffractogram of sample 10-PTA-116.

APPENDIX G2 Deposit-scale maps of gamma-ray spectrometry analyses.

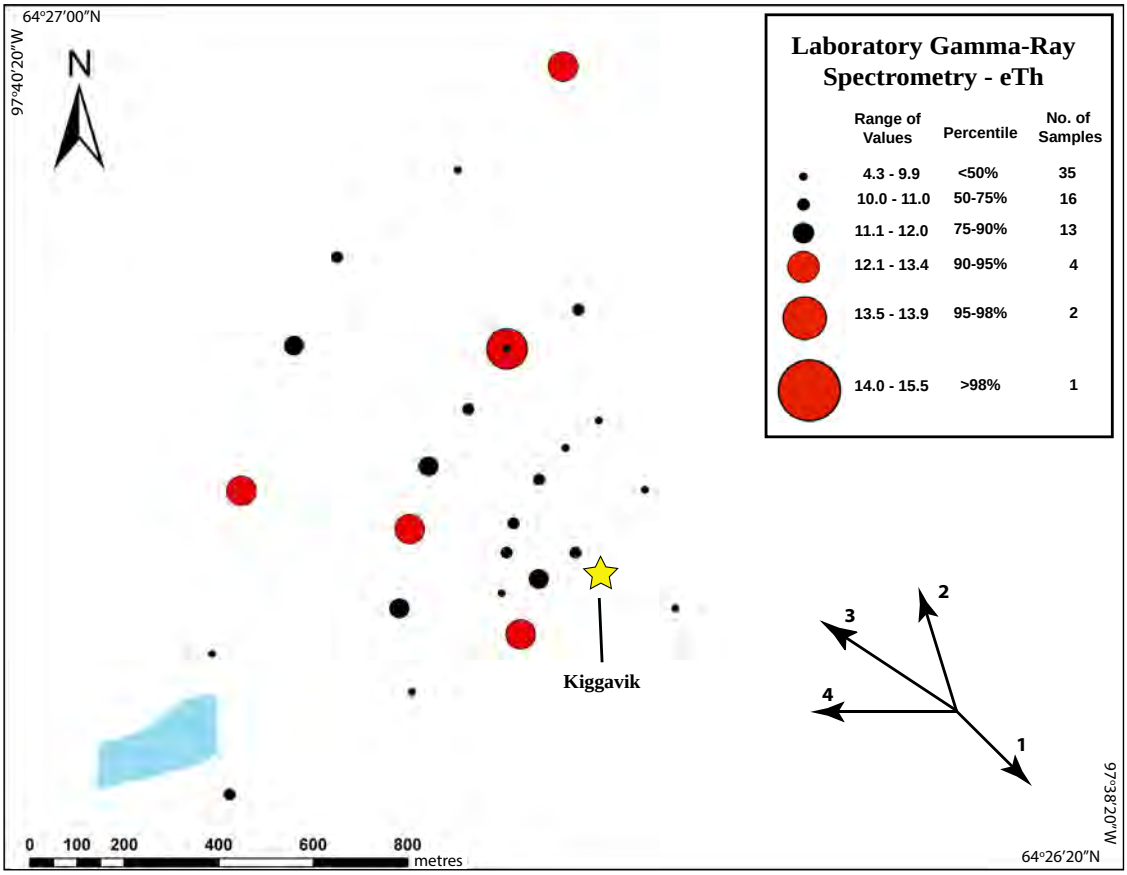

Appendix G2 Map 1. Deposit-scale map of the study area showing eTh values determined by gamma-ray spectrometry .

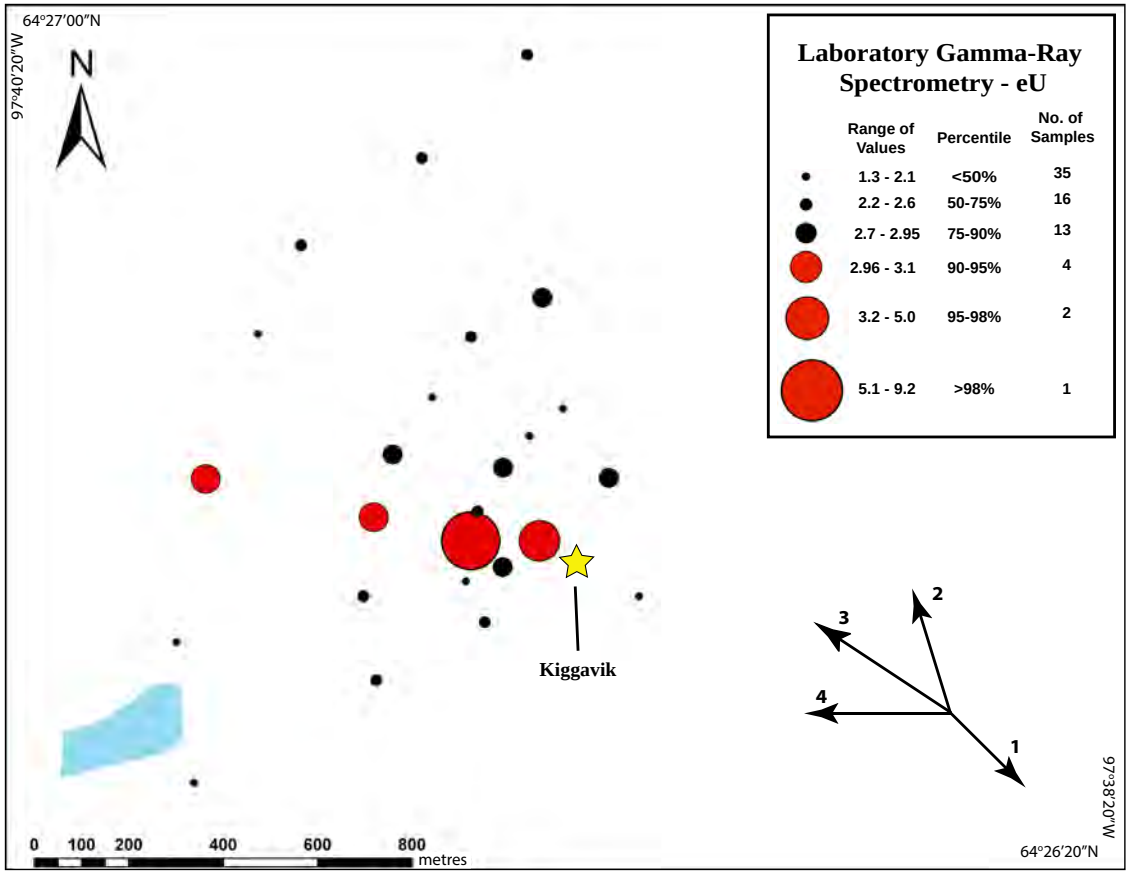

Appendix G2 Map 2. Deposit-scale map of the study area showing eU values determined by gamma-ray spectrometry .

APPENDIX G2 continued.

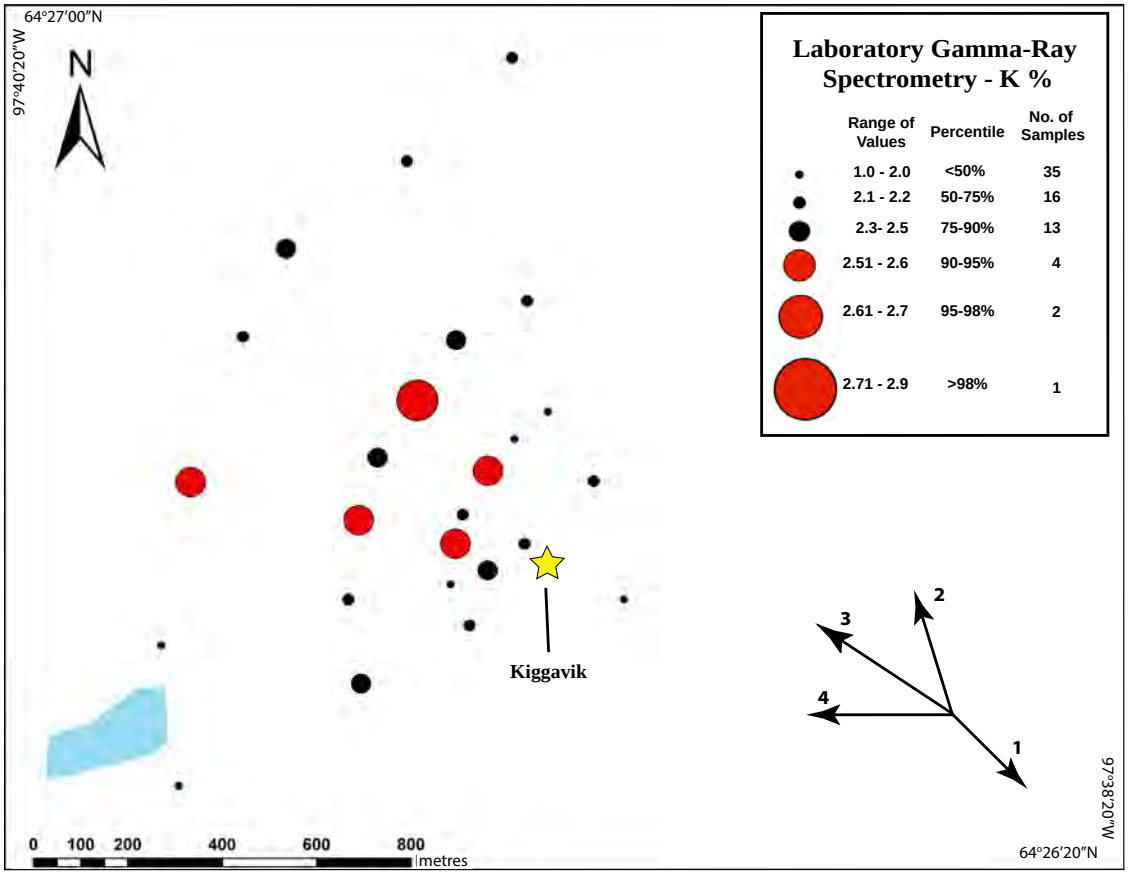

Appendix G2 Map 3. Deposit-scale map of the study area showing K contents (in weight percent) determined by gamma-ray spectrometry.

APPENDIX G3 Regional-scale maps of gamma-ray spectrometry analyses.

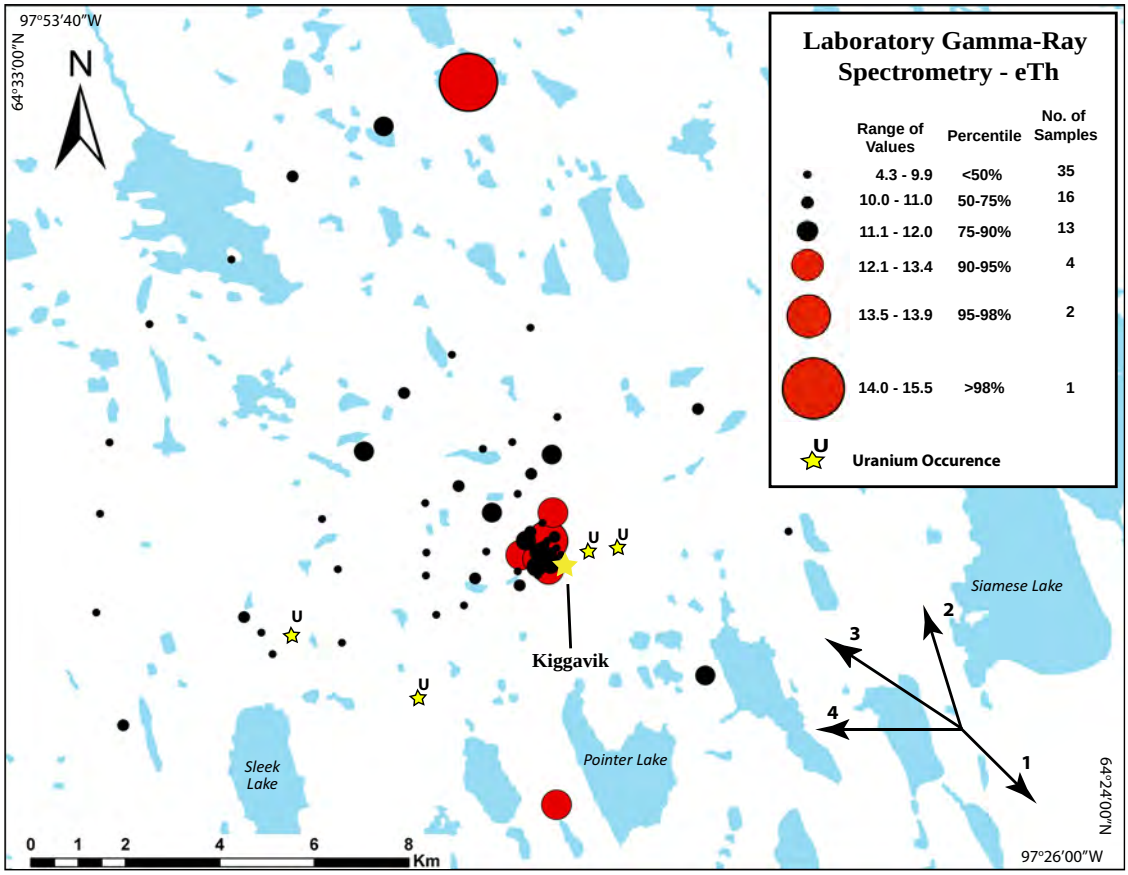

Appendix G3 Map 1. Regional-scale map of the study area showing eTh values determined by gamma-ray spectrometry.

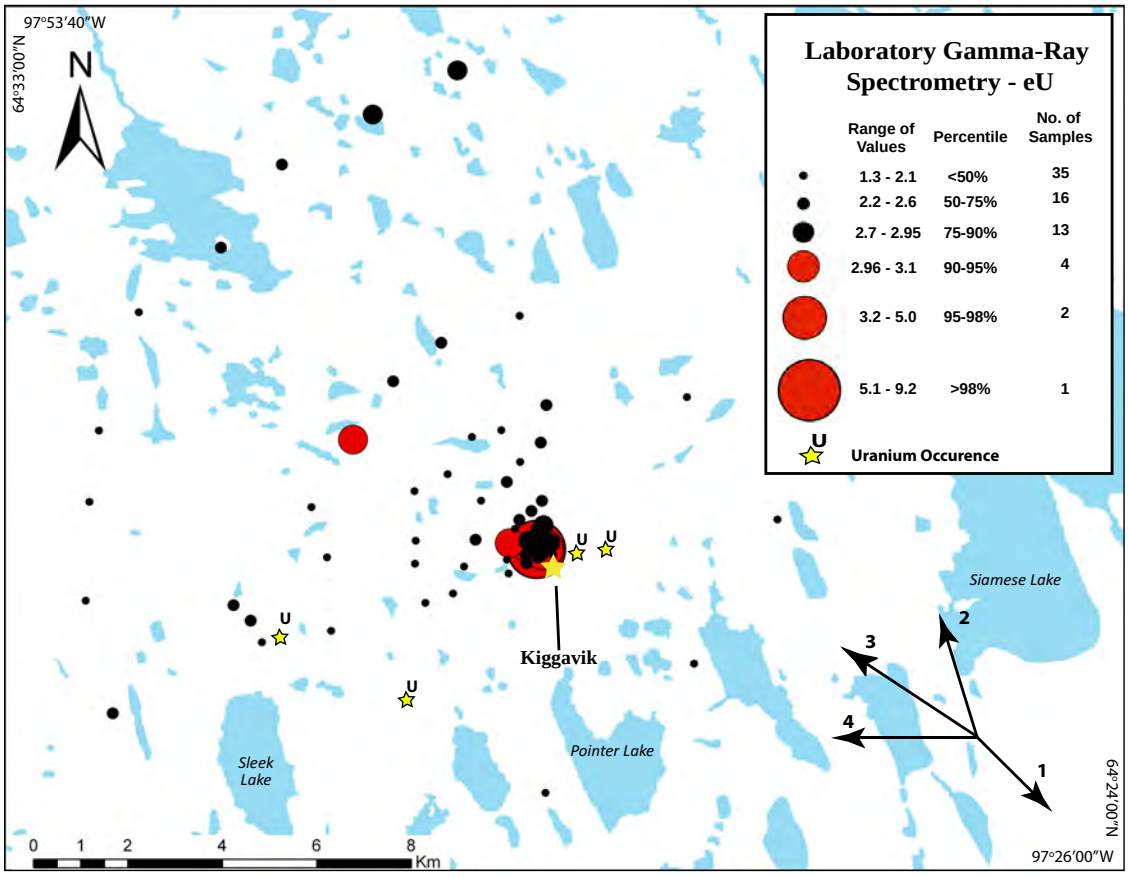

Appendix G3 Map 2. Regional-scale map of the study area showing eU values determined by gamma-ray spectrometry .

APPENDIX G3 continued.

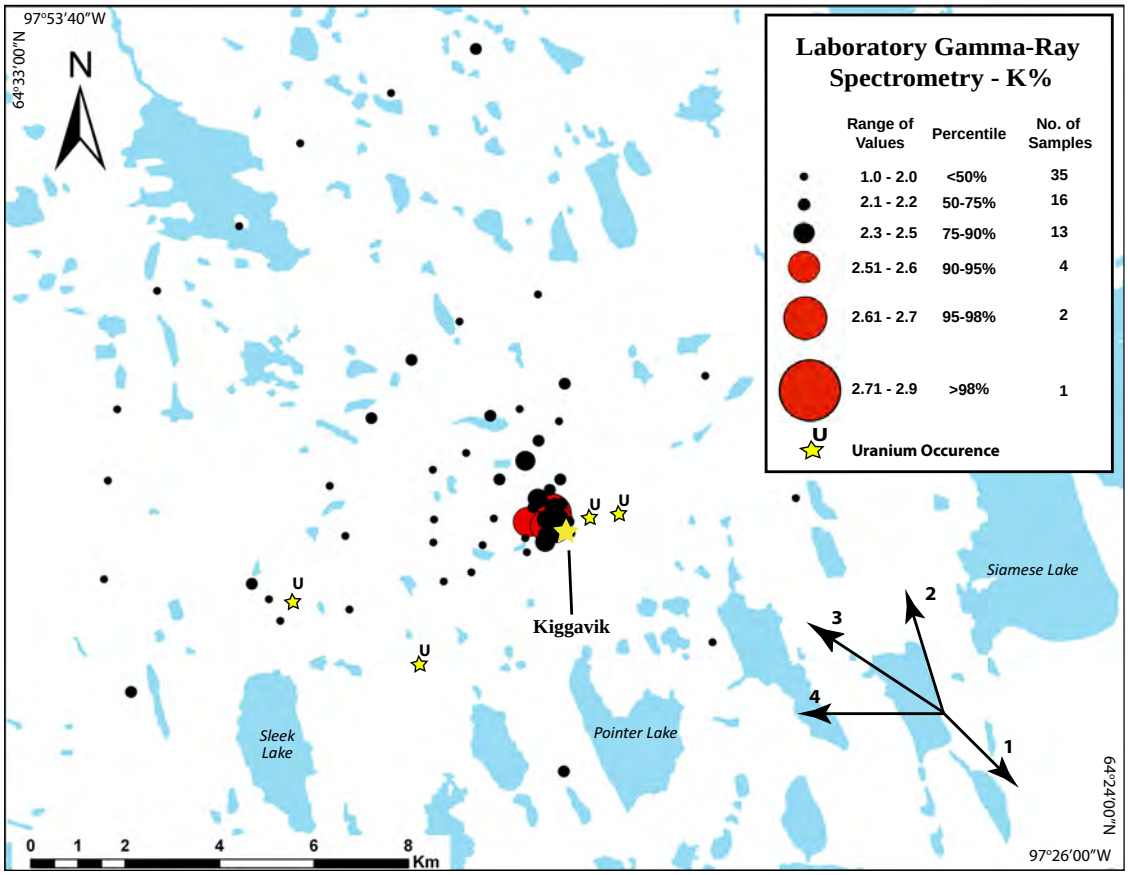

Appendix G3 Map 3. Regional-scale map of the study area showing K contents (in weight percent) determined by gamma-ray spectrometry.

APPENDIX H2 Photographs of pebble counts at each sample site sorted by lithology.

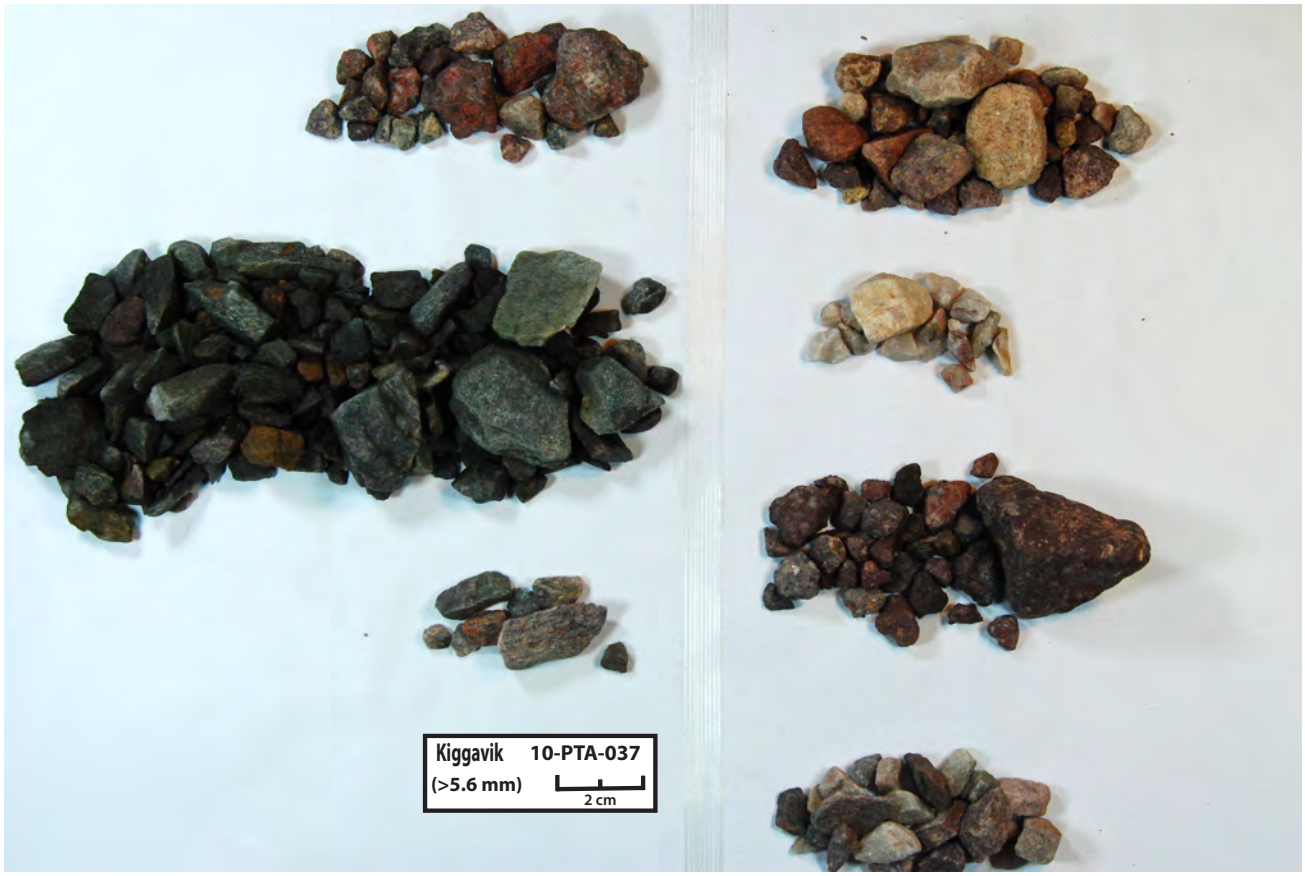

APPENDIX H2 continued.

APPENDIX H2 continued.

APPENDIX H2 continued.

APPENDIX H2 continued.

APPENDIX H2 continued.

APPENDIX H2 continued.

APPENDIX H2 continued.

APPENDIX H2 continued.

APPENDIX H2 continued.

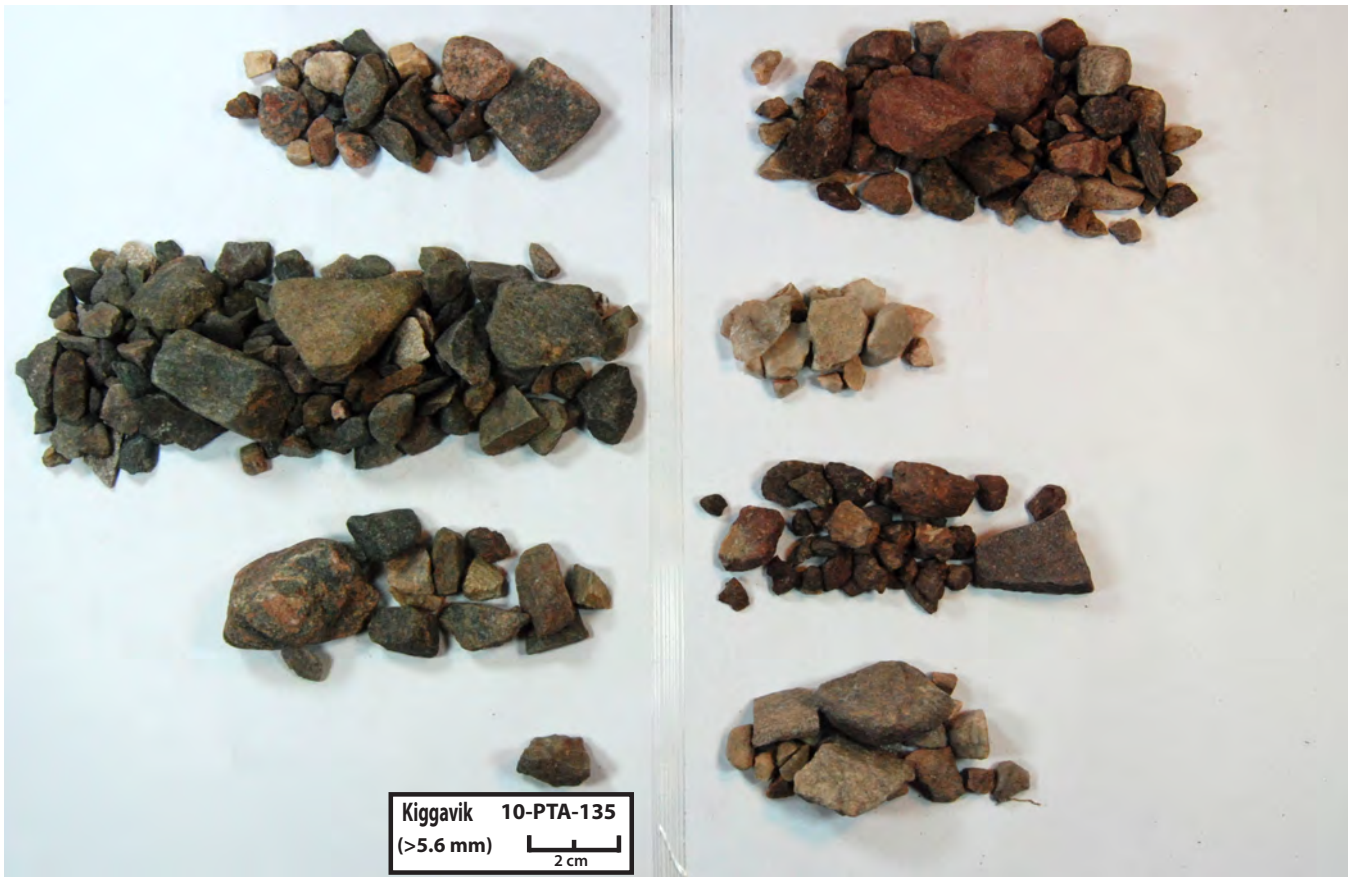

APPENDIX H3 Maps of the study area with lithological pebble counts.

Appendix H3 Map 1. Map of the study area illustrating the number of granitoid gneiss pebbles recovered at each sample site.

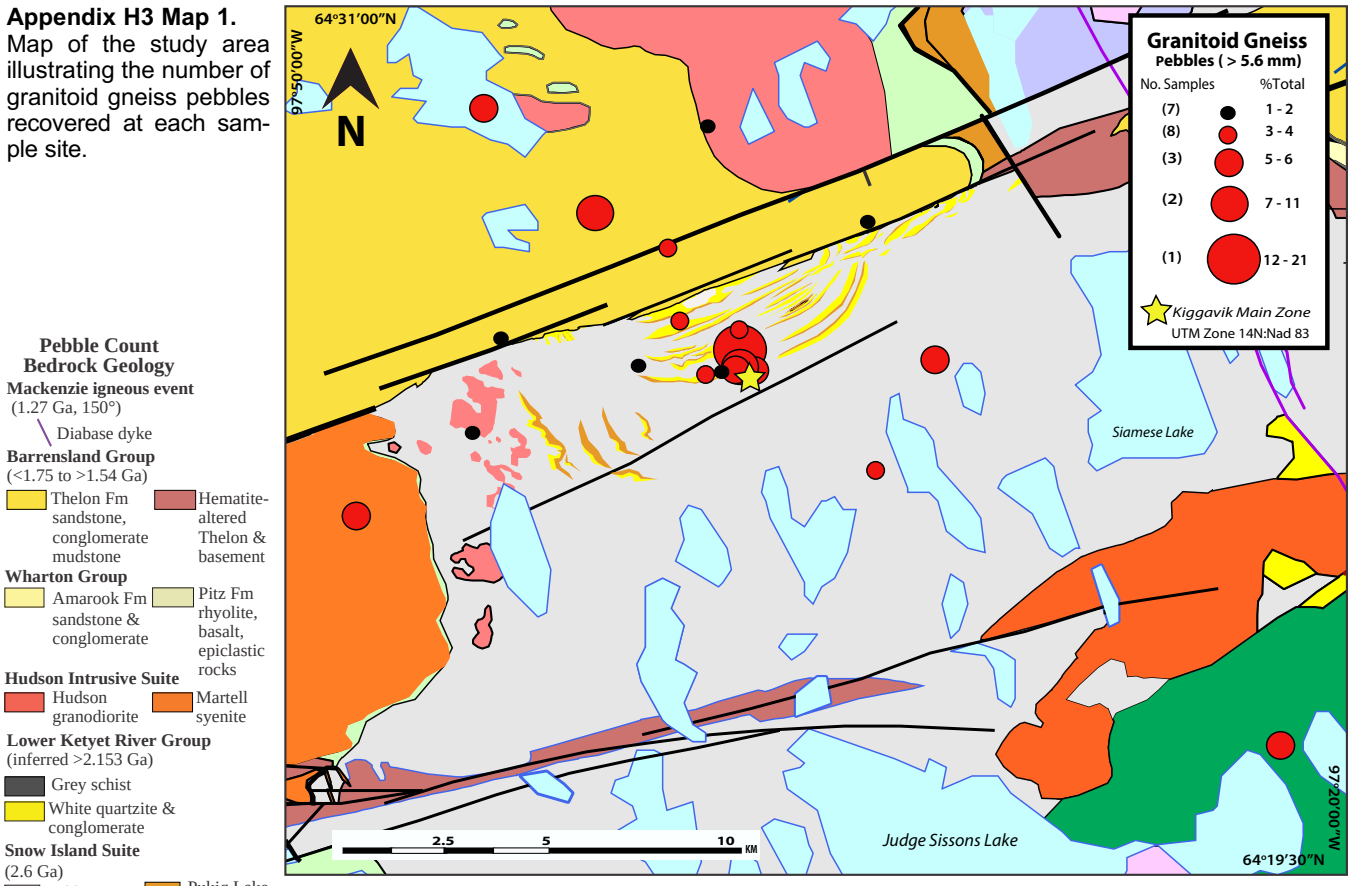

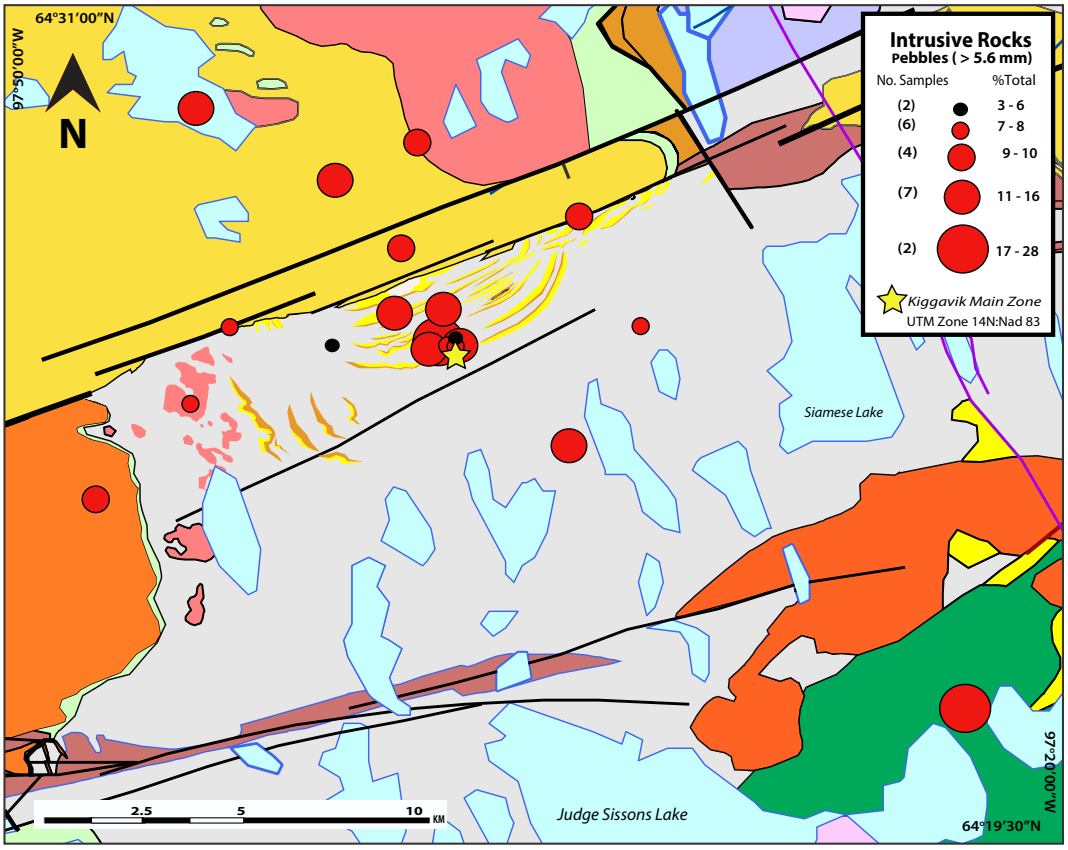

Appendix H3 Map 2. Map of the study area illustrating the number of pebbles of intrusive rock recovered at each sample site.

APPENDIX H3 continued.

Appendix H3 Map 3. Map of the study area illustrating the number of metasedimentary pebbles recovered at each sample site.

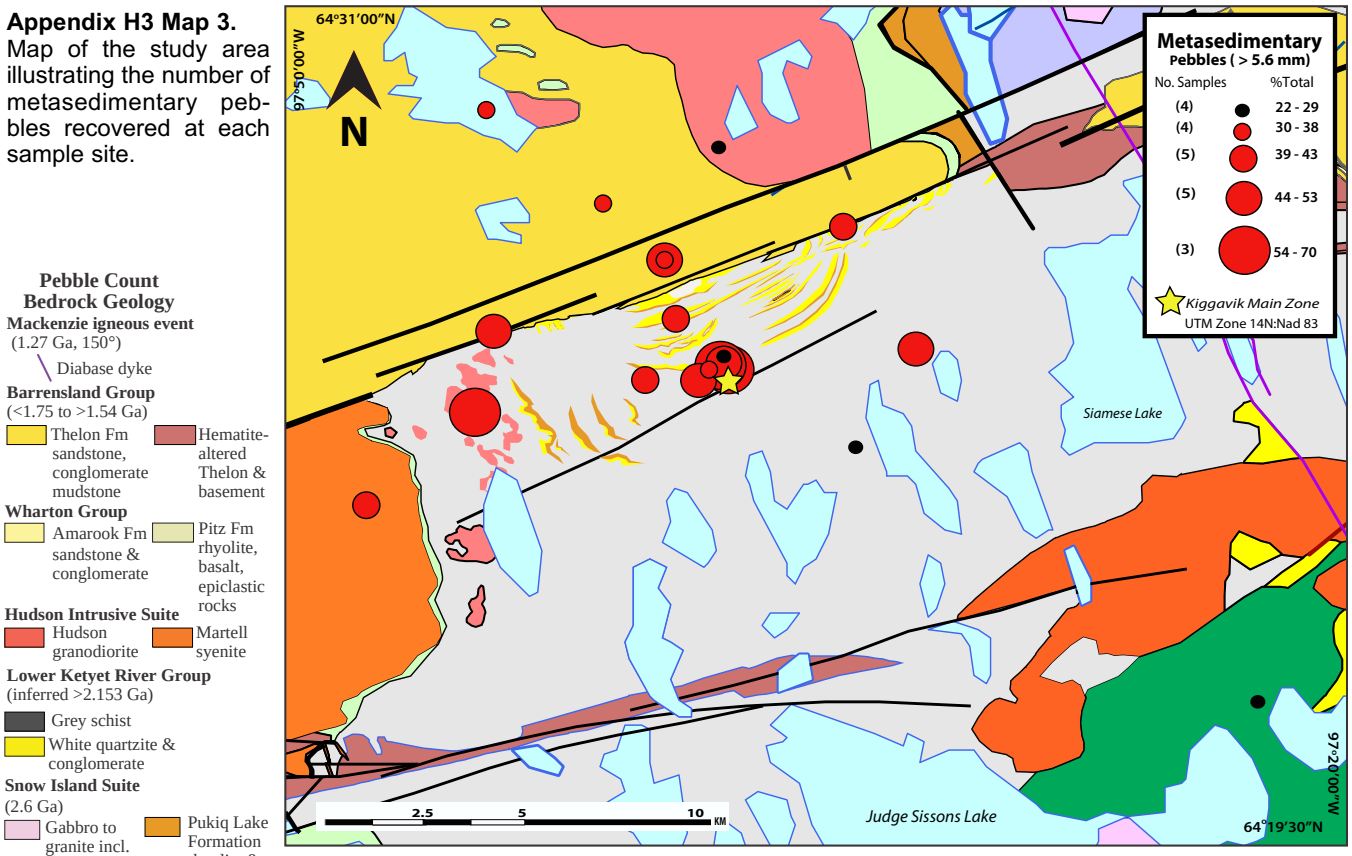

Appendix H3 Map 4. Map of the study area illustrating the number of Pitz volcanic pebbles recovered at each sample site.

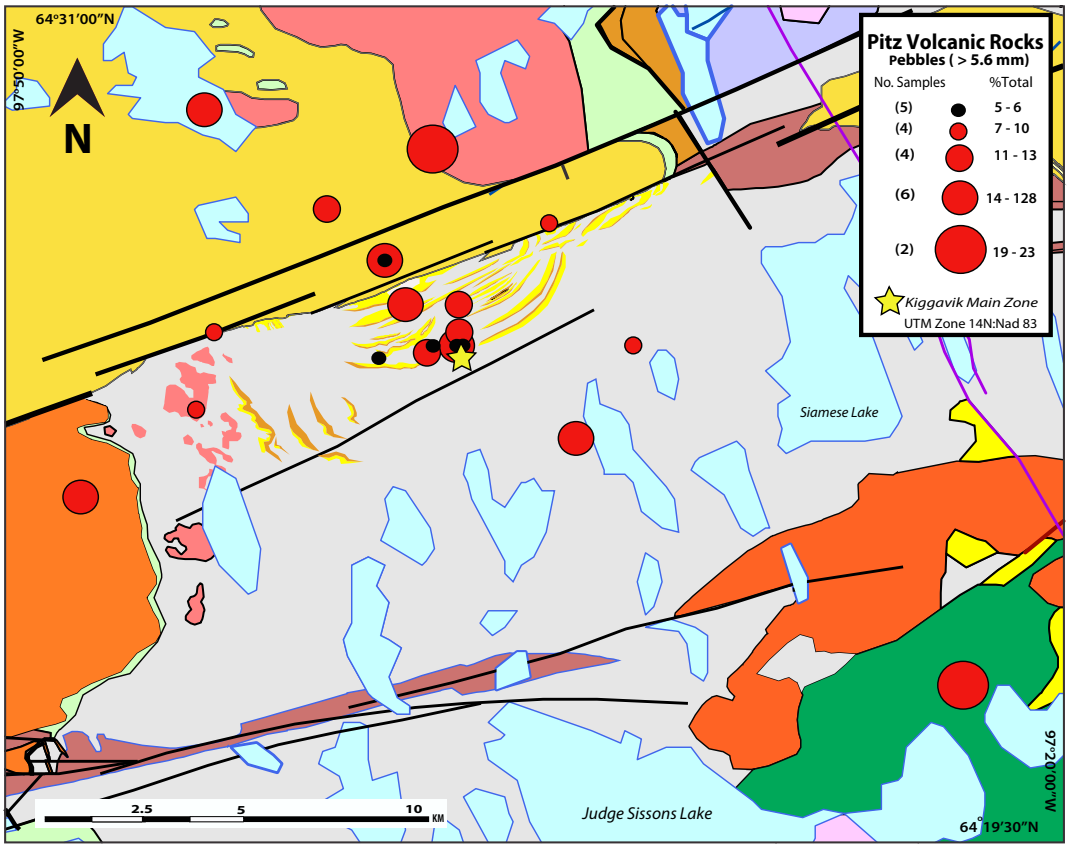

APPENDIX H3 continued.

Appendix H3 Map 5. Map of the study area illustrating the number of quartzite pebbles recovered at each sample site.

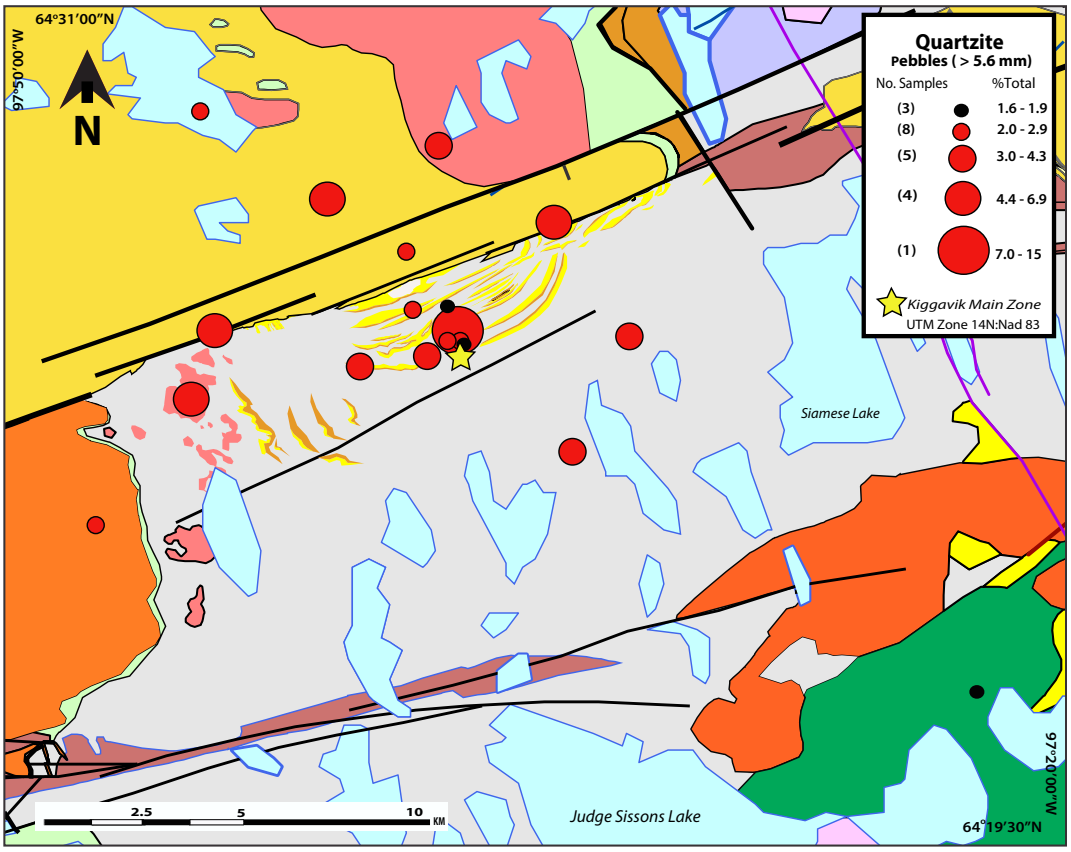

Pebble Count Bedrock Geology

Mackenzie igneous event (1.27 Ga, 150°)
- Diabase dyke

Barrensland Group (<1.75 to >1.54 Ga)
- Thelon Fm sandstone, conglomerate mudstone
- Hematite-altered Thelon & basement

Wharton Group
- Amarook Fm sandstone & conglomerate
- Pitz Fm rhyolite, basalt, epiclastic rocks

Hudson Intrusive Suite
- Hudson granodiorite
- Martell syenite

Lower Ketyet River Group (inferred >2.153 Ga)
- Grey schist
- White quartzite & conglomerate

Snow Island Suite (2.6 Ga)
- Gabbro to granite incl. Judge Sissons Pluton
- Pukiq Lake Formation rhyolite & epiclastics

Marjorie Hills assemblage (<2.63 Ga)
- Metasedimentary & metavolcanic gneiss
- BIF

Woodburn Lake Group (Neoarchean)

Amarulik assemblage (<2.68 Ga)
- Greywacke, intra-formational breccia

Pipedream assemblage (2.71 Ga)
- Feldspathic greywacke, local graphitic schist

Halfway Hills assemblage (2.73 Ga)
- Ultramafic to felsic volcanic and sedimentary rocks

Archean basement gneiss
- Undifferentiated granitoid gneiss & amphibolite, possible basement to WLG

Regional Fault

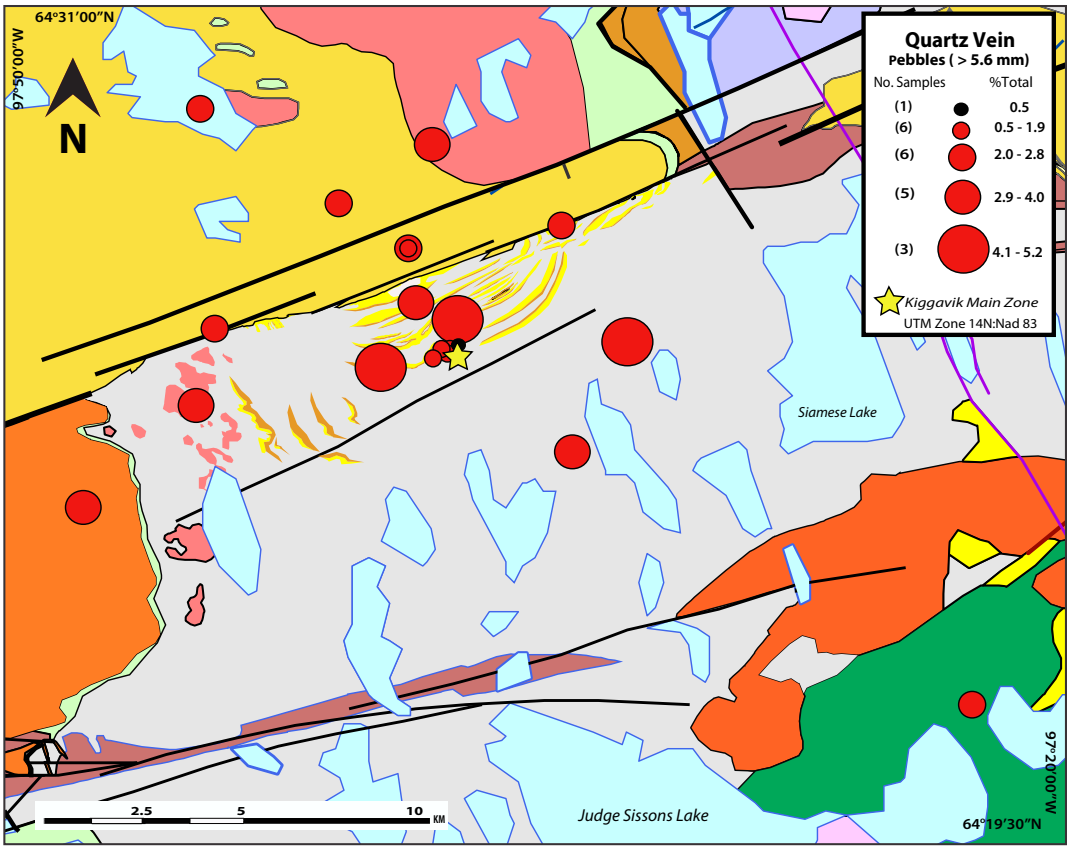

Appendix H3 Map 6. Map of the study area illustrating the number of quartz vein pebbles recovered at each sample site.

APPENDIX H3 continued.

Appendix H3 Map 7. Map of the study area illustrating the number of Thelon Formation pebbles recovered at each sample site.

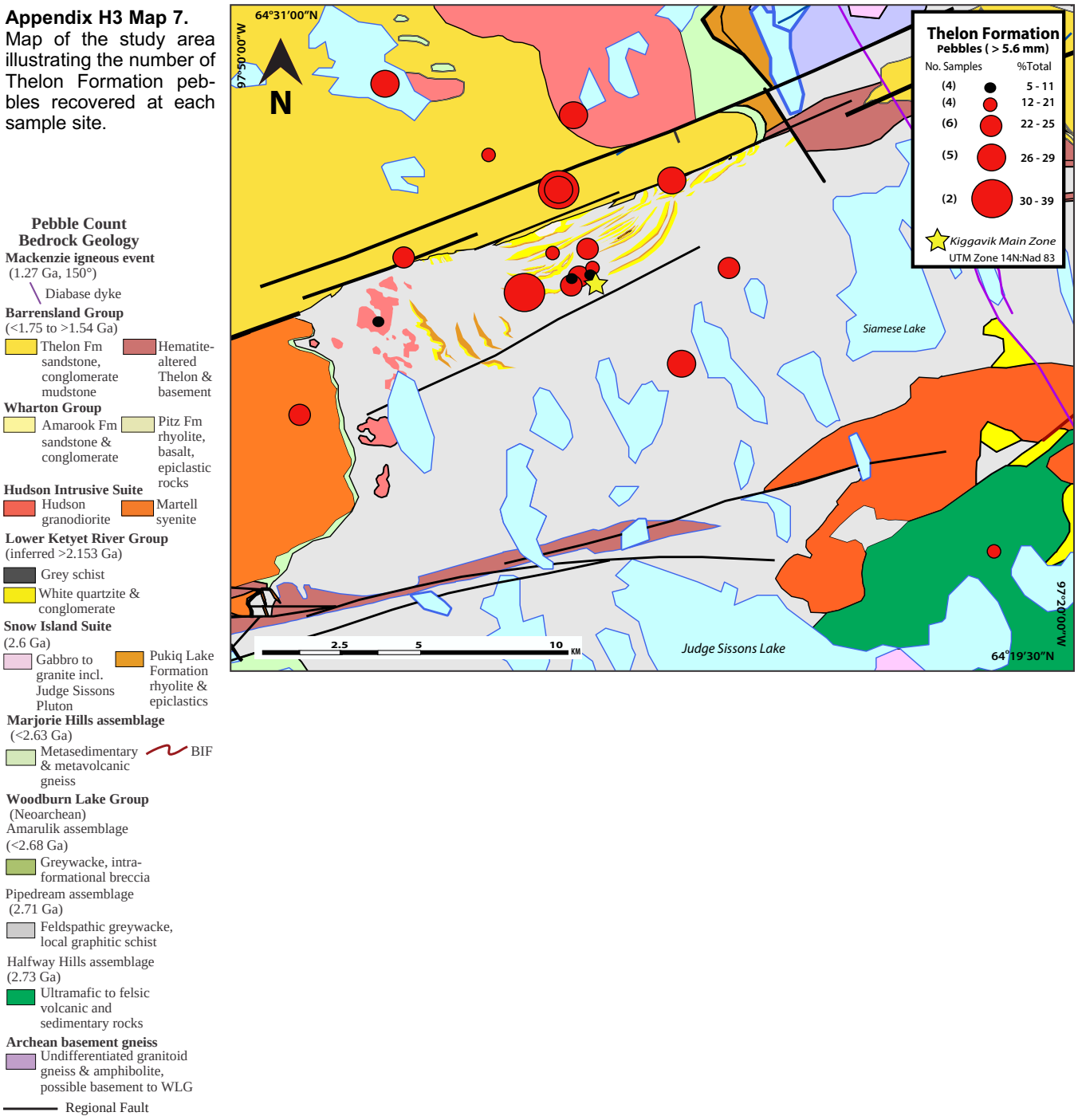

APPENDIX I1 Statistical plots of selected element content in the <0.002 mm fraction.

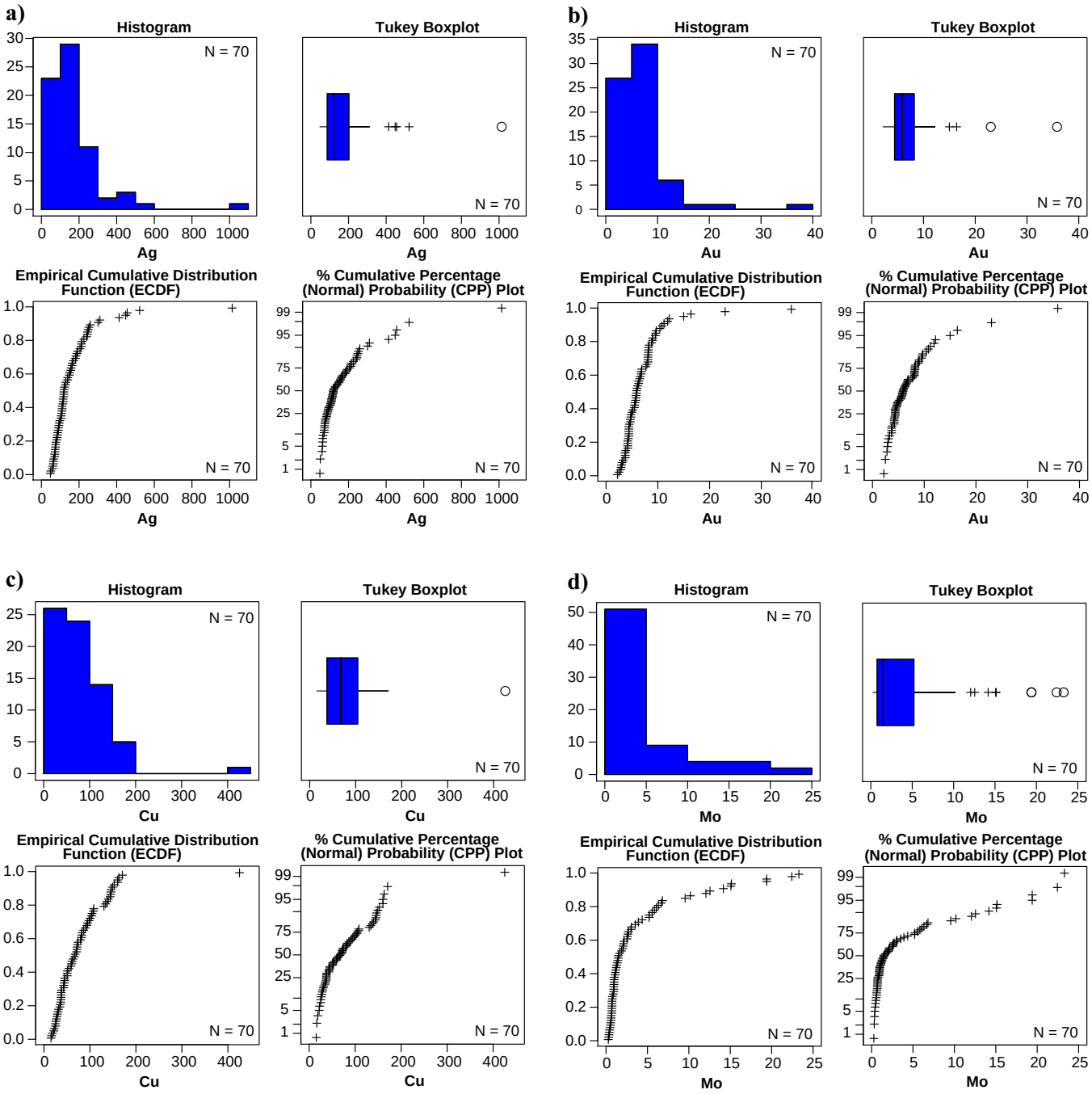

Appendix I1. Statistical plots of selected element content in the <0.002 mm fraction of the sample suite excluding sample 11-PTA-117 (with the exception of plot g): **a)** Ag, **b)** Au, **c)** Cu, and **d)** Mo. Continued on the next page.

APPENDIX I1 continued.

e)

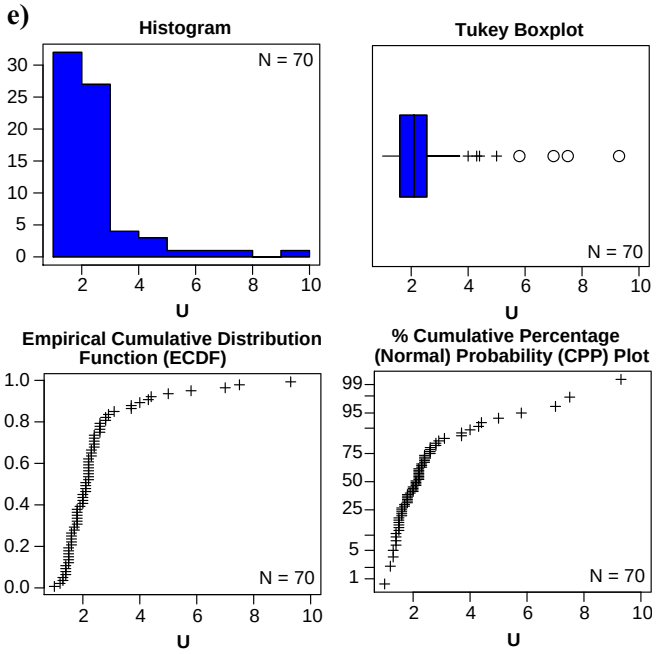

f)

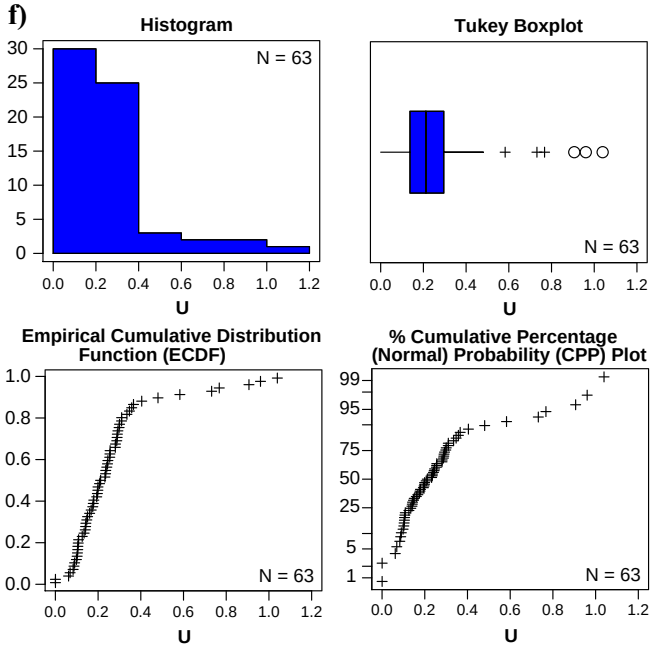

g)

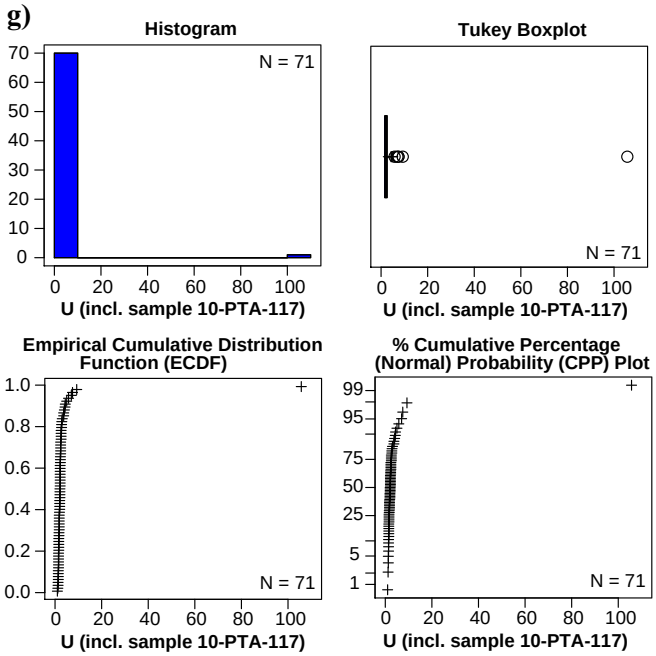

Appendix I1. Continued: **e)** U, **f)** U determined by HNO_3, and **g)** U content including sample 11-PTA-117.

APPENDIX I2 Statistical plots of selected element content in the <0.063 mm fraction.

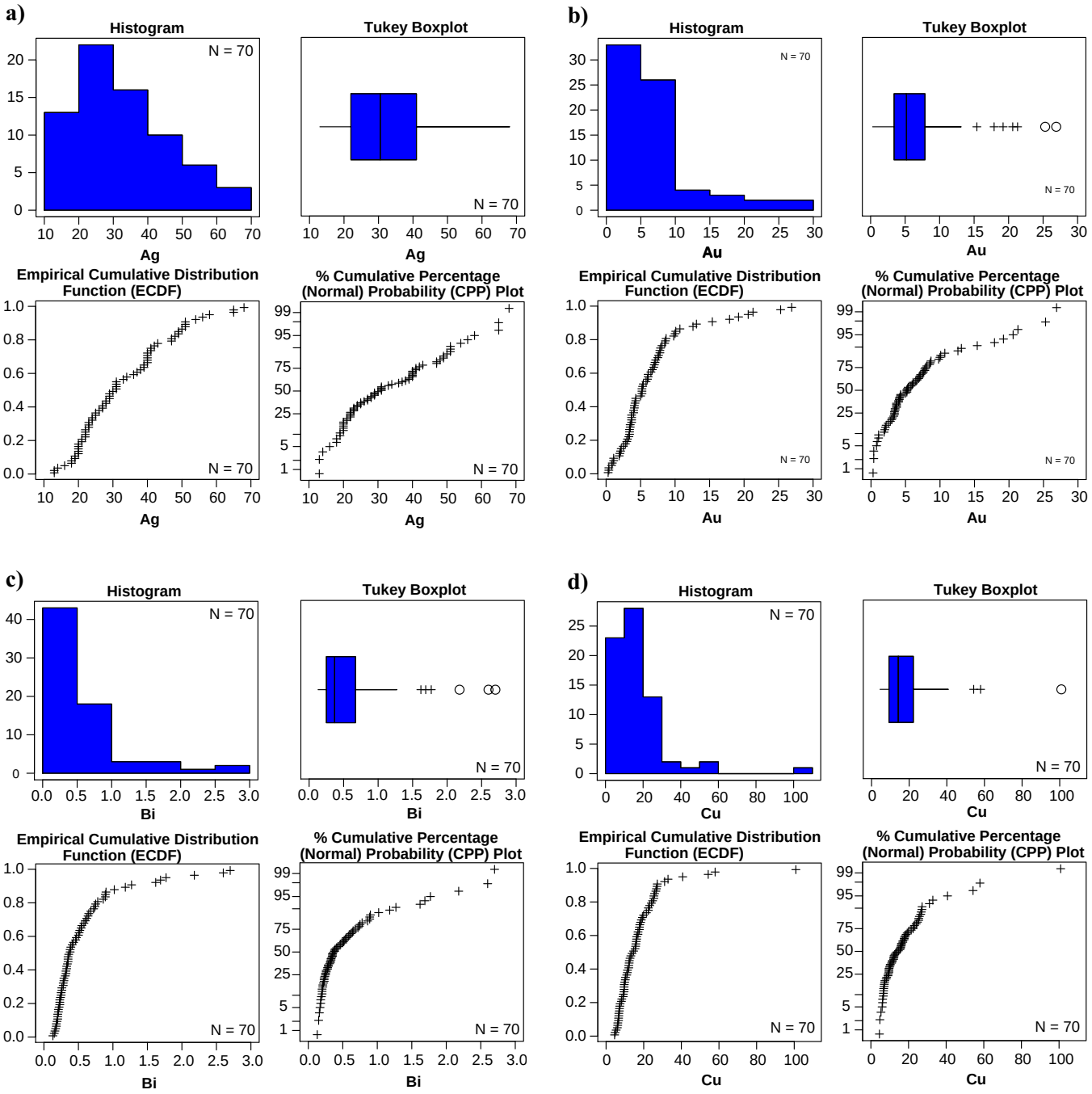

Appendix I2. Statistical plots of selected element content in the <0.002 mm fraction of the sample suite excluding results from sample 11-PTA-117: **a)** Ag, **b)** Au, **c)** Bi, and **d)** Cu. Continued on the next page.

APPENDIX I2 continued.

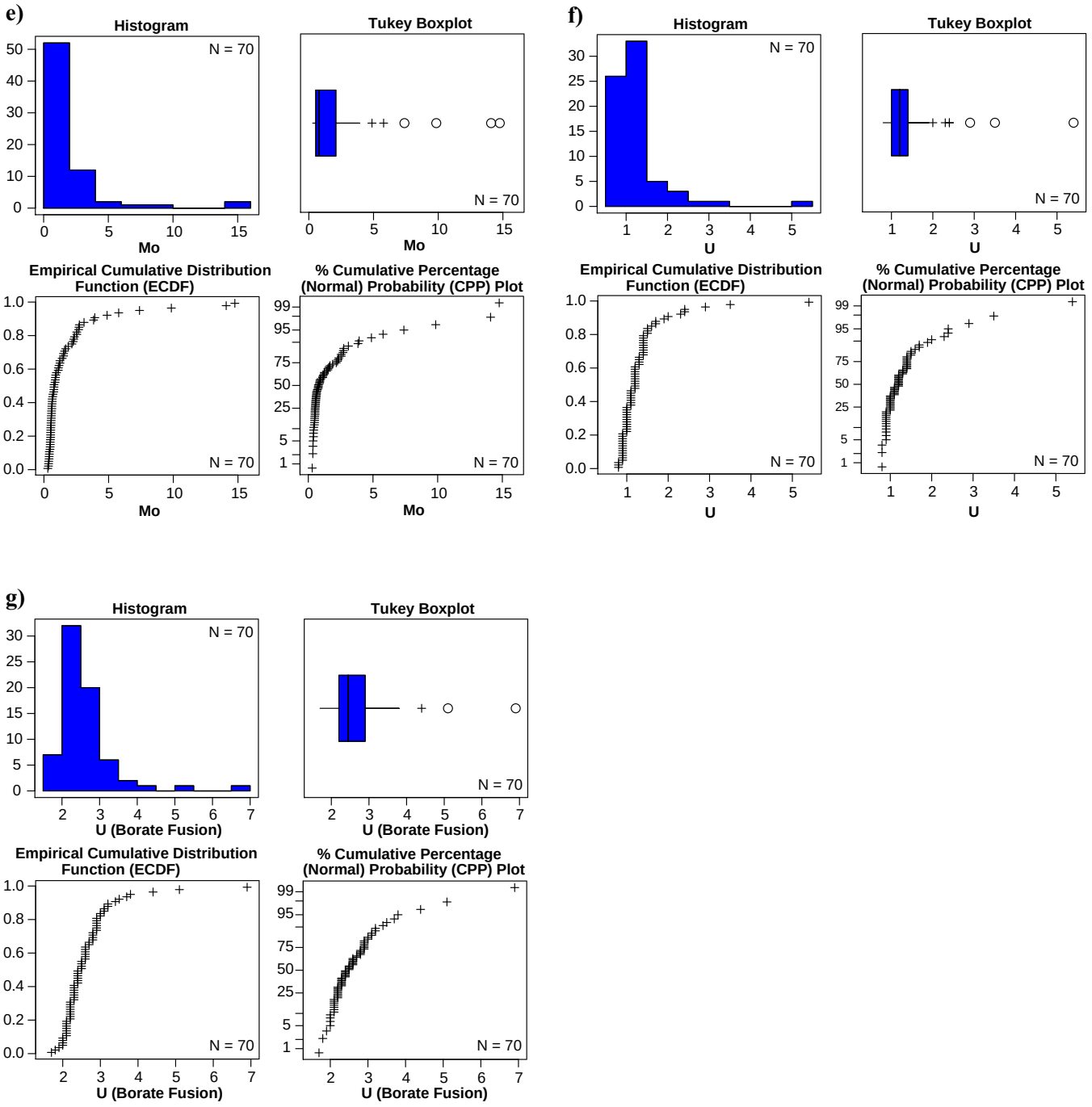

Appendix I2. Continued: **e)** Mo, **f)** U, and **g)** U determined by borate fusion.

APPENDIX J1. Deposit-scale geochemistry maps of selected elements in the <0.063 mm fraction.

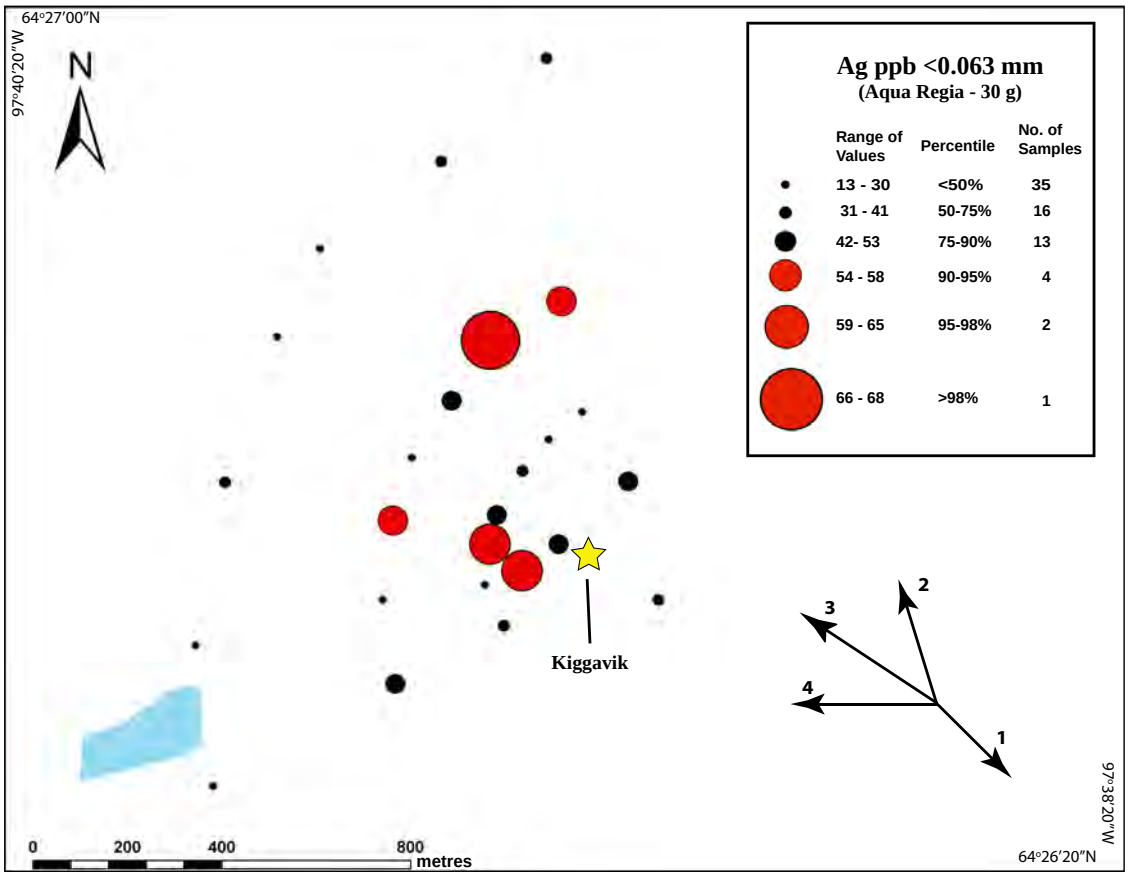

Appendix J1 Map 1. Deposit-scale map of the study area showing the Ag content in the <0.063 fraction at each site.

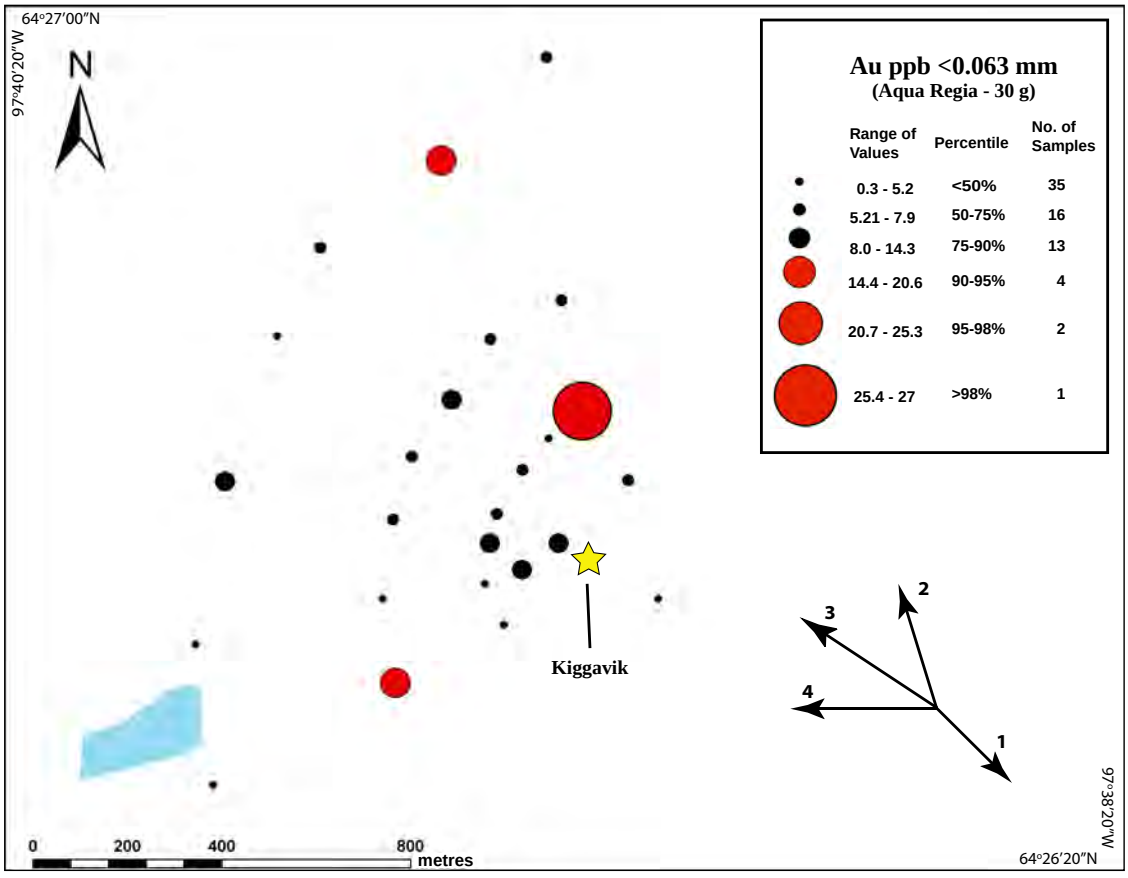

Appendix J1 Map 2. Deposit-scale map of the study area showing the Au content in the <0.063 fraction at each site.

APPENDIX J1 continued.

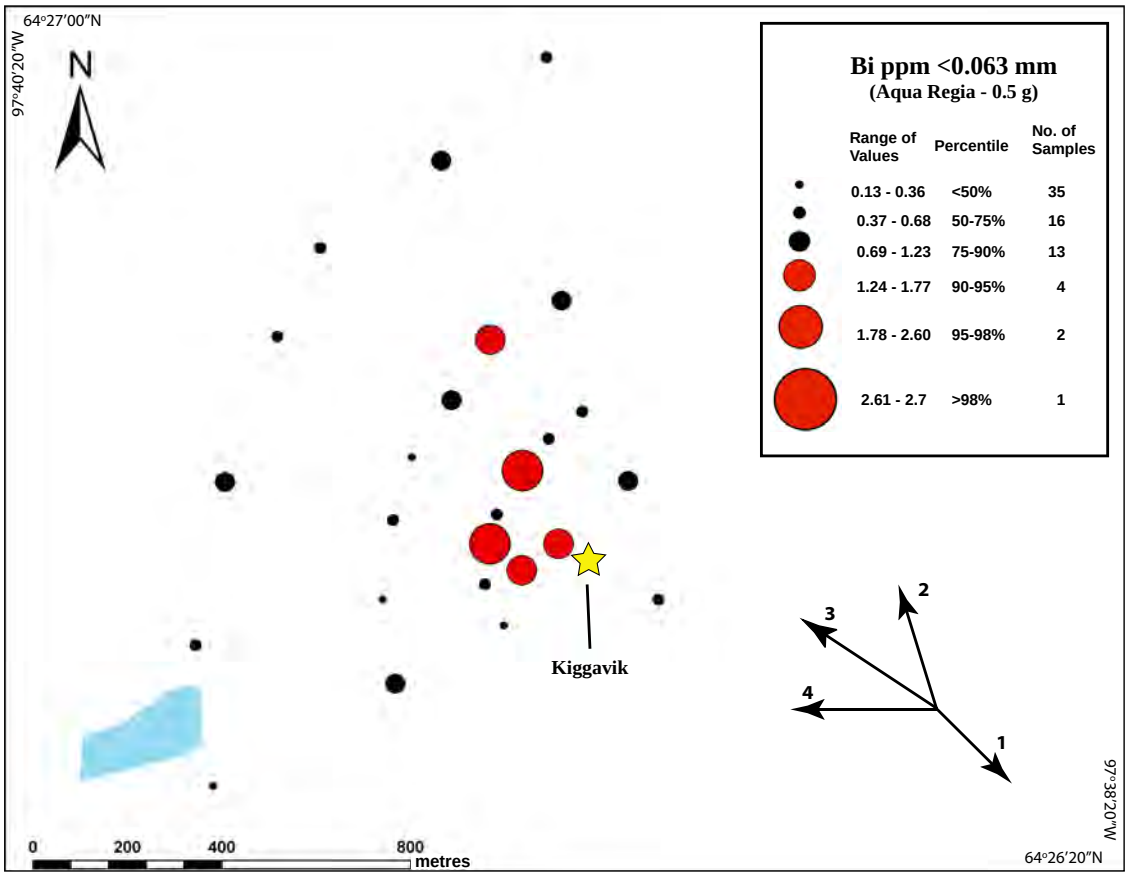

Appendix J1 Map 3. Deposit-scale map of the study area showing the Bi content in the <0.063 fraction at each site.

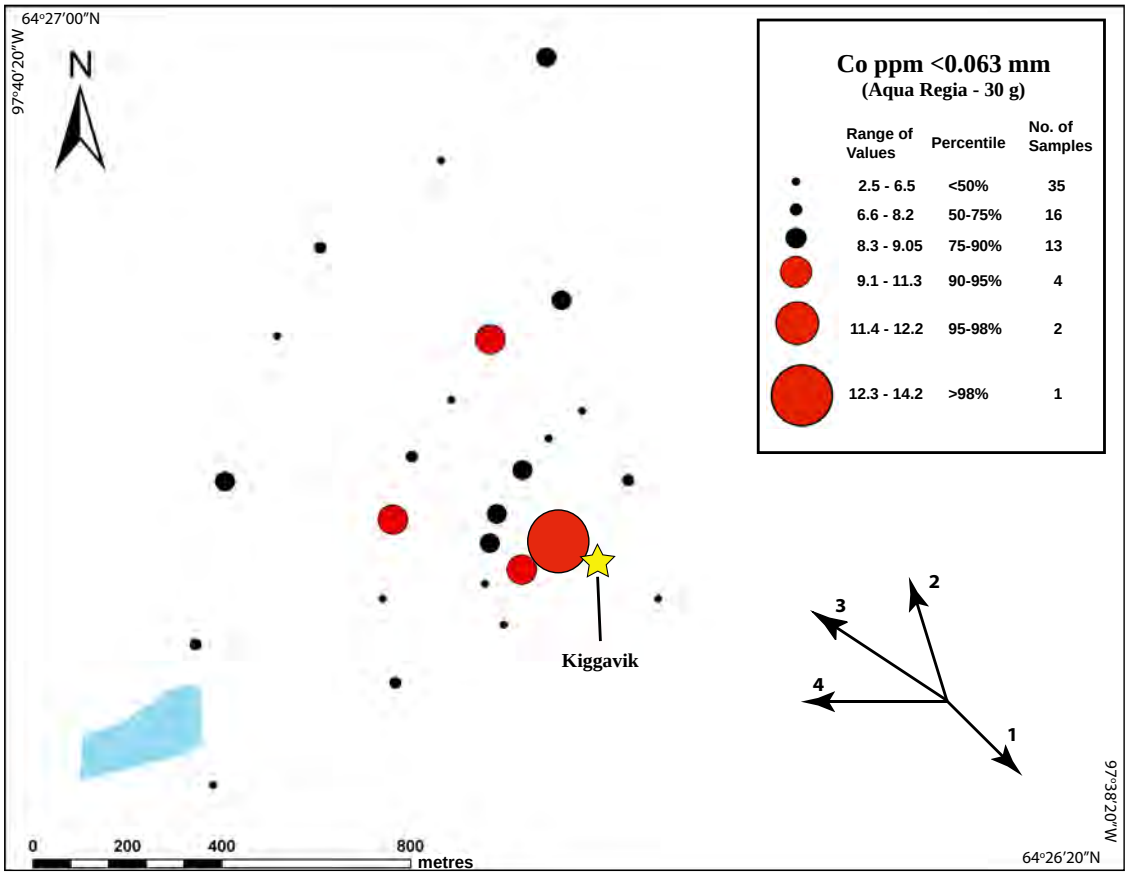

Appendix J1 Map 4. Deposit-scale map of the study area showing the Co content in the <0.063 fraction at each site.

APPENDIX J1 continued.

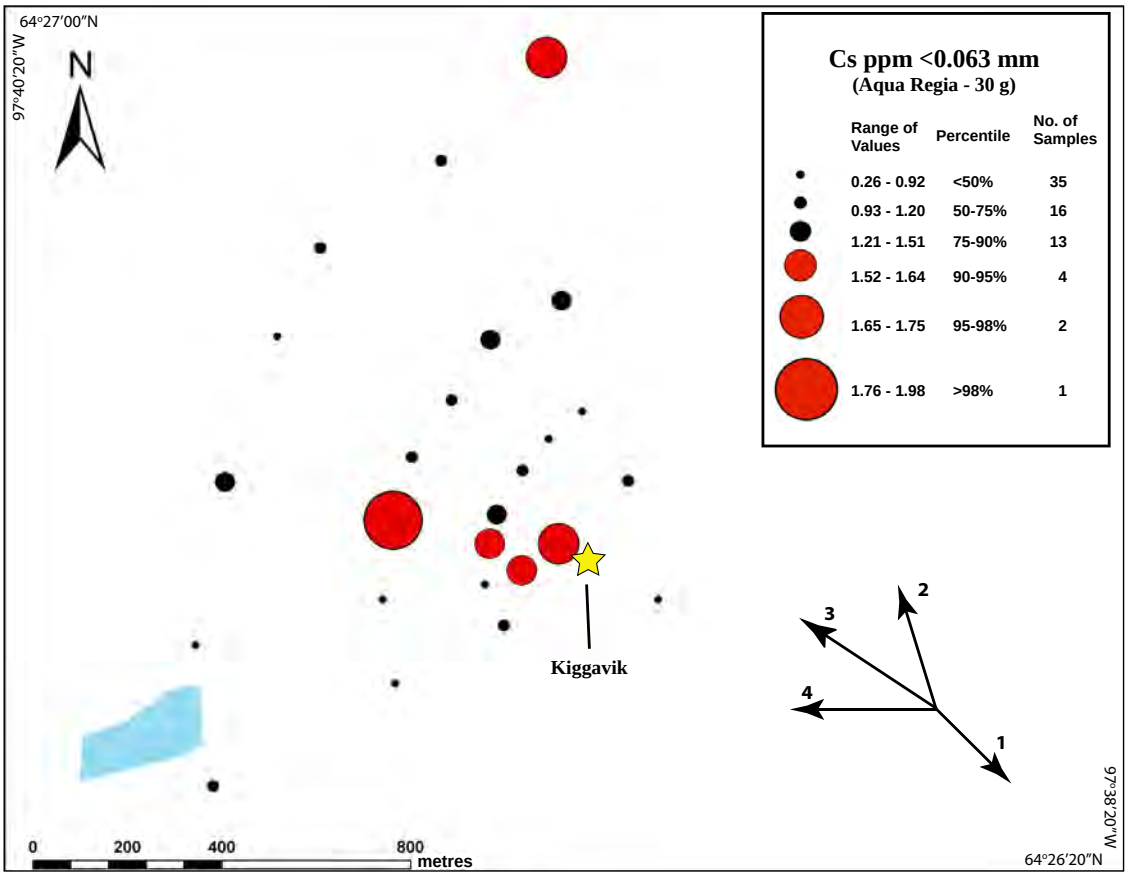

Appendix J1 Map 5. Deposit-scale map of the study area showing the Cs content in the <0.063 fraction at each site.

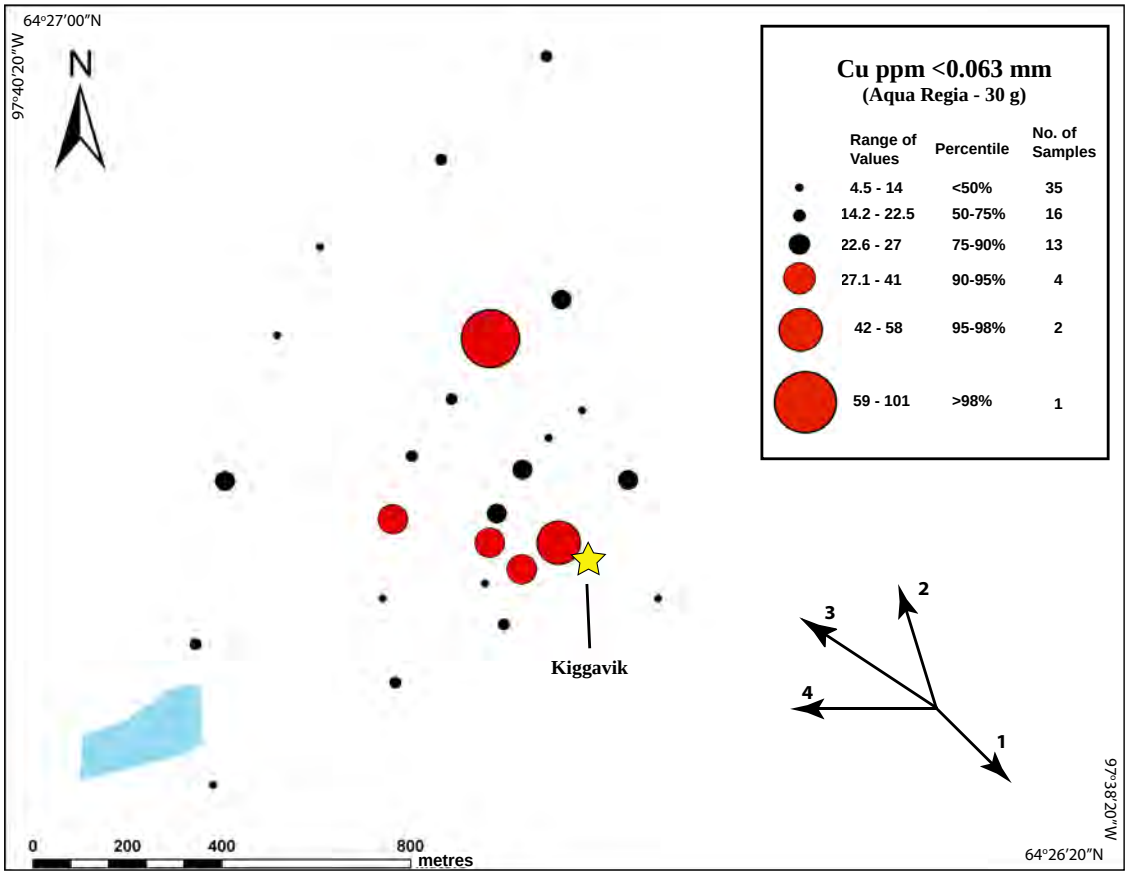

Appendix J1 Map 6. Deposit-scale map of the study area showing the Cu content in the <0.063 fraction at each site.

APPENDIX J1 continued.

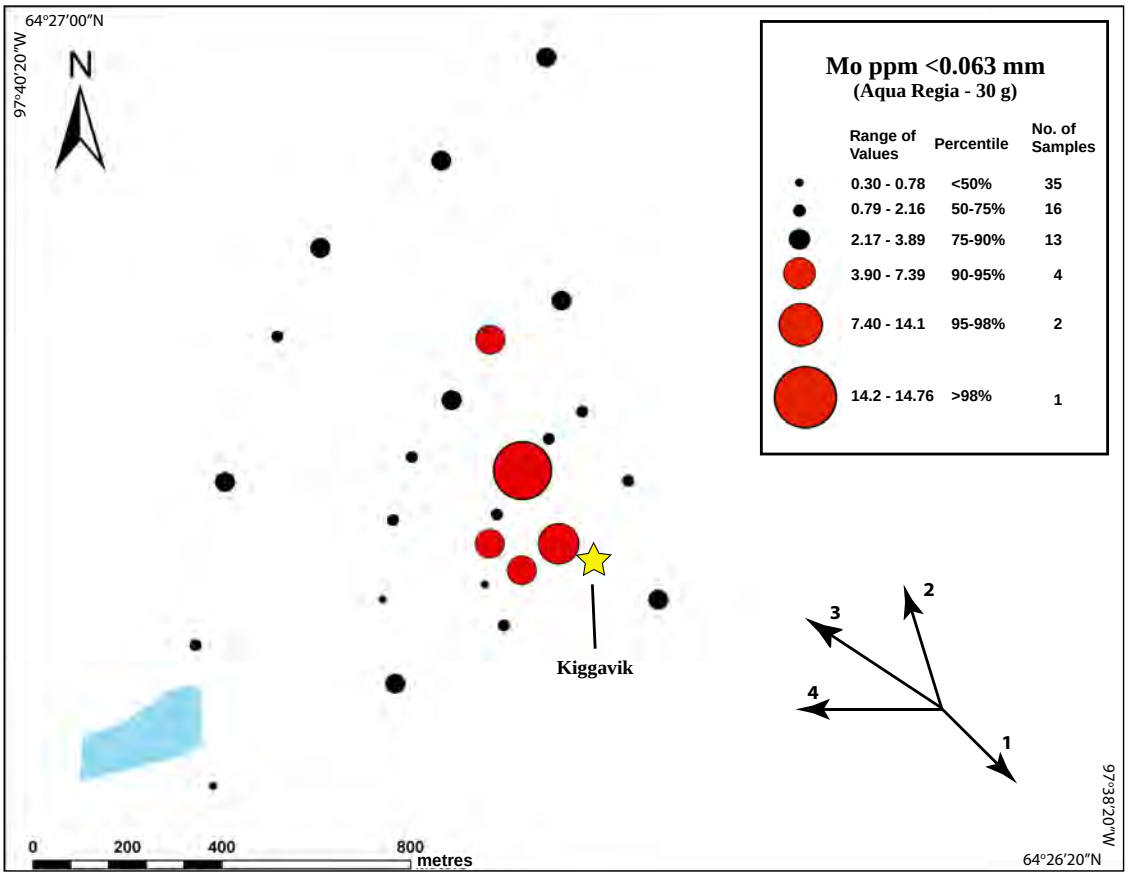

Appendix J1 Map 7. Deposit-scale map of the study area showing the Mo content in the <0.063 fraction at each site.

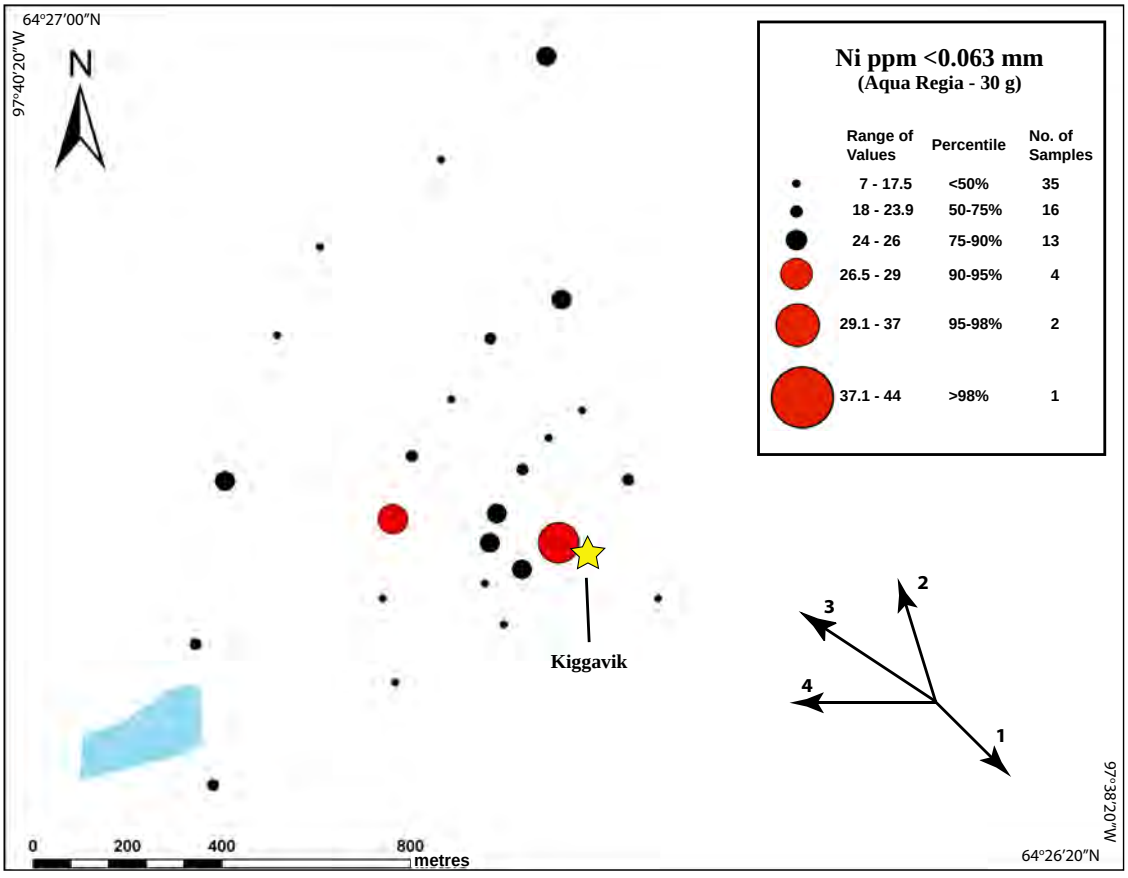

Appendix J1 Map 8. Deposit-scale map of the study area showing the Ni content in the <0.063 fraction of each sample.

APPENDIX J1 continued.

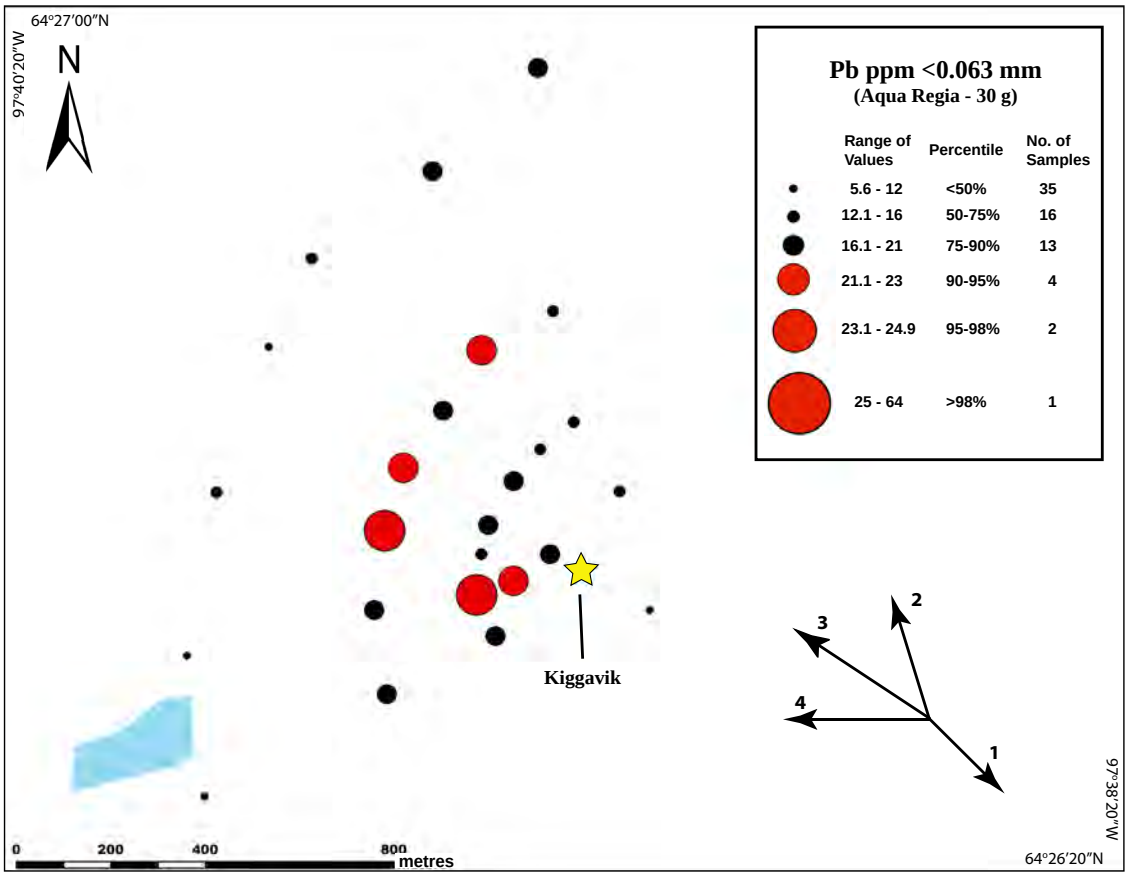

Appendix J1 Map 9. Deposit-scale map of the study area showing the Pb content in the <0.063 fraction at each site.

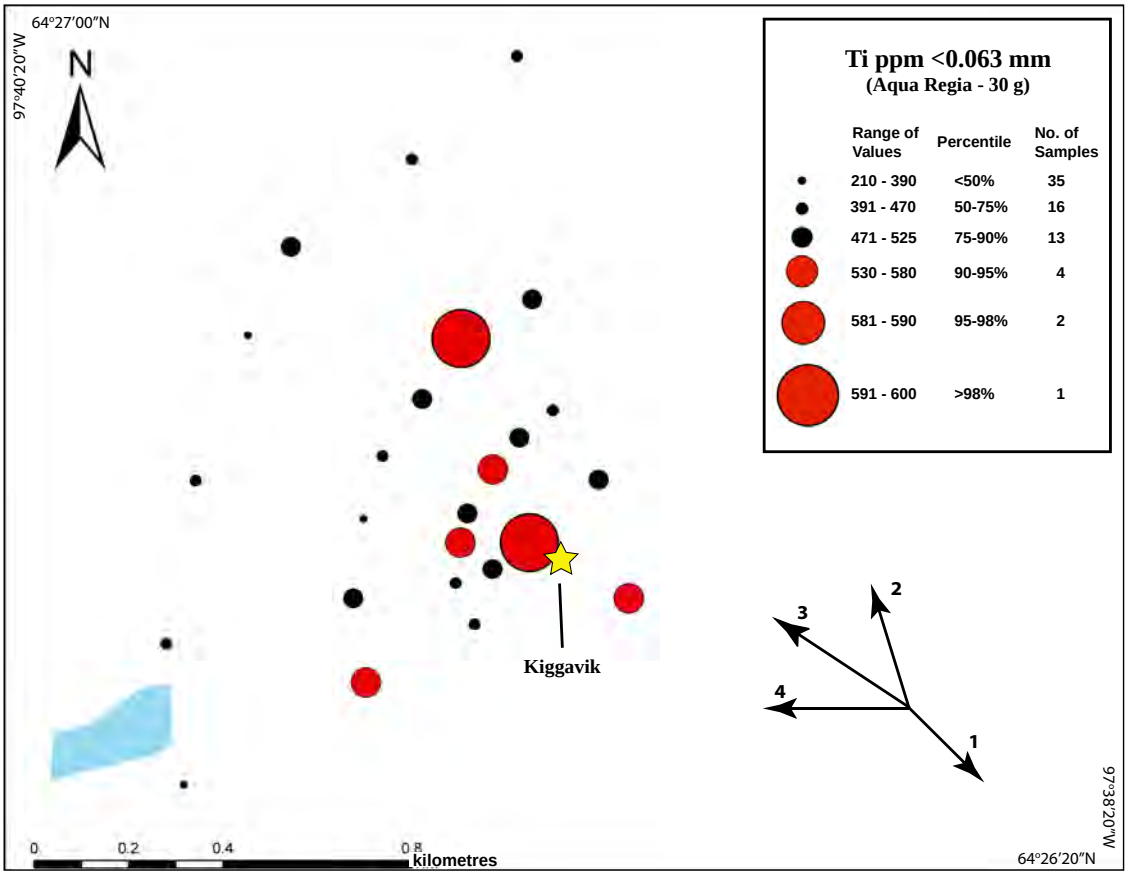

Appendix J1 Map 10. Deposit-scale map of the study area showing the Ti content in the <0.063 fraction at each site.

APPENDIX J1 continued.

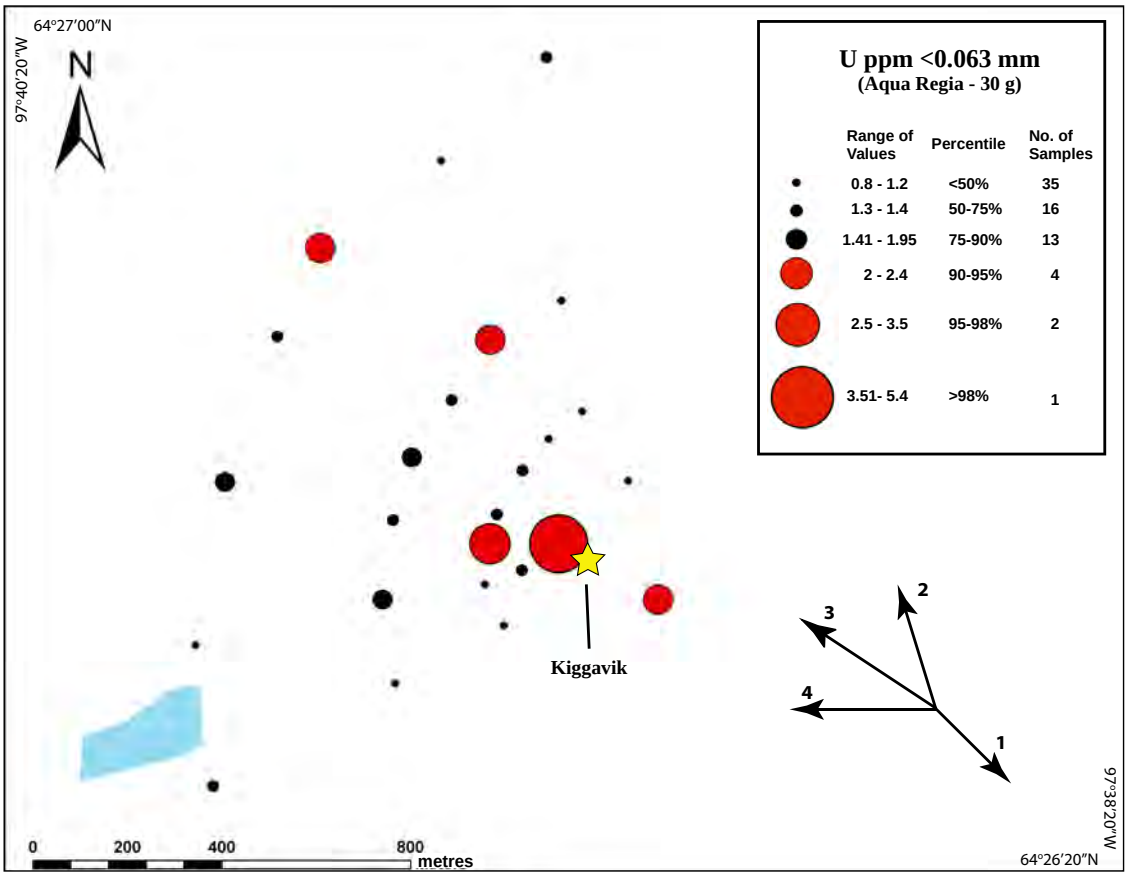

Appendix J1 Map 11. Deposit-scale map of the study area showing the U content (determined by aqua regia) in the <0.063 fraction at each site.

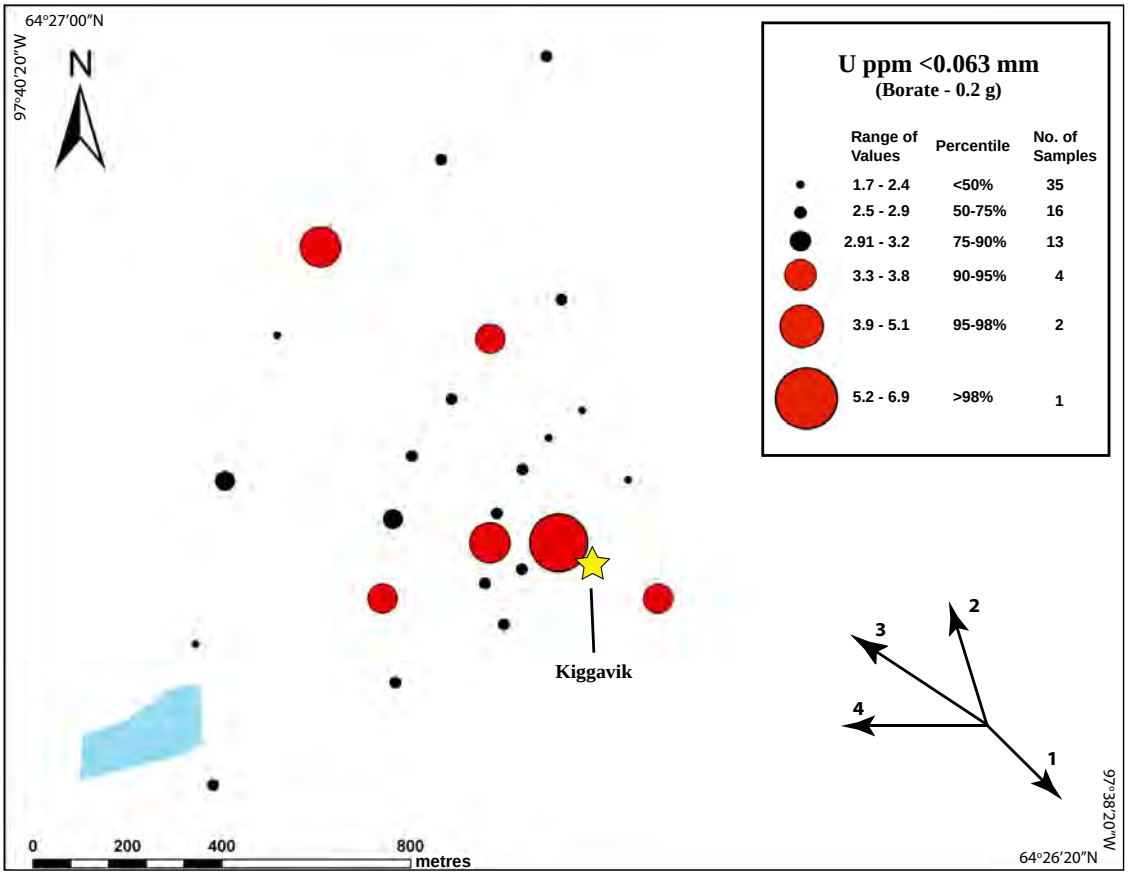

Appendix J1 Map 12. Deposit-scale map of the study area showing the U content (determined by borate fusion) in the <0.063 fraction at each site.

APPENDIX J1 continued.

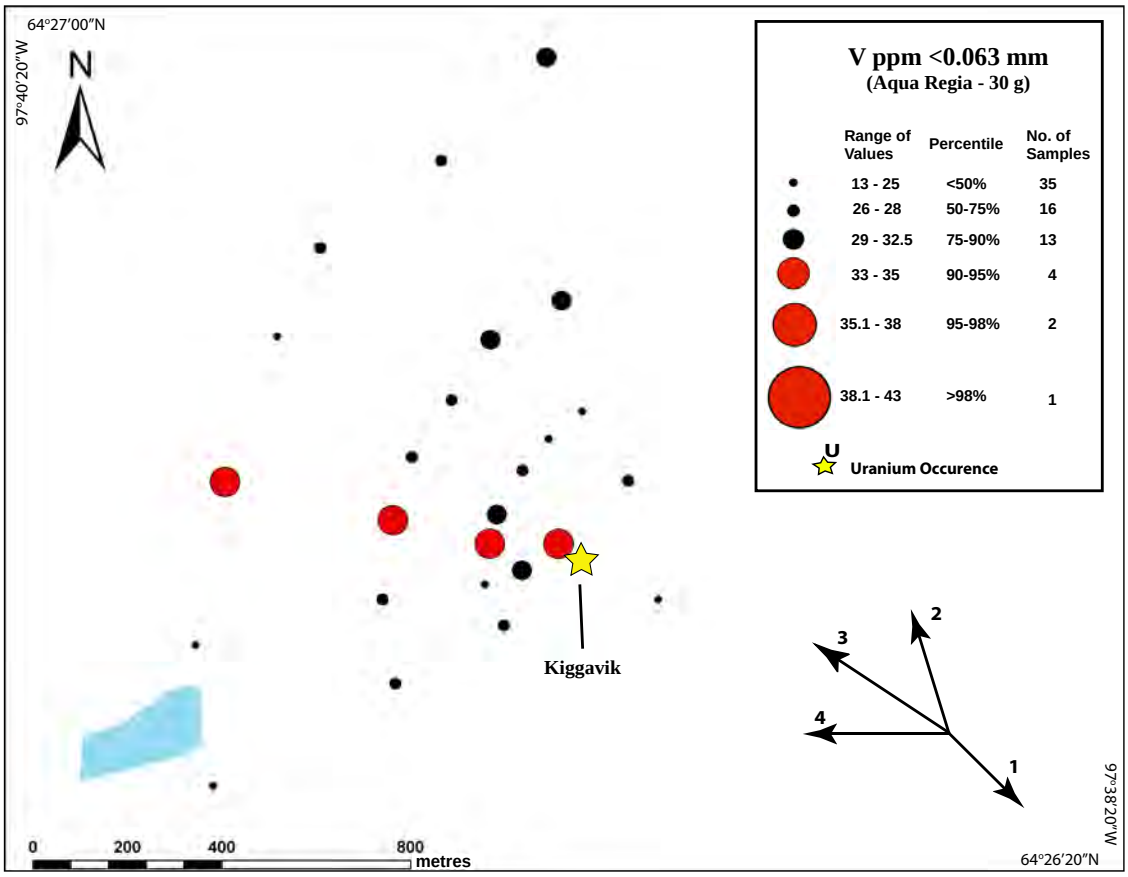

Appendix J1 Map 13. Deposit-scale map of the study area showing the V content in the <0.063 fraction at each site.

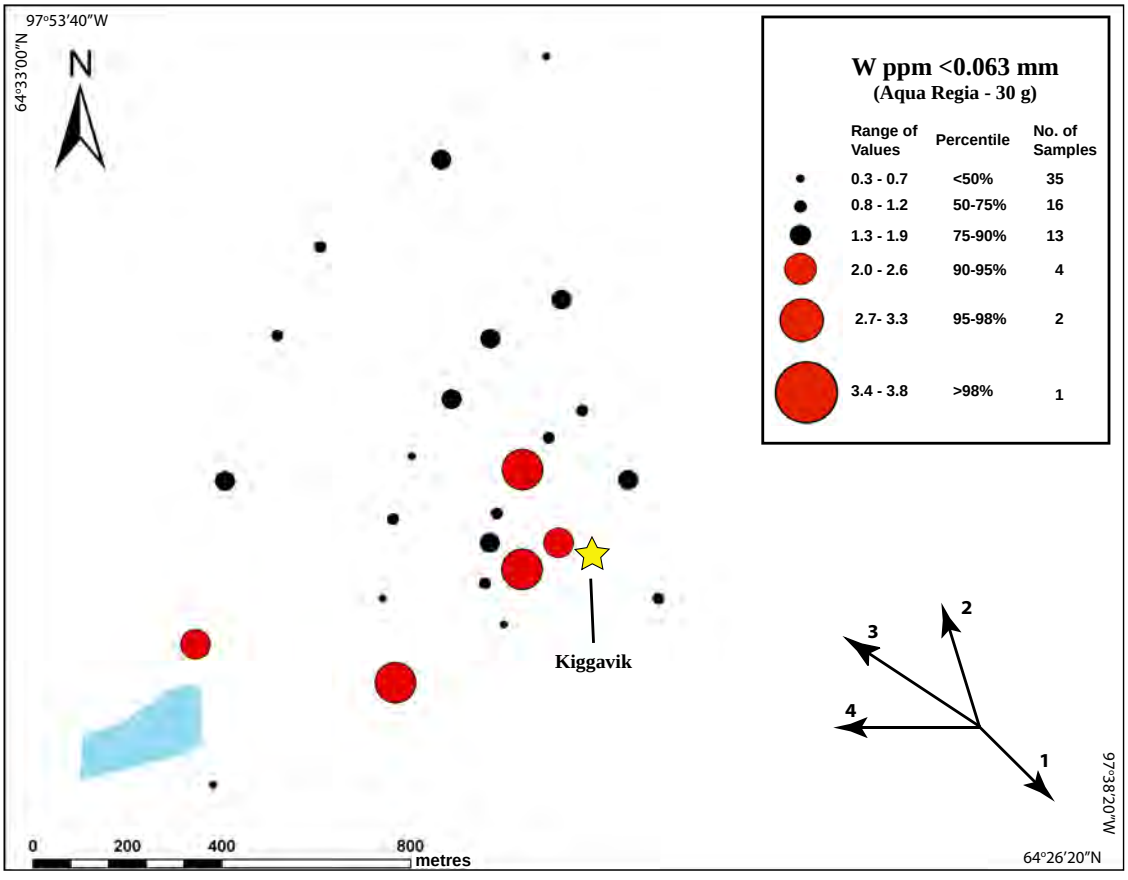

Appendix J1 Map 14. Deposit-scale map of the study area showing the W content in the <0.063 fraction at each site.

APPENDIX J2. Regional-scale geochemistry maps of selected elements in the <0.063 mm fraction.

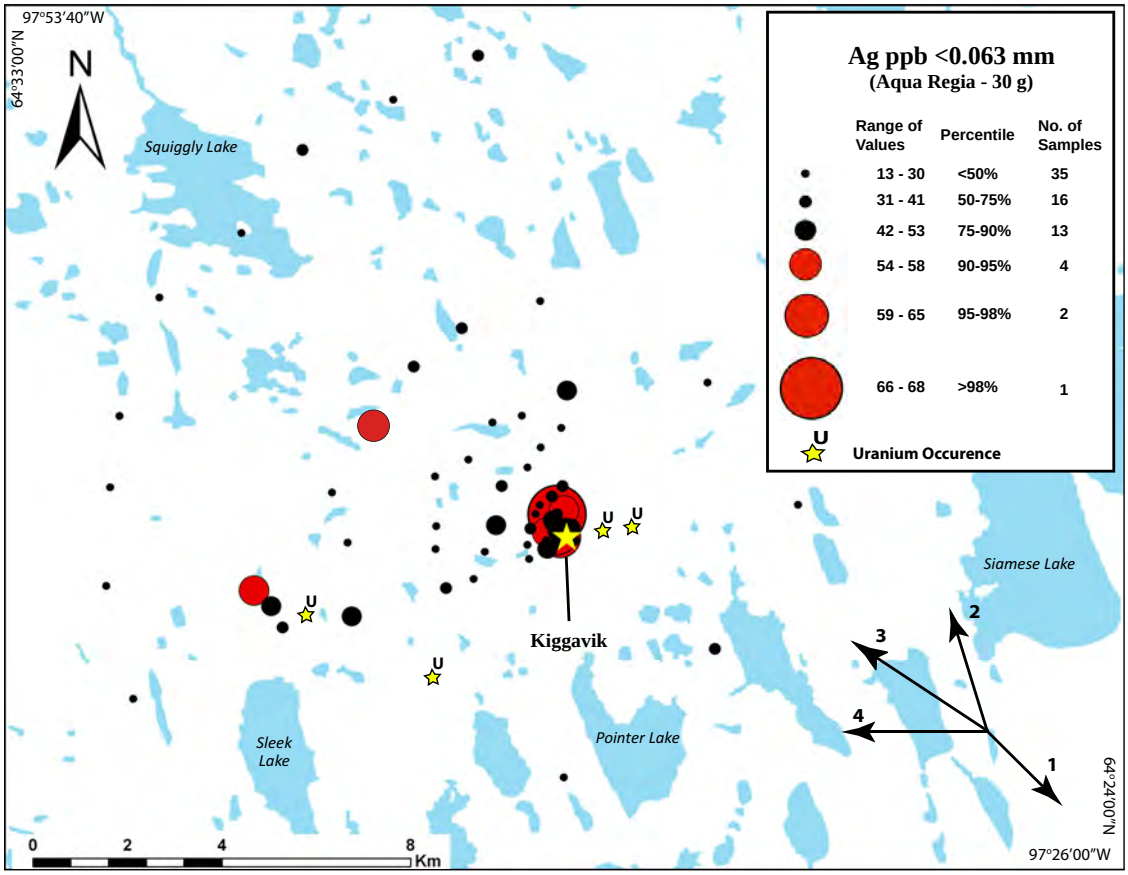

Appendix J2 Map 1. Regional-scale map of the study area showing the Ag content in the <0.063 fraction at each site.

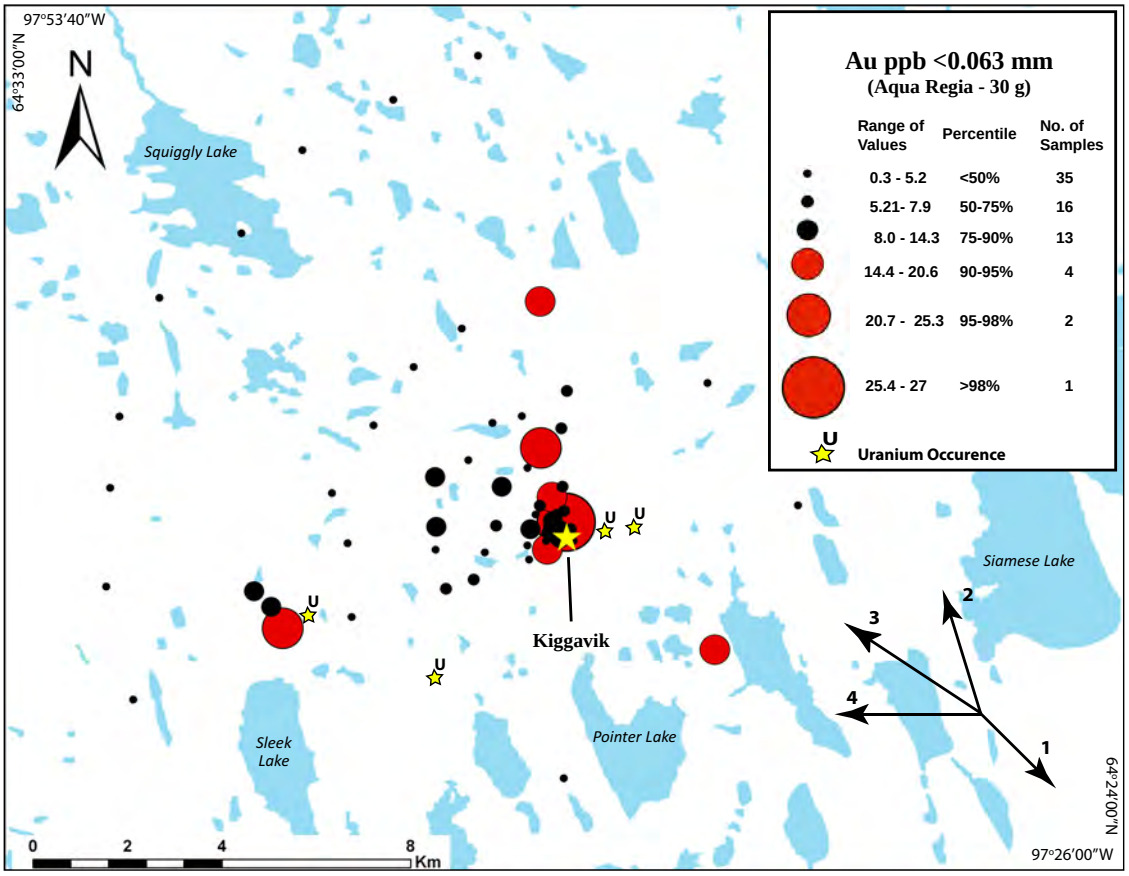

Appendix J2 Map 2. Regional-scale map of the study area showing the Au content in the <0.063 fraction at each site.

APPENDIX J2 continued.

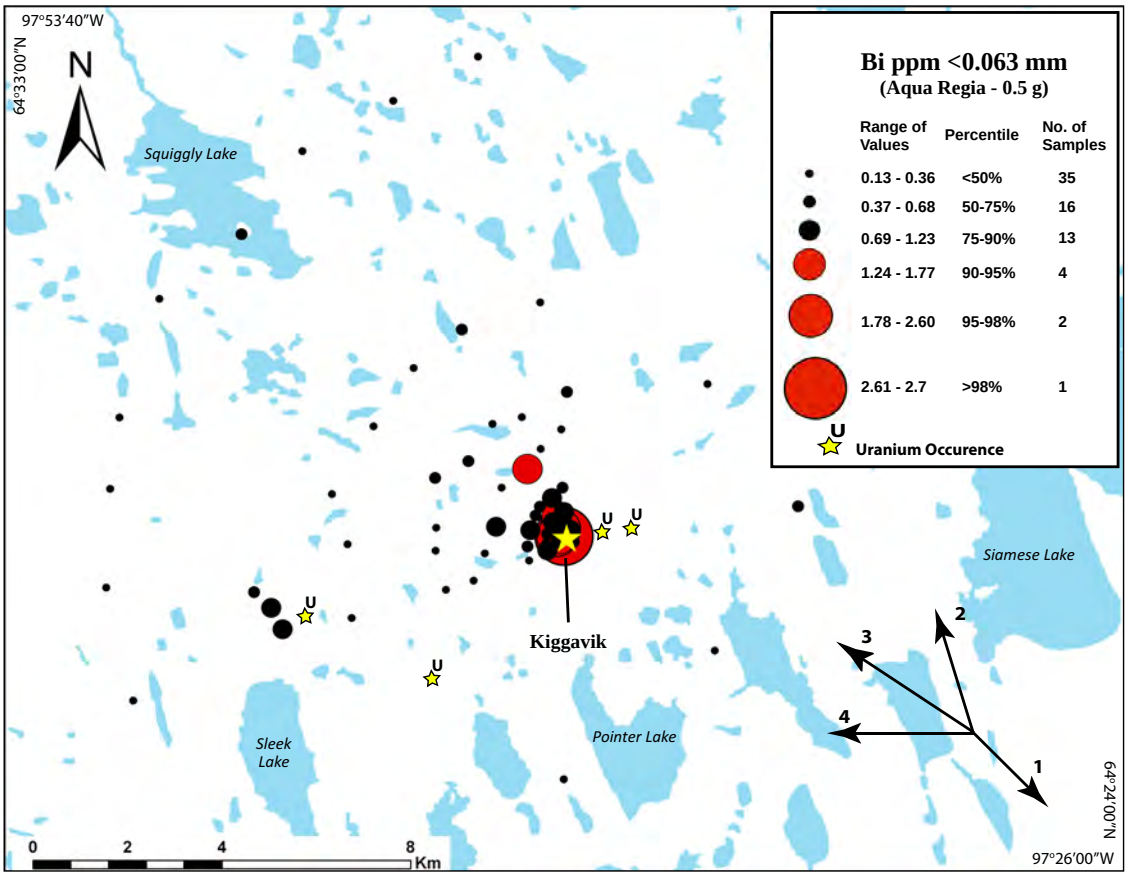

Appendix J2 Map 3. Regional-scale map of the study area showing the Bi content in the <0.063 fraction at each site.

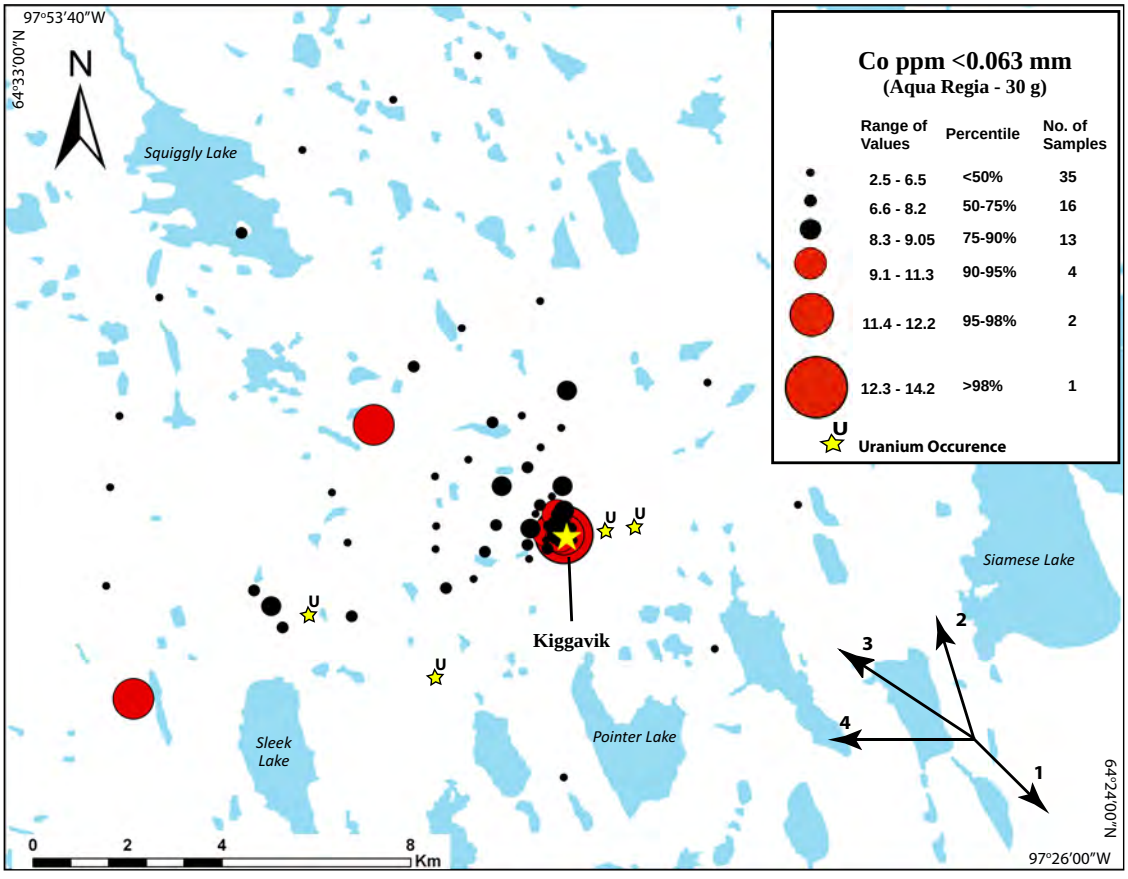

Appendix J2 Map 4. Regional-scale map of the study area showing the Co content in the <0.063 fraction at each site.

APPENDIX J2 continued.

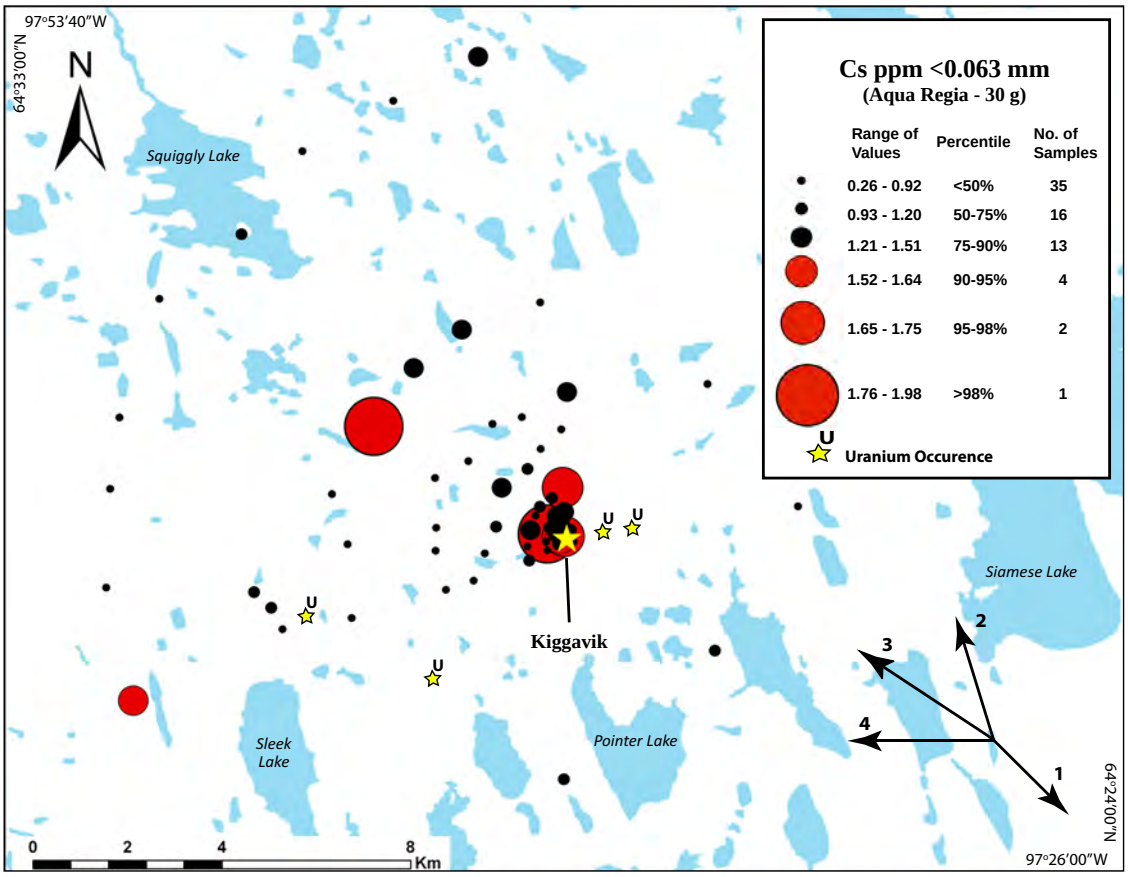

Appendix J2 Map 5. Regional-scale map of the study area showing the Cs content in the <0.063 fraction at each site.

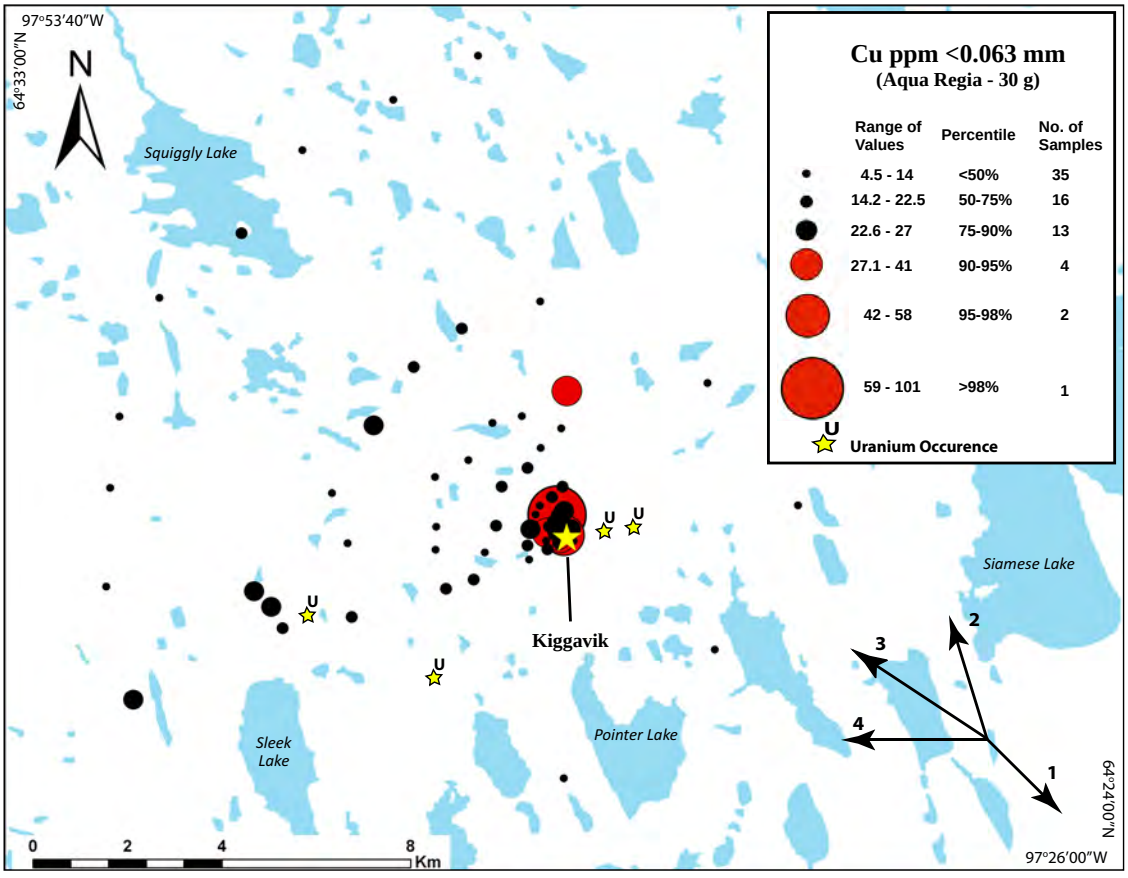

Appendix J2 Map 6. Regional-scale map of the study area showing the Cu content in the <0.063 fraction at each site.

APPENDIX J2 continued.

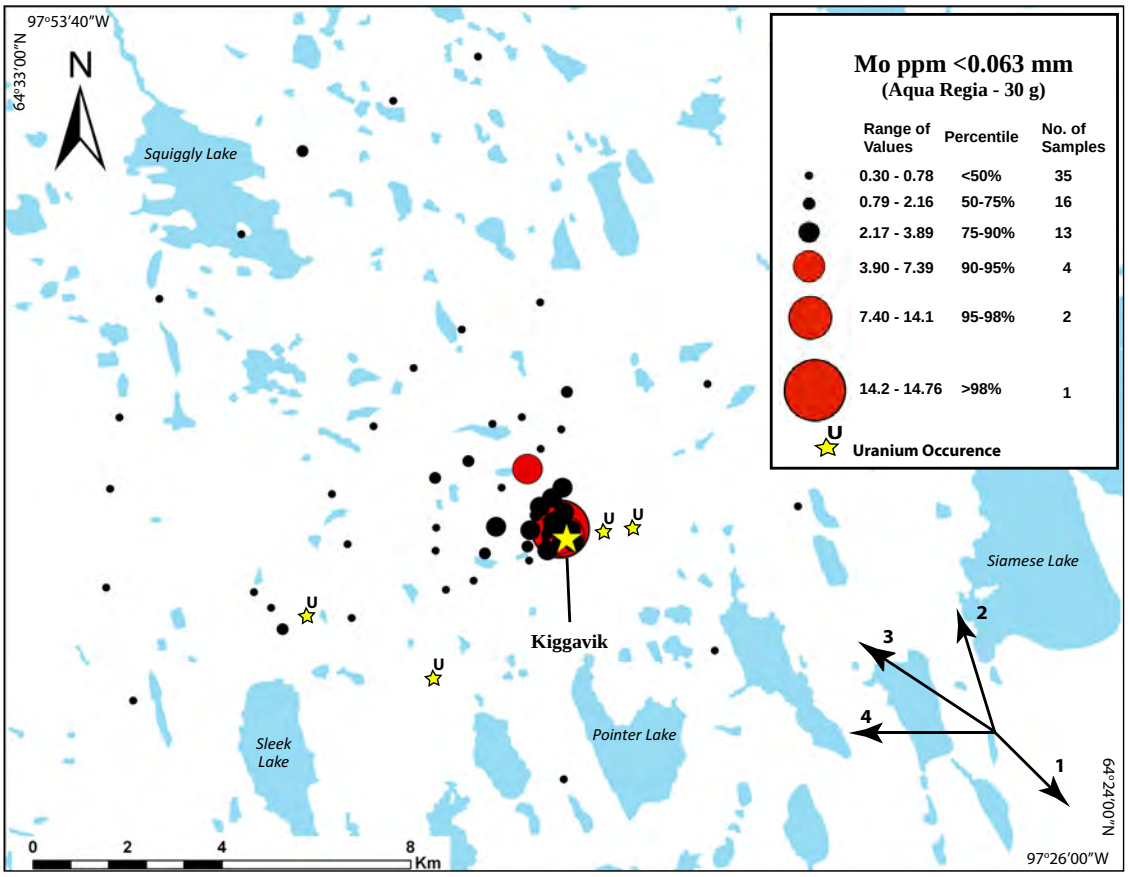

Appendix J2 Map 7. Regional-scale map of the study area showing the Mo content in the <0.063 fraction at each site.

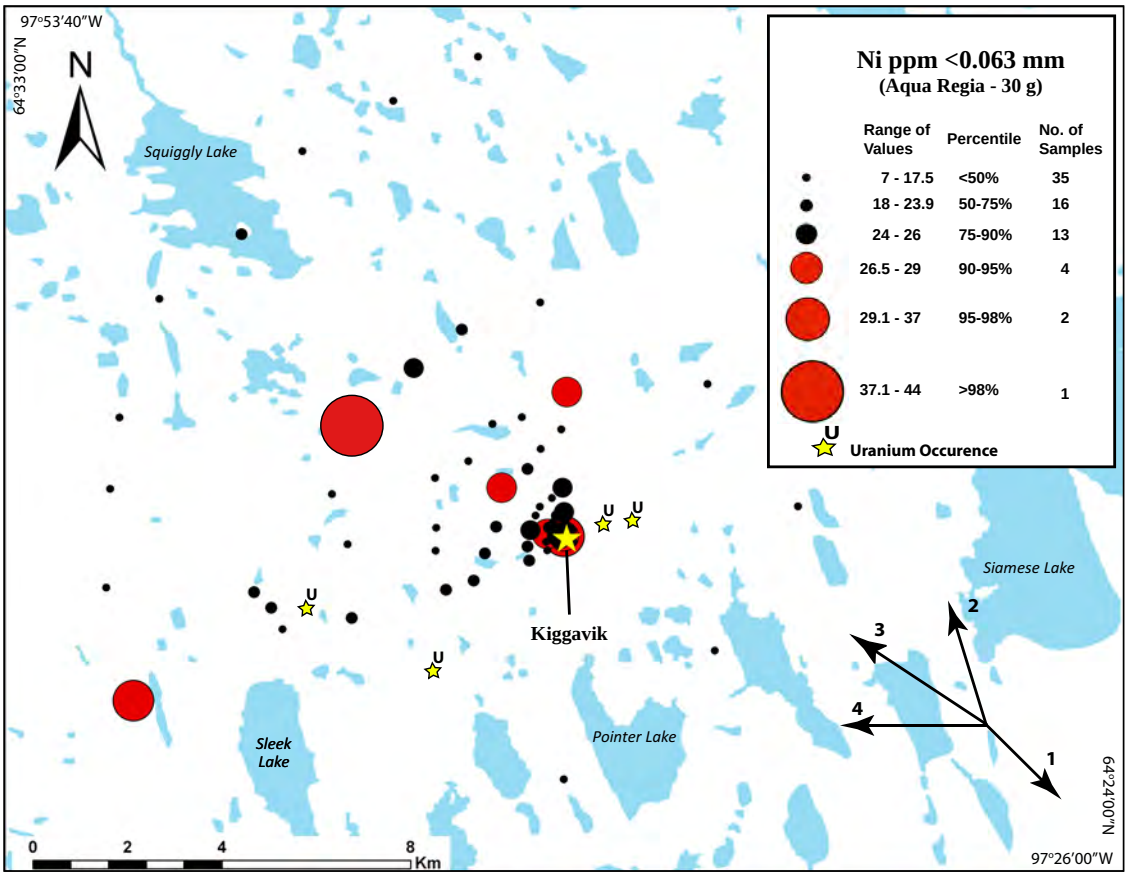

Appendix J2 Map 8. Regional-scale map of the study area showing the Ni content in the <0.063 fraction at each site.

APPENDIX J2 continued.

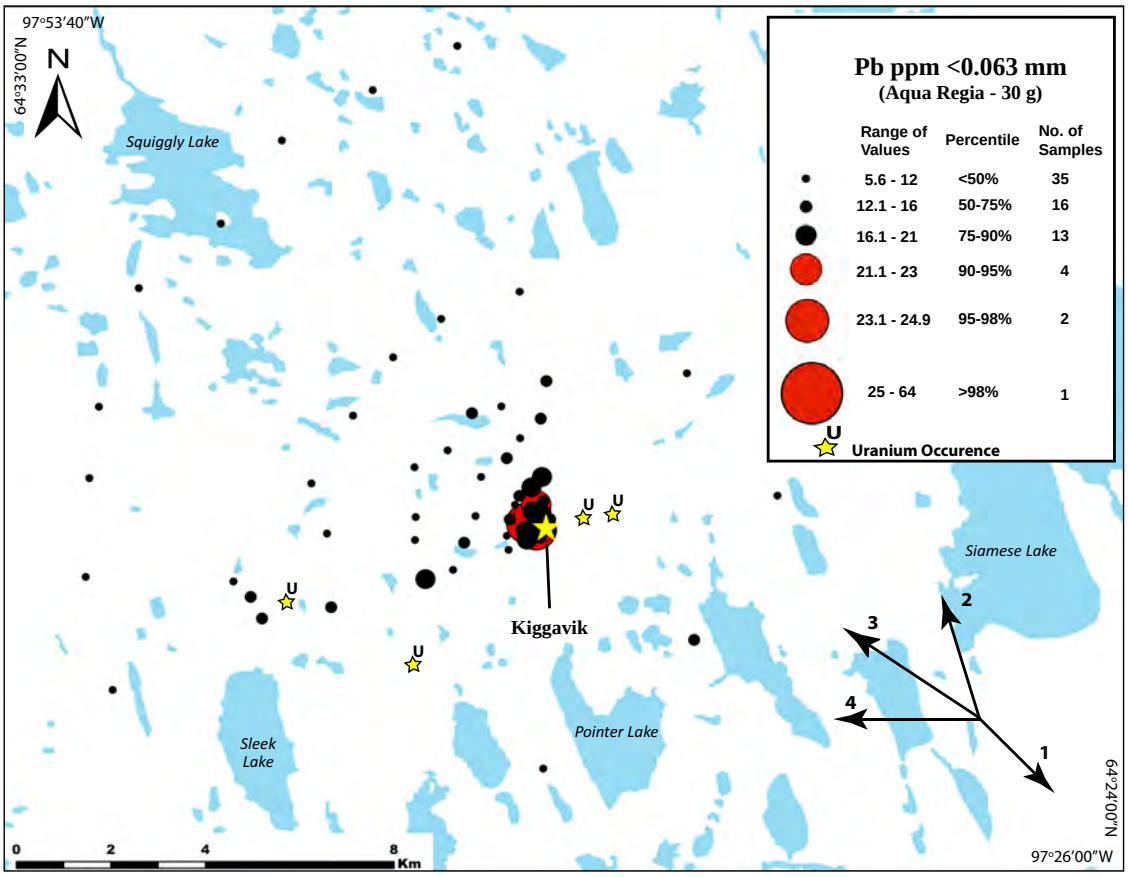

Appendix J2 Map 9. Regional-scale map of the study area showing the Pb content in the <0.063 fraction at each site.

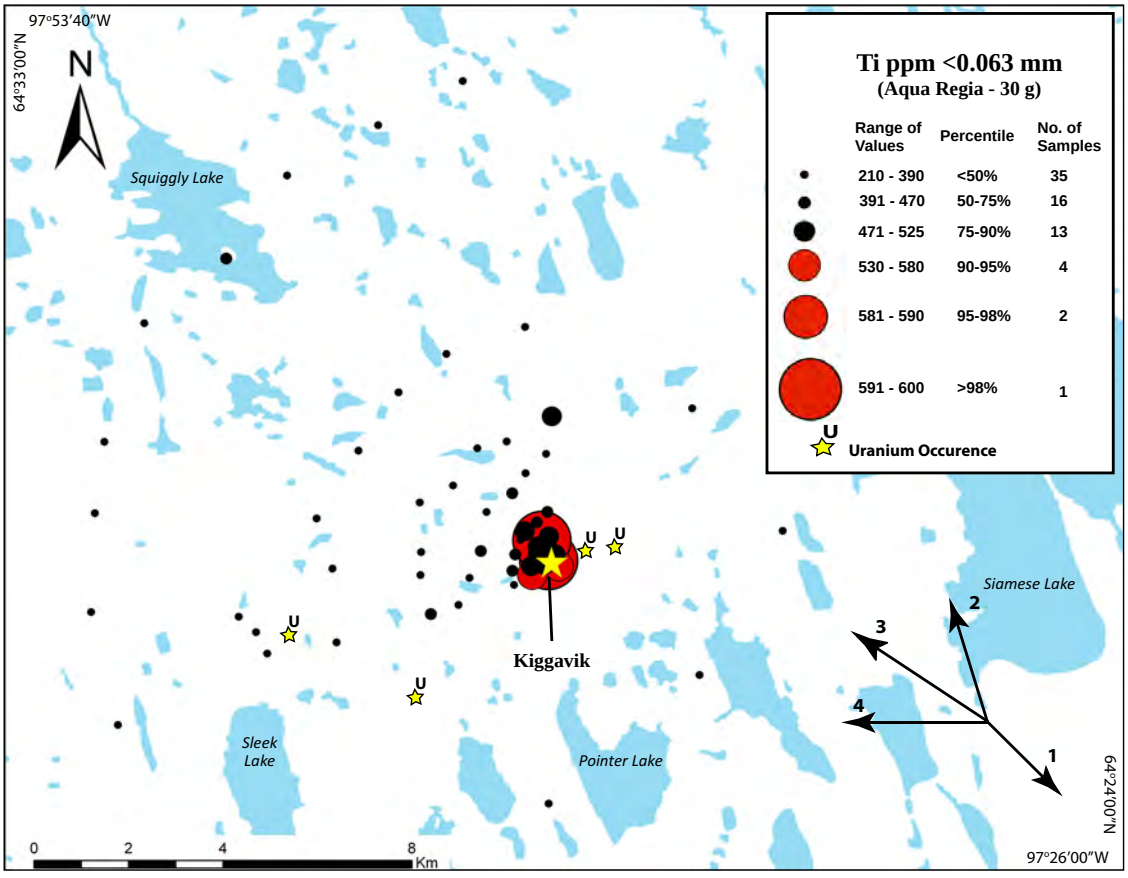

Appendix J2 Map 10. Regional-scale map of the study area showing the Ti content in the <0.063 fraction at each site.

APPENDIX J2 continued.

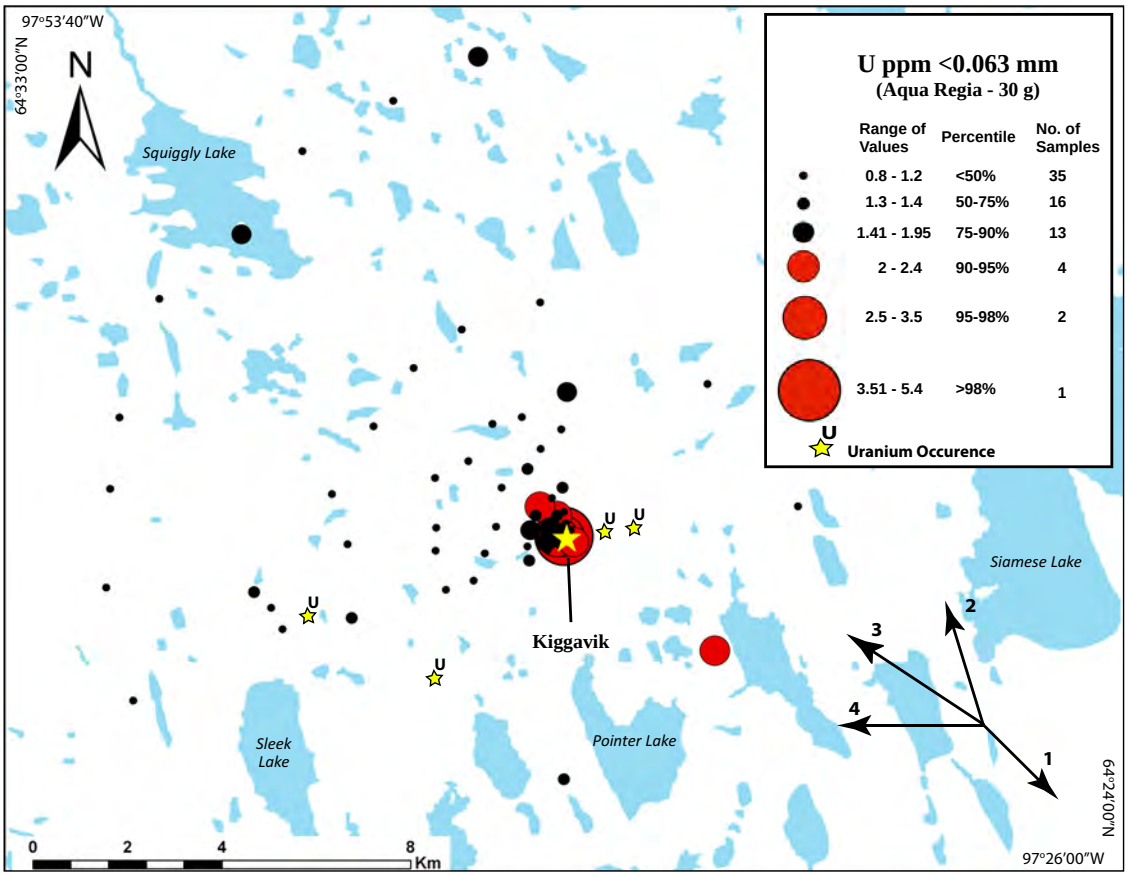

Appendix J2 Map 11. Regional-scale map of the study area showing the U content (determined by aqua regia) in the <0.063 fraction at each site.

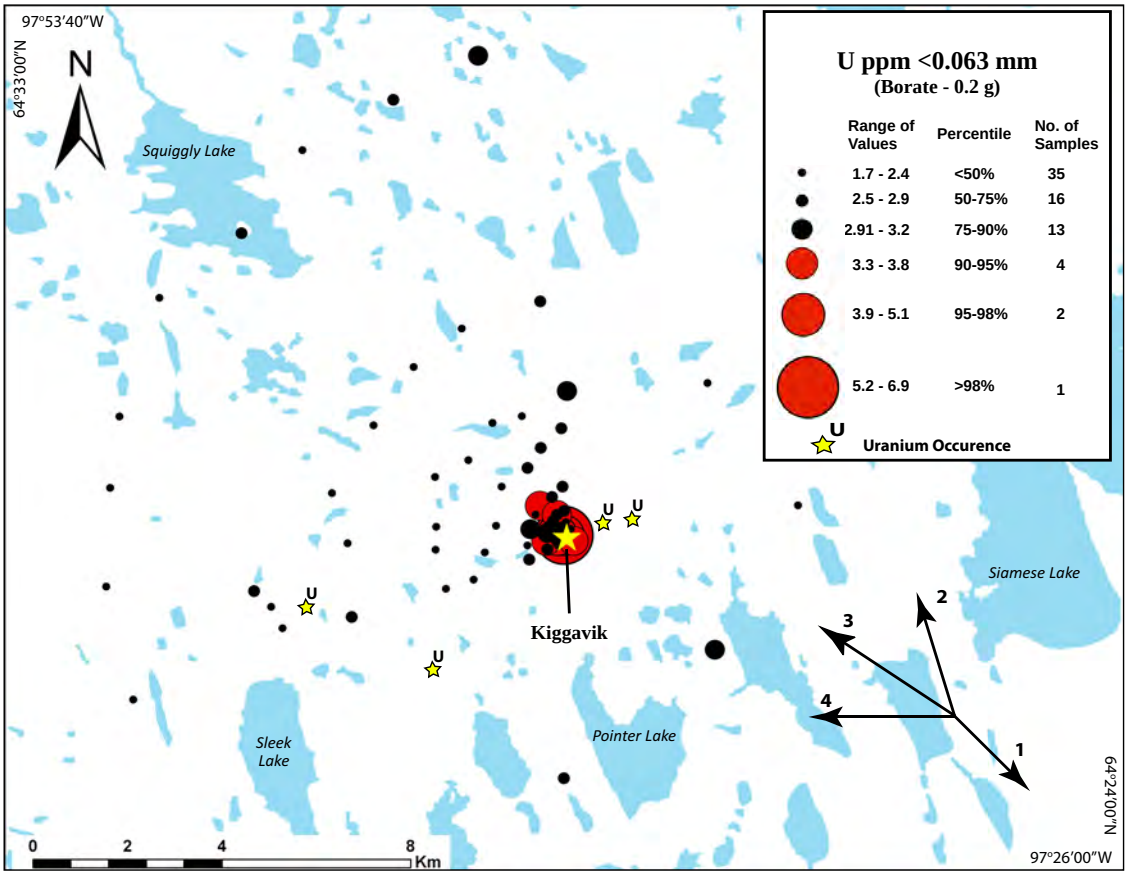

Appendix J2 Map 12. Regional-scale map of the study area showing the U content (determined by borate fusion) in the <0.063 fraction at each site.

APPENDIX J2 continued.

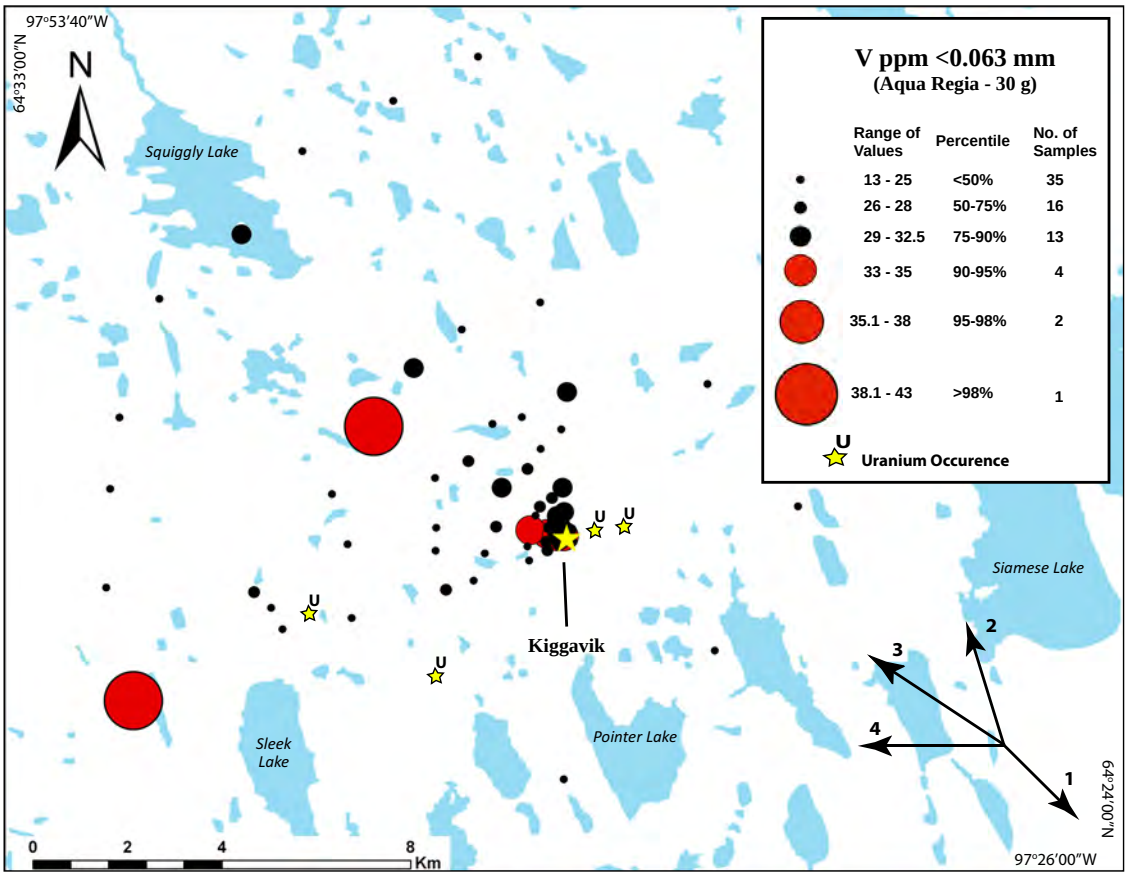

Appendix J2 Map 13. Regional-scale map of the study area showing the V content in the <0.063 fraction at each site.

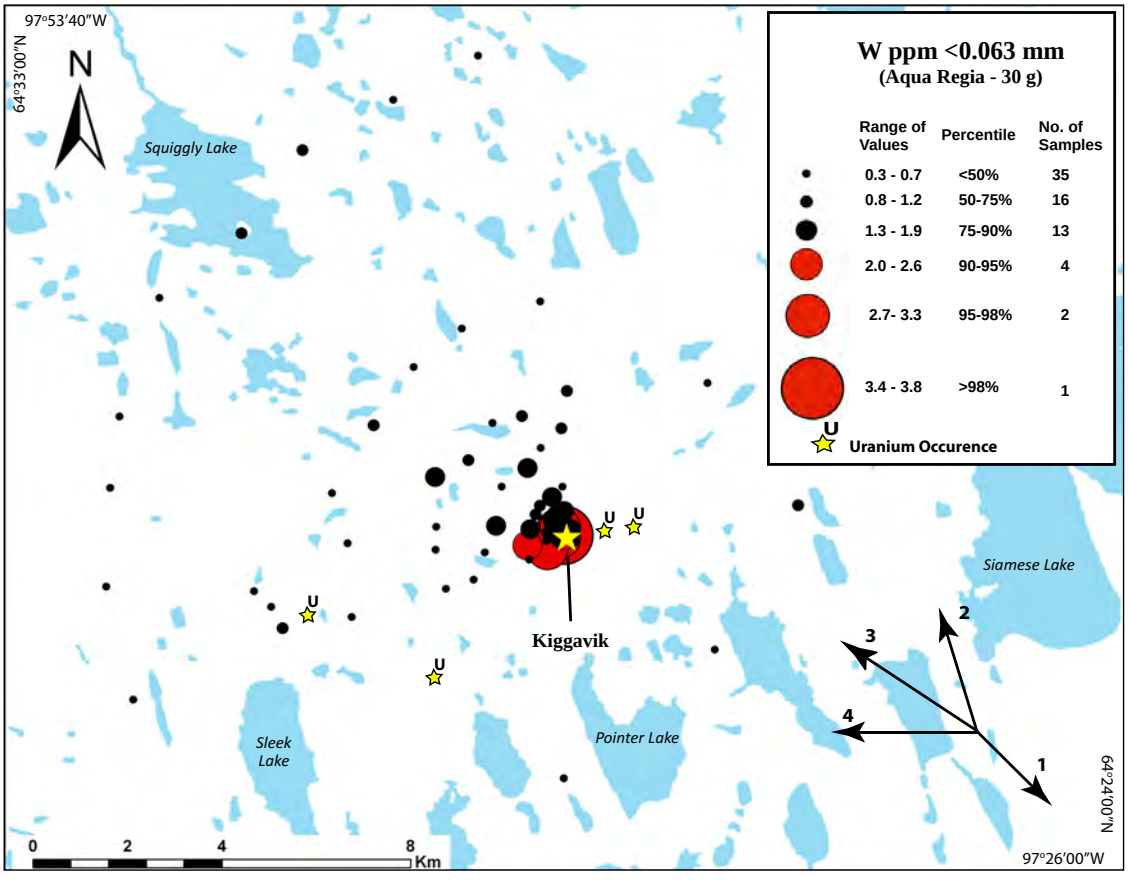

Appendix J2 Map 14. Regional-scale map of the study area showing the W content in the <0.063 fraction at each site.

APPENDIX K1. Deposit-scale geochemistry maps of selected elements in the <0.002 mm fraction.

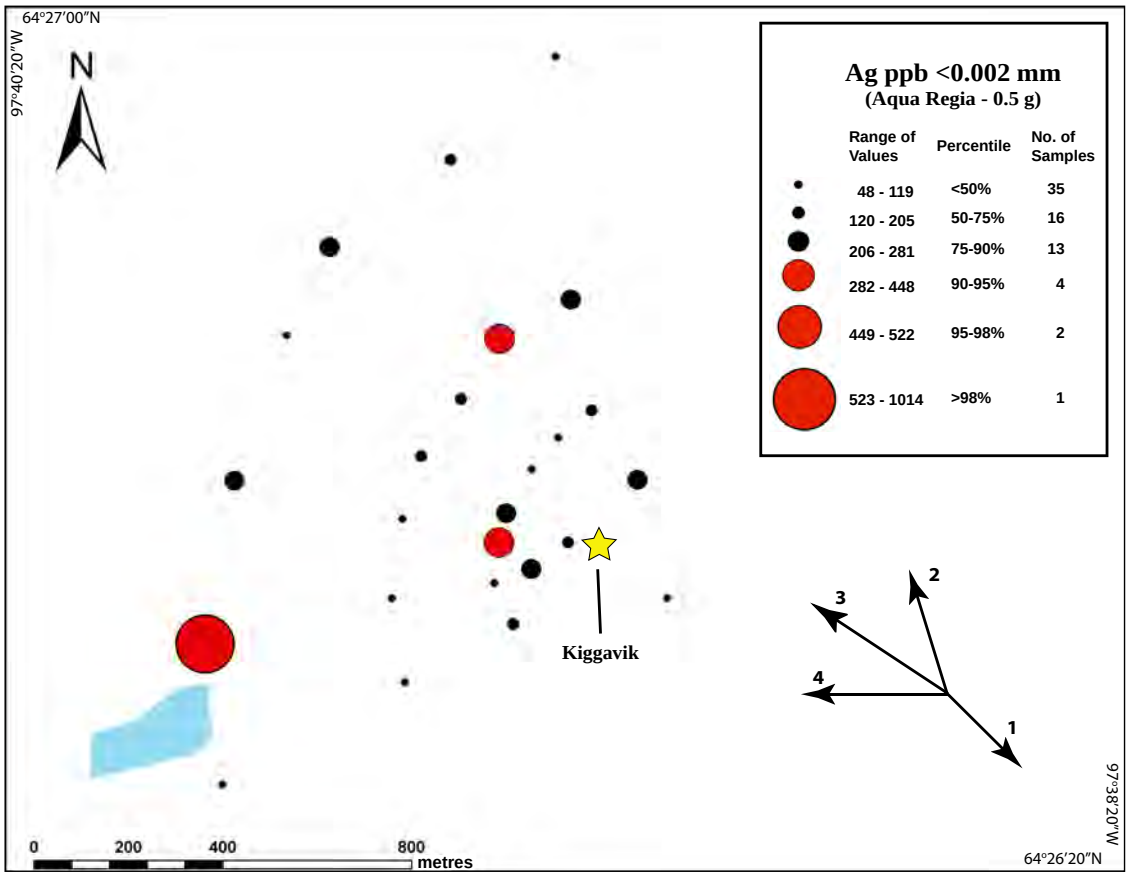

Appendix K1 Map 1. Deposit-scale map of the study area showing the Ag content in the <0.002 fraction at each site.

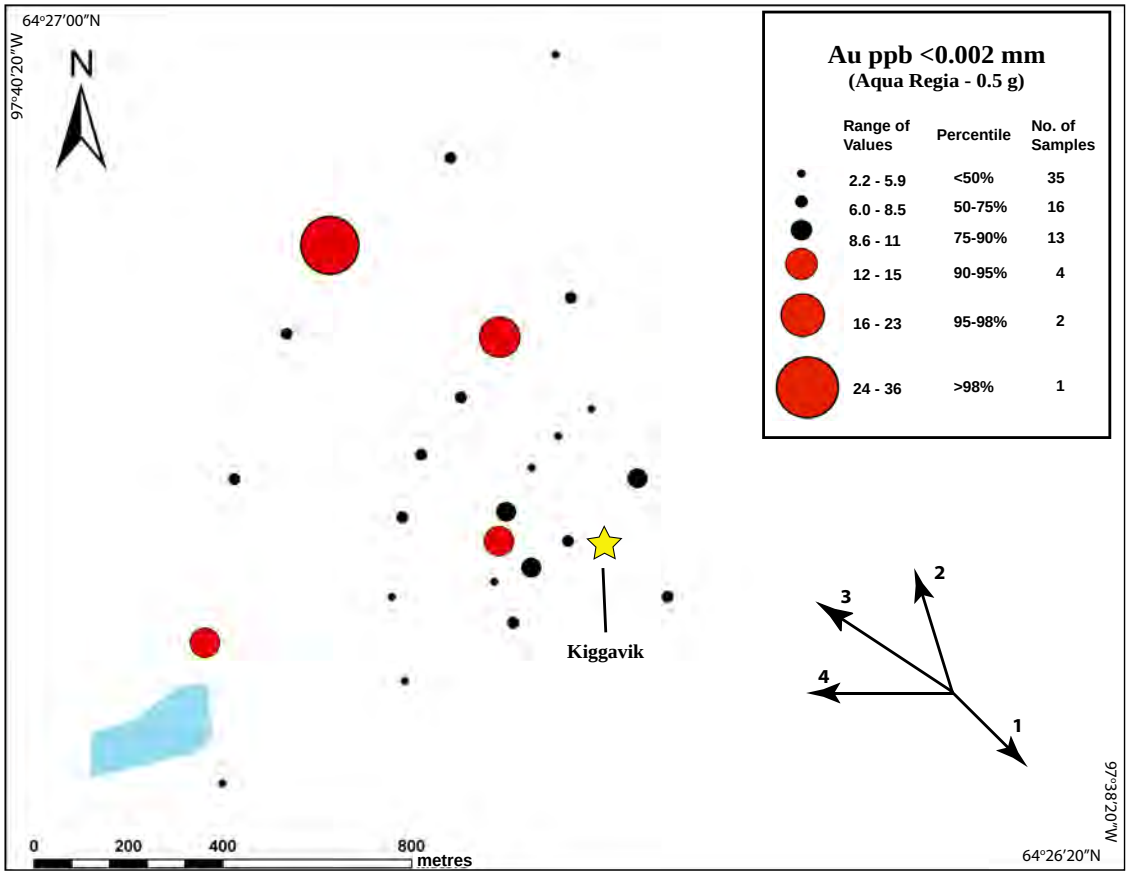

Appendix K1 Map 2. Deposit-scale map of the study area showing the Au content in the <0.002 fraction at each site.

APPENDIX K1 continued.

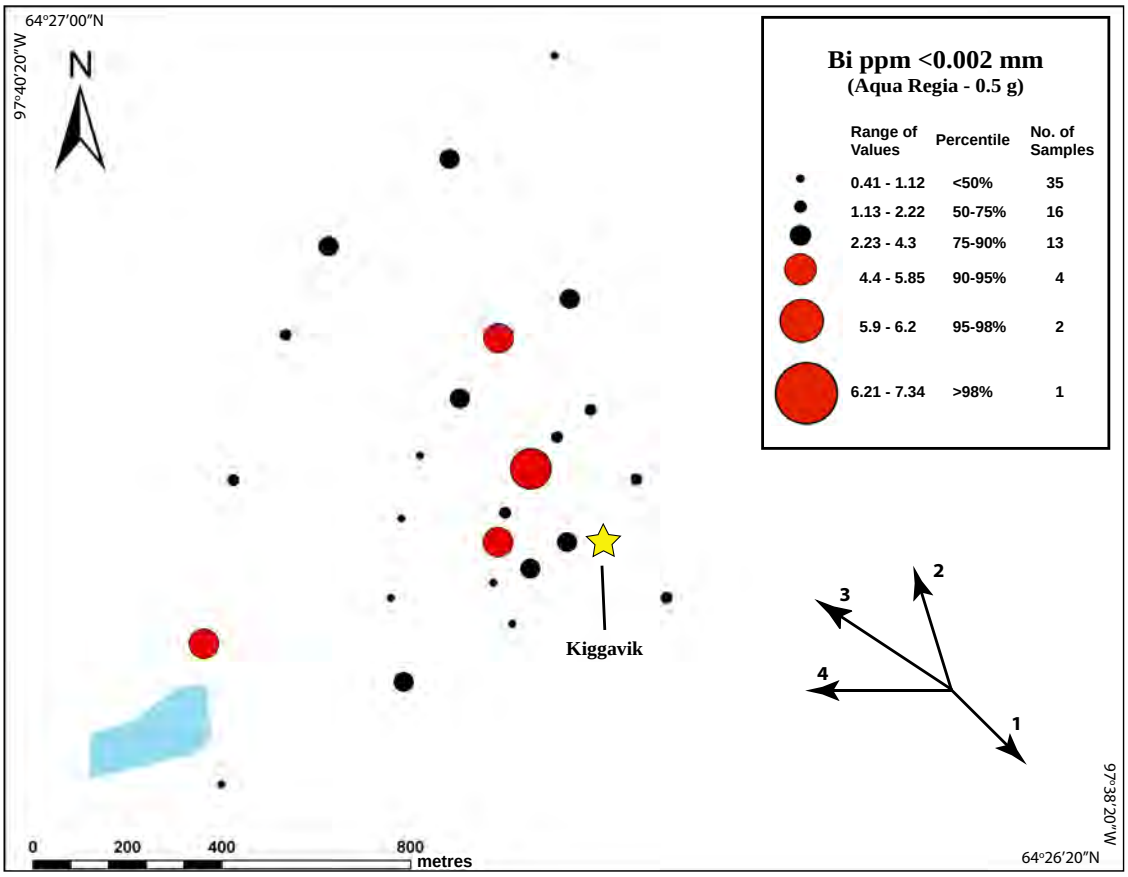

Appendix K1 Map 3. Deposit-scale map of the study area showing the Bi content in the <0.002 fraction at each site.

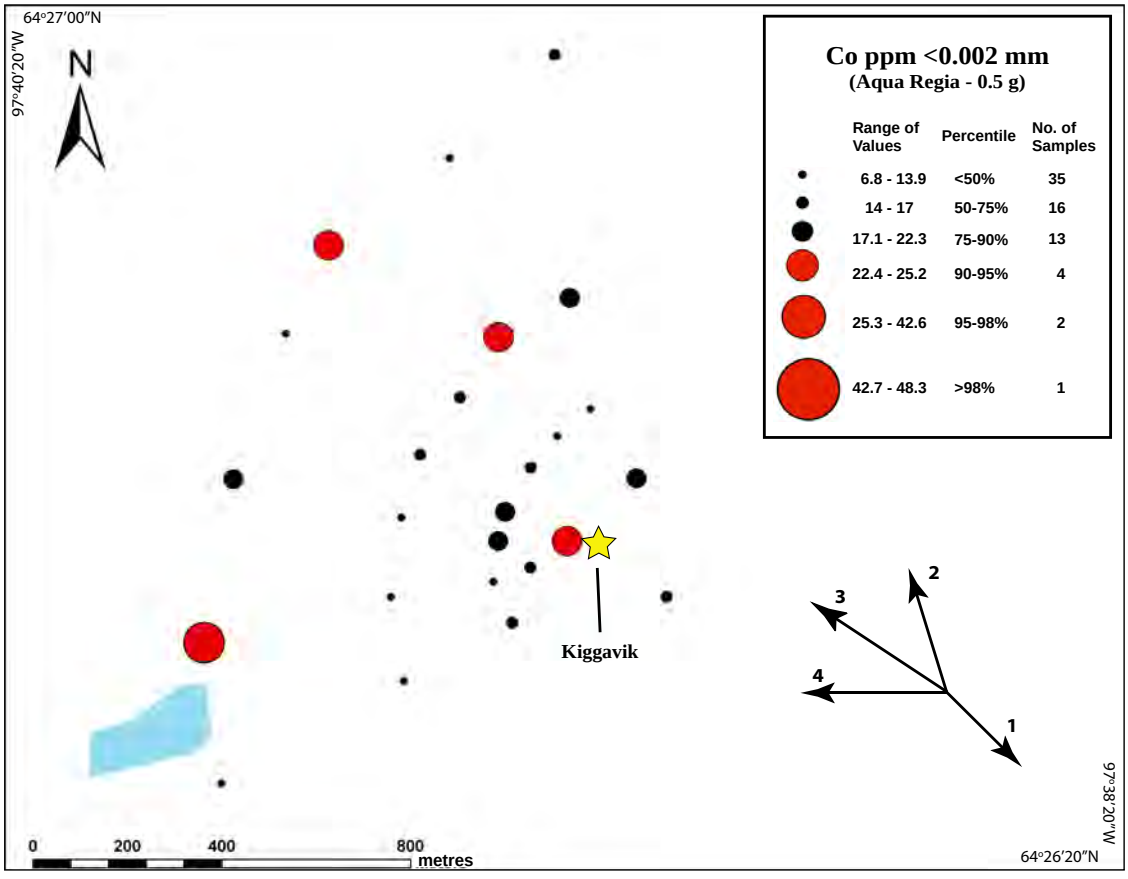

Appendix K1 Map 4. Deposit-scale map of the study area showing the Co content in the <0.002 fraction at each site.

APPENDIX K1 continued.

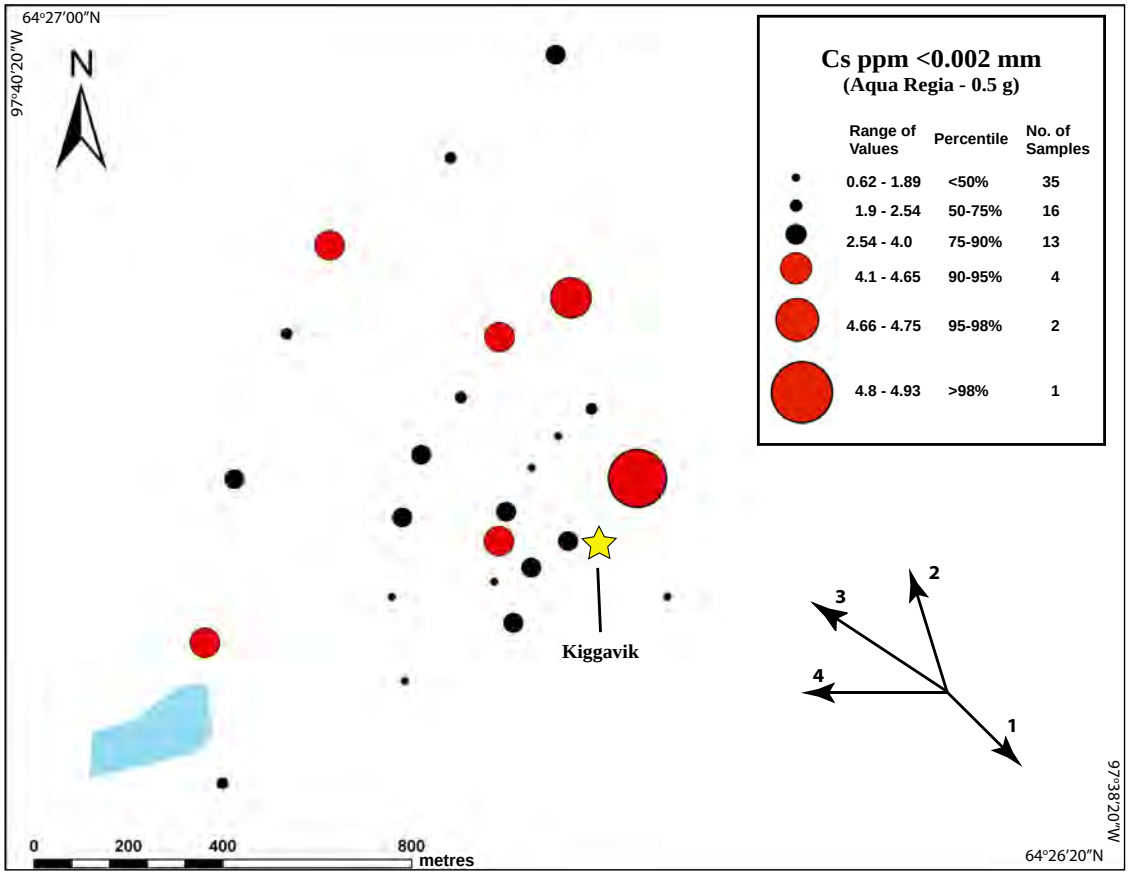

Appendix K1 Map 5. Deposit-scale map of the study area showing the Cs content in the <0.002 fraction at each site.

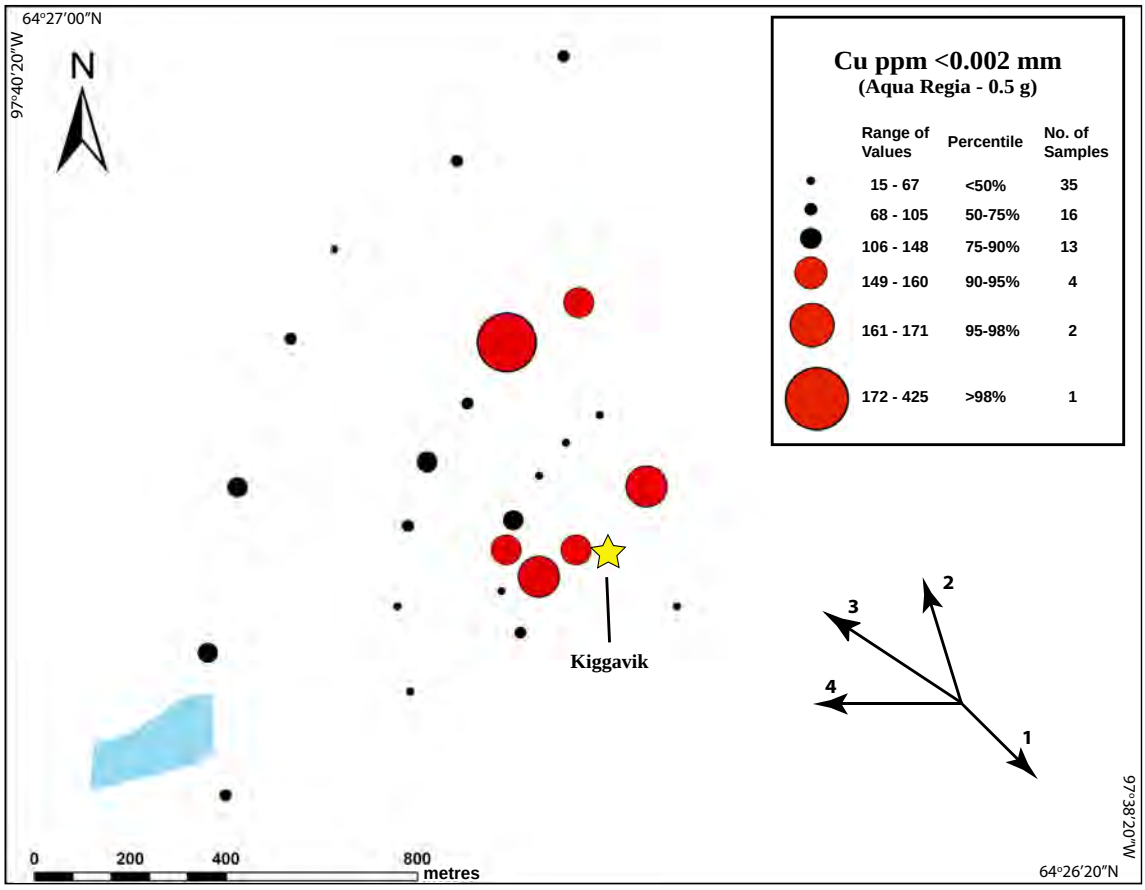

Appendix K1 Map 6. Deposit-scale map of the study area showing the Cu content in the <0.002 fraction at each site.

APPENDIX K1 continued.

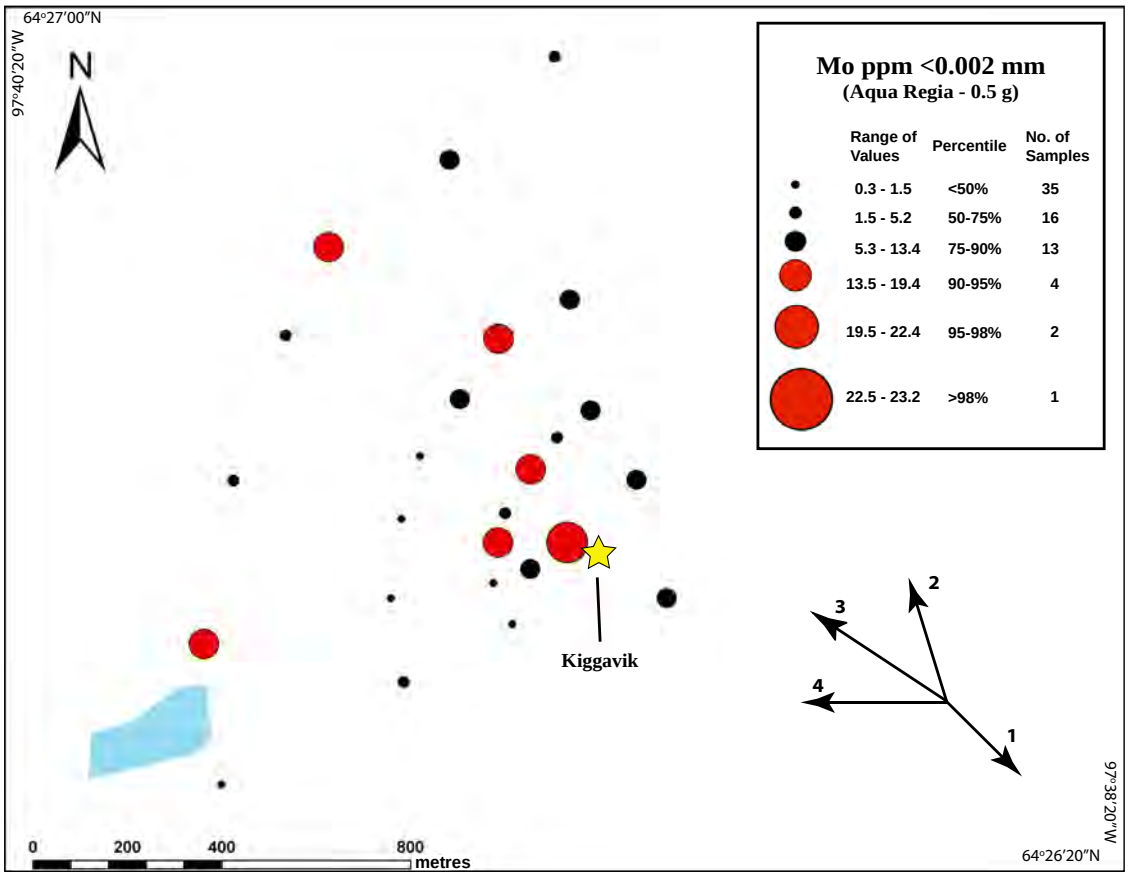

Appendix K1 Map 7. Deposit-scale map of the study area showing the Mo content in the <0.002 fraction at each site.

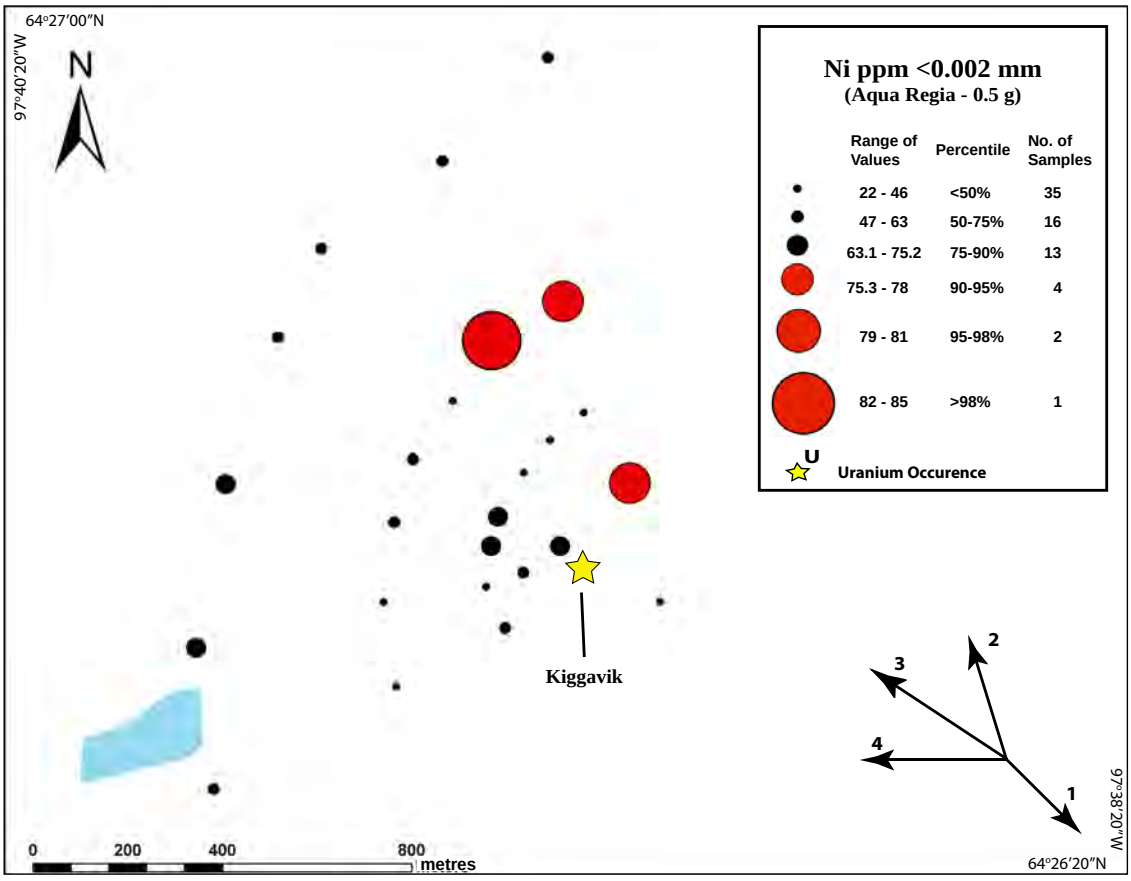

Appendix K1 Map 8. Deposit-scale map of the study area showing the Ni content in the <0.002 fraction at each site.

APPENDIX K1 continued.

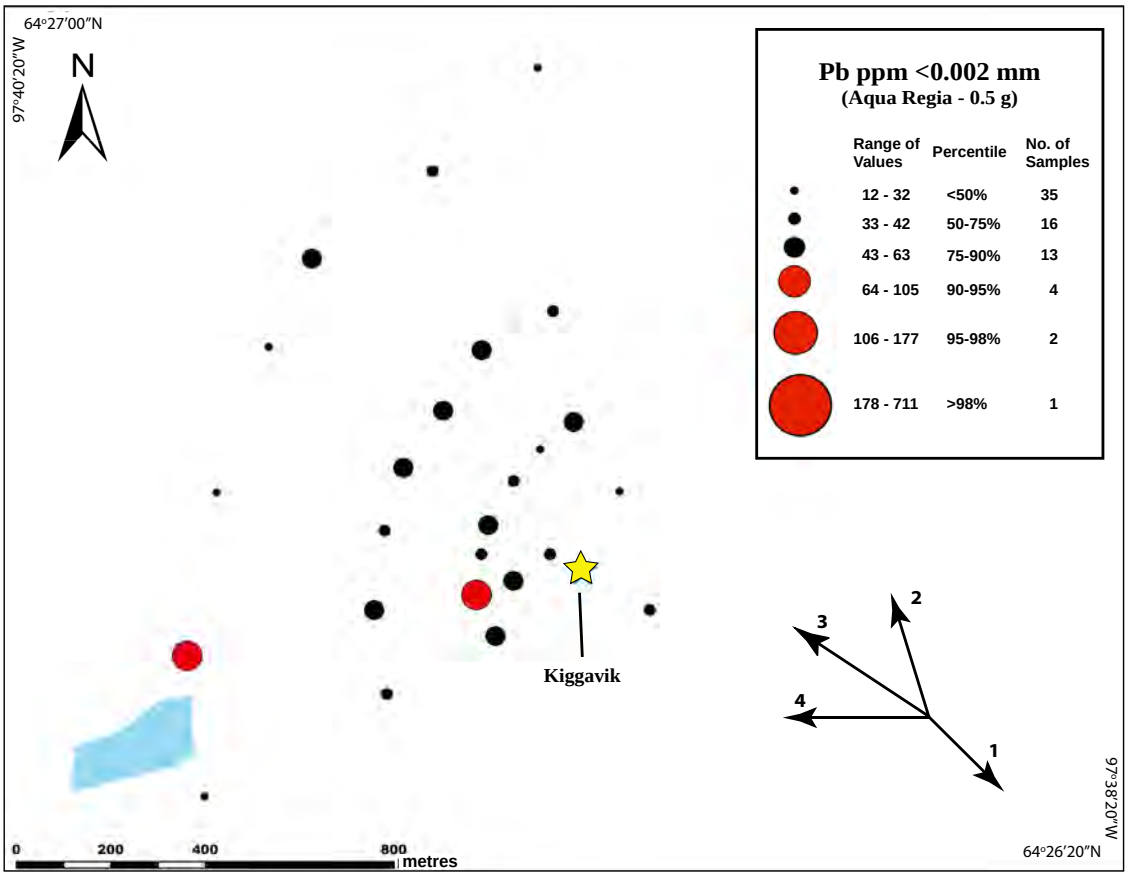

Appendix K1 Map 9. Deposit-scale map of the study area showing the Pb content in the <0.002 fraction at each site.

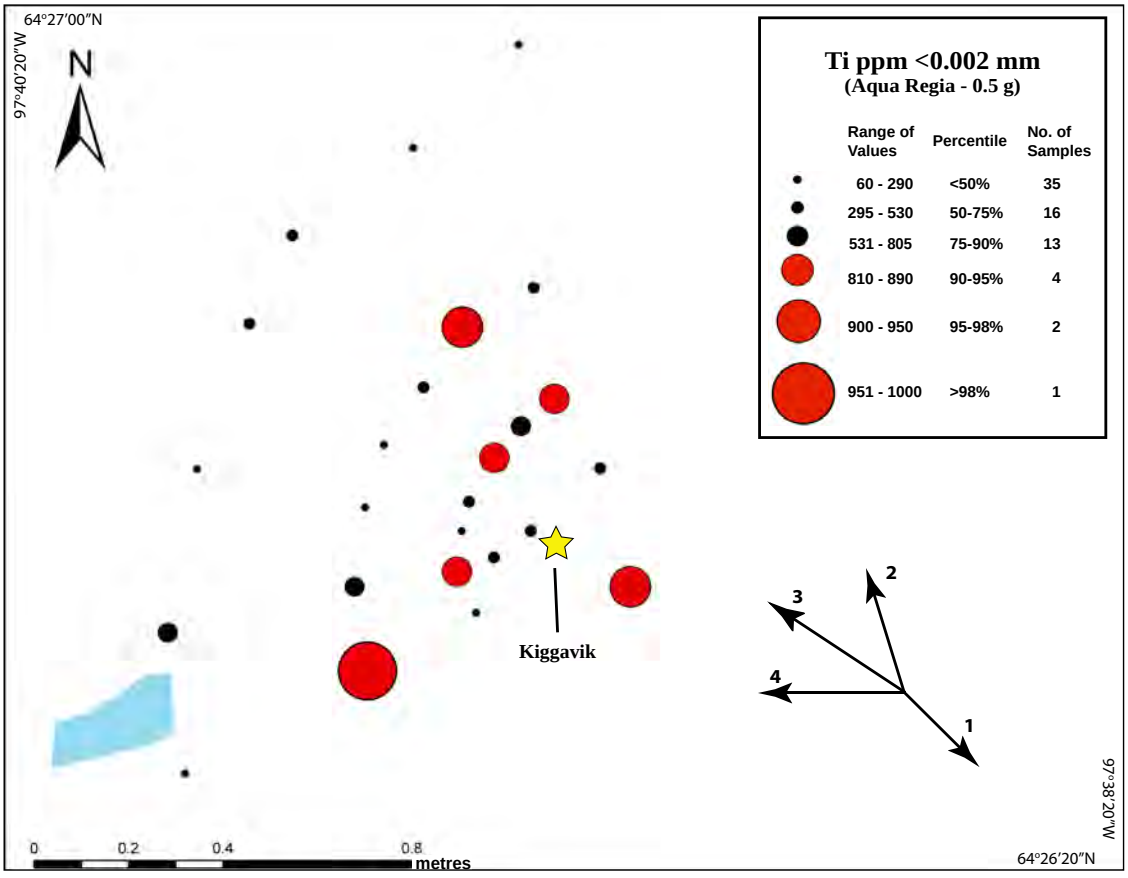

Appendix K1 Map 10. Deposit-scale map of the study area showing the Ti content in the <0.002 fraction at each site.

APPENDIX K1 continued.

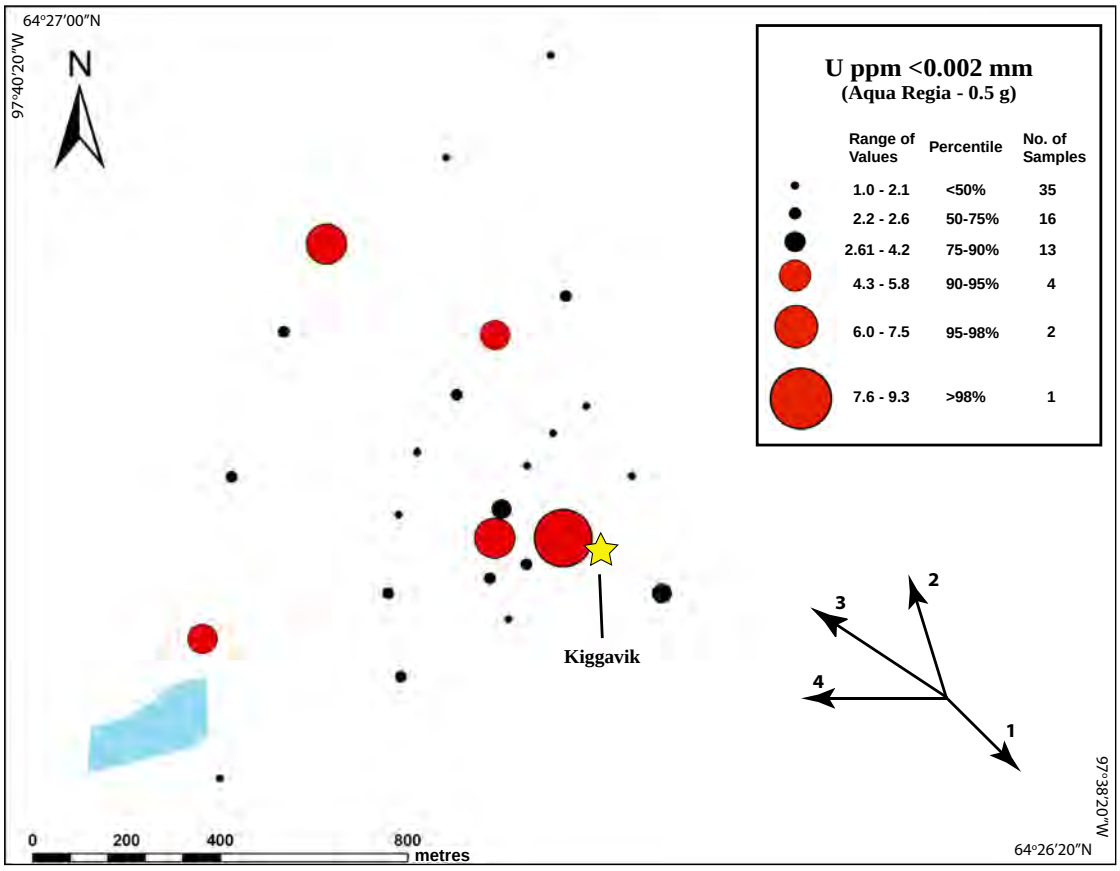

Appendix K1 Map 11. Deposit-scale map of the study area showing the U content (deteremined by aqua regia) in the <0.002 fraction at each site.

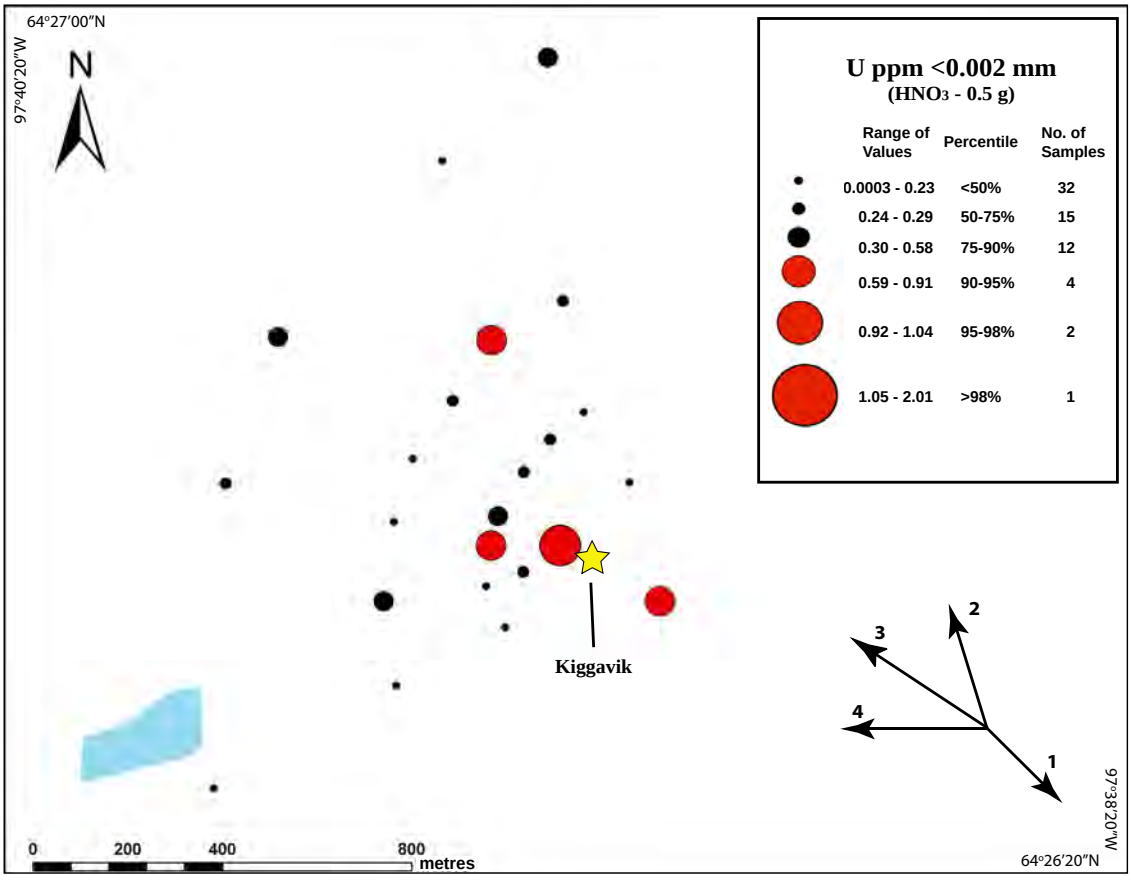

Appendix K1 Map 12. Deposit-scale map of the study area showing the U content (determined by HNO_3) in the <0.002 fraction at each site.

APPENDIX K1 continued.

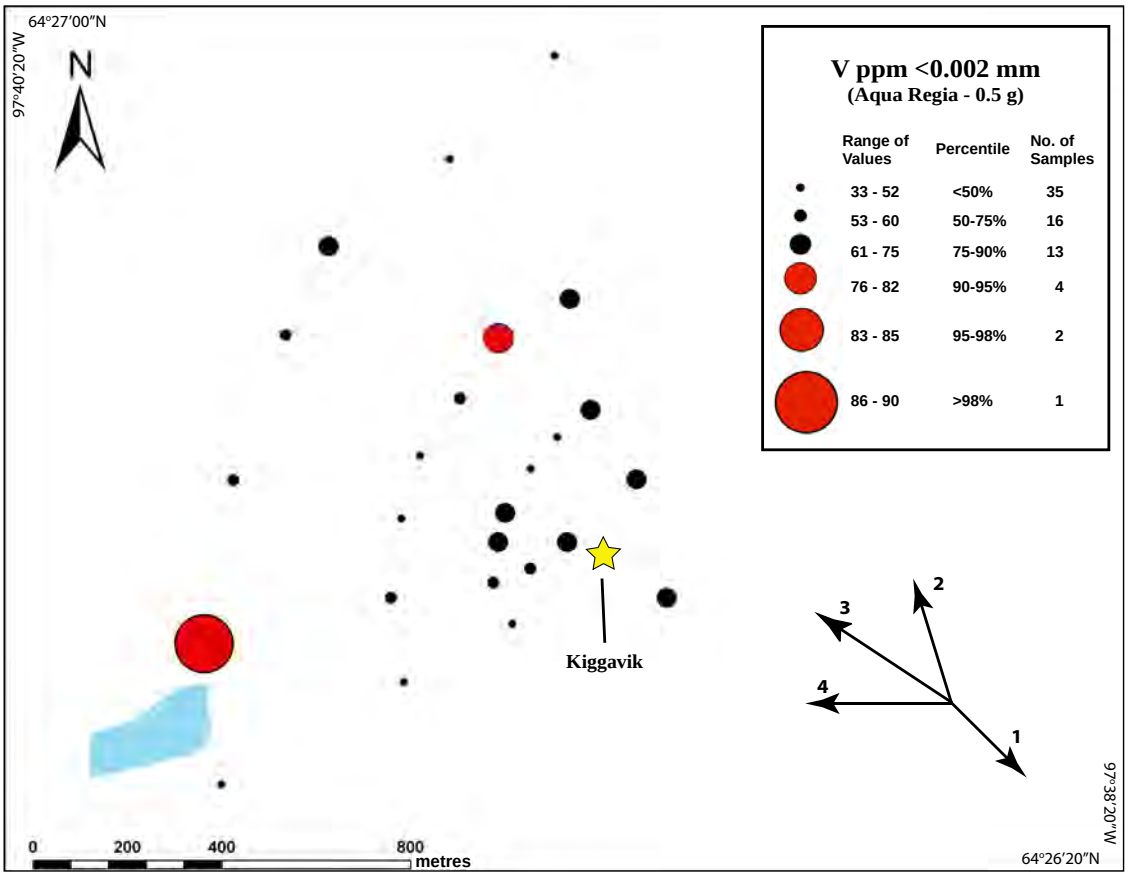

Appendix K1 Map 13. Deposit-scale map of the study area showing the V content in the <0.002 fraction at each site.

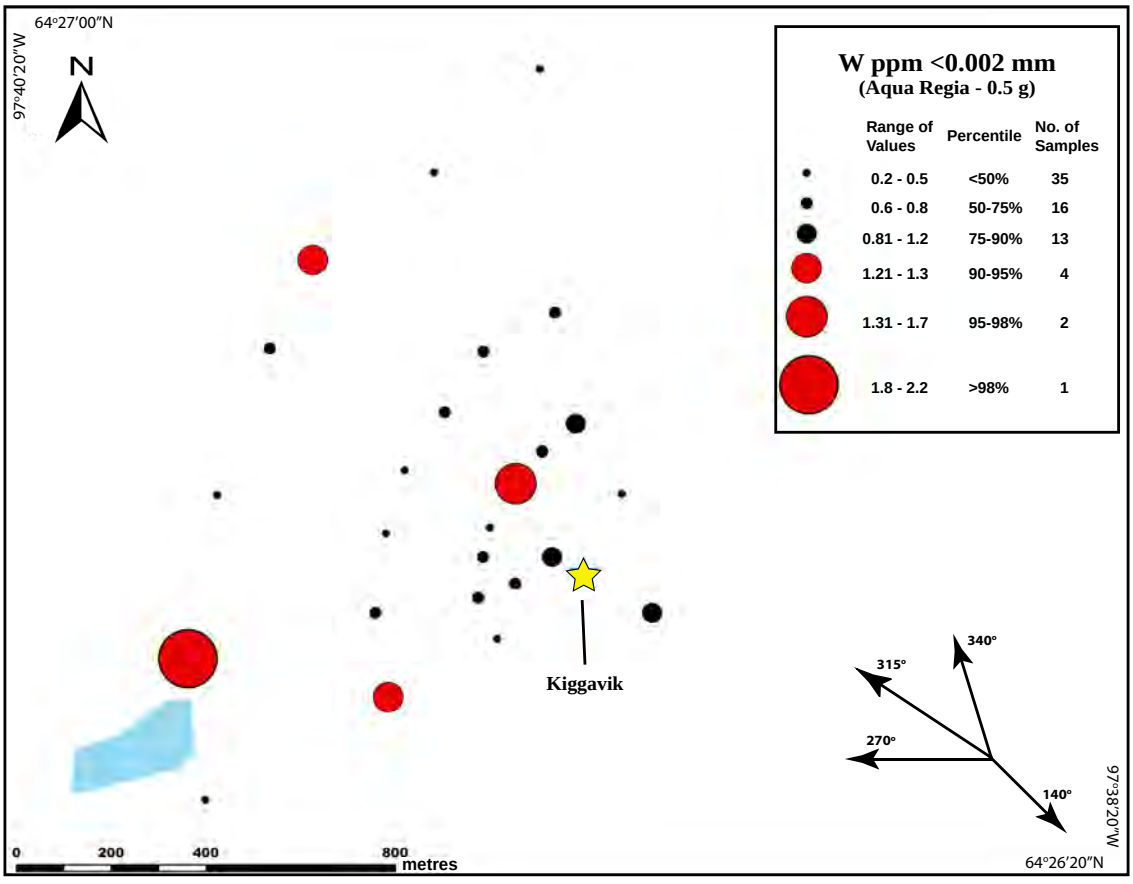

Appendix K1 Map 14. Deposit-scale map of the study area showing the W content in the <0.002 fraction at each site.

APPENDIX K2. Regional-scale geochemistry maps of selected elements in the <0.002 mm fraction.

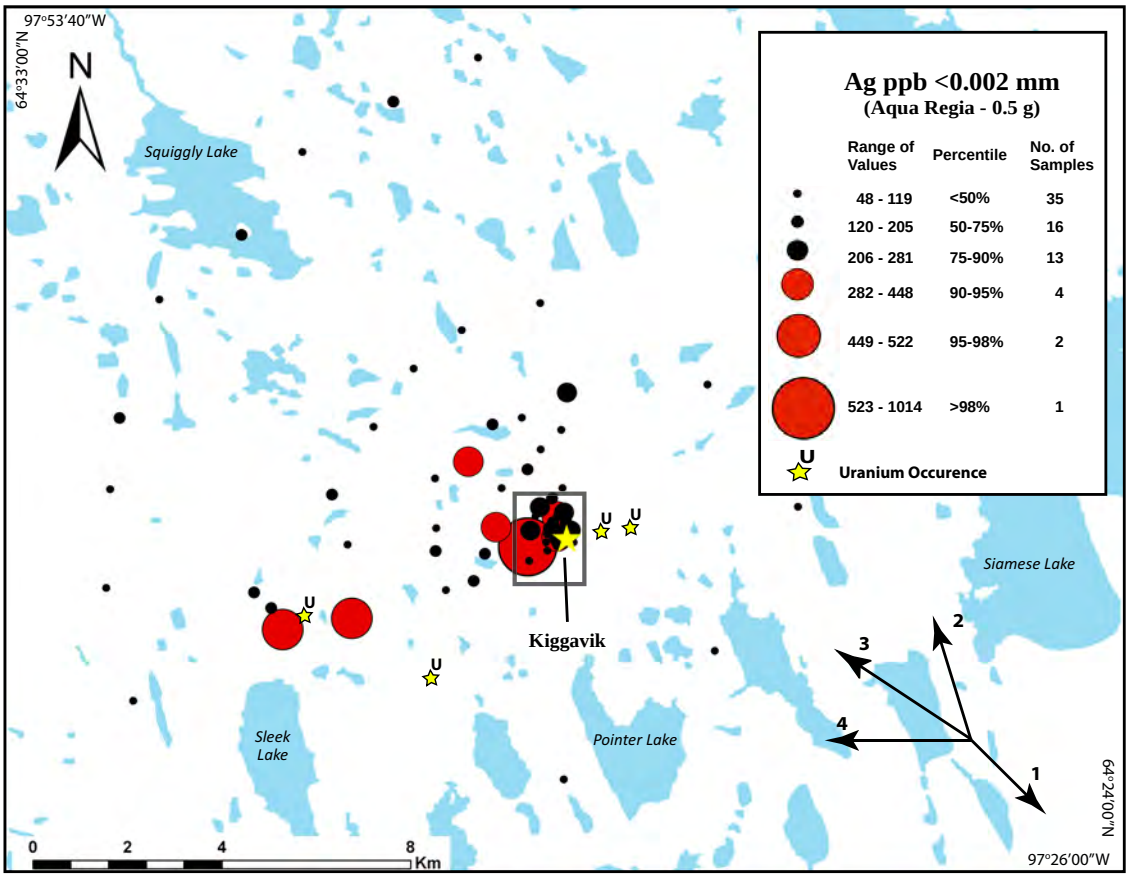

Appendix K2 Map 1. Regional-scale map of the study area showing the Ag content in the <0.002 fraction at each site.

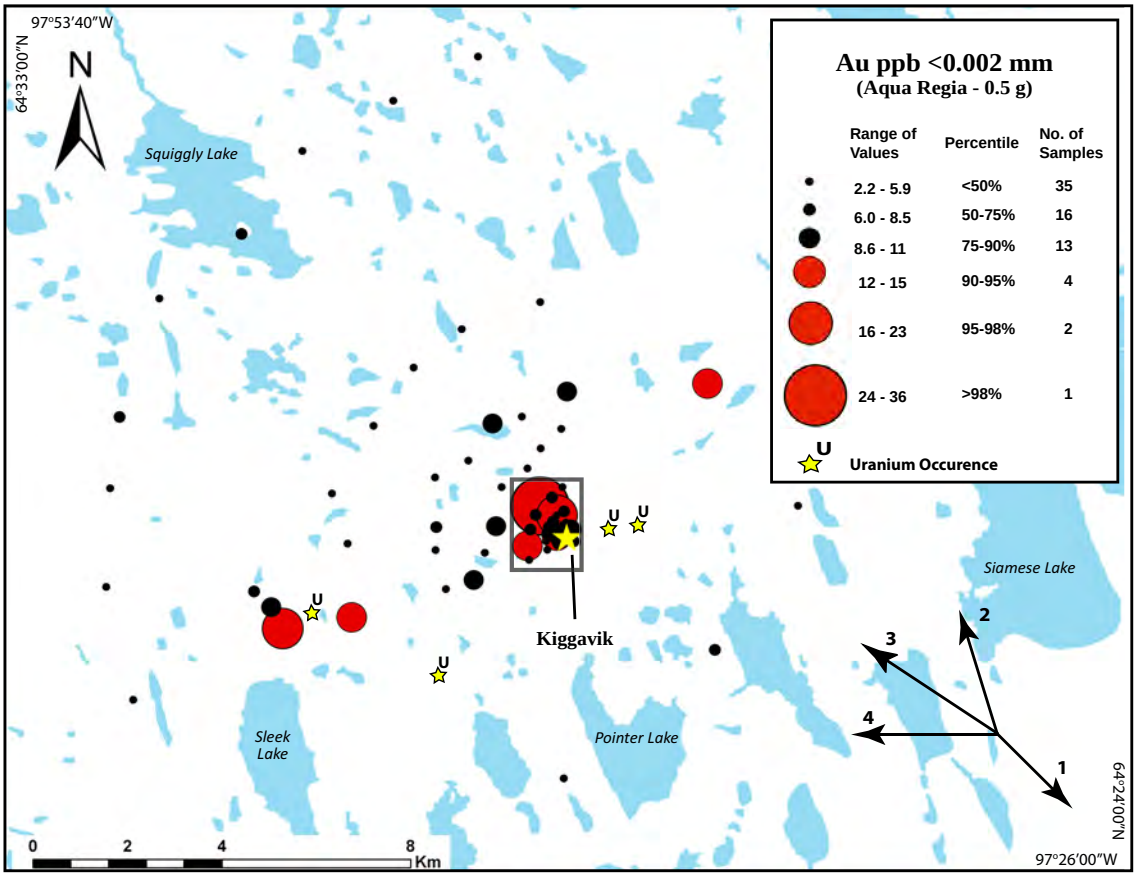

Appendix K2 Map 2. Regional-scale map of the study area showing the Au content in the <0.002 fraction at each site.

APPENDIX K2 continued.

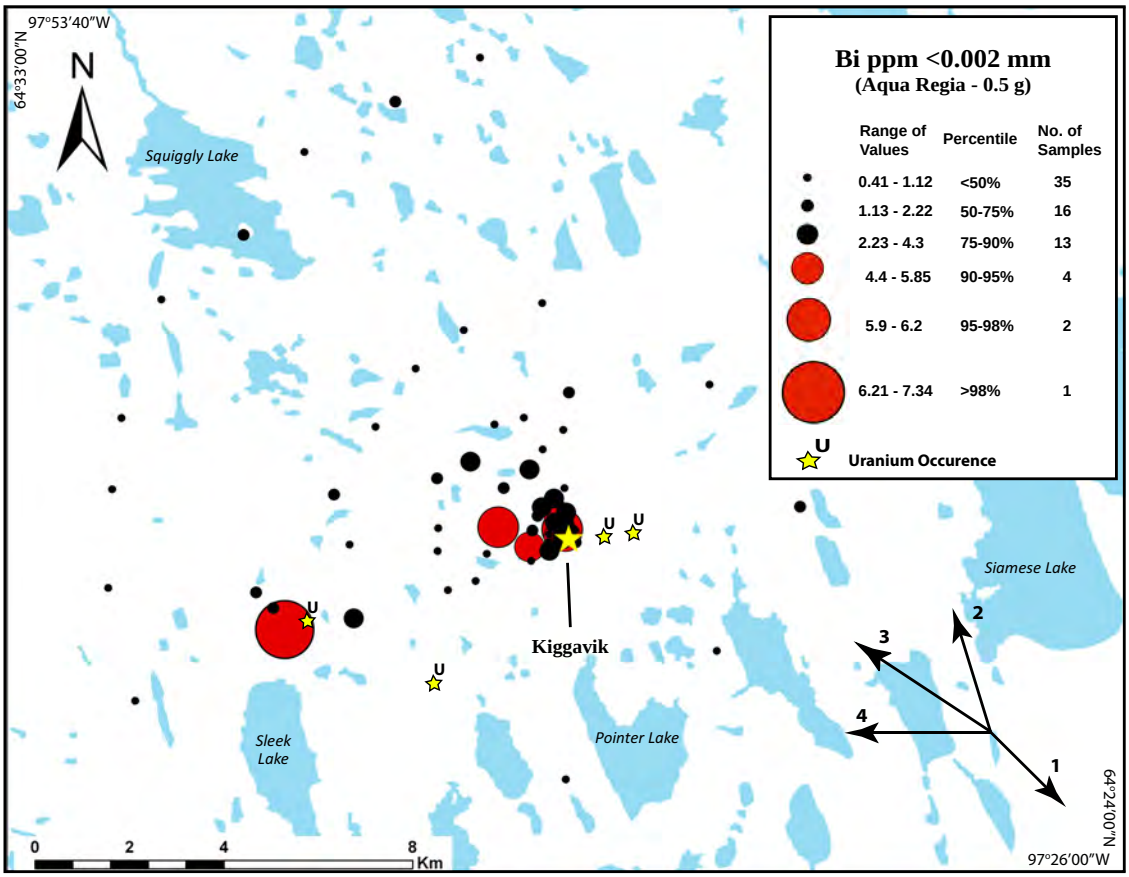

Appendix K2 Map 3. Regional-scale map of the study area showing the Bi content in the <0.002 fraction at each site.

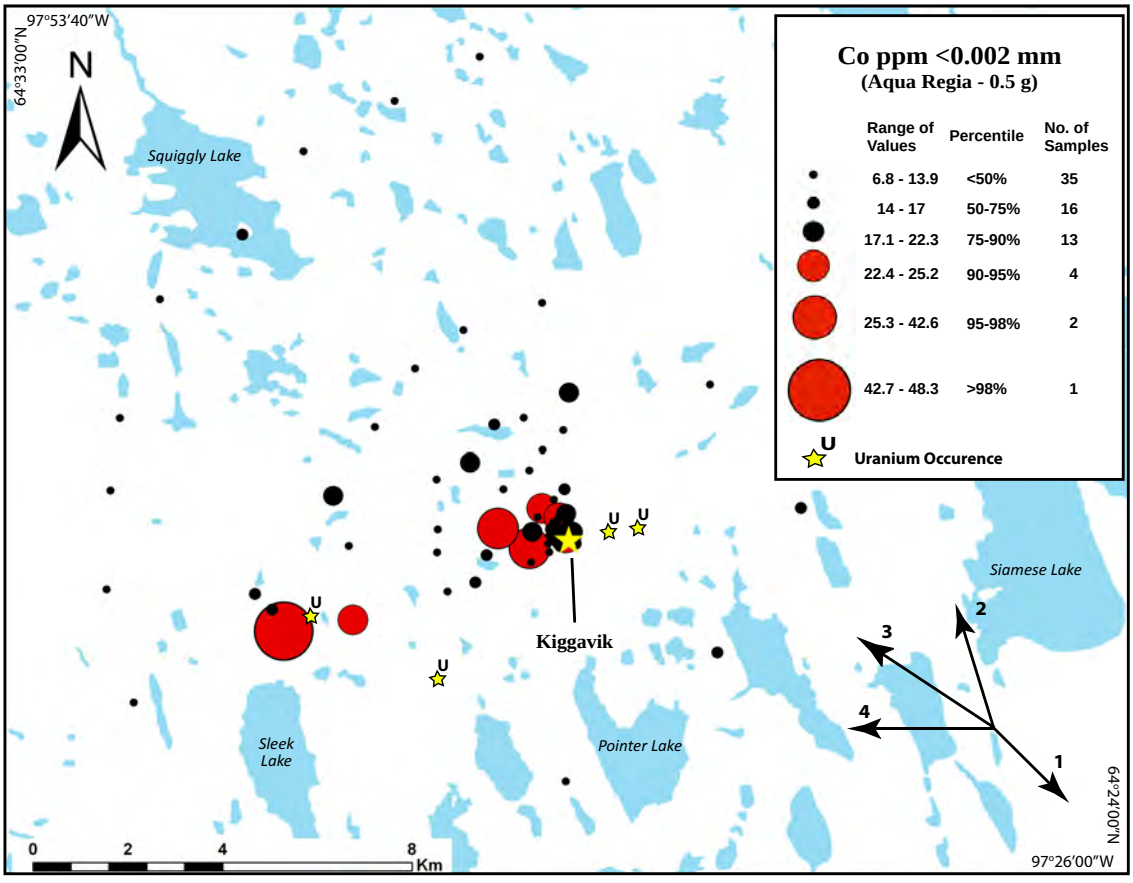

Appendix K2 Map 4. Regional-scale map of the study area showing the Co content in the <0.002 fraction at each site.

APPENDIX K2 continued.

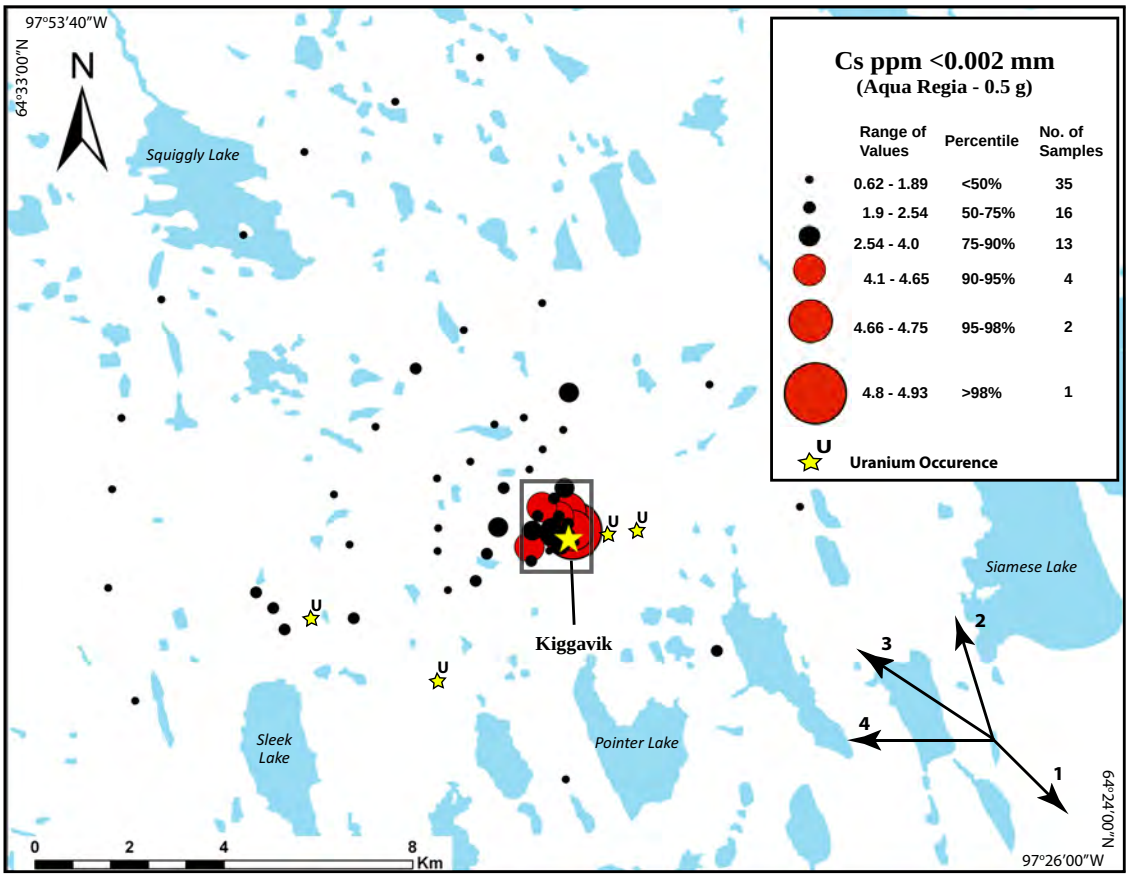

Appendix K2 Map 5. Regional-scale map of the study area showing the Cs content in the <0.002 fraction at each site.

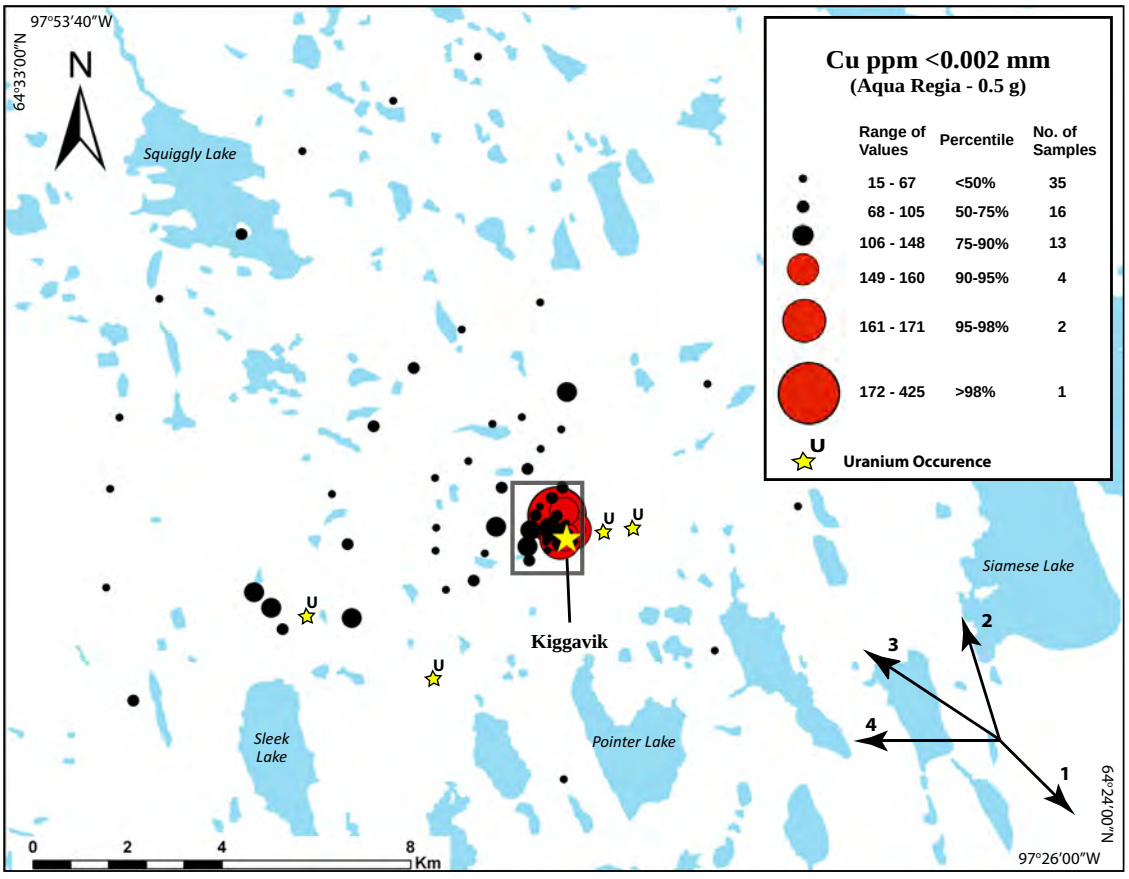

Appendix K2 Map 6. Regional-scale map of the study area showing the Cu content in the <0.002 fraction at each site.

APPENDIX K2 continued.

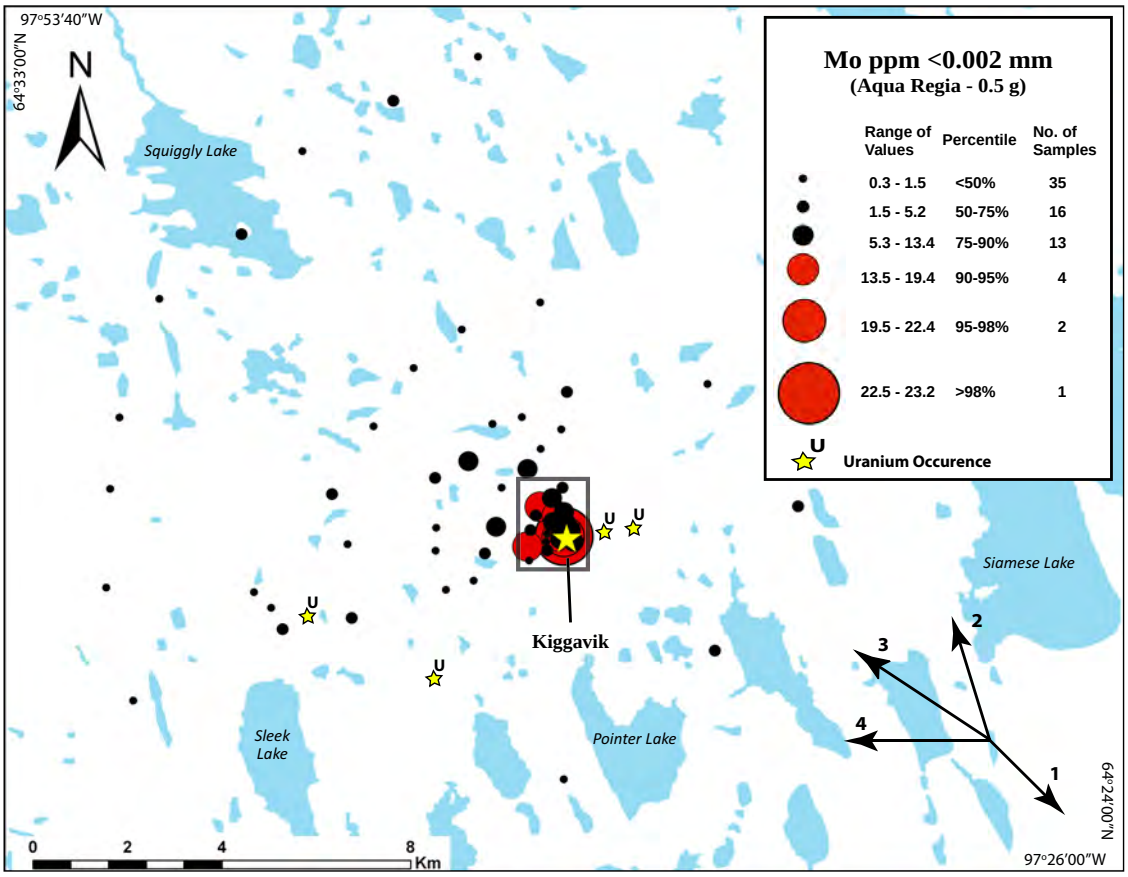

Appendix K2 Map 7. Regional-scale map of the study area showing the Mo content in the <0.002 fraction at each site.

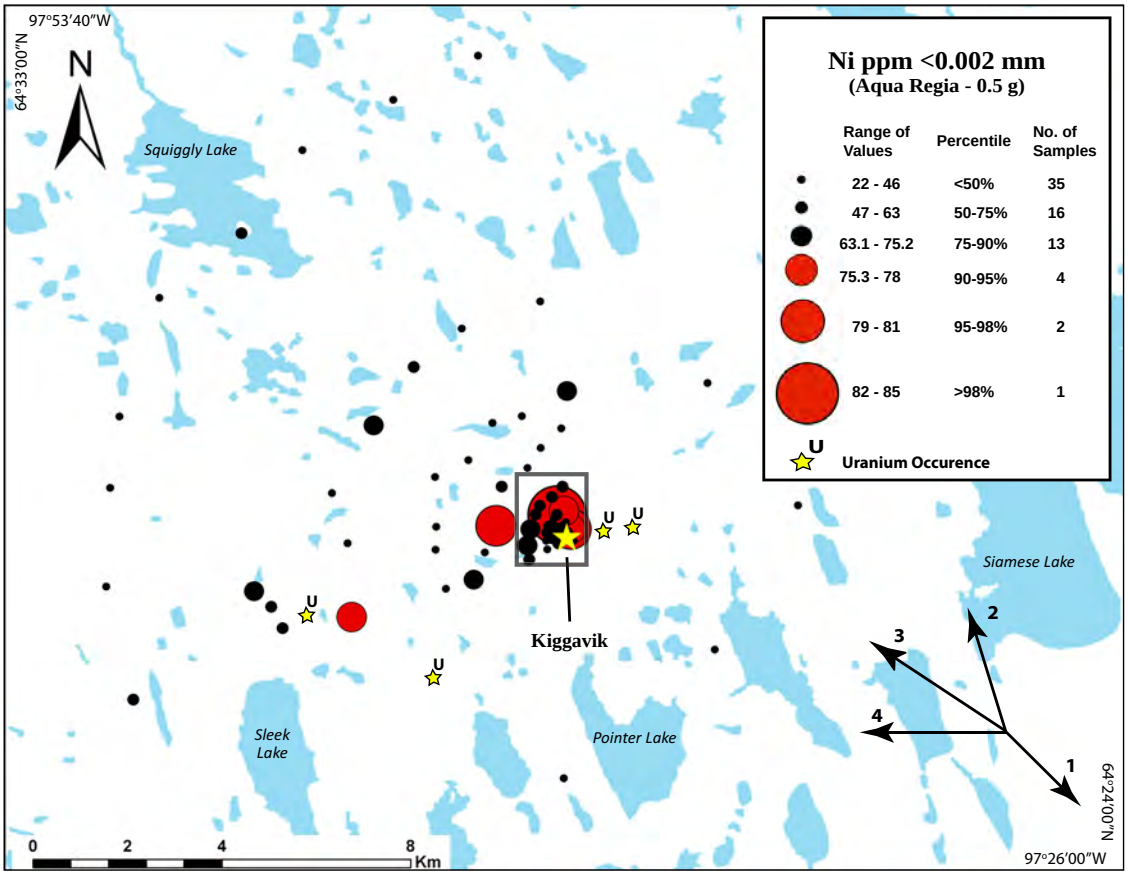

Appendix K2 Map 8. Regional-scale map of the study area showing the Ni content in the <0.002 fraction at each site.

APPENDIX K2 continued.

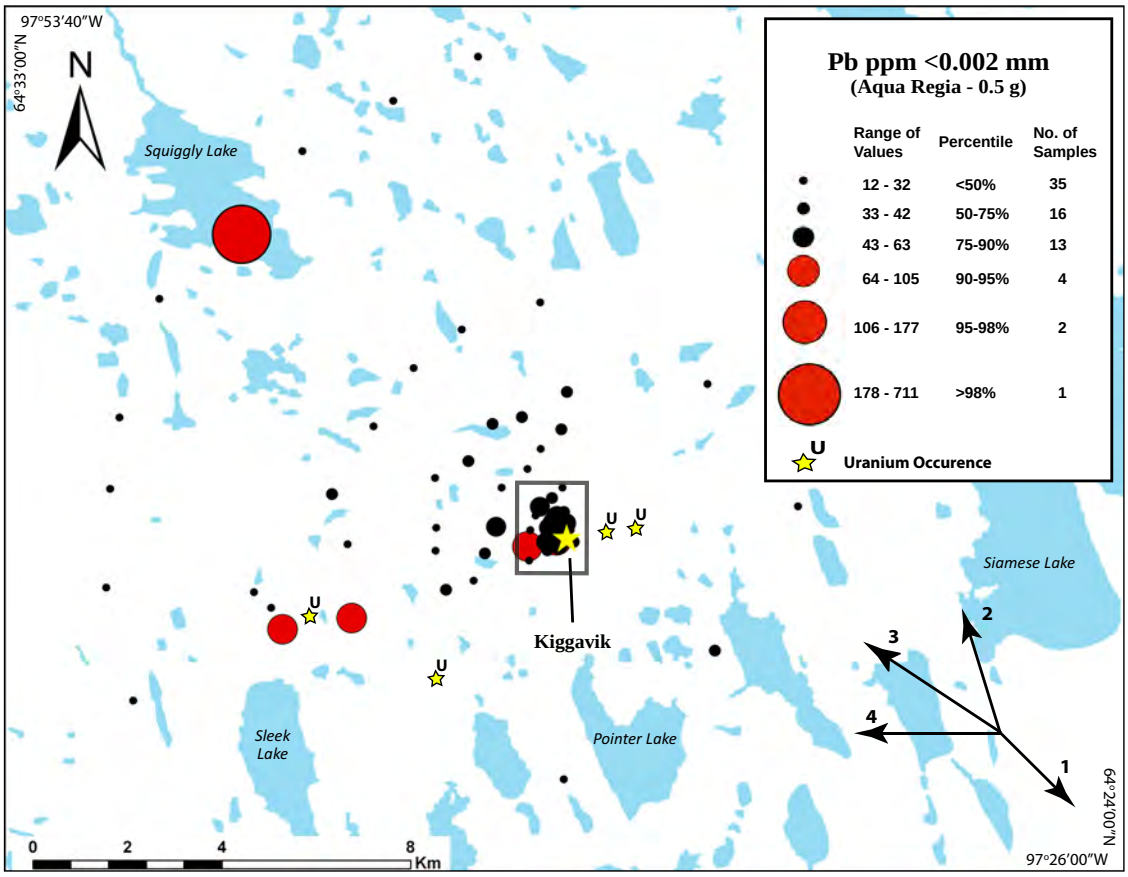

Appendix K2 Map 9. Regional-scale map of the study area showing the Pb content in the <0.002 fraction at each site.

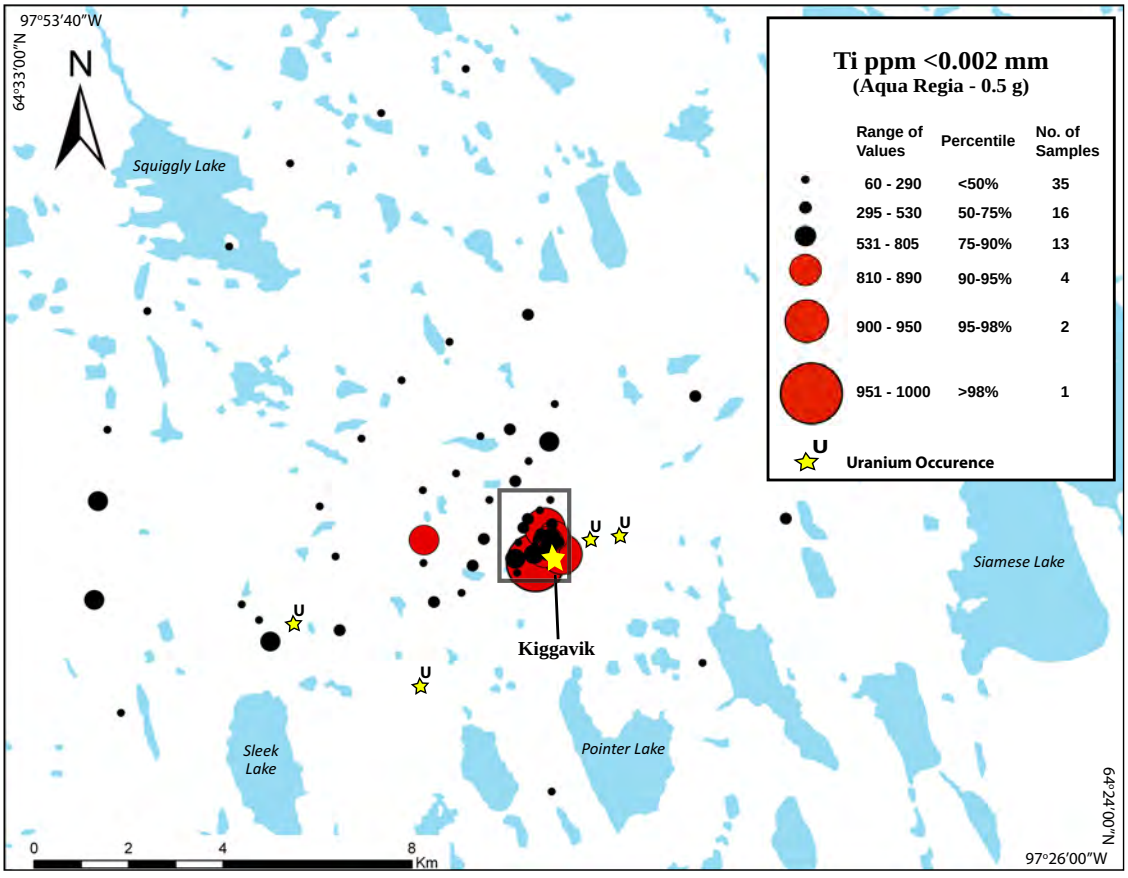

Appendix K2 Map 10. Regional-scale map of the study area showing the Ti content in the <0.002 fraction at each site.

APPENDIX K2 continued.

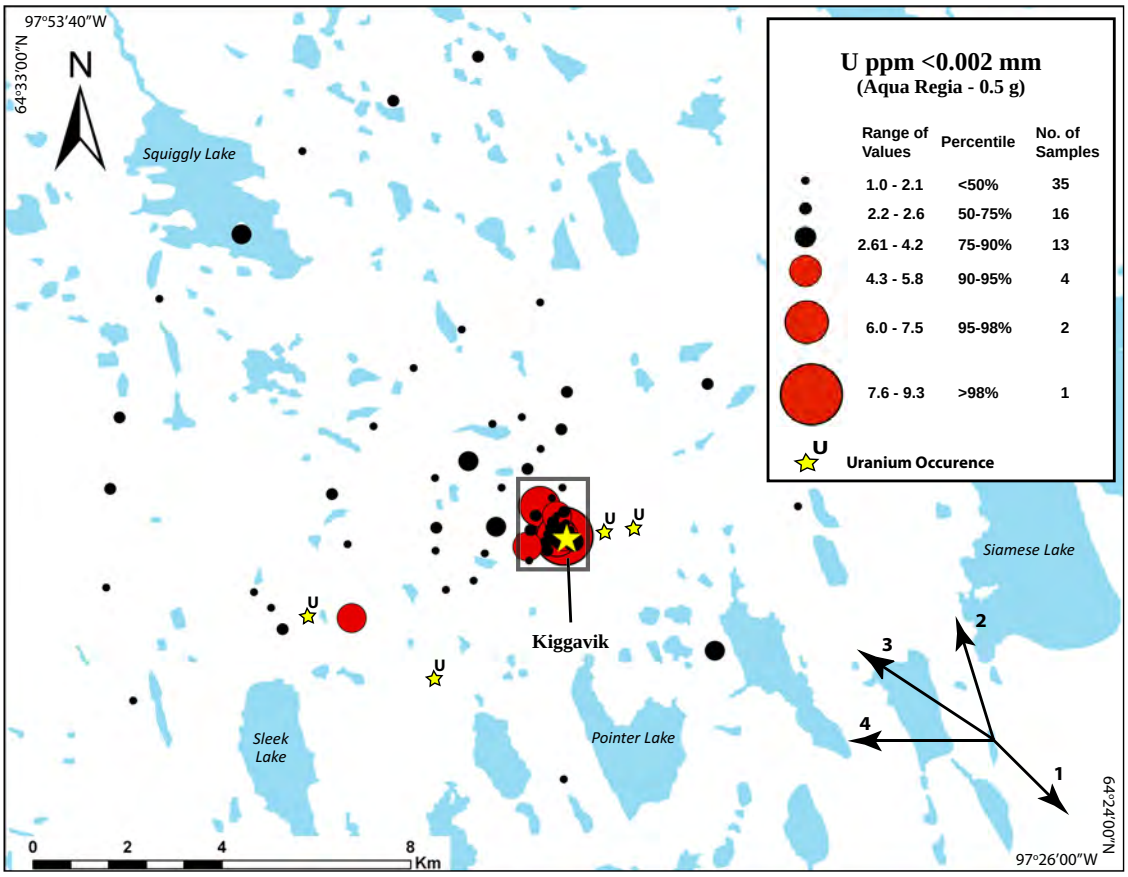

Appendix K2 Map 11. Regional-scale map of the study area showing the U content (determined by aqua regia) in the <0.002 fraction at each site.

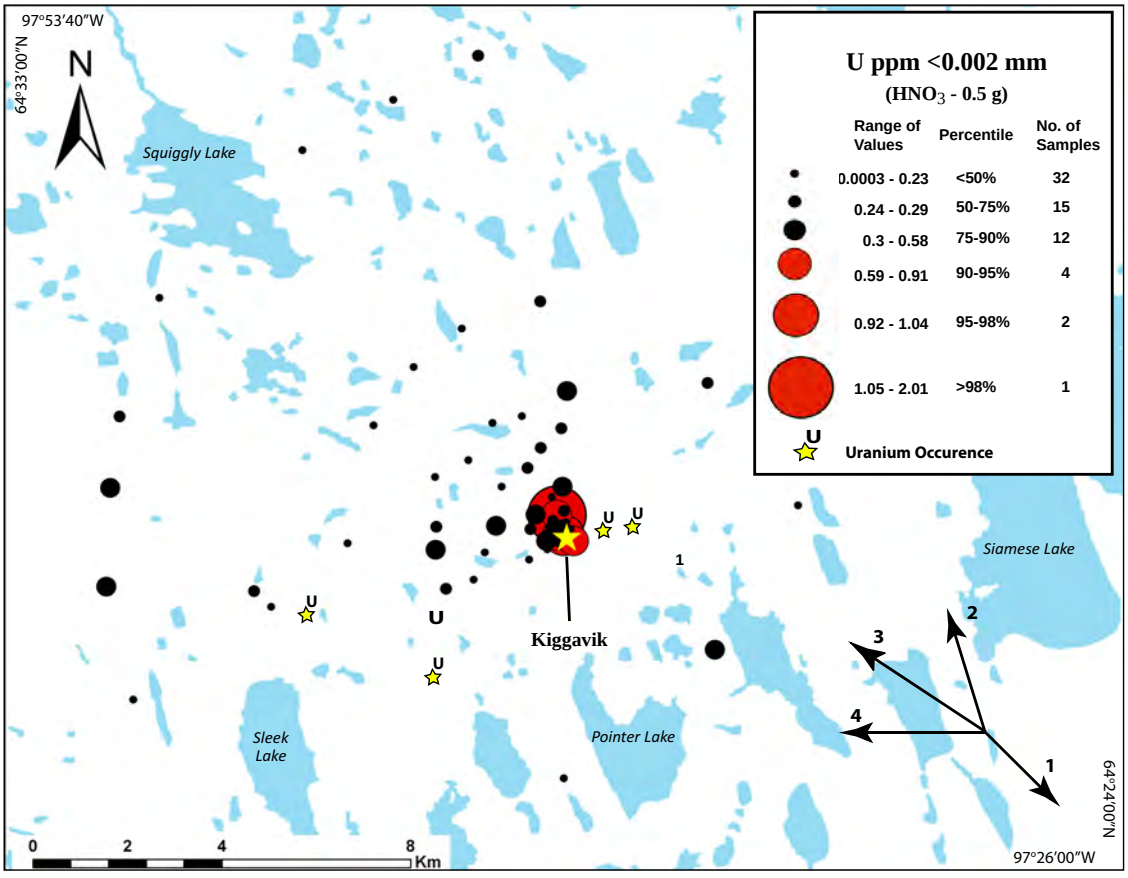

Appendix K2 Map 12. Regional-scale map of the study area showing the U content (determined by borate fusion) in the <0.002 fraction at each site.

APPENDIX K2 continued.

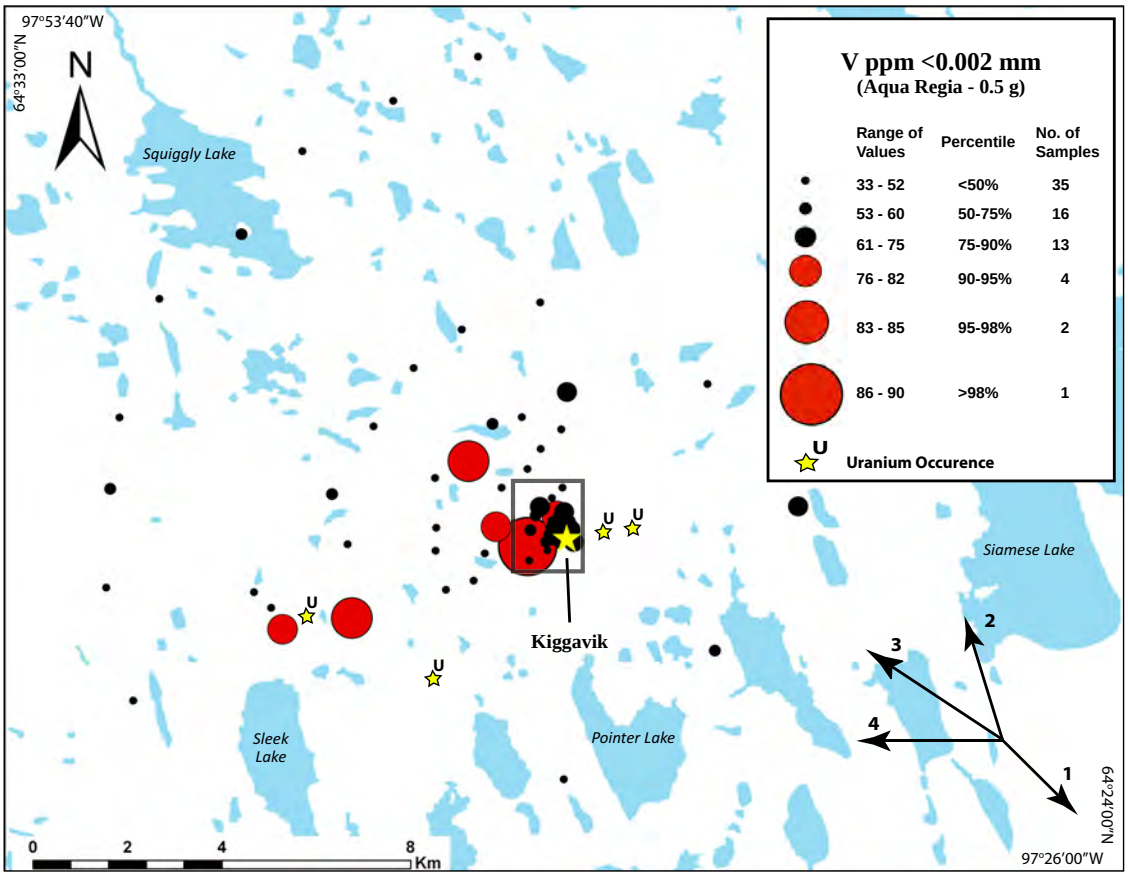

Appendix K2 Map 13. Regional-scale map of the study area showing the V content in the <0.002 fraction at each site.

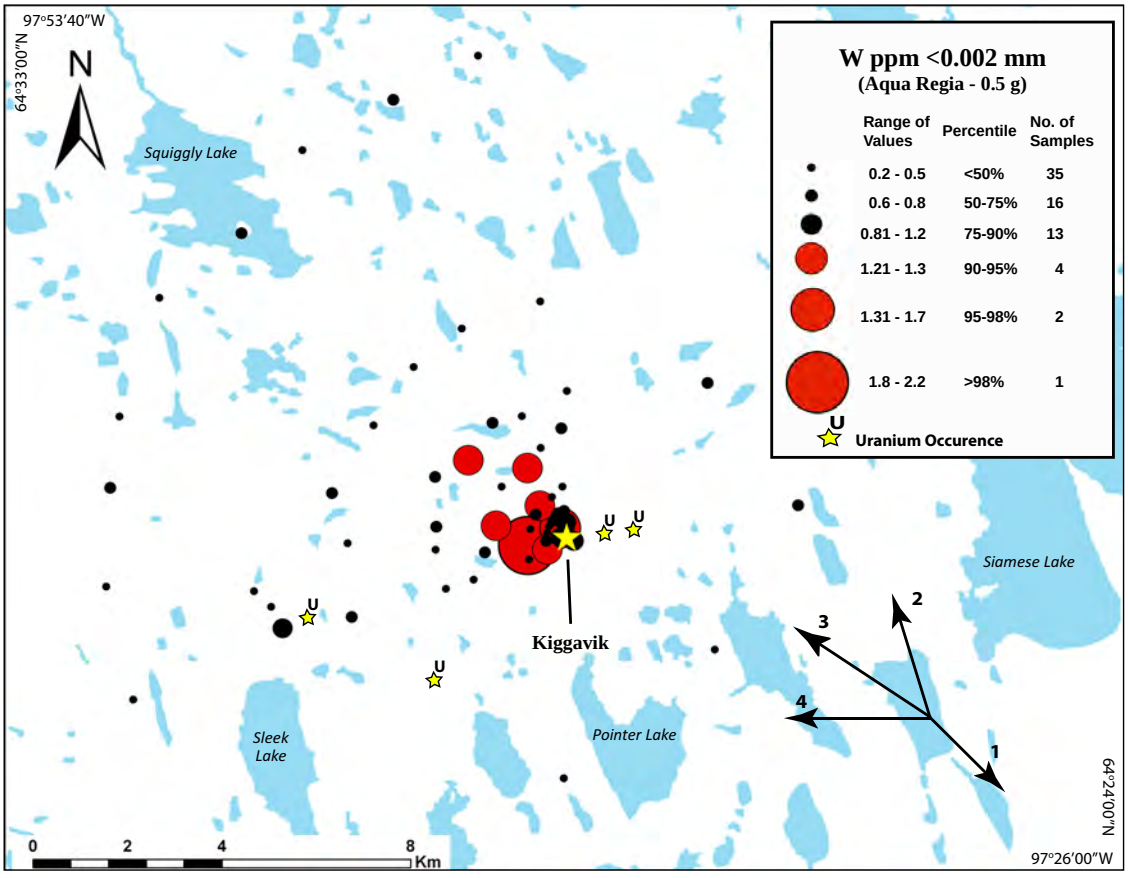

Appendix K2 Map 14. Regional-scale map of the study area showing the W content (analyzed by borate fusion in the <0.002 fraction at each site.